THE ROLE OF UNFOLDED PROTEIN DEPOSITS IN CARDIAC DYSFUNCTION

A thesis submitted to

IMPERIAL COLLEGE

NATIONAL HEART AND LUNG INSTITUTE

for the degree of

DOCTOR of PHILOSOPHY

By

Davide Gianni

2

Per aspera ad Astra

DECLARATION OF ORIGINALITY

I, Davide Gianni, declare that this thesis is my own work and has not been submitted in any form for another degree or diploma at any university or other institute of tertiary education. Information derived from the published and unpublished work of others has been acknowledged in the text and a list of references is given in the bibliography.

Davide Gianni

ABSTRACT

In this study we investigated the role of unfolded proteins as a toxic insult for cardiomyocytes in idiopathic dilated cardiomyopathy (DCM).

We first confirmed the presence of amyloid fibers in DCM cardiomyocytes by histological and ultrastructural analysis, showing their preferentially intracellular distribution. These molecular species seem to coexist with low-complexity β-folded precursors (oligomers) which in our experiments could promote increase of systolic Ca^{2+} in normal cardiomyocytes and alterations of contractility.

Our results suggest that these molecular species trigger the overexpression of UPR components such as GRPs, Chop and Caspase 12. In addition we demonstrated the presence of interactions between presenilins (PS) and Serca2a, suggesting a regulatory role of these Alzheimer's-related proteins on the Ca^{2+} pump. The genetic analysis of the presenilin genes in DCM samples identified two undescribed mutations in the promoter of PS1, which appeared to inhibit the expression of the protein. The quantification of the presenilin levels showed a considerable decrease of PS2 associated with an increase of PS1.

In order to characterize the protein(s) involved in the aggregasomes, we developed a series of purification protocols, which, unfortunately, did not identify a single protein species. As an alternative approach, we focused on the identification of transcripts differentially expressed in iDCM. Our study introduces an innovative three-group analysis in which we used amyloid samples to eliminate the interference related to the accumulation of unfolded peptides and deriving from the progression of HF. Interestingly we recognized a limited number of iDCM-specific genes, including nestin and DSCR1, which are normally correlated to neural development.

In conclusion, our findings open intriguing perspectives to increase our knowledge of the etiology and progression of DCM. However further investigation is required to identify the protein(s) involved in the formation of the aggregasomes and the role of these molecular structures in the etiology of the disease.

ACKNOWLEDGMENTS

This work would not have been possible without the supervision of Dr. del Monte at Harvard Medical School, who always represented a model both as a person and as a scientist. Although my presence in her laboratory was concomitant with important changes in her carrier, she always contributed with extraordinary effort and guidance in helping my development as the scientist I am today.

I also owe my deepest gratitude to my supervisor at Imperial College, Prof. Harding, for the strong support and encouragement she offered even in the most difficult moments of my program.

I would like also to express my gratitude to Dr. Fulci and Dr. Esteves for the valuable and wise advices they provided.

Lastly, I'd like to thank my family for the financial support during these years and, in particular, my wife Erika for her strong support and for understanding the difficulties that often were present during the completion of my program.

Davide Gianni

TABLE OF CONTENTS

INDEX OF FIGURES

20

INDEX OF TABLES

CHAPTER 1

INTRODUCTION

1.1 Heart Failure

1.1.1 Definition

Cardiovascular diseases (CDV) are currently one of the most frequent causes of mortality in Western countries. In the UK alone every year nearly 238,000 people die of heart and circulatory diseases, representing about one third of the total deaths. Congestive heart failure (HF), in particular, is officially recorded as the cause of death in 11,500 cases/year. However, this number is considered a large underestimate of the actual deaths mainly because of the current guidelines on death certificates, which explicitly discourage from recording HF as the underlying cause of death (2001).

Heart failure is the end stage of several conditions of different etiologies leading to abnormal hemodynamics with low cardiac output and accumulation of blood upstream to the heart. In the long term these defects lead to a progressive deterioration of cardiac function and premature cardiomyocyte death.

Different clinical classifications for HF have been proposed based on the diverse hemodynamic characteristics (Table 1.1).

Table 1.1. Main classification methods for heart failure.

Criteria	Classification
Localization of the defect	**myocardial** **cardiac** (includes valve defects) **circulatory** (includes hypertension, stenosis, anemia, hepatic and liver diseases)
Localization of the ventricular dysfunction (only for HF due to defects within the heart)	**Left** **Right**
Type of defect	**Forward:** impaired capacity of pumping the blood **Backward:** impaired filling of the chambers
Alteration of the ejection fraction (EF)	**Diastolic:** EF>45% **Systolic:** EF<45%

A first classification is based on the localization of cause of the inadequate cardiac output. According to this classification it is possible to identify three different categories of HF: myocardial failure, heart failure (which includes valve genetic defects inducing the regurgitation of blood from the ventricles to the atria) and circulatory failure (which derives from hypertension, anemia, aortic stenosis, fluid retention secondary to renal or hepatic diseases) (Braunwald, 1996).

When the cause of the failure is within the heart, a clinical distinction is usually made to identify the ventricle producing the abnormal function. In most cases HF is determined by dysfunctions originating in the left ventricle. Right ventricle failure, instead, is usually secondary to the presence of congenital heart diseases or to conditions affecting the lung (e.g., multiple emboli, chronic lung diseases or pulmonary hypertension). However, the distinction between left and right failure is a simplification of the disease: the two ventricles work as two pumps in series, so impairment of one inevitably affects the correct function of the second.

A further distinction in the HF group is related to the type of defect causing the dysfunction. According to what was proposed by James Hope back in 1832, a failing condition is referred as forward if the insufficient cardiac output is due to the incapacity of the ventricle to pump the blood out of the cavity or backward if the low output is due to defects leading to an incomplete filling of the chamber (e.g., valve anomalies or ventricle hypertrophy associated with reduced ventricular volume (Hope, 1832).

A last classification of HF is instead based on the evaluation of the ejection fraction (EF). EF is defined as the ratio between stroke volume and telediastolic volume. According to this definition, HF is considered diastolic when the EF is preserved or systolic when the EF is lower than 45%. In this last case the failing condition is usually due to increased diastolic volume rather than reduced stroke volume.

Despite the different classification proposed, HF is characterized by a series of common molecular defects leading to a decreased contractility of the cardiomyocyte including alterations in the energetic metabolism, in the contractile apparatus and in the molecules involved in the homeostasis of the cell (Table 1.2). Failing cardiomyocytes are characterized by significantly decreased contents of ATP and

Table 1.2. Molecular defects in heart failure.

Category	Alterations

Contractile apparatus	- Decreased Ca^{2+}-dependent Mg^{2+} ATPase activity
	 - Reduction of cross bridges and slower cycling
	 - Reduction of relative amount of myofibrils
	 - Isoform changes (TnT, Myosin light chain)
	    - Change of phosphorylation states (TnI)
	    - Increased Ca^{2+} sensitivity (debated)

Energetics	- Reduced fatty acid oxidation - Increased glycolysis - Decreased phosphocreatine:ATP ratio - Decreased and structurally abnormal mitochondria - Reduced expression of th electron transport chain components
Calcium homeostasis	- Increased cytosolic Ca^{2+} concentration during diastole - Prolonged Ca^{2+} transient - Progressive decrease of Ca^{2+} in cellular storage - Decrease of L-type Ca^{2+} channels - Impaired coupling between L-type Ca^{2+} and Ryanodine receptor - Increased activity of the sarcolemmal Na^{+}/Ca^{2+} exchanger - Increased phospohrylation of PLN kinase
Signal transduction	- Decrease in β-adrenoceptor - Decreased activity of the adenylyl cyclase-cAMP-PKA pathway - Increased desentization of in β-adrenoceptor - Increased levels of inhibitory G-proteins

phospocreatine, i.e., the molecule allowing a rapid diffusion of the energy produced in the mitochondria (Taha and Lopaschuk, 2007). The processes leading to the reduction of ATP include decreased capillary density and, in hypertrophy-related HF, increased diameter of the cardiomyocyte. These characteristics generate limited capacity of oxygen and nutrients to reach all the mitochondria of the cell and, therefore, produce impairment in the production of ATP. The effects of the decreased availability of ATP on the cardiomyocyte mainly affect high energy demanding processes of the cell such as the contractile function and homeostasis. In this condition cardiomyocytes switch
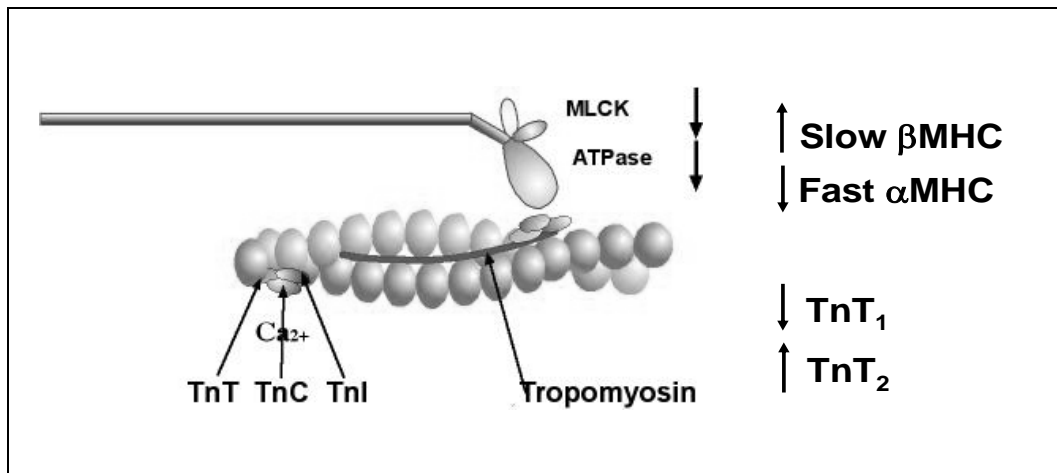
Figure 1.1. Major modification of the contractile apparatus in HF. HF samples show ~20% decrease in myofibrillar proteins, including the myosin light chain kinase (MLCK) and reduction of the ATPase activity. HF is also characterized by isoform transition in the myosin heavy chain (MHC, leading to reduced cross-bridge cycling) and troponin T (TnT, leading to decrease Ca^{2+} sensitivity). (Picture: courtesy of Dr. del Monte)

their energy source from high efficiency β-oxidation of fatty acids to anaerobic glycolysis, leading to the accumulation of lactate and, consequently, to acidosis. The molecular changes in the contractile apparatus affect different proteins, mainly causing isoform shifts leading to altered Ca^{2+} sensitivity and eventually depressed contractility (Del Monte and Hajjar, 2008). These proteins include myosin light and heavy chains, actin, troponin T and many cytoskeletal proteins such as titin, α-actinin, myosin binding protein C and fibronectin. In particular, failing cardiomyocytes present increased content of myosin heavy chain β combined with decreased level of the isoform α. This is associated with diminished velocity of contraction (Figure 1.1) (Nakao et al., 1997).

Additional anomalies of failing cardiomyocytes involve the ion transport systems (Figure 1.2) (Del Monte and Hajjar, 2008). In the sarcoplasmic reticulum (SR) the molecules affected by the failing condition are mainly the sarco/endoplasmic reticulum Ca^{2+} ATPase (SERCA) and the ryanodine receptor (RYR). Both the proteins show decreased content in HF (Go et al., 1995, Currie and Smith, 1999). However RYR is also characterized by an impaired activity (Terentyev et al., 2008). This effect is probably delivered by increased distance between the cisternae and the T-tubule in the dyadic space, leading to a decreased sensitivity to the Ca^{2+} released by
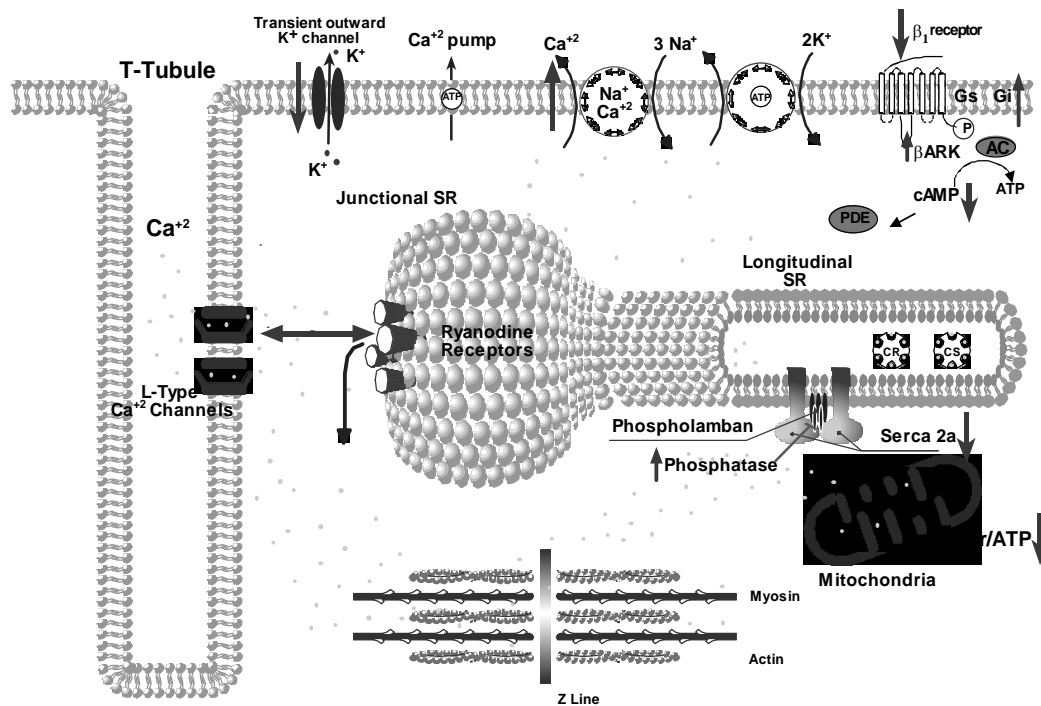
Figure 1.2. Principal modification in the Ca^{2+} handling in HF myocytes. HF cardiomyocytes show significant alteration of many proteins related to the regulation of the Ca^{2+} homeostasis. In particular the levels of Serca2a on the sarcoplasmic reticulum, β$_1$ receptor and K$^+$ channels on the sarcolemma appear decreased. Phospolamban phosphatase, β adrenergic receptor kinase (βARK) and the Na$^+$/Ca^{2+} exchanger are increased. Of note the dyadic space between the ryanodine receptor and the voltage-sensitive L-type channels is increased, leading to a decreased release of sarcoplasmatic Ca^{2+} following the arrival of action potentials. (From: del Monte, 2003)

the L-type channels during the depolarization of the membrane (Cannell et al., 2006). The decreased content in SERCA is further aggravated by the action of phospholamban (i.e., the inibitor of SERCA), which appear increased in HF (Kiss et al., 1995). The combination of these events lead to impaired Ca^{2+} handling characterized by progressive decrease of the ion content in the SR reticulum combined to increased levels in the cytosol. According to recent studies, these alterations can produce effects on the calcium sparks including increased duration and width of the event, leading to increased RYR activity (Lindner et al., 2002). However, the reduced levels of Ca^{2+} stored in the SR counterbalance this increase leading to a general impairment of the E-C coupling (Figure 1.3).
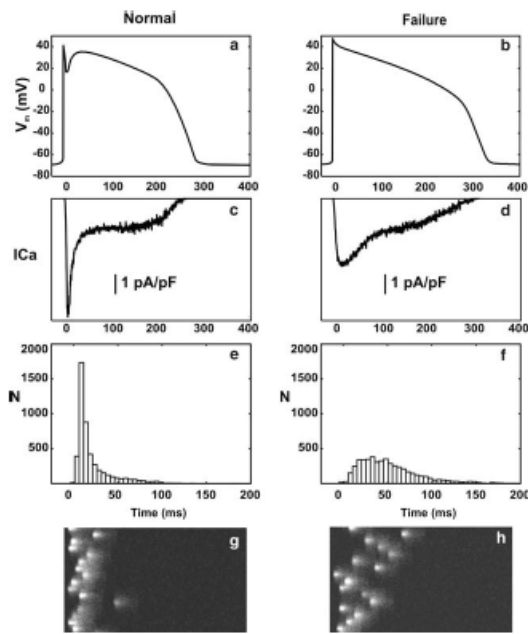
Figure 1.3. Calcium sparks non-failing (left) and failing (right) cardiomyocytes. Failing cardiomyocytes are characterized by altered depolarization of the cell membrane (a and b). This defect is related to altered Ca^{2+} current in the cells and, in particular, to decrease amplitude of the incoming current (c and d) mainly due to different temporal distribution of Ca^{2+} sparks (e,g and f,h). (From: Lindner, 2002)

Other molecular alterations in HF are related to the modification of proteins of the sarcolemma and, in particular, molecules involved in the ion transport system such as the channels Kv4.2 and Kv4.3 (Wickenden et al., 1998). The reduction of these channels is associated to defects in the repolarization of the membrane causing the prolongation of the action potential (Figure 1.4).
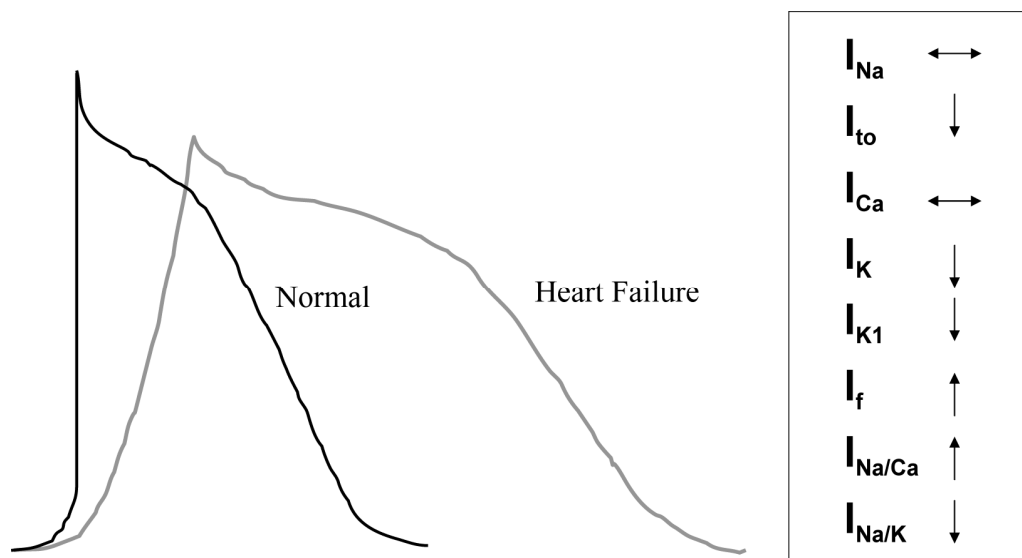
Figure 1.4. Schematic representation of the membrane depolarization in failing and non-failing cardiomyocytes and main ion current alterations.

1.1.2 Causes of Heart Failure

HF is caused by diseases or other factors that affect the cardiac function. The most common cause of HF is coronary artery disease (He et al., 2001). This disease is characterized by the progressive accumulation of atheromatous plaques within the coronary arteries producing a total or partial block of the blood supply to the cardiac muscle with deleterious effects on the cardiomyocyte metabolism in the affected region. Depending on the extension of the region affected, the myocardial infarction might have a lethal outcome or it might produce permanent damage to the myocardium, decreasing the efficiency of the heart in the long term.

Alternatively, in about 30% of cases, HF arises from recognizable etiologies including hibernating myocardium, hypertension, cardiac hypertrophy, myocarditis, congenital valvular defects (congenital or acquired), genetic and amyloidosis (Hare, 2004).

In the remaining cases HF develops without a recognizable cause and the heart function progressively deteriorates and is accompanied by morphological changes of the heart with dilatation of the chambers and altered geometry towards a more spherical shape. These cases are classified as idiopathic dilated cardiomyopathy (DCM) and will be discussed in detail in chapter 1.2.

1.1.3 Clinical Characteristics

The different forms of HF share similar signs and symptoms despite the diverse etiologies that might be involved. A physical exam of HF patients shows gaining of weight and presence of higher body temperature (<38° C) ascites, hepatomegalia, pale skin, diminished pulse, systemic venous hypertension, signs of increased adrenergic activity such as cyanosis of the digits due to vasoconstriction and, in the heart, cardiomegaly, systolic murmurs, pulse alternans and gallop sounds (Braunwald, 1996).
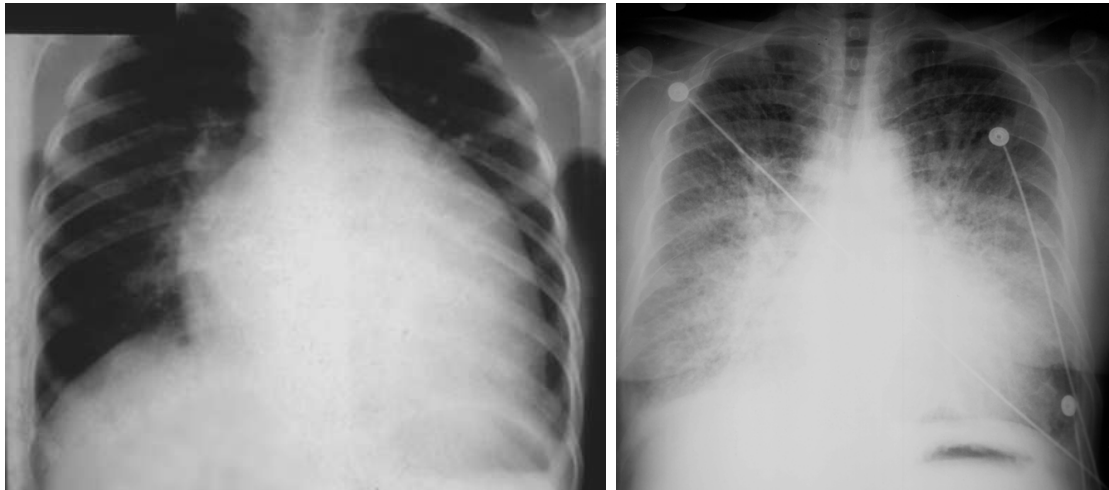
Figure 1.5. Chest X-ray of non-failing and failing subjects. HF patients (right) show evidence of pulmonary edema due to the increase of the lung capillary pressure. (From: Davies, 2000 (left panel), http://ehalth.gov.mt//impaedcard/issue/issue2/0310/031 (right panel))

HF patients present respiratory problems ranging from lung congestion to pulmonary edema that develop as a consequence of the increased pressure in the pulmonary veins. This abnormality produces an increase in pressure in the alveolar capillary circulation that supports fluid diffusion into the extracellular space. In physiological conditions the excess of extracellular fluid is removed via the lymphatic vessels. However, when the capacity of the lymphatic system is saturated, the fluid starts accumulating (Figure 1.5), with consequent impairment in the O_2-CO_2 exchange. The formation of edema in the lungs is therefore associated to dyspnea that exacerbates during the night's sleep: spending hours in horizontal position, in fact, induces the reabsorption of fluids in particular from the lower limbs, where they have been confined by gravity during the normal daily activities.

A second characteristic of HF consists in the occurrence of fatigue and weakness. In the past these symptoms were related to decreased perfusion of the skeletal muscles associated to the decreased cardiac output. However recent reports showed the presence of a more complex mechanism involving a myopathy condition related to the accumulation of lactic acid deriving from glycolysis. According to this theory, the inflammation process and, in the most severe cases, apoptosis have a considerable role in limiting the muscular activity (Katz, 1990).

In the most severe cases, HF can induce cerebral symptoms in addition to the anomalies previously mentioned (Heckman et al., 2007). Symptoms such as headache, confusion, memory impairment, delirium and disorientation can arise especially in patients affected by HF and showing the presence of cerebral arteriosclerosis plaques that further limit the blood flow in the central nervous system.

1.1.4 Progression of heart failure

HF is commonly described as a chronic disease that gradually tends to become worse, leading to serious impairment of the vital activities and, eventually, death.

It is generally agreed that cardiac cells lack significant proliferative capacity due to their terminally differentiated nature. In fact, only a limited pool of cells with proliferative capacity have been identified in specific areas of the heart (Messina et al., 2004, Urbanek et al., 2006), which, however are not sufficient to replace the defective fibers and restore the original architecture and function of the organ. Therefore, cardiomyocytes have evolved different solutions to contrast the decreased cardiac output.

A first group of responses is related to modifications of the geometry and structure of the organ to pump more blood and provide more pressure (Braunwald, 1996). In the first phases of heart failure the heart usually enlarges assuming either an eccentric or a concentric shape. The first is commonly associated with a faster degeneration of the organ function, while the latter provides a short-term improvement of the cardiac condition since it is associated to an increase in cardiomyocyte size and, therefore, to the increase of the contracting muscular mass of the ventricle. In the long term, though, the heart is not able to sustain the continuous hypertrophic stimulation and starts a maladaptive process involving muscle degeneration and weakening (Katz, 1990).

At a cellular level the progression of HF is normally associated with changes in the components of the extracellular matrix. During the first phases of HF there is an increased production of collagen III that enhances the elasticity of the tissue. When the condition becomes chronic the collagen III is replaced by collagen I, which is

characterized by a higher mechanical resistance. This response provide a stronger support for the contraction on one side but on the other the deposition of fibrotic material in the extracellular space can damage the cardiomyocytes or interfere with the conduction of the action potential (Weber et al., 1987, Chapman et al., 1990, Marijianowski et al., 1995).

Other molecular alterations that have been related to the progression of HF are instead related to the neurohormonal regulation system of the heart. In fact, several groups reported sensitive reduction of specific adrenergic receptors (β_1) in correlation with the severity of the disease (Engelhardt et al., 1996). This characteristic is usually associated with a general desensitization of the β-adrenergic cascade, which lead to attenuation of the stimulatory effects of the PKA signaling pathway (Ungerer et al., 1993).

Additional responses to HF are instead mediated by the circulatory system. In fact adequate pressure and perfusion of vital organs can be delivered by general vasoconstriction and by partially diverting the blood flow form less critical tissues (Braunwald, 1996). These mechanisms may produce beneficial effects in the short term; however their action in the long term is considered deleterious since they induce a continuous and progressively increasing need of correction by the adaptive mechanisms.

1.2 Dilated Cardiomyopathy

1.2.1 Definition

Dilated Cardiomyopathy (DCM) consists of a group of diseases of different etiologies, which can affect the function of one or both ventricles. Regardless of the cause, DCM is characterized by ventricular dilatation, contractile dysfunction and often symptoms of congestive HF. DCM can arise as a consequence of coronary artery disease, viral and bacterial infections, genetic mutations, excessive and chronic alcohol consumption, prolonged exposure to toxic substances and, in some cases,
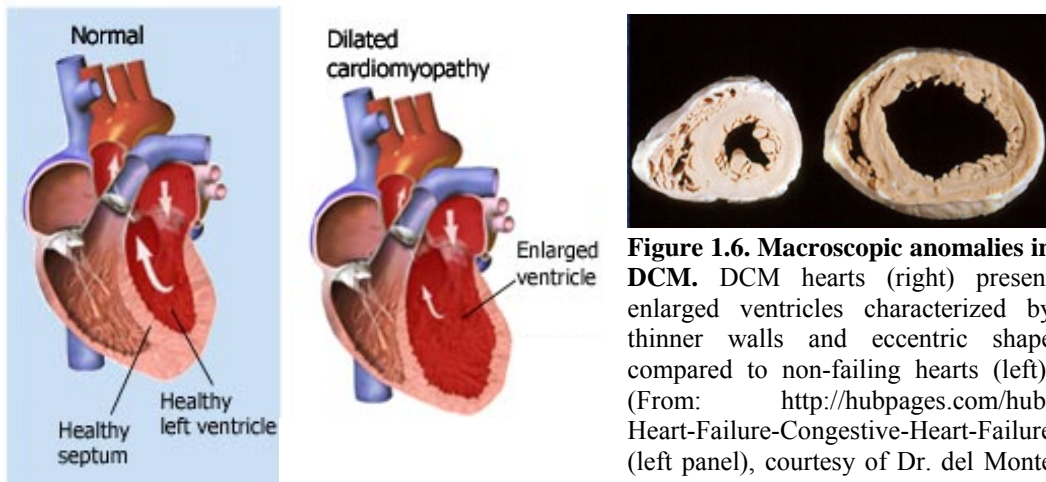
Figure 1.6. Macroscopic anomalies in DCM. DCM hearts (right) present enlarged ventricles characterized by thinner walls and eccentric shape compared to non-failing hearts (left). (From: http://hubpages.com/hub/ Heart-Failure-Congestive-Heart-Failure (left panel), courtesy of Dr. del Monte (right panel).

from pregnancy (Braunwald, 1996). In about 30% of the patients, though, the specific noxa cannot be identified. In these cases the condition is referred as idiopathic.

DCM generally becomes manifest with a gradual and eccentric dilatation of the left ventricle that becomes more spherical with consequent alteration of the hemodynamics properties (Figure 1.6) These characteristics are usually associated with anomalies of the walls that become thinner and lose stiffness. In some patients the walls may present increased thickness compared to normal individuals. However this form of hypertrophy is not proportional to the severe enlargement observed in the ventricular cavity (Vikstrom et al., 1998).

At the cellular level the major anomalies consists of the presence of large areas of interstitial and perivascular fibrosis, necrosis and, occasionally, cell infiltration. The cardiomyocytes appear in part hypertropic and in part atrophic (Figure 1.7) (Seidman and Seidman, 2001).

Molecular analysis of late stage DCM-affected hearts revealed abnormalities in
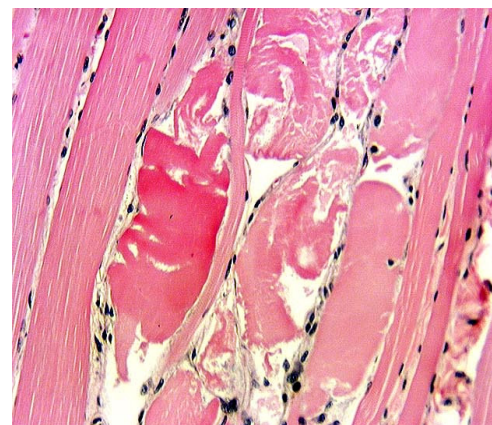
Figure 1.7. Histological anomalies in failing hearts. Failing hearts present large areas characterized by fiber disorganization, necrosis and deposition of fibrotic material.

Ca^{2+} handling and changes in the expression level and function of key regulatory proteins for excitation-contraction coupling (Davidoff and Gwathmey, 1994). More specifically, DCM is characterized by a deficient Ca^{2+} reuptake into the SR during relaxation that leads to a persistent high concentration of Ca^{2+} in the cytosol and to a progressive decrease of the Ca^{2+} stocks in the SR. This condition is further aggravated by the switch from the highly efficient fatty acid metabolism to glycolysis, that produce a decrease of the ATP produced in the cells and, therefore, to an impairment of the active transport of Ca^{2+} across the SR membrane operated by SERCA2a. In addition to the impairment of contractility, high levels of Ca^{2+} in the cytosol can produce activation of several critical pathways including apoptosis.

1.2.2 Genetic Causes of Dilated Cardiomyopathy

Genetic DCM is commonly inherited as a dominant autosomal trait, even if other forms of inheritance might occur (Karkkainen and Peuhkurinen, 2007). This condition is usually characterized by high mortality, late onset and incomplete penetrance; therefore in the past it has been remarkably difficult to obtain large families to identify candidate genes.

The known genetic mutations related to DCM are grouped in two major categories depending whether the failing condition is inherited in association with other disorders. Most of the mutations not having a phenotype limited to the heart are related to skeletal muscle diseases, but also associations to hematologic, skin or hearing disorders exist.

Familial DCM has been associated to different classes of genes by linkage analysis. These include genes codifying for cytoskeletal, sarcomeric, calcium handling and energetic-related proteins. A small portion including tafazin and EYA4 still has unknown biological function and, therefore, have not been classified in any of the categories mentioned above (Schonberger et al., 2005, Philipp et al., 2007) (Table 1.3).

Alterations of cytoskeletal molecules impair the capability of the cell to efficiently transfer the contractile force produced by the sarcomeres to the adjacent cells and to

Table 1.3. Gene involved in familiar forms of DCM

Gene	Symbol	Locus	Additional phenotype
Lamin A/C	LMNA	1p1-q21	Conduction disease, skeletal myopathy
Cardiac troponin T2	TNNT2	1q32	
Titin	TTN	2q31	Conduction disease
Desmin	DES	2q35	Skeletal myopathy
δ-Sarcoglycan	SGCD	5q33	Skeletal myopathy
Desmoplakin	DSP	6p23-q4	Wooly hair, keratoderma
Phospholamban	PLN	6q22.1	
Metavinculin	MVCL	10q22-q23	Mitral valve prolapse
Cypher	LDB3	10q22.3-q23.2	Left ventricular noncompaction
Cardiac myosin binding protein C	MYBPC3	11p11.2	
Cardiac muscle LIM protein	CLP	11p15.1	
ATP-sensitive K channel	ABCC9/SUR2	12p12.1	Arrhythmias
β myosin heavy chain	MYH7	14q12	
Cardiac actin	ACTC	15q14	
α-tropomyosin	TMP1	15q22	
Dystrophin	DMD	Xp21	Skeletal myopathy
Tafazzin	TAZ	Xq28	Skeletal myopathy
Eye absent homolopgus 4	EYA4	6q23-q24	Skeletal myopathy, sensrineural hearing loss
Teletonin	TCAP	17q12	Limb girdle muscular dystrophy
Cardiotrophin	CTF1	16p11	
Potassium inwardly-rectifying channel	KAPT	11q24	Arrhythmias
Unknown		2q14-q22	
Unknown		6q12-q16	
Unknown		9q13-q22	
Unknown		9q22-q31	
Unknown		19q13.2	Conduction disease

the extracellular matrix. This category includes proteins such as the cardiac muscle LIM protein (encoded by CLP), cipher (LBD3), δ-sarcoglycan (SGCD) desmoplakin (DSP), dystrophin (DMD), telethonin (TCAP), vinculin (VCL) and desmin (DES) (Norgett et al., 2000, Itoh-Satoh et al., 2002, Sylvius et al., 2003, Arimura et al., 2004, Chang and Potter, 2005, Shimizu et al., 2005). The later, in particular, seems to be related to the formation of intracellular amyloid bodies when mutated.

Other forms of genetic-inherited DCM are related to mutations of sarcomeric proteins. In particular mutations producing alterations of the Ca^{2+} sensitivity or of the mechanical properties of the sarcomere have been described in titin (TNN), cardiac actin (ACTC), tropomyosin (TPM1) and myosin heavy chain (MYH7) (Tesson et al., 2000, Daehmlow et al., 2002, Chang and Potter, 2005).

Genetic mitochondrial syndromes represent an additional cause of cardiomyopathy due to the high demand of energy related to the cardiac activity. This category of mutations have been described in genes encoding proteins such as SUR2a and KATP (Bienengraeber et al., 2004), i.e., two components of a K^+ channel that seems to be related to the susceptibility to Ca^{2+} overload.

A last category of DCM-related mutations includes the control of the calcium in the cytosol; in particular mutations in phospholamban (PLN) have been reported to be associated with a decreased sensitivity to β-adrenergic phosphorylating stimuli and, therefore, with a decrease control on the dissociation of PLN from SERCA2a, with consequent increased inhibition of the activity of the pump (Schmitt et al., 2003, DeWitt et al., 2006, Medin et al., 2007). However, the role of PLN in the etiology DCM is still under debate since recent contrasting reports have appeared suggesting the presence of a delicate equilibrium in the fine regulation of the reuptake of Ca^{2+} in the SR. In fact, on one side the ablation of the molecule activity mediated by negative dominant mutants such asK3E/R14E and V49A or by small interfering RNA has been shown to produce enhanced contractility and capacity of rescuing from the failing phenotype (He et al., 1999, Minamisawa et al., 1999, Suckau et al., 2009), while on the other mutations such as L39stop, R14del or R9C have been related to the development of DCM (Haghighi et al., 2003, Schmitt et al., 2003).

1.2.3 Clinical Characteristics of Dilated Cardiomyopathy

The clinical manifestations of dilated cardiomyopathy are generally related to the development of HF (Chapter 1.1.3)

In many cases DCM can develop for months or even years in an asymptomatic form, but when the left ventricular function becomes severely impaired the patients are affected by sense of fatigue, weakness and pulmonary congestion as observed in HF.

A physical examination of DCM patients usually reveals the presence of systemic embolism concentrated in particular in the legs and a diminished stroke volume that manifests as low systolic pressure and narrow pulse pressure. The auscultation of the heart shows gallop sounds often associated to systolic murmurs due to the regurgitation of the mitral valve and, in some cases, arrhythmias (Braunwald, 1996).

Echocardiography is considered the most reliable way to diagnose DCM currently available. In this exam the heart ventricle clearly shows spherical eccentric shape and thin walls (figure 1.8); according to Henry et al., DCM is diagnosed if the following criteria are met (Henry et al., 1980):

- Ejection fraction <45%;

- Fractional shortening <25%;

- Left ventricle end diastolic volume >112% compared to the average corrected for the age and body surface.

- Exclusion of different ethiologies (CAD, alcohol consumption, congenital defects, etc.)
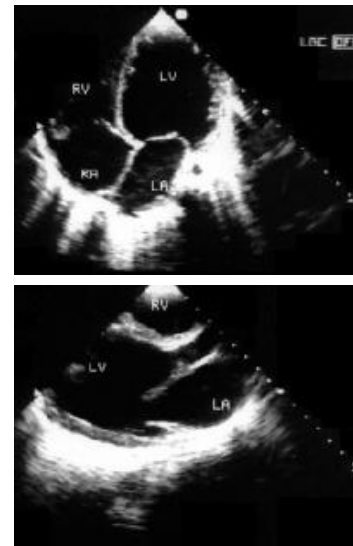
Figure 1.8. Anatomic anomalies of DCM by echocardiography. (From http://www.drmarcelonogueira. med.br/exames/EXAMES.htm

1.2.4 Progression

Dilated Cardiomyopathy is a chronic disease consisting of a progressive deterioration of the cardiac structure and function. The lethality of DCM is extremely high: about one third of the patients affected dies within 1 year from the diagnosis while the survival rate at 5years drops to 25% (Keogh et al., 1990). Surprisingly, the prognosis

and the mortality of DCM are not associated to the ventricular function, probably because of the different etiologies involved in the disease.

The only effective treatments currently available for DCM consist of the implantation of a left ventricle assisting device (temporarily) or in surgical transplant. The later, in particular, triples the survival rate at 5 years. However, cardiac transplant is an option not always available due to the difficulty of finding compatible donors.

1.2.5 Animal Models of Dilated Cardiomyopathy

The study of animal models represents an interesting opportunity for better understanding the molecular mechanisms associated with complex diseases and to test new potential therapeutic approaches. As mentioned above, DCM can develop in asymptomatic form for many years. Therefore the condition usually presents late stage features at the time of diagnosis. The high mortality rate within one year from diagnosis and the difficulties in obtaining patient consent further compromise the possibility of acquiring a significant number of samples for research purposes.

These problems can be partially solved by focusing part of the research on animal models. Many animal models for DCM have been identified in the past, including spontaneous and transgenic/induced.

DCM can arise spontaneously in some dog breeds such as Boxers, Doberman Pinschers and English Cocker Spaniels (Tidholm and Jonsson, 2005). Canine DCM can present two different histological phenotypes respectively characterized by fat infiltration in the myocardium or by the presence of wavy muscular fibers. This feature has been typically observed in humans as a consequence of ischemia and only occasionally of DCM. In some cases the canine form is characterized by the presence of both the histological characteristics.

However, the use of large animals is often considered ineffective due to the combination of high housing costs and the long time before the disease becomes manifest. These reasons increase the interest of investigators towards the development of models that are easier to study such as rodents. Many genetic murine models of

DCM are currently available. Most of them have been developed after identifying the homolog genetic defect in humans. In other instances, instead, the molecular defect has been first studied in the mouse and then confirmed in patients (e.g., desmin, δ-sarcoglycan, LIM). However, no clear correlations between murine and human defects have been yet reported for some mutations (Ross, 2002).

Somatic gene transfer represents a valid alternative to obtain the expression of a certain gene/mutation in the heart when transgenic or knockout mice for a specific protein are not available. The most efficient method currently available for the in vivo transfer is the use of viral vectors such as adonoviral, adeno-associated, lentiviral and, in general, viral vectors with capacity of infecting non-dividing cells as the cardiomyocytes (Lyon et al., 2008). Many different delivery routes have been tested in the past, including systemic or intramyocardial injection. However, the most efficient seems to be intracoronary injection. This procedure is based on the injection of the viral vector downstream to the aortic valve in conjunction with temporal occlusion of the ascending aorta tract. A permeabilizing agent such as adenosine is usually administered in combination with the virus in order to facilitate the diffusion of the viral particles from the capillary vessels (Wright et al., 2001).

A different approach for generating DCM models in rodents consists of increasing the afterload by creating a surgical constriction of the ascendant aortic tract. This process usually leads to the development of a compensating hypertrophy in the short term (about 3 months after the procedure) that progressively degenerates to dilated cardiomyopathy in about 6 months (Kleinman et al., 1978).

1.3 Heart Diseases and Protein Folding

In the last few years increasing interest has developed in the involvement of protein folding defects in cardiac diseases.
In particular, data obtained in Dr. Robbins' lab showed that mutations in genes encoding proteins such as desmin and Aβ-crystallin (CryAβ) have dementrial effects

on the cardiac activity. Desmin is a protein belonging to the intermediate filaments involved in the architecture of the cytoskeleton. Its role in muscular cells is related to forming a scaffold around the Z-disks in order to connect these structures with the sarcolemmal cytoskeleton and with the myofibrils (Bar et al., 2004). CryAβ, instead, is the most abundant small heat shock protein in the heart (Longoni et al., 1990). This molecule is focused on the maintenance of the integrity of the cytoskeleton by controlling the structural conformation of desmin (Wang et al., 2002, Wang et al., 2003). Although overexpression of desmin and/or CryAβ has not been related to any pathological phenotype, mutations in the coding sequences of these proteins have been associated with accumulation of insoluble electron-dense cytoplasmic deposits composed primarily by desmin and CryAβ, but also involving other cytoskeletal proteins such as tubulin, vimentin and dystrophin. These aggregates can lead to restrictive, hypertrophic or dilatative cardiomyopathies in the long term (Wang et al., 2002). In particular, the substitution of an arginine residue with a glycine in position 120 of CryAβ seems to produce a dominant autosomal syndrome characterized by evidences of HF and, eventually, premature death in transgenic mice. As confirmation, the abrogation of the expression of CryAβ^{R120G} decreases the content of desmin aggregates and improves the viability of the animals (Sanbe et al., 2005). Additional studies also showed that these transgenic mice as well as other models of desmin-related myopathies are characterized by alterations of the unfolded protein response and of the ubiquitin-mediated protein degradation (Chen et al., 2005, Liu et al., 2006).

Similar anomalies were also observed in some familiar forms of hyperthrophic cardiomyopathy (FHCM): recent reports showed that some of the FHCM-related cardiac myosin binding protein-C (MYBP-c3) mutations induce preferential degradation of the aberrant protein by the proteasome (Sarikas et al., 2005, Bahrudin et al., 2008, van Dijk et al., 2009). This process seems associated with changes in the conformational state of the protein. In fact Bahrudin et al showed that the preference of the proteasome for the mutated protein can be drastically altered only when a single amino acid located in a critical region is replaced with another with significantly

different chemical properties (Bahrudin et al., 2008). According to the author the whole process leads to saturation of the proteasome system with the aberrant polypeptide and to consequent accumulation of all the other cellular proteins needing proteosomal degradation.

Interestingly, the hypothesis of the impaired proteosome activity has been validated in animal models of other cardiovascular diseases such as pressure-overload (Tsukamoto et al., 2006) and myocardial ischemia (Powell et al., 2005).

A detailed picture of the quality control of protein folding and of the toxicity deriving from the accumulation of aberrant proteins will be discussed in detail in the next section.

1.4 Protein folding

The structural and catalytic functions of proteins are performed by creating sophisticated three-dimensional structures in which specific chemical groups interact with each other and with the surrounding environment. Differently from nucleic acids (in which the biological function is solely depending on the nucleotide sequence), protein function is related to both their amino acidic sequence and their conformation. In fact, the specificity of a particular region in interacting with a particular molecule derives from the compatibility between the sterical structure and the chemical properties.

The process of folding is totally dependent on the thermodynamic properties of the polypeptidic chains involved with no participation of kinetics (Govindarajan and Goldstein, 1998). The final (and active) three-dimensional structure of a protein, in fact, is solely related to the lower and most stable energy level possible for the polypeptide, which is generally reached when compatible groups are interacting with each other. For example, hydrophobic residue-enriched regions (i.e., mainly
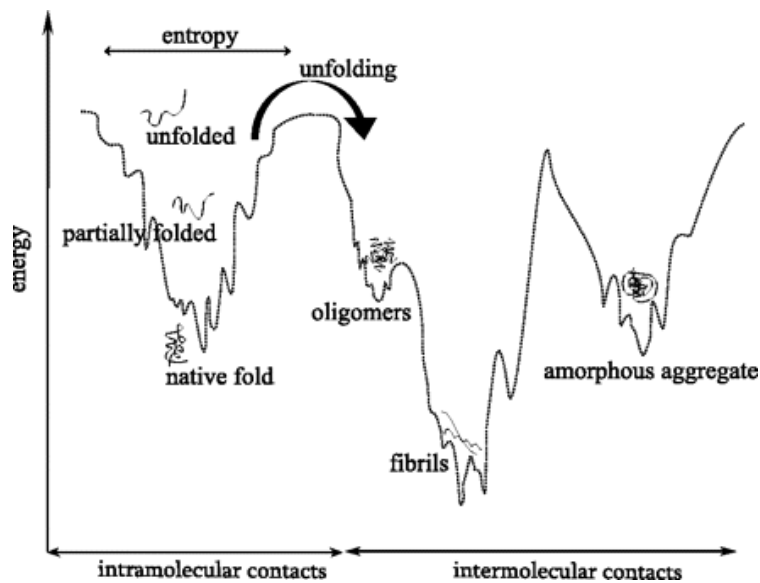
Figure 1.9. Landscape theory of protein folding. Different energetic conformation are available in proteins. The functional is usually characterized by the lower and most stable energy content. (From: Herczenik, 2008)

composed by aa such as leucine, valine, methionine and phenylalanine) have the tendency to fold inwards the centre of the protein to maximize their distance from the aqueous environment. Instead, charged residues and the amino and carboxyl unpaired groups at the two ends of the polypeptide chain are usually external and interacting with water. It has been calculated that for a 100 aa peptide the total number of energy states is in the 10^5 range, even if the total number of configuration patterns related to biological activity have been estimated to be 10^3-10^4 (Lehninger, 1993). Small proteins can usually assume independently their correct folding. Large polypeptides, instead, can fold during the translation process assuming intermediate structures that may be thermodynamically stable, although they do not represent the lowest energy state possible (Young et al., 2004). The recovery of the functional conformation normally requires an energy-consuming step to unfold the molecule. Therefore these states are called energy pits (Figure 1.9). In order to prevent dissipation of large amounts of ATP to resolve energy pits, eukaryotic cells and prokaryotic organisms have developed a class of proteins responsible for the control of the protein folding called chaperones. Chaperones are defined as "a family of unrelated classes of proteins that mediates the correct assembly of other polypeptides, but are not themselves components of the final functional structure" (Ellis and van der Vies, 1991).

Figure 1.10. Chaperones and chaperonins. Chaperones (Hsp70) have an important role in stabilizing the nascent peptides inhibiting the formation of three-dimensional incorrect conformations. Chaperonins (TCiP), instead, promote the folding of the protein by isolating the unfolded peptide in their lumen. Both chaperone and chaperonins activities are ATP-dependent. (From: Lodish, Cell biology, 4th Ed.)
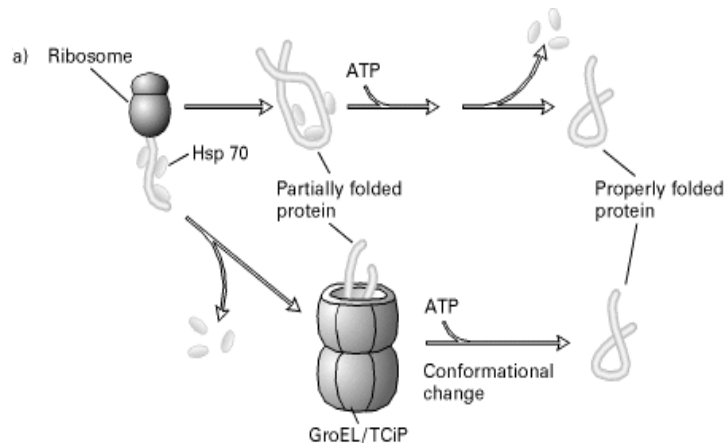
These proteins are grouped into two families respectively called molecular chaperones and chaperonins and related to two different functions. Chaperonins are directly involved in folding polypeptide chains; instead molecular chaperones seem to be related to the stabilization of the high energy intermediates of nascent proteins and to the prevention of energy pits (Figure 1.10)(Horwich et al., 2007).

Chaperonins are structurally characterized by the presence of two identical monomers forming a barrel-like structure (Carrascosa et al., 2001, Young et al., 2004). This can accommodate the unfolded protein in the lumen and promote the correct folding by isolating the protein from the external environment. The energy required for this process is delivered by the hydrolysis of a molecule of ATP. Examples of chaperonins are heat shock protein (Hsp) 60 in eukaryotes and GroEL in the prokaryotes (Figure 1.11).

Molecular chaperones are instead mostly represented by the Hsp70 family. These
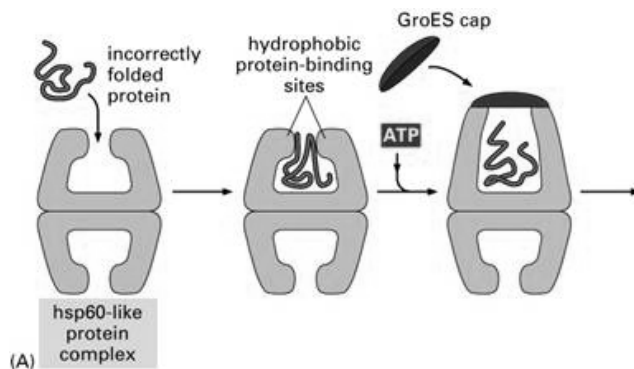
Figure 1.11. GroES/HSP60-mediated folding. Incorrectly folded proteins are isolated from the cytosol and refolded in the lumen of the chaperon. The dissolution of the incorrect folding requires energy that is provided by ATP hydrolysis. (From: Alberts, Molecular biology of the cell, 4th Ed.)

proteins are characterized by the presence of hydrophobic regions which are exposed following the hydrolysis of ATP into ADP+P_i. These regions bind unfolded peptides at high specificity and promote folding into their functional state. The correctly folded peptides are then released following a structural re-arrangement of the chaperone caused by the substitution of ADP with ATP (Saibil, 2008).

A third group of chaperone proteins has been identified in relationship to the control of the architecture of the cytoskeleton rather than of the folding process. These peptides include α-B crystallin and Hsp27, which respectively stabilize the actin-desmin interaction and the aggregation of filaments of actin (Dillmann, 1999).

Chaperones have an important role in determining the kinetics of the reaction besides adjuvating the folding of proteins into the most thermodynamically favorable energy state: if the folding process were merely associated to a combinatorial event, the correct folding for a 100 aa protein would require up to several hours. Instead in the cells chaperones reduce the duration of this process to micro- or milliseconds (Lehninger, 1993).

Chaperones are highly conserved proteins that are largely distributed throughout the entire cell and its organelles. Their activity is highly important in several physiological processes (Ellis and van der Vies, 1991) such as:

1. Protein synthesis: during the elongation of the polypeptidic chain, the free amino-terminal region can fold in non-efficient structures.

2. Protein transport between cellular compartments: the protein involved in the biochemical and structural functions in the organelles (with the exception of few peptides that are locally produced in the mitochondria) are produced in the cytosol and then transported through the lipid membrane of the organelles. The translocation of the protein is usually achieved if the protein has a linear structure. After the transport, the protein requires the presence of local chaperons to re-estabilish the correct folding structures.

3. Stress response: extreme variations in pH, temperature, ion concentration or the presence of free radicals produce conditions that can irreversibly alter the conformation of the proteins.

4. Protein-protein interaction. During normal physiological reactions, some oligomeric complexes change their structure and transiently expose some domains normally involved in protein-protein interaction.

In some cases the correct folding for particular proteins is achieved through the interaction of different chaperones and co-chaperones. In particular the activity of Hsp70 is usually performed in combination with a different chaperone called Hsp90 (Figure 1.12) (Young et al., 2001, Pearl and Prodromou, 2006). Hsp90 is a homodimer in which each subunit is characterized by an ATP-binding site on the
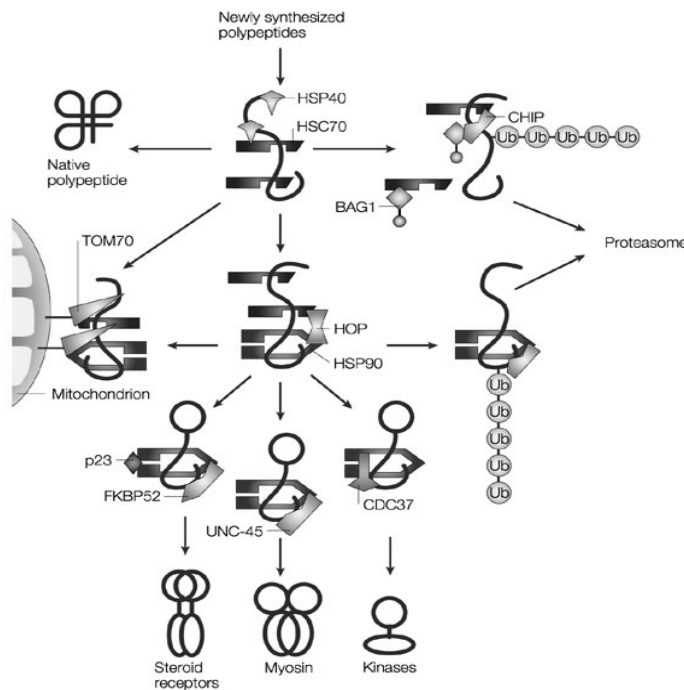
Figure 1.12. Chaperonins-mediated folding of nascent proteins. Newly synthesized polypeptides are bound by the 70-kDa heat-shock cognate protein (HSC70), which works together with its 40-kDa heat-shock protein (HSP40 or HDJ1) or HDJ2 cofactor. Some polypeptides fold with the assistance of HSC70, whereas others are passed to the 90-kDa heat-shock protein (HSP90). The tetratricopeptide repeat (TPR)-clamp co-chaperone Hsp-organizing protein (HOP) organizes the transfer of animal steroid-receptor proteins from HSC70 onto HSP90 and might function similarly for other substrate polypeptides. Other TPR-clamp co-chaperones (shaded pink) help HSC70 and HSP90 in various functions. The immunophilin 52-kDa FK506-binding protein (FKBP52) functions in HSP90-dependent steroid-receptor folding, together with the HSP90 co-chaperone p23. UNC-45 functions with HSP90 in myosin folding. CDC37 is unrelated to the TPR-clamp cofactors and works with HSP90 in the folding of certain kinases. TPR-clamp interactions also recruit HSC70 and HSP90 for protein sorting. Some mitochondrial precursor proteins are delivered by HSC70 and HSP90 to the import receptor 70-kDa translocase of the outer mitochondrial membrane (TOM70) for import into the organelle. The U-box ubiquitin-ligase CHIP (carboxyl terminus of HSC70-interacting protein) contacts HSC70 or HSP90 to attach polyubiquitin onto substrate polypeptides, which results in these substrates being targeted to the proteasome for degradation. Finally, the HSC70-regulatory co-chaperone BCL2-associated athanogene-1 (BAG1) can assist in targeting the HSC70-bound polyubiquitylated polypeptides to the proteasome. Ub, ubiquitin. (From: Young, 2004)

amino terminus. The presence of binding produces conformational rearrangements of the structure of Hsp90 that promote the retention of unfolded proteins and the conversion of their three-dimensional conformation. The mechanism involved in the activity of Hsp90 is not completely understood, but it seems to involve the co-participation of different co-chaperones such as HOP (that allows Hsp90 interaction in the Hsp70 machinery), p23, (that stabilizes the Hsp90 homodimer), and Hsp40 (that participates in the interaction between HSC70 and the unfolded protein).

The activity of the Hsp70-90 complex can be modulated by interaction with several co-chaperones. For example, mitochondrial proteins are relocated into the mitochondria by the cytosolic Hsp70-90 complex only when linked to TOM70, i.e., a protein located on the external membrane of the organelle acting as an import receptor (Young et al., 2004).

In other cases the Hsp70-90 complex is involved in the degradation of the unfolded protein by promoting its ubiquitination and the consequent proteolysis in the proteasome. The co-chaperones involved in this activity are CHIP and BAG1 (Hohfeld and Jentsch, 1997, Connell et al., 2001).

1.4.1 The endoplasmic reticulum: principal functions

The endoplasmic reticulum (ER) consists of an extensive network of tubules and cisternae, which is present in all the eukaryotic cells and extends throughout the cytosol forming a series of convolutions supported by the cytoskeleton (Wolfe, 1993). The main role of ER consists in the production and post translational modification of protein for the ER itself, the cytosolic membrane, the cytoplasmic organelles (including the Golgi apparatus, lysosomes, endosomes, secretory vesicles) and for secretion. It has been calculated that about one third of the total proteins produced in an average cell are processed in the ER. In order to undergo the post-translational modification and, ultimately, to perform their function, all the proteins entering the ER need to assume a correct three-dimensional conformation. This step is monitored by complex mechanisms of control. The most common process involves the action of a class of proteins called lectins, including calreticulin and calnexin (Ellgaard and

Helenius, 2003). These chaperones are specialized in folding glycosylated protein. Two distinct forms of glycosylation are available in the cell, *O*-glycosylation and N-glycosylation, even if only the latter is processed in the ER. During this process a preformed precursor oligosaccharide (composed of *N*-acetylglucosamine, mannose, and glucose and containing a total of 14 sugars) is transferred to the amide group of aspargine by the oligosaccharyl transferase. This enzyme is located on the internal side of the ER membrane and directly glycosylates peptides during the ribosomal synthesis and translocation through the membrane. This reaction is facilitated by a molecule of dolichol lipid anchoring the oligosaccharide in its activated form (i.e., linked through a high-energy phosphate bond) to the membrane in proximity of the oligosaccharyl transferase.

After N-glycosylation the polysaccharide chains are trimmed in different steps leading to complex glycosylation patterns. This step, in particular, seems to be related to the lectin-mediated control of the correct folding. Initially the precursor oligosaccharide terminates with three residues of glucose. During the maturation, these molecules are progressively removed. If the protein is not correctly folded, it is retained in the ER by calnexin and calreticulin and one molecule of glucose is added to the polysaccharide chain by the (UDP)-glucose:glycoprotein glucosyltransferase (UGGT). This procedure promotes a new folding attempt.

The lectin complex can perform its folding assistance activity only on glycosylated proteins. The folding of most of the other peptides in the ER, instead, is processed by by GRP78 and GRP94, respectively the analog of the cytoplasmatic Hsp70 and Hsp90 (Argon and Simen, 1999, Ni and Lee, 2007).

Different proteins including Grp170 and the co-chaperone ERdj3 seem to be involved in the formation of the Grp78-94 complex (Meunier et al., 2002, Ni and Lee, 2007). However the specific molecular mechanisms are still unclear.

A third folding pathway in the ER is associated to the activity of the small heat shock protein hsp47 and is specifically involved in the processing of procollagen (Hirayoshi et al., 1991, Natsume et al., 1994).

In many proteins the stability of the three-dimensional structure after folding is significantly increased by the oxidative environment of the ER lumen and by the action of protein disulfide isomerase (Weissman and Kim, 1993). This enzyme catalyzes the oxidation of the sulfhydryl groups present on cysteines and form strong covalent bonds between two non-adjacent residues.

All the processes described to this point involving the translocation and the folding of the proteins and are generally confined to the rough ER. The portion of the ER lacking ribosomes, instead, is called smooth ER and is specialized in different activities. The smooth ER is mainly related to the export of the mature proteins to their relative final location by a system based on vesicles. Moreover it is a critical location for production and exportation of membrane lipids such as phospholipids, cholesterol and ceramide (Wolfe, 1993).

In particular cell types the smooth endoplasmic reticulum acquires specific functions related to the activity of the cell. For example, organs that produces large amounts of steroid hormones such as the testis and ovaries are characterized by a significantly extended ER network. In hepatocytes, instead, the ER has a major role in producing proteins secreted in the blood. In addition the ER of hepatocytes is specialized in the metabolism of lipids, including the detoxification of potentially harmful lipophilic molecules through the cytochrome P450 pathway.

Myocytes, instead, contain a specialized form of endoplasmic reticulum called sarcoplasmic reticulum (SR). The SR is the most important Ca^{2+} storage in the cell. When a contraction signal reaches the cell, the SR is triggered to release large amounts of the ion into the cytosol. This allows the interaction of the actin and myosin fibers and, consequently the contraction.

It is interesting to observe that most of the chaperones operating in the ER are sensitive to oscillations of the Ca^{2+} concentration. In normal conditions the total concentration of Ca^{2+} in the myocyte SR is in the mM range, but it can change significantly during the contraction/relaxation cycles. In order to maintain the Ca^{2+} concentration always at a level compatible with the correct function of the proteins in

the lumen, the calcium cycling activity and the post-transaltional modification machinery are located in different regions of the SR (Papp et al., 2003). In addition the SR evolved molecular buffers such as calsequestrin, which bind the cation and keeps the level of free Ca^{2+} constant.

1.4.2 Response to the accumulation of unfolded peptides

In normal conditions about one third of the protein translocated into the ER cannot acquire a correct folding. Therefore in an average cell large amounts of proteins are exposing domains normally not present on the protein surface. In some cases these domains may be able to unspecifically interact with functionally correct proteins, leading to interference to the normal activities of the cell.

For this reason, the control of the level of unfolded proteins is an issue of considerable importance. In the SR/ER this function is achieved through the combination of three different pathways activated by three different sensors/effectors: the activating transcription factor 6 (ATF6), the inositol-requiring enzyme 1 (IRE1) and the PRK-associated kinase (PERK) (Zhang and Kaufman, 2006). The events triggered by the activation of these three peptides are commonly referred to as unfolded protein response (UPR). The UPR consists is a series of modifications in different cellular compartment leading to alterations of the nuclear transcription, alteration of the protein synthesis, increased catabolism of the proteins and, when the excess of unfolded proteins cannot be resolved, to apoptosis (Zhao and Ackerman, 2006).

ATF6, IRE1 and PERK are transmembrane molecules located across the ER membrane. In absence of unfolded proteins, the luminal domains of these proteins bind Grp78, preventing the activation of the UPR (Figure 1.13). Several events can trigger the dissociation of Grp78 from the UPR molecular sensors, including large presence of newly synthesized peptides or the persistence of conditions inducing the denaturation of existing peptides (e.g., temperature increase, altered ion concentration). Grp78 binds the unfolded peptides immediately after the separation from IRE1, ATF6 and PERK, protecting the hydrophobic domains and inhibiting their
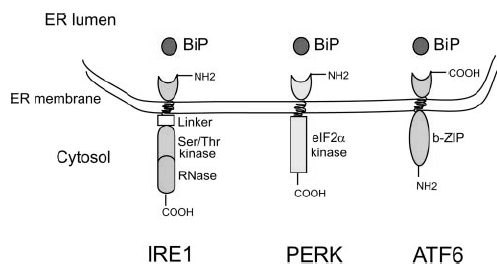
Figure 1.13. Sensor of ER stress: IRE1, PERK, ATF6. IRE1, PERK, ATF6 are transmembrane proteins located on the membrane of the endoplasmic reticulum. In absence of unfolded proteins these molecule are kept in inactive form by binding BiP/GRP78. (From Zhang, 2004)

export of the polypeptidic chains from the ER. This process leads to the homodimerization of IRE1 and PERK and their concomitant activation achieved by autophosphorylation. ATF6, instead, is translocated to the Golgi apparatus where it is processed into its active form.

The IRE1 pathway is the best characterized of the three, mainly because of several studies conducted on its yeast homolog, Ern1p (Zhang and Kaufman, 2006). The cytosolic domain of IRE1 is characterized by an intrinsic RNAse activity that is activated after the ER-stress induced-homodimerization and phosphorylation (Figure 1.14) (Shamu and Walter, 1996). The active molecule specifically recognizes the mRNA for XBP1 (HAC1 in yeast) and induces splicing of a 26 nucleotide-long internal sequence (Yoshida et al., 2001, Calfon et al., 2002, Back et al., 2005). This event produces a translational frame shift of the 3' region of the mRNA that leads to the production of the active XBP1 molecule. XBP1 has been characterized as a potent transcription factor acting at nuclear level. After the cytosolic synthesis, the molecule is translocated to the nucleus of the cell where it binds a sequence commonly found in the promoters of UPR activated genes and, in particular, of ER-specific chaperones such as calreticulin, GRP94 and Grp78. This sequence, called ERSE (endoplasmic reticulum stress response element), is characterized by a minimal core $(CCAAT(N_9)CCACG)$ that interacts with XBP1, allowing the assembly of the transcription apparatus (Yoshida et al., 1998).

Figure 1.14. Transcriptional regulation upon ER stress. Upon accumulation of unfolded protein in the ER lumen, BiP release from IRE1 permits dimerization to activate its kinase and RNase activities to initiate XBP1 mRNA splicing. Spliced XBP1 mRNA encodes a potent transcription factor that binds to UPRE or ERSE sequences in many UPR target genes. BiP release from ATF6 permits ATF6 transport to the Golgi compartment where full-length ATF6 (90kDa) is cleaved by S1P and S2P proteases to yield a cytosolic fragment (50kDa) that migrates to the nucleus to activate transcription of UPR responsive genes. U-Pr, unfolded protein. (From Zhang, 2006)
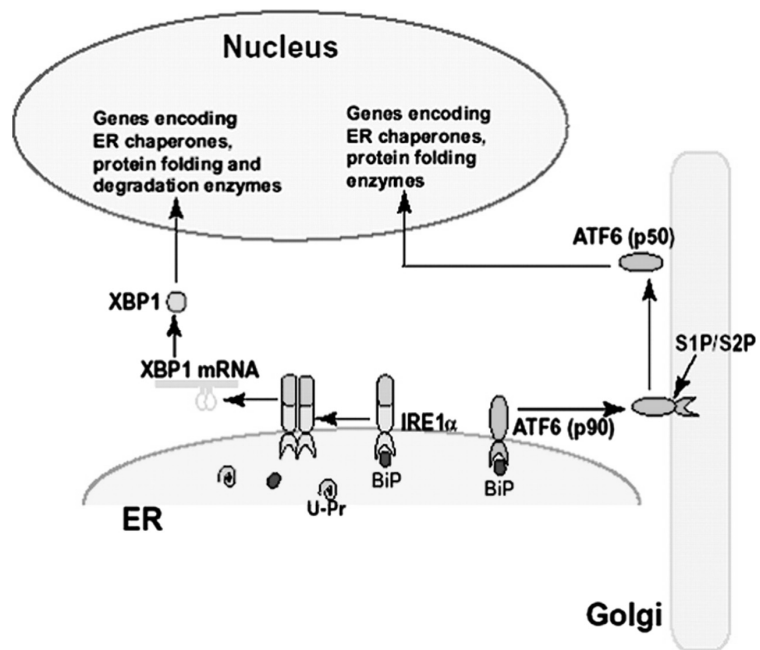
ERSE sequences represent a target also for ATF6 (Yoshida et al., 1998). ATF6 is normally present in the SR/ER membrane as a 90 kDa (ATF6α) or 110 kDa (ATF6β) inactive protein (Figure 1.14) (Haze et al., 1999). The dissociation of Grp78 allows the relocation of the molecule to the Golgi apparatus through vesicular trafficking, where it is cleaved by site-1 protease (S1P) and site-2 protease (S2P). This event induces the release of a 50 kDa cytosolic fragment that migrates to the nucleus, where it combines with the transcription factor NF-Y (Yoshida et al., 2000). This complex recognizes ERSE sequence in the genome, producing activation of genes encoding ER chaperones and other proteins related to the maturation and degradation of peptides. Of note, recent studies reported that in some cases the transcription of ATF6 is regulated by the activity of XBP1, and, indirectly, by IRE1 (Lee et al., 2003).

The activation of the IRE1 and ATF6-mediated responses requires the transcription and translation of new sets of proteins. It has been shown that the whole process may require up to one or two hours. PERK activity, instead, is mainly achieved through

modulation of the protein synthesis apparatus in the cytosol, producing effects within minutes (Kaufman, 2004).

The activation of PERK is achieved similarly to what observed in IRE1: after the dissociation of Grp78, two molecules of PERK combine forming a homodimer in which they activate each other by autophosphorylation (Figure 1.15) (Bertolotti et al., 2000). The cytosolic domain of active PERK interacts with the soluble protein elongation factor eIF2α, inducing its phosphorylation. In the non-phosphorylated form eIF2α is a key protein in the initiation of the translation process since it stabilizes the ribosome-tRNA^{met}-methionine interaction (Kaufman, 2004). The phosphorylation of eIF2α on Ser51 mediated by PERK produces a general destabilization of the protein synthesis apparatus, leading to a reduced protein production (Harding et al., 2000a, Harding et al., 2000b). However, a limited group of proteins can be translated efficiently in presence of phosphorylated eIF2α (P-eIF2α). These proteins are usually characterized by the presence of multiple 5' untranslated open reading frames (uORF) on the mRNA sequence. uORFs prevent the translation of the codifying ORF in normal conditions by inducing the release of the ribosome from the nucleic acid. In ER stress conditions, instead, the P-eIF2α promotes the activity of the ribosome on these ORF (Kaufman, 2004). An example of this complex regulation mechanism derives from the activating transcription factor 4 (ATF4) that is transported in the nucleus after translation (Harding et al., 2000b). Here it induces the transcription of genes involved in the amino acid metabolism and transport, oxidation-reduction reactions and ER-stress induced apoptosis (Harding et al., 2003).
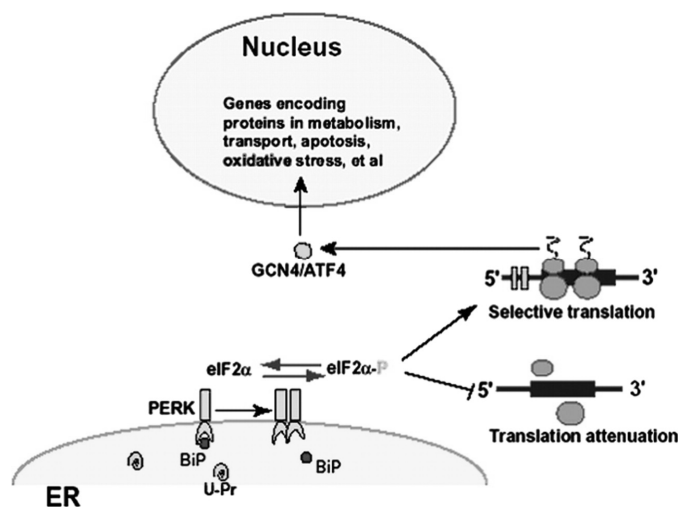
Figure 1.15. Translational regulation upon ER stress. Upon accumulation of unfolded protein in the ER lumen, PERK is released from BiP, thus permitting its dimerization and activation. Activated PERK phosphorylates eIF2 to reduce the frequency of the mRNA translation initiation in general. However, selective mRNAs, such as GCN4 or ATF4 mRNA, are preferentially translated in the presence of phosphorylated eIF2 . U-Pr, unfolded protein. (From Zhang, 2006)

56

A second mechanism included in the UPR consists in the activation of the catabolic pathway. This process is called ER-associated degradation (ERAD) and is mediated by several proteins expressed under the control of the IRE1-XBP1 pathway (Werner et al., 1996, Zhao and Ackerman, 2006). In particular the ERAD is generally triggered when continuous accumulation of unfolded and partially folded proteins is not balanced by a proportional increase of chaperones to stabilize their unfolded state.

Several mechanisms are involved in the recognition of the aberrant proteins to be degraded, including the recognition of exposed hydrophobic pathways, unpaired cysteines or immature glycan chains.

Immature glycoproteins are addressed to the ERAD by the α-mannosidase, which acts on the oligosaccaridic chains removing the terminal four sugars (Molinari et al., 2003, Oda et al., 2003) (Figure 1.16). This enzyme doesn't have specificity for unfolded proteins; in facts it interacts stochastically with any protein present in the ER (Wang and Hebert, 2003). Therefore the probability of a particular protein to be processed by α-mannosidase is directly proportional to the duration of its stay in the ER, which is usually prolonged in proteins incurring multiple folding attempts. After this step the protein binds calnexin and the endoplasmic reticulum degradation-enhancing 1,2 mannosidase-like protein (EDEM). This complex is then translocated across the
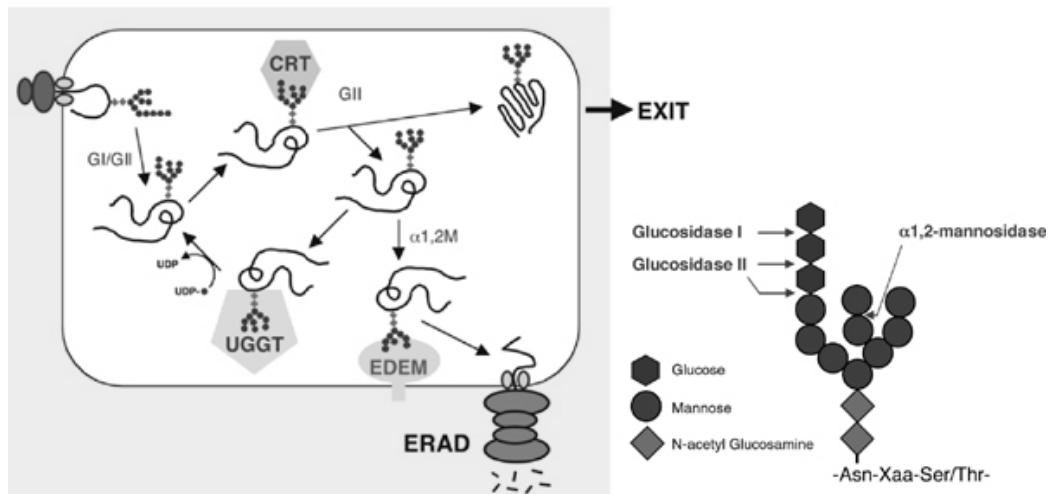
Figure 1.16. Mechanism of action of the calreticul/mannosidase on the control of the protein folding in the ER. Unfolded glycopeptides are kept in the ER by the calreticulin (CRT)/ glucose transferase (UGGT) system until they reach the correct conformation. In particular conditions, i.e. when all the glucose on the oligosaccharide chain are removed, the glycoprotein becomes substrate of the a-mannosidase. The removal of a molecule of mannose induce the binding of the peptide with EDEM and the export to the cytoplasm. (From: http://www.bijvoet-center.nl/cpc/ research/CNX)

membrane with a process that involves a channel –probably Sec61 operating in reverse (Sitia and Braakman, 2003) mode or derlin-1- with the co-participation of p97 ATPase (Ye et al., 2004) (which provides the energy necessary for the complete unfolding of the protein) and other proteins that prevent the backsliding of the polypeptide into the ER (UBX (Schuberth and Buchberger, 2005), Rad23p (van Laar et al., 2002) and Dsk2p (Medicherla et al., 2004)). The protein sequence entering the cytosol is immediately covalently linked to preformed chains of ubiquitin by the ubiquitin protein ligase E3 (Glickman and Ciechanover, 2002). The ubiquitinated polypeptide is then delivered to the cytosolic apparatus for protein degradation, i.e., the proteasome.

The proteasome is a large cytosolic complex (2 MDa) composed by two multimeric subunits, 19S and 20S, respectively involved in the regulation of the proteasome function and in the proteolytic activity (Voges et al., 1999) (Figure 1.17). The 20S complex is formed by 28 subunits encoded by 14 different genes and arranged in four axially stacked heptameric rings. The central lumen of the cylindrical structure of the 20S represents the active site and it is delimited by two copies of each of the proteolytic subunits (Groll and Huber, 2003) (β_1, β_2, β_5). All the substrates reach this region through two 13 Å pores located at both the ends of the barrel (Lowe et al., 1995). The activity of the 20S subunit is regulated by the presence of one or two 19S subunits that work as gates for the catalytic site (Goldberg, 2003). The 19S complex is
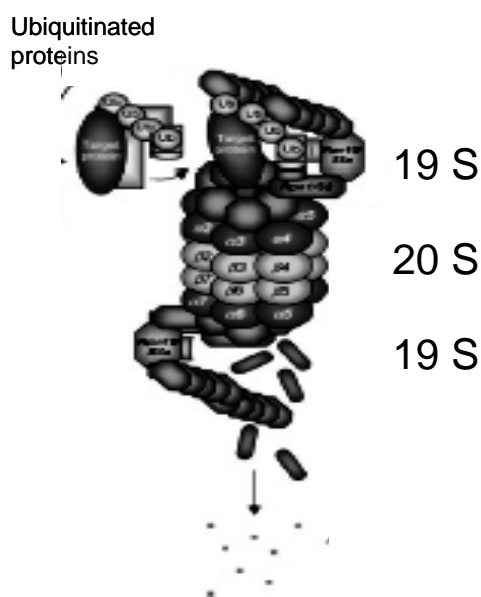
Figure 1.17. Proteasome-mediated degradation of ubiquitinated proteins. Ubiquitinated proteins interact with the 19S subunit of the proteasome inducing the opening of the lid of the complex and the linearization of the peptide. This allows the degradation of the protein in the 20S subunit lumen. (From Hermann, 2007)
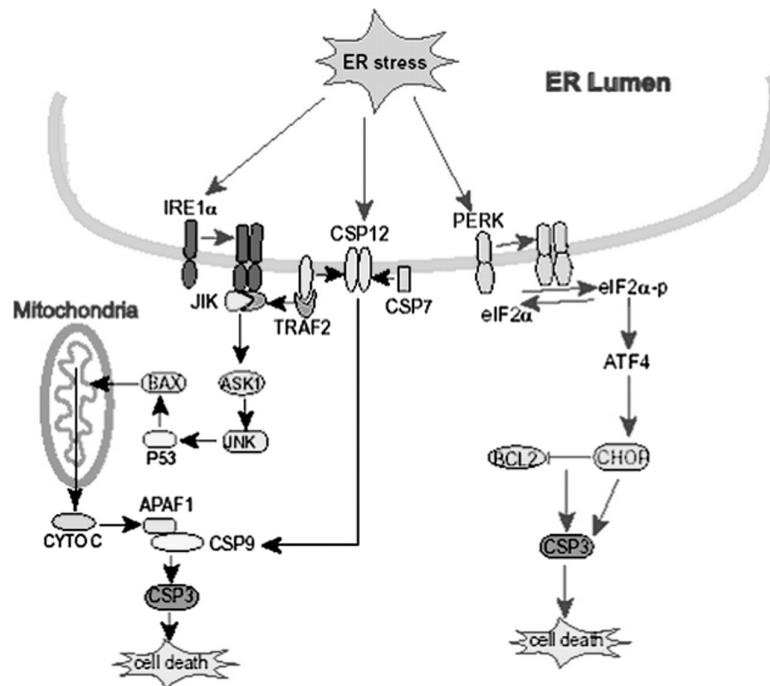
Figure 1.18. Apoptosis mediated by UPR signaling. Upon ER stress, activated IRE1 can recruit JIK and TRAF2 to activate ASK1 and JNK, leading to activation of mitochondria/Apaf1-dependent caspases. Upon activation of the UPR, c-Jun-N-terminal inhibitory kinase (JIK) release from procaspase-12 permits clustering and activation of procaspase-12. Caspase-12 activates procaspase-9 to activate procaspase-3, the executioner of cell death. Activated PERK phosphorylates eIF2 , that enhances translation of ATF4 mRNA. ATF4 induces transcription of the pro-apoptotic factor CHOP, that can inhibit expression of apoptotic suppressor BCL2. CSP, caspase; CYTO C, cytochrome C. (From: Zhang, 2006)

formed by 20 subunits responsible for different activities including binding the incoming protein, dissociating the ubiquitin chain, opening the catalytic core, dissolving the three-dimensional structure.

In some cases the combination of the control of the transcription and the ERAD-mediated proteolysis is insufficient to resolve the ER-stress induced by the overload of unfolded proteins (Zhao and Ackerman, 2006). Consequently the cell activates three different apoptotic pathways respectively initiated by IRE1, caspase 12 and PERK (Figure 1.18) (Nakagawa et al., 2000, Schroder and Kaufman, 2005, Xu et al., 2005). IRE1 can bind the c-Jun-N-terminal inhibitory kinases (JIK) upon dissociation form Grp78. This allows the recruitment of the cytosolic adapter TRAF2 to the

external side of the ER membrane. This molecule activates the apoptosis-signaling kinase 1 (ASK1) that induce the activation of the JNK protein kinase and of the mitochondria/APAf1-dependent caspase cascade (Nishitoh et al., 2002).

Caspase 12, instead, is present in the cell as a transmembrane protein of the ER that is activated directly by ER stress. Active caspase 12 induces activation of the cytosolic caspase 3 (i.e., the actual effector of the apoptotic process) by activating caspase 9 (Morishima et al., 2002).

The third apoptotic cascade induced by ER-stress is related to the action of ATF4, a transcription factor induced by the PERK/eIF2α pathway (Harding et al., 2000a, McCullough et al., 2001, Ma et al., 2002). ATF4 induces the transcription of CHOP, a strong proapoptotic transcription factor that opposes the antiapoptotic activity of Bcl2 by inhibiting its transcription (Maytin et al., 2001).

1.4.3 Amyloid aggregation and effects of the unfolded proteins on cell function

Unfolded proteins have a tendency to aggregate forming structures with different levels of complexity. Three main different models have been proposed to represent the mechanics of this process: the cross spine, the end to end and the domain swapping models (Bennett et al., 2006).

The end to end mechanism is characterized by the capacity of preserving the functional folding of the protein. The aggregates progressively form sequentially to the establishment of hydrogen bounds between the monomers. In general this event is triggered by a single point mutation that alters the properties of the surface of the protein. Typical examples of polypeptides aggregating following the end to end model include superoxide dismutase 1 (Elam et al., 2003), hemoglobin (Marenduzzo et al., 2006) and transthyretin (Correia et al., 2006), leading respectively to amyotrophic lateral sclerosis, sickle cell anemia and transthyretin-related amyloidosis.

Domain swapping has been mainly related to proteins characterized by two structurally different regions interacting with each other and separated by a random-

coiled loop. Domain swapping consists in the formation of aggregates deriving from the interaction of a domain with the complementary domain of an adjacent molecule of the same protein (Bennett et al., 2006). This process can be limited to two molecules swapping the domains to each other (close end domain swapping) or can involve a series of molecules forming a chain (open end domain swapping). The process is generally not related to any modification of the molecular interactions between the subunits of the protein and doesn't require any formation of new hydrogen bonds or hydrophobic interactions.

The cross spine model, instead, induces the formation of the highly ordered structure that aggregates forming macroscopical deposits called amyloid plaques. In this model adjacent β-sheets belonging to different polypeptidic chains are linked by intermolecular hydrogen bonds. Electron microscopy analysis of these structures revealed a long unbranched filament pattern with a diameter ranging from 65 to 130 Å (Sipe and Cohen, 2000). In addition X-ray crystallographic diffraction studies showed that the structure is characterized by the presence of 2 main reflection signals deriving respectively from the interstrand and the intersheet distances, respectively corresponding to about 4.8 Å and 10.7 Å (Stromer and Serpell, 2005) (Figure 1.19). Although the orientation of adjacent β-sheets (parallel vs. antiparallel) is still debated, the β-sheeted structure is recognized as a common feature of all the amyloidogenic
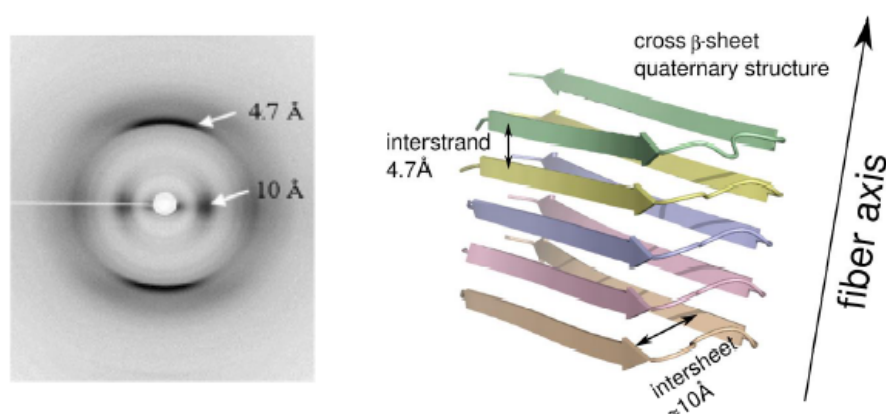
Figure 1.19. Xray diffraction and computer-based reconstruction of amyloid. Cristallography studies (a) shows the presence of different spots (4.7 and 10 A) respectively representing the interstrand and the intersheeet distances (b). (From: Fowler, 2007)

proteins despite of their primary sequence and their functional conformation.

From the molecular point of view, amyloid is composed by small oligomers (i.e., β-sheeted structures formed by a limited number of proteins) that progressively aggregate forming increasingly complex structure such as protofibers and amyloid fibers (Dobson, 2003). The aggregation seems to be a process related to the amino acid composition of the peptide, although no specific patterns have been yet identified.

The process of amyloid formation follows two different models depending on the kinetics and thermodynamics of the reaction. In thermodynamically unfavorable reactions the initial polymerization is characterized by a long lag phase during which a core of unfolded protein is built. After the formation of the nucleus, the polymerization occurs rapidly. This model is referred as nucleated polymerization. In other cases, instead, the aggregation in complexes is thermodynamically favorable and the formation of the complex follows linear kinetics. This second polymerization pathway seems to be the most common in cells, since the amyloid structure represents a significantly stable protein conformation.

Regardless of the kinetics of the reaction, the aggregation is characterized by a two step-model called docking-locking model (Esler et al., 2000, Dobson, 2003, Glabe and Kayed, 2006). The docking step consists of the aggregation in complexes of oligomers and protofibers. At this stage the transition from one state to another is regulated by a thermodynamic equilibrium, making the process reversible. The locking phase, instead, consists in the terminal and irreversible deposition of fibers that is sustained by the continuous production of the amyloidogenic protein (Figure 1.20).

The first report related to the deposition of filaments following the cross spine model was published in 1906, when Alois Alzheimer described the presence of deposits of unknown nature in the brain of patients affected by dementia. Afterward the presence of these deposits has been observed in different diseases including neurological disorders such as Parkinson and Creuzfelt-Jacobs disease and non neurological conditions such as systemic amyloidosis and diabetes (Zhao and Ackerman, 2006)
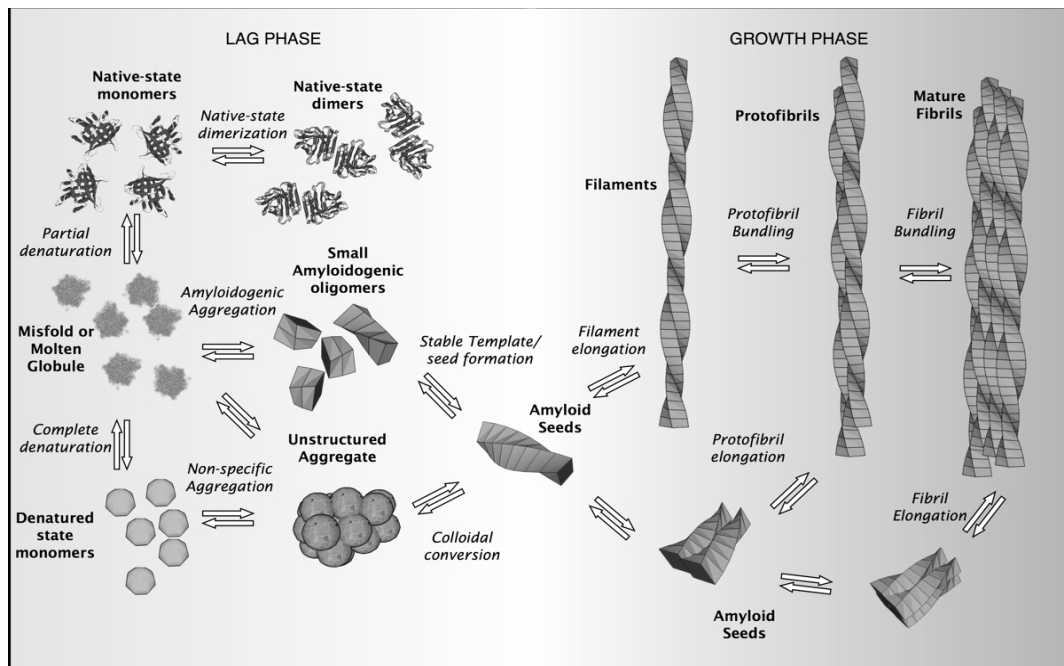
Figure 1.20. Different aggregation states of unfolded peptides. (From http://talaga.rutgers.edu/ research/images/Amyloid%20Mechanisms-2-tm.jpg)

(Table 1.4). In these diseases the deposits of amyloid are mainly composed by one protein.

As previously mentioned, protein function is a direct consequence of correct folding. Therefore, the accumulation of unfolded and misfolded protein in the cell can lead to a significantly diminished activity of the proteins involved in the deposits (Dobson, 2003). For example, cystic fibrosis is a severe disease resulting from the deletion of an aa in the polypeptidic sequence of a chloride channel located on the cell membrane. This mutation produces general instability in the three-dimensional conformation of the protein that leads to the retention of the immature peptide in the ER with consequent loss of the activity of the channel.

In other cases misfolded proteins gain toxic functions due to the acquisition of a three-dimensional structure favoring unwanted interaction with other proteins of the cell. Although this last aspect of the effects of amyloid has been widely studied, it is still debated which state of the amyloid aggregation process is producing damage to the cell (Glabe, 2008). In particular two major hypotheses have been formulated. Experimental data obtained from the study of Alzheimer's amyloid β (Aβ) show that

Table 1.4. Human diseases related to protein unfolding

Disease	Protein(s) involved
Cystic fibrosis	CFTR
Marfan Syndrome	Fibrillin
Nephrogenic Diabetes Insipidus	Amylin
Systemic Amyloidos	Light Ig chain, SAA, TTR, b2 microglobulin
Amyothrophic Lateral Sclerosis	SOD1
Alzheimers's Disease	Beta Amyloid
Creutzfeldt-Jacob Disease	PrP
Parkinson's Disease	a-Synuclein, Parkin
Marinesco-Sjogren syndrome	SIL1
Pelizaeus-Merzbacher disease	PLP1
Batten disease	PPT1
Huntington disease	huntintin
Bipolar disease	XBP1
Spinocerebellar ataxia	SCA3
Sporadic inclusion body myositis	APP
Wolcott-Rallison syndrome	PERK
Wolfram syndrome	WSF1
Hereditary tyrosinemia	FAH
Diabetes mellistus (type 2)	Amylin
Familial hypercholesterolemia	LDLR
Z α1-antitripsin deficiency	A1AT

the administration of exogenous Aβ fibers induces cell death and neuronal loss in vitro and in vivo (Yankner et al., 1989, Koh et al., 1990, Kowall et al., 1991, Reyes et al., 2004). Other reports, instead, showed that oligomers are the principal mediators of toxicity (Lashuel et al., 2002a, Lashuel et al., 2002b, Walsh et al., 2002, Caughey and Lansbury, 2003, Baglioni et al., 2006, Novitskaya et al., 2006).

The toxicity deriving from the accumulation of unfolded proteins seems to involve two different cellular pathways: Wnt and apoptosis.

Wnt signaling represents an important pathway in development, oncogenesis (Coombs et al., 2008) as well as in neurodegenerative disorders such as autism and schizophrenia (De Ferrari and Moon, 2006). The principal modulator of the Wnt pathway is GSK-3β (Chong et al., 2005) (Figure 1.21). This protein is regulated by the interaction of soluble extracellular Wnt with a membrane receptor called frizzled. The process induces the activation of the aberrant protein that inhibits the activity of GSK-3β and, eventually, promotes the increase of intracellular β-catenin. β-catenin
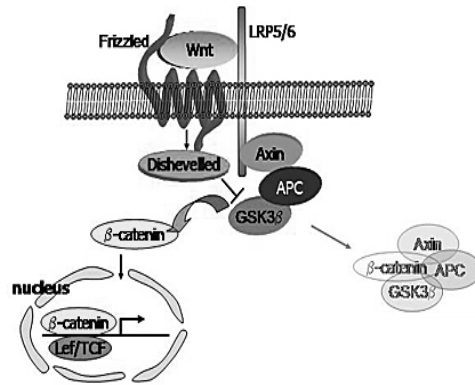
Figure 1.21. Wnt/GSK3b Pathway and activation of b-catenin induced genes.
The presence of aberrant proteins induces the release of β-catenin that translocate to the nucleus and modulates the transcription patterns by combining with other nuclear factors. In absence of aberrant proteins, β-catenin is phosphorylated by GSK-3β and transported to the proteasome for degradation. (From: http://www.anatomy.unimelb.e du.au/researchlabs/deIongh/proj ects.html

translocates to the nucleus where it combines with other nuclear factors to modify transcription. The activation of GSK-3β produces phosphorylation of β-catenin and its proteasome-mediated degradation. Several experiments showed that the administration of substances inhibiting GSK-3β such as lithium induced an increased resistance of cells to the effects of Aβ, suggesting that intracellular fiber aggregation produces effects related to the decrease of β-catenin (Hedgepeth et al., 1997, Inestrosa et al., 2005).
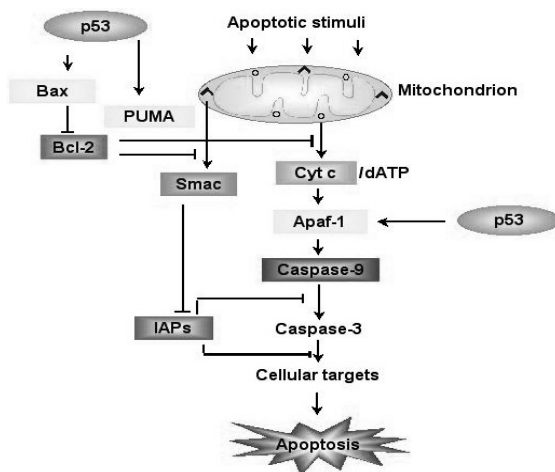
Figure 1.22. Apoptosis cascade following the activation of p53 by the interaction with amyloid structures. (From: http://www. weizmann.ac.il/home/ligivol/apoptosis_project/ap optotic_pathways.html)

The second pathway involved in the Aβ-mediated cell death is related to direct activation of the apoptotic pathway. Recent reports show that the administration of Aβ produces unbalance between the proapoptotic and antiapoptotic proteins interacting with p53 (Esposito et al., 2004) (Figure 1.22). In particular, cells exposed to Aβ present higher levels of bax and diminished bcl2, inducing activation of p53 and of the caspase-3 mediated apoptosis. This process

seems to be related to altered homeostasis of Ca^{2+} that is direct and immediate consequence of the administration of Aβ. Different hypotheses have been proposed to explain the correlation between Ca^{2+} dysregulation and Aβ. One of the most attractive theories suggests that Aβ fibers directly inserts within the cellular membranes, producing destabilization of the lipid layer, formation of cation conducing pores, activation of receptors and oxidative stress (Demuro et al., 2005).

Some studies also suggested a role for activation of the necrotic pathways following the presence of Aβ in the cells with consequent cytosolic vacuolization, Golgi apparatus disorganization and absence of DNA damage. However, the specific mechanisms involved in the Aβ-mediated necrosis are still unclear (Behl et al., 1994).

1.5 Systemic Amyloidosis

1.5.1 Definition

Amyloidosis consists of a group of pathologies characterized by deposition of protein material deriving from the aggregation of a specific protein. The polypeptide involved usually loses the functional folding and acquires a β-sheeted three-dimensional structure, which is associated with decreased solubility and with formation of 6.5-13 nm thick fibrils of indefinite length (Hirschfield, 2004).

The different forms of amyloidosis can be grouped in two main categories depending on the localization of the protein deposits: if the fibers are located in one specific organ, the amyloidosis is referred as localized. Instead if the fibers are transported in the blood and deposit in several organs, the amyloidosis is called systemic (Selkoe, 2003).

A second classification of the forms of amyloidosis is based on the molecular event that produces the fiber agglomeration (Buxbaum, 2004). According to this definition type I amyloidosis is related to the aggregation of a protein physiologically in equilibrium between amyloigenic and soluble form (Figure 1.23). This typically
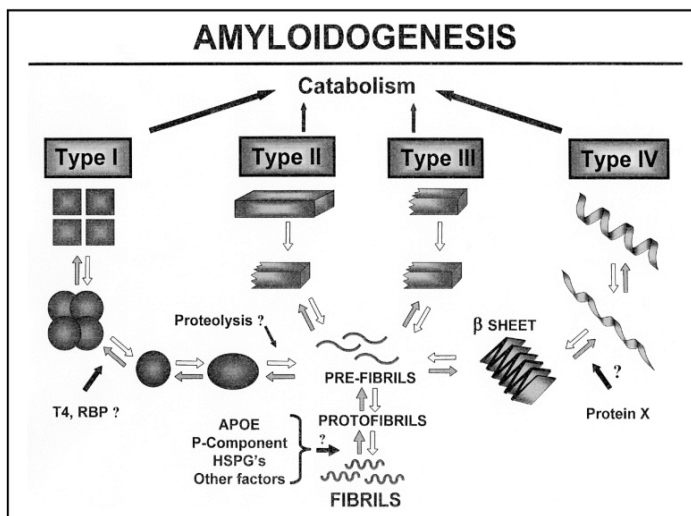
Figure 1.23. Classification of the different forms of amyloid based on the mechanisms of aggregation. Amyloid fibers can derive from different aggregation processes including aggregation of proteins in thermodynamic equilibrium between a functional and an amyloigenic form (type I), aggregation of fragments derived from proteolysis (type II) or degradation (type (III) or aggregation of proteins containing mutations (type IV). (From: Buxbaum, 2004)

occurs in transthyretin amyloidosis (Kelly et al., 1997). Type II and III amyloidosis are respectively due to incomplete digestion of a soluble precursor or to the formation of insoluble peptides from the physiological cleavage of a precursor. Instead, Type IV amyloidosis is essentially due to specific mutations that destabilize the functional folding of a protein (e.g., PrP in prion disease (Prusiner, 1998)).

The accumulation of a non-functional and non-compliant material in a metabolic active tissue or organ has been shown to be sufficient to induce a pathologic condition even in absence of an inflammatory response (Sousa et al., 2001). Although the specific cellular mechanism inducing toxicity has still to be elucidated, many studies reported the activation of the apoptotic pathway through the activation of NF-κB (Bales et al., 1998).

At the moment no effective therapies for systemic amyloidosis are available. However survival rate for these patients has been increasing in the last few years thanks to novel therapeutic approaches decreasing the production of the amyloidogenic peptide and to the recent advances in organ transplantation for the most severe cases.

1.5.2 Causes of amyloidosis

Amyolidosis can arise from different causes including genetic mutations, chronic infections (e.g., tuberculosis, osteomyelites), chronic inflammatory diseases, aging and presence of neoplasias such as multiple myeloma. At the moment, about 25 different amyloigenic peptides have been recognized. Of these, 12 can lead to the systemic form of the disease (Buxbaum, 2004).

The most common systemic amyloidosis is represented by the immunoglobulin light chain amyloidosis (AL). This condition is usually secondary to multiple myelomas or malignant lymphomas, in which the uncontrolled expansion of B lymphocyte clones results in the overproduction of light immunoglobulin chains (Hirschfield, 2004). These peptides are then secreted into the plasma where they aggregate in amyloid fibers and reach all the peripheral organs through the vascular system.

Amyloid A (AA) is another common form of amyloidosis especially in the developing countries, where the occurrence of untreated chronic infections is still high. AA is considered a type II amyloidosis since it caused by the deposition of protein fragments derived from the degradation of the serum amyloid A; during inflammation the degradation rate of this peptide fail to meet the actual need, leading to a progressive accumulation of toxic products (Buxbaum, 2004).

Transthyretin amyloidosis (ATTR) is instead a condition originating in the liver since this organ is the major producer of serum albumin. ATTR is usually not related to overexpression of transthyretin but it is associated to the presence of point mutations that induce structural modifications of the protein. TTR is normally secreted in the serum as a homotetramer (Saraiva, 2002). However the presence of just one molecule carrying amyloidogenic mutations produces structural changes affecting the whole quaternary structure of the protein and, eventually, the formation of amyloid deposits.

In addition TTR seems to participate in other forms of amyloidosis; in fact the amyloid senile deposits (which are commonly found in almost all the individuals over 80 years old especially in the atria, in the aorta and occasionally around the

vasculature of lung and other organs) contain large amount of this protein (Westermark et al., 2003).

1.5.3 Clinical characteristics of systemic amyloidosis

Amyloid deposits can occur in all the organs, even if the most commonly involved are kidneys, heart, gastrointestinal (GI) tract, peripheral nerves, and liver.

At a first examination, patients show peripheral edema as a result of heart and nephrotic failure, hepatomegalia and purpura, which derives from the accumulation of amyloid fibers in the subendothelium of the capillary leading to increased fragility of the vessels. For this reason bleeding is a frequent complication of amyloidosis. This is further aggravated in AL since light chains seem able to bind and inhibit the coagulation factor X (Enjeti et al., 2005).

As mentioned, the nervous system is a frequent target of the deposition of amyloid. This leads to weakness and sensorimotor peripheral neuropathy.

Occasionally systemic amyloidosis also manifests with localized aggregates of light chains in the skin, in the lungs, in the respiratory tract and in the urinary system.

1.5.4 Amyloidosis in the heart

The heart is one of the most sensitive targets for systemic amyloidosis (Figure 1.24). Amyloid infiltration in the cardiac tissue is initially clinically undetectable. However the progression of the deposition in the long term produces different non-specific effects including congestive heart failure, orthostatic hypotension, impaired conduction and restrictive cardiomyopathy, which is characterized by
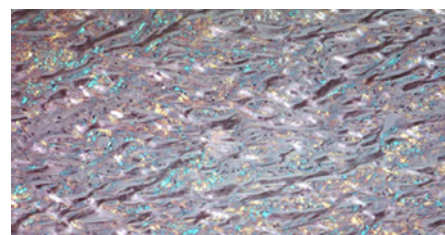
Figure 1.24. Congo red staining of amyloidosis myocardium in polarized light. Due to its capacity of binding β-sheeted structures, Congo red is used for diagnosis of amyloidosis, giving a green signal in polarized light.
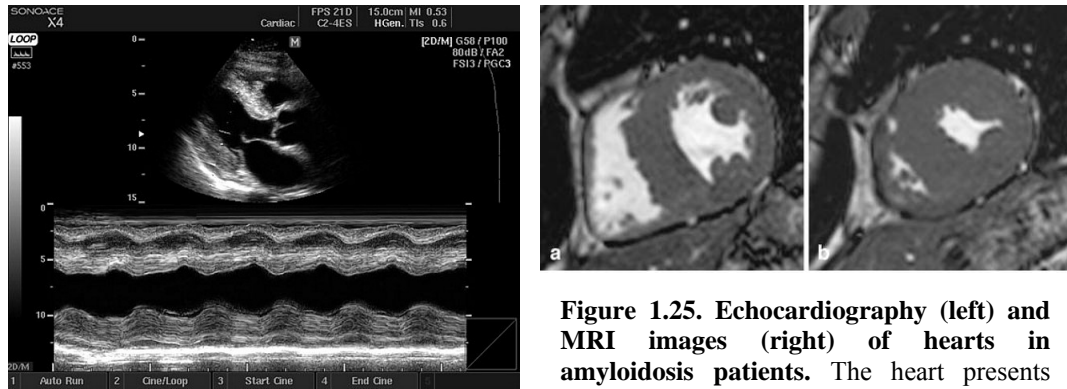
Figure 1.25. Echocardiography (left) and MRI images (right) of hearts in amyloidosis patients. The heart presents lower elasticity that leads to a limited ejection fraction as shown by the MMode in the echocardiogram and by the diastolic and systolic diameter of the chambers by MRI. (From: http://www.medison.ru/uzi/eho404.htm (left panel), Van Geluwe, 2006 (right)).

peripheral edema and stiffness of the myocardium leading to improper filling of the chambers. When the failing condition becomes symptomatic the average survival is usually no longer than one year, although improvements can derive from heart transplant (Van Geluwe et al., 2006).

Echocardiography and pathological observation of the amyloidosis-affected heart shows a mild atrial enlargement usually not associated by significant ventricular dilatation. An increased thickness of the walls is instead a common feature due to the interstitial amyloid deposition (Figure 1.25).

Occasionally some patients present deposits in the coronary arteries that can cause anginal symptoms similar to what is observed in coronary artery disease (Mesquita et al., 2005, Neben-Wittich et al., 2005).

1.6 Alzheimer's Disease

1.6.1 Definition

"*A. reports a case of illness, which was observed at the asylum in Frankfurt/Main and which was submitted for the examination of the central nervous system by director Sioli. The case has clinically presented such an aberrant picture, that it was impossible to classify it according to known diseases. It shows anatomically a picture, which differed from all other findings, known so far. […] She is temporally and locally completely disoriented. From time to time she says that she does not understand the whole matter, does not find her way. She greets the doctor as if he visits her and apologizes for not having finished her work, she shouted, he will slit her, or she turns him away, using phrases, which indicate that she thinks he could say something against her female honor. […] From time to time she is completely lunatic, carries her bedclothes around, cries for her husband and her daughter and seems to suffer from acousma. […] Her memory is extremely disordered. If you show her some objects, she names them correctly, but shortly after she has forgotten everything. […] Her gait is normal, she uses her hands equally. The patellar reflexes exist. The pupil reacts.[…] The autopsy reveals an atrophic brain without macroscopical focuses. The major brain vessels are arteriosclerotically modified. With the help of preparations, which are made by Bielschowsky's silver stain, very strange changes of neurofibrils appear. In the inside of a cell, which seems otherwise to be normal, one or more fibrils stand out due to their special thickness and their feature to impregnate. Further on, many parallel-running fibrils appear modified in the same way. Then they affiliate to close bundles [tangels] and appear gradually on the surface. Finally the nucleus and the cell itself break down, and only an unfurled bundle of fibrils shows the position, where a ganglion cell has lain before.[…]*"

With these words in 1906 Alois Alzheimer presented an unusual case of psychiatric illness and specific histomorphological alteration observed in the brain of a 51 year-

old woman, Augusta D. This is the first report regarding a neurodegenerative disease which was later classified as Alzheimer's disease (AD).

AD is a major cause of dementia in the Western countries, representing about 45% of the total amount of the diagnosed cases and affecting a total of about 700,000 individuals in the UK. In general AD has minimal incidence below the fifth decade, but it gradually increases with aging. AD cases can be classified as early (≤ 65 years old) or late onset (≥ 65 years old) depending on the age the patients show the first symptoms. The development of AD is usually a sporadic event, although most of the cases of early onset AD have been associated to Mendelian transmission of the disease (familiar AD or FAD, 5-10% of the total).

1.6.2 Clinical characteristics

The presence of plaques in the brain is a clear indication of AD. However it is pratically impossible to obtain a biopsy of brain tissue from living patients; therefore diagnosis of AD is usually performed on clinical observation aimed to the identification of behavioral and neurological profiles that can be associated with the neuropathy.

The most common sign correlating to early stage AD consists in a progressive decline of the mnemonic functions characterized by a tendency to forget name and events and to reveal personal preserved information. Over time, the patients also gradually show difficulties in learning deriving from short term memory impairment.

In addition, the patients present general alteration of different neurological functions including executive functions, language and visual-spatial abilities. These characteristics progressively degenerate to a severe form of dementia in which the patient has difficulties in naming objects, produces empty fluent speech and experience a relevant spatial disorientation.

AD usually develops with a long course that can range between years and decades. However, the disease becomes clinically manifest only when the brain presents severe and irreversible damages. This characteristic produced increasing efforts in the possibility of diagnosing AD at very early stages. In particular, imaging technologies

have been very useful in developing new diagnostic tools. For example a common alteration in the brain of AD patients consists in significant focal atrophy of the medial temporal lobe structures. This anomaly can be observed by MRI in preclinical stages of the disease (Figure 1.26a). Further alterations are associated to a bilateral hypoperfusion of the nervous system especially localized in the temporal and parietal lobes and, occasionally, in the frontal lobes, which can be detected by single photon emission computed tomography (Figure 1.26b).
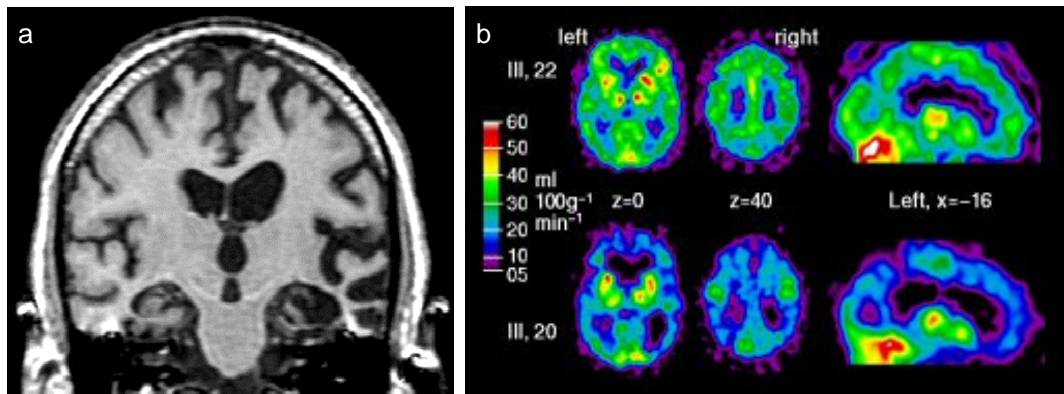
Figure 1.26. In vivo imaging of AD. Panel a shows the MRI scan of a suspected AD case characterized by unilateral tempoparietal atrophy. Panel b, instead, shows the activity of different cerebral area detected by sPET in a normal (up) and a diseased brain (down). (From: http://www.radgray.com/mri-articles/alzheimer-disease (left))

1.6.3 Pathological characteristics

AD brains show evidence of diffuse neuronal degeneration in specific regions of the brain during post mortem analysis. In particular, hippocampus and temporal cortex generally present marked cytostructural alteration even at early stages of the disease. These regions are characterized by proteinaceus plaques that progressively induce atrophy and that gradually deposit in the surrounding areas of the brain. In the long term this results in marked degeneration of the tempo-parietal cortex combined to decreased cholinergic projections to the frontal cortex, to the hippocampus and to the amigdala (DeKosky et al., 1985, Zubenko et al., 1989).

From the histological point of view AD is characterized by formation of plaques and tangles in the cortical areas associated to a progressive loss of cortical neurons. At the
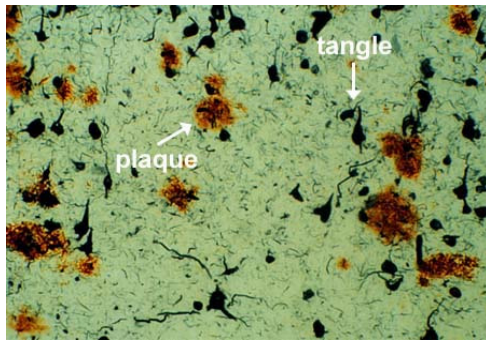
Figure 1.27. Silver staining of AD brain sample. Post-mortem analysis of AD brain tissue by silver staining shows the presence of extracellular plaques and intracellular tangles. (From: www.ladulab.anat.uic.edu)

moment, post mortem histological analysis represents the only available method for a precise diagnosis of the disease (Figure 1.27).

Senile plaques consist of 20-200 μm extracellular deposition of amyloid material. The neurons surrounding these aggregates are usually characterized by alteration of their typical shape, although it is still not clear whether they maintain normal activity (Rogers et al., 1996).

The senile plaque core is composed by fibers of Aβ, i.e., a 40-42 aa long peptide deriving from the posttranslational cleavage of the amyloid precursor protein (APP). Aβ aggregates can be divided in two major groups, classic and diffuse, depending on the presence of neuronal degeneration in the surrounding area. In addition, senile plaques are usually present in combination with an inflammatory response mediated by the microglia. (Figure 1.28)

Tangles, instead, consist of intracellular agglomerates of filaments. These deposits are mainly localized in the cytoplasm and around the nucleus of the neuron, although occasionally they diffuse into the dendrites (Figure 1.29). Ultrastructural evaluation of the tangles revealed a double helix structure with a diameter of 20-24 nm. Each helix
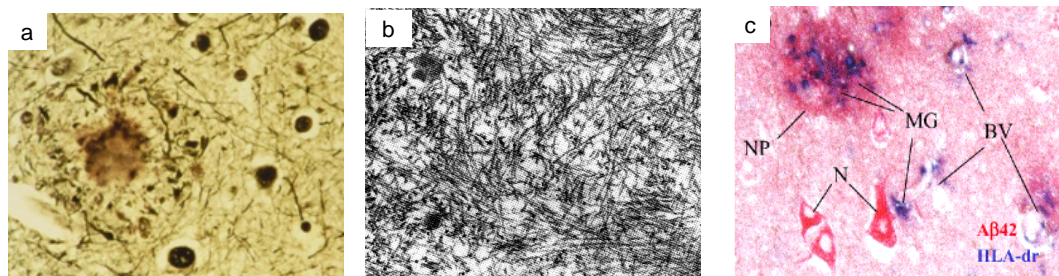
Figure 1.28. Amyloid plaques in AD brain. Panel a shows a high magnification image of an amyloid plaque detected by silver stain. Panel b illustrates the structure of the amyloid fibers by electron microscopy. Panel c, instead, shows the presence of microglial cells on the border of the plaques and of neurons (MG in blue). (From: Nagele, 2003)

is formed by 4-8 protofilaments of tau, a 55 kDa cytoskeletal protein highly expressed in the brain. This protein is normally related to the assembly of the microtubules of the cell. However it can form insoluble intracellular deposits especially in the hippocampal and in the cortical neurons when hyperphosphorylated,

1.6.4 Proteins involved

Amyloid precursor protein (APP)

APP is a single pass transmembrane glycoprotein with a molecular weight of 110-130 kDa. This protein is encoded by a large gene (over 170 kBp) mapping on chromosome 21q21 (Korenberg et al., 1989); the gene contains 19 exons that can be alternatively spliced to give three main isoforms. APP_{695} is the shortest isoform and is created by assembling exons 1-6 and 9-18 with the exclusion of 13a. APP_{751} and APP_{770}, instead, contain a serine protease inhibitor domain called serpin domain and encoded in exon 7. These two isoforms are respectively obtained by the combination of exons 1-7+9-18 without 13a and 1-18 without 13a (Tanaka et al., 1988). Expression of APP has been detected in a broad number of tissues, even if the brain shows the most abundant levels (Tanzi et al., 1988). In particular APP_{695} is mainly present in neurons while APP_{751} and APP_{770} are more expressed in glial cells.

The biological function of APP is still unknown although different theories have been formulated including a potential role in cell adhesion and in neuroprotection (Priller et al., 2006). According to some hypotheses APP present a domain resembling the serin-protease inhibitor. This region may be involved in the inhibition of the coagulation pathway by specifically blocking the activity
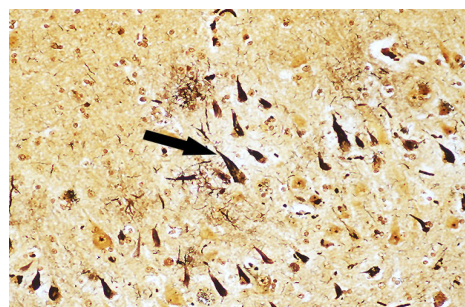
Figure 1.29. Silver stain detection of accumulation of hyperphosphorylated tau in neurons showing the typical flame shape (arrow). (From: http:// www. oumedicine.com/body.cfm?id=2881)

of XIa factor, i.e., a serin-protease involved in the process. Nishimoto et al, instead, suggested a hypothetic role for APP in signal transduction: a specific mutation of APP, in fact, seems to alter the activation of a G_0 protein leading to an increased release of Ca^{2+} from the cell storages (Nishimoto et al., 1993). An additional theory associates APP to vesicle trafficking along the axon due to its capacity of binding chinesine-I, an ATPase belonging to the molecular motor class and related to anterograde transportation in the cell (Kamal et al., 2001).

Some investigators attempted to clarify the biological function of APP by developing knockout mice. However these models failed to show increased lethality or pathologic conditions, probably due to the presence of amyloid precursor like protein 1 and 2 (APLP1 and APLP2). These two proteins are characterized by high sequence homology with APP and, apparently, seem to be able to partially replace it. Indeed, triple deficient mice for APP, APLP1 and APLP2 are not viable (von Koch et al., 1997, Heber et al., 2000).

APP processing

In physiological conditions, APP is matured through several post-translational proteolytic steps operated by the secretase complexes (Figure 1.30). The first phase of the process occurs during the transport of the molecule to the membrane and involves
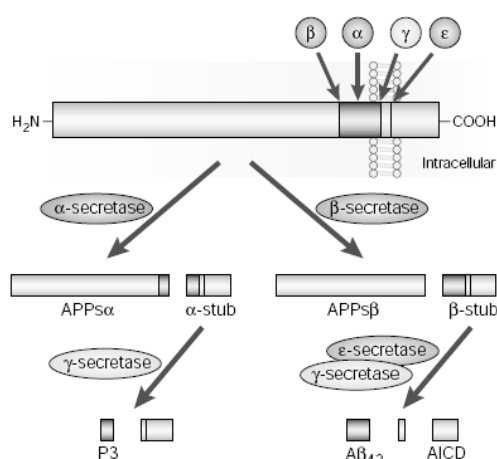
Figure 1.30. Schematic processing pathways of APP operated by α, β, ε and γ secretases. (From: LaFerla, 2002)

the α-secretase, i.e., a protease belonging to the A disintegrin and metalloproteases (ADAM) family. α-secretase cleaves a large portion of the N terminus of the peptide (called s-APP$_α$) and releases it in the vesicular lumen or in the extracellular space. s-APP$_α$ seems related to a neuroprotective activity; In fact this fragment is apparently able to significantly decrease the toxic effects

of high intracellular Ca^{2+} content subsequential to cellular damage or, in hippocampal neurons, to glutamate stimulation (LaFerla, 2002).

The remaining portion of APP after α-secretase-mediated cleavage consists in an 83 aa transmembrane peptide called CTF. This fragment can be further processed by a different enzymatic complex γ-secretase. This enzyme produces a proteolytic cleavage in the transmembrane domain releasing a 3 kDa peptide called p3, which is commonly present in the amyloid plaques even if not directly involved in the aggregation process.

Alternatively, full length APP can be processed by β-secretase, a transmembrane glycoprotein usually located on the membrane of the Golgi apparatus or on the cellular membrane. Two different forms of the enzyme have been identified, named β-site APP cleaving enzyme (BACE) 1 and 2, which are respectively characterized by specific tissue distribution. β-secretase cleaves APP into a soluble fragment (s-APP$_\beta$) and a 99 residue transmembrane peptide (CTF$_\beta$). Similarly to what observed for CTF, the latter can be further processed by γ-secretase. This event leads to the pro production of β-amyloid (Aβ), a 4 KDa peptide that has amyloidogenic properties. γ-secretase processing can cleave CTF in two different positions (711 and 713) producing respectively a 42 aa and a 40 aa fragments called Aβ$_{42}$ and Aβ$_{40}$. In normal conditions the balance between production and degradation of these molecules is achieved mainly through the insulin degrading enzyme pathway and, in part, the proteasome system (Schmitz et al., 2004). In AD, instead, the content of Aβ$_{40}$ and Aβ$_{42}$ are significantly increased. Although both the fragments are involved in the formation of amyloid plaques, it seems that Aβ$_{42}$ is the main responsible for the aggregation. This represents a result of the marked hydrophobicity of the molecule conferred by the presence of two extra highly hydrophobic residues (Haass et al., 1992, Shoji et al., 1992, Yoshiike et al., 2003).

In addition recent reports showed the presence of an alternative processing pathway of CTF$_\beta$ involving a different secretase (ε-secretase) that cleaves and releases the intracellular domain of APP (AICD). The functional role of this peptide is still unknown but it seems to be related to the calcium homeostasis through the regulation of the inositol triphosphate pathway (Leissring et al., 2002).

γ-secretase

γ-secretase represents a particular group of endoproteases that catalyzes the cleavage of target sequences in transmembrane domains. The catalytic region of the γ-secretase complex is formed by presenilin 1 (PS1) or presenilin 2 (PS2) (Tolia and De Strooper, 2008). These two proteins are mainly localized in the ER and in the Golgi apparatus, although recent reports showed their presence in the cytoplasmic, in the nuclear and in the endosomial membranes (Walter et al., 1996, Cupers et al., 2001).

PS1 and PS2 are encoded in two different genes (*PSEN1* and *PSEN2*) located respectively on 14q24.3 and 1q32-q42. The translation of these genes produces two proteins of 463 and 448 aa characterized by high amino acid homology (67%) and a series of structural analogies. PS1 and PS2 are 8-pass transmembrane proteins with a molecular weight of 49 and 50 kDa, which present cytoplasmic N and C termini. The catalytic core of the proteins is located in a highly conserved large cytoplasmic loop between the transmembrane domain 6 and 7, corresponding to the sequence included between aa 378 and 406 (Figure 1.31). In particular this region contains 2 aspartic
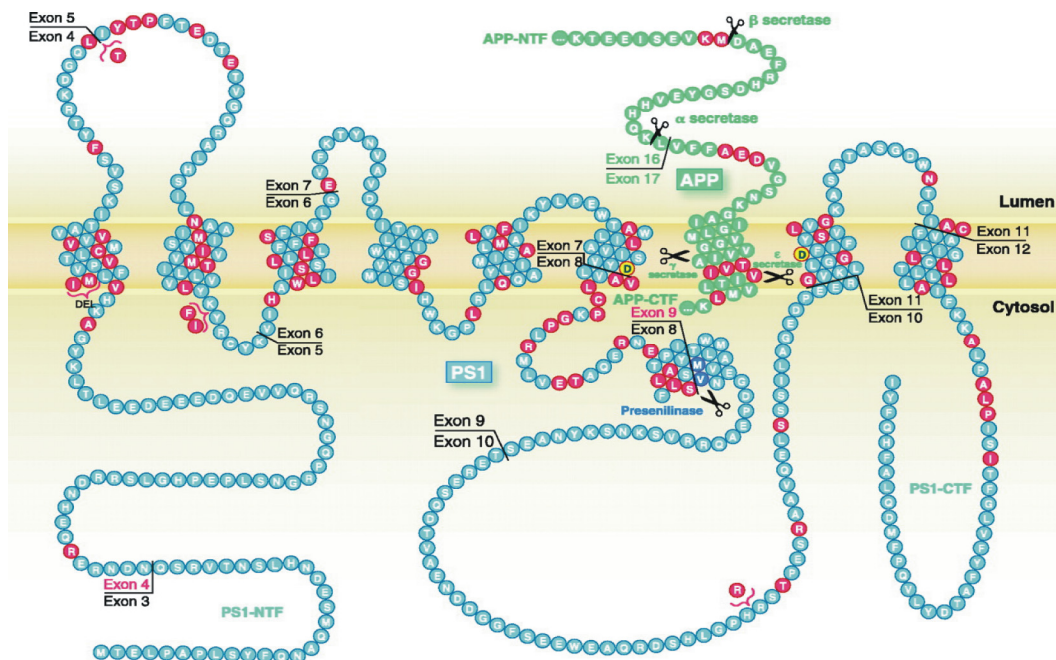
Figure 1.31. Structure of PS1 (blue) and localization of APP-NFT (green) in the catalytic site located between transmembrane helices 6 and 7 that contain two critical aspartate residues in position 257 and 385 (yellow). The proteolysis sites of both proteins are marked by scissor simbols. The amino acids marked in red represent some of the mutation described as related to AD. (From: Hardy, 2002)

acid residues (Asp$_{257}$ and Asp$_{385}$) that are directly responsible of the cleavage of Aβ (Wolfe et al., 1999).

Full length PSs require a activation step in order to perform their physiological function. This process consists in the cleavage of the protein in the catalytic loop most probably mediated by autocatalysis with the co-partecipation of co-factors (Takasugi et al., 2003). The proteolysis of PS produces a 30 kDa N terminal fragment (NTF) and a 20 kDa C terminal fragment that dimerize to form the γ-secretase core.

γ-secretase, though, is a high molecular weight enzymatic complex (150-250 kDa) composed by several other proteins with accessory function, including Pen-2, nicastrin, Aph-1, δ- and β-catenin (Figure 1.32) (De Strooper, 2003, Capell et al., 2005). In particular Pen-2 seems to be related to the correct assembly of the γ-secretase complex, while the other elements of the enzyme have a role in stabilizing the structure of PS (Steiner et al., 2002, Tolia and De Strooper, 2008). Nicastrin, for example, is a transmembrane glycoprotein that binds the N and the C termini of the presenilin stabilizing its structure and its interaction with APP. Therefore, the role of this protein in the γ-secretase complex is necessary for the proteolytic activity of the enzyme; dominant negative mutant forms of nicastrin, in fact, produce a drop in the formation of Aβ (Chen et al., 2001).

Figure 1.32. The γ-secretase complex and domains involved in the processing of APP. (From: http://www. biochemie.abi.med.u ni-muenchen.de/ haass/gamma-secretase/index.html)
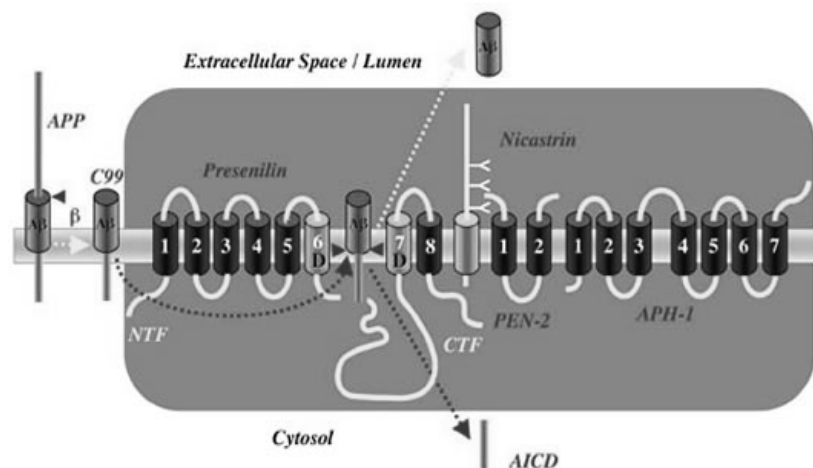
Table 1.5. Genes mutated in the familial forms of AD

Gene	Location	Described mutations	Biochemical alteration
APP	21q21	16	Increased Aβ generation and aggregation Increased Aβ42/Aβ40 ratio
PSEN1	14q24	140	Increased Aβ42/Aβ40 ratio
PSEN2	1q42	10	Increased Aβ42/Aβ40 ratio

1.6.5 Causes of AD

AD is a complex disease that produces a pathological phenotype deriving from concomitant interaction of environmental factors and genetic background.

Only a limited amount of mutations in the APP, PS1 and PS2 genes have full penetrance autosomal inheritance leading to AD (Table 1.5). These alterations usually produce the early-onset familiar forms of AD (EOFAD), which affects about 5% of the total number of AD cases and which develope clinically explicit AD condition by the age of 65. To date about 160 mutations in these genes have been associated to EOFAD, although most of them (~140) have reported in the PS1 gene. These modifications produce direct alterations of the biochemical processing of APP that lead to increased levels of Aβ with preferential production of $A\beta_{42}$. Mutated forms of PS1 have also been related to anomalies in the activity of protein kinases such as glycogen synthase kinase 3β (GSK-3β), protein kinase A (PKA), mitogen-activated protein kinase (MAPK) and cyclin-dependant kinase 5 (cdk5). These enzymes seem to be involved in the alteration of the architectural structure of the cytoskeleton by modifying the phospshorylation state of tau, which can aggregate in tangles and destabilize the microtubules when present in the hyperphosphorylated form. This process leads to the degeneration of the axon and to the loss of the synapses deriving from it (Maccioni et al., 2001, Mandelkow et al., 2003).

Table 1.6. Risk factors genes for AD (sporadic form)

Gene	Location	Biochemical dysfunction
A2M	12p13	Aβ clearance
ADAM9	8p11	α-secretase
ADAM10	15q21	α-secretase
ADAM17	2p25	α-secretase
APH1A	1q21	γ-secretase
BACE1	11q23	β-secretase
BACE2	21q22	β and α-secretase
IDE	10q23	Aβ/AICD clearance
LRP1	12q13	Aβ clearance
NCSTN	1q23	γ-secretase
NEP	3q25	Aβ clearance
PEN2	19q13	γ-secretase
PLAT	8p11	Aβ degradation (via plasminogen)
PLAU	10q22	Aβ degradation (via plasminogen)
PLG	6q26	Aβ degradation (via plasminogen)
ECE2	3q27	Aβ clearance

The analysis of the pedigree of late-onset cases of AD (LOAD) by segregation or twin study allowed the identification of more that three dozen genes that were mutated in AD. However, most of the genetic anomalies described are considered as risk factors rather than as primary cause of the disease. In fact, these alterations are considered neither necessary nor sufficient for the development of the disease (Table 1.6), unlike the mutations described in EOFAD. The most significant association to AD in this group is considered the polymorphism of the apolipoprotein E (APOE) gene on chromosome 19q13. The role of this protein in the pathogenesis of AD is still not clear, although some reports suggested that Aβ is able to bind the lipoprotein receptor on the cellular surface by interacting with the low-density lipoprotein receptor-related protein (LPR) (Figure 1.33). The interaction of extracellular APOE with the lipoprotein receptor produces the internalization of the complex and its translocation to the lysosome, where it undergoes a degradation process (Shibata et al., 2000). Other hypotheses, instead, suggest a specific role for APOE in binding Aβ in the extracellular space and in facilitating its removal from the deposition site. Each APOE allele seems to have peculiar capacity for Aβ clearance: the variant ε2, for example, has been associated to a more efficient clearance of the β-amyloid, while the presence of the ε4 allele seems related to the accumulation of the insoluble fibers (Hone et al., 2005, Tanzi, 2005).
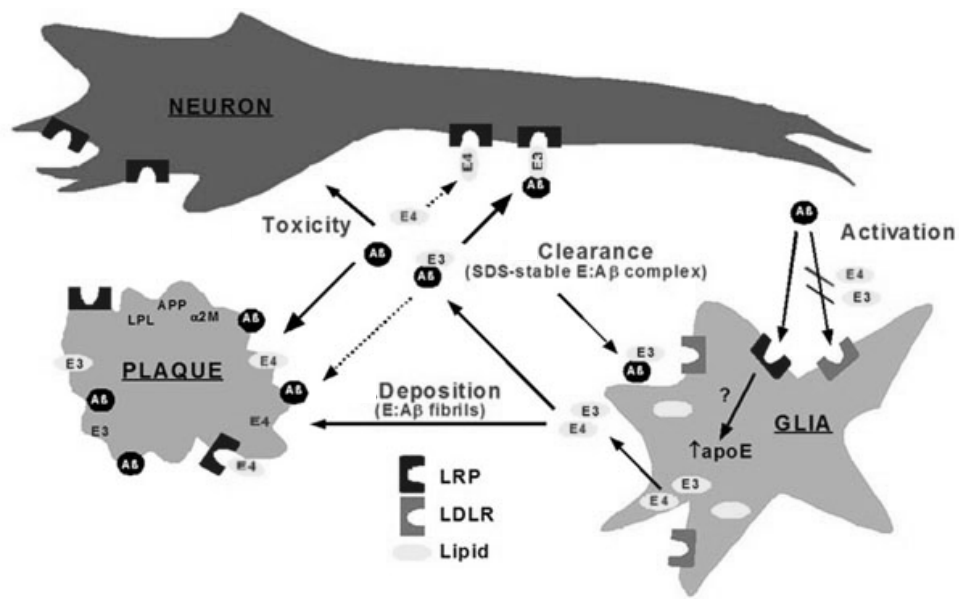
Figure 1.33. Mechanism of action of different APOE isoforms on the clearance of extracellular amyloid. Extracellular amyloid (Aβ) bind preferentially some forms of APOE such as ε3. This process allows the internalization of the APOE-Aβ complex in the cell and its degradation. Other isoforms of APOE and in particular ε4 have lower affinity for Ab. This produces an increased content of extracellular Aβ that can accumulate in plaques and that activates the astrocytes inducing production of APOE in order to facilitate the removal of free Aβ. (From: LaDu, 2000)

Other LOAD-associated genes are instead associated to different steps of the Aβ metabolism ranging form biosynthesis (e.g., α-secretase, β-secretase, elements of the γ-secretase such as PEN2, APH1A and Nicastrin) to the degradation (e.g., insulin degrading enzyme, neprilysin, urokinase-type plasminogen activator). However, these genes are still considered functional and/or positional candidates due to contrasting data about their role in the pathogenesis of AD.

As mentioned, LOAD is a multifactor disease in which non-genetic elements contribute to the development of the condition besides the genetic background. In fact, several studies reported that factors including level of education (Evans et al., 1997), dietary habits (Mayeux and Sano, 1999), exposure to heavy metals, head injuries (Lye and Shores, 2000)or history of cardiovascular diseases such as hypercholesterolemia, hypertension or stroke have an important role in AD etiology.

1.6.6 Ca^{2+} alteration in AD

An interesting aspect of most of the proteins involved in AD is their involvement in the regulation of Ca^{2+} signaling.

The secreted form of APP, for example, seems to have a role in the protection of the cell against toxic increases of intracellular Ca^{2+}, which are induced by injury or by overstimulation with glutamate in the neurons. This activity is thought to be mediated through the activation of the guanylate cyclase and the subsequent increase of cGMP. Therefore, any perturbation to the normal maturation of APP could lead to the accumulation of Ca^{2+} and to apoptosis. This process is further aggravated during deposition of Aβ, mainly because the fibers seem to infiltrate the lipid layer of the membranes forming cation pores that allow uncontrolled diffusion of Ca^{2+}.

A second hypothesis on the regulatory role of APP in calcium signaling has been related to a direct involvement of the AICD fragment, similarly to what observed with the NICD fragment deriving from proteolysis of notch (Leissring et al., 2002).

The mechanisms of action of the presenilin on the Ca^{2+} regulation, instead, have not been completely clarified. In particular it seems that some mutation of PS1 and PS2 can interact indirectly on the inositol-3-phosphate (Ins-3P) receptor on the ER inducing a increased release of Ca^{2+} (Chan et al., 2000). According to recent theories, these mutations are related to a loss of the intrinsic capacity of the PSs to form low-conductance divalent cation channels. This event leads to an overload of Ca^{2+} in the ER and to a significantly increased release during the opening of the Ins3P-regulated channels (Tu et al., 2006) (Figure 1.34).

PSs seem also to control Ca^{2+} levels in the cell through indirect pathways involving several calcium-related proteins related to ER free Ca^{2+} binding (calsenilin and calmyrin) (Stabler et al., 1999) and Ca^{2+} release from the ER (sorcin, RyR) (LaFerla, 2002, Stutzmann et al., 2006).
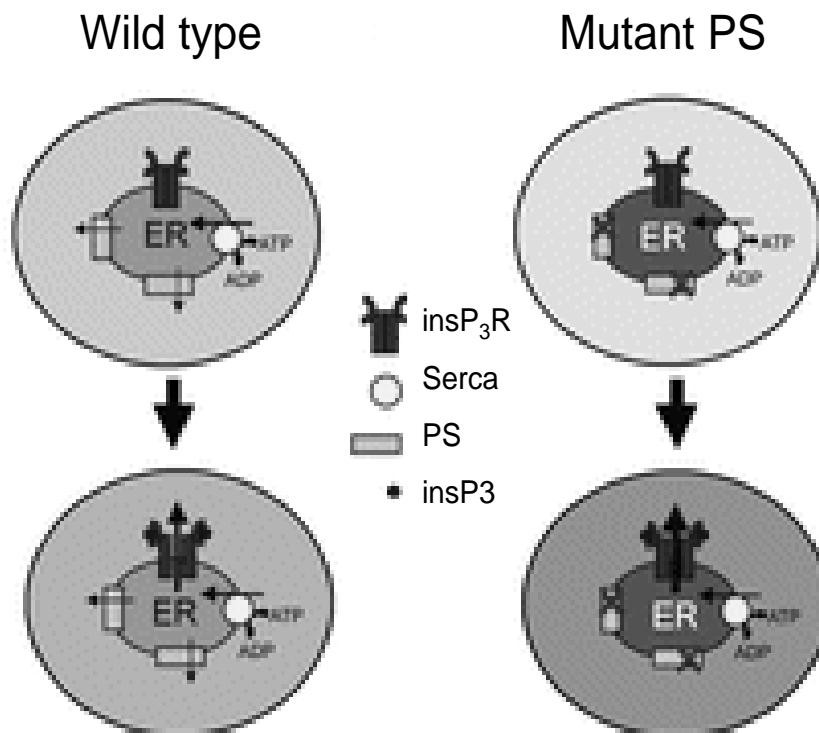
Figure 1.34. Proposed effects of PS mutation on the InsP-3 pathway. In wild type cells the Ca^{2+} internalized by the ER through SERCA normally leaks through a constitutive channel formed by the PSs. Mutations of the PS genes block the Ca^{2+} leaking from the ER leading to an overload of Ca^{2+} in the ER that results in an abnormal release upon opening of the InsP-3-regulated channels on the ER. (From: Tu, 2006)

1.6.7 Vascular defects associated to AD

In the last decade cardiovascular diseases have been related to cognitive impairment, showing in particular the correlation between AD and hypertension or CAD.

Neuropathological analysis of the brain of non-demented individuals affected by critical CAD (cCAD, i.e., occlusion of one coronary artery greater than 75%) often revealed significant deposition of Aβ in the brain compared to same age controls (Sparks et al., 1990). These data have been confirmed by animal studies in which the deposition of Aβ was induced by administration of a high cholesterol diet and reverted by the deprivation of cholesterol. The mechanism underlying this process is still unclear but it seems to involve the activation of microglia and alteration in the

metabolism of cholesterol. These affect the normal cleavage of APP, shifting the secretase activity from α to β cleavage (Sparks, 1996, Urmoneit et al., 1998).

The reports showing correlation between cCAD and deposition of Aβ were able to show the occurrence of intracellular fibrils of tau only in a limited number of cCAD patients. The study of brain damages in hypertensive heart disease, instead, revealed the concomitant presence of Aβ and tangles (Prince et al., 1994, Sparks et al., 1995, Petrovitch et al., 2000) that is probably due to the increased possibility of generating of silent brain infarcts and thrombosis, two risk factors that have been linked to AD (Qiu et al., 2003, Cechetto et al., 2008).

Aims

In the last few years an increasing number of previously unrelated disorders have been associated to adverse effects deriving from the accumulation of non-functional aggregates of unfolded proteins forming amyloid fibers (Selkoe, 2003). These aberrant deposits can arise from point mutations destabilizing the polypeptide structure or perturbation of the normal homeostasis of the cell.

Several studies have investigated the correlation between formation of β-sheeted structures and alterations of the Ca^{2+} homeostasis: molecules such as amylin, prion protein and $A\beta_{42}$ seem able to randomly create cation pores in the membranes (Mirzabekov et al., 1996, Lin et al., 1997, Kawahara and Kuroda, 2000), producing non-regulated ion migration. However, this cause-effect relationship is still considered controversial since some groups reported evidences of Ca^{2+} dysregulation in the brain before the detectable formation of amyloid fibers. In addition Ca^{2+} dysregulation was also observed in non-neural tissues normally not affected by the presence of $A\beta_{42}$ (Yoo et al., 2000).

As previously discussed, DCM hearts are characterized by a marked Ca^{2+} handling impairment that may be sufficient to disturb the correct post-translational modification of the protein chains in the sarcoplasmic reticulum. In fact, most of the enzymes involved in these processes –including the chaperones GRP78 and GRP94- are totally functional only when Ca^{2+} concentrations are kept within specific ranges. For this reason the SR in normal cardiomyocytes is spatially sub-compartmentalized in different regions for calcium cycling and protein folding, respectively enriched in pumps and ion channels or chaperones and calcium buffering proteins (Papp et al., 2003).

The potential deleterious effects of anomalies of the UPR system and of the presence of unfolded proteins in HF have been confirmed by an increasing number of reports in the last few years. Activation of the UPR system have been described both in humans and in rodent models of HF (Okada et al., 2004, Dally et al., 2009), which showed sensitive increase of GRP78 levels and initiation of the CHOP-regulated ER-mediated apoptotic pathway. Similar conclusions were reached by Hamada et al. (Hamada et al., 2004), which investigated the development of dilated cardiomyopathy in

transgenic animals with compromised UPR quality control system. These observations are consistent with ultrastructural morphological findings suggesting increased extension of the ER network in failing cardiomyocytes (Maron et al., 1975) and with other studies showing incapacity of the cell to efficiently degrade the peptides accumulation in a time-effective manner, which eventually leads to accumulation of poly-ubiquitinated proteins including the pro-apoptotic factor p53 (Birks et al., 2008).

Interesting confirmations of the role of the UPR in the etiology of HF derive from a recent paper showing clear correlation between pharmacologically-induced inhibition of the proteasome and heart failure (Voortman and Giaccone, 2006, Hacihanefioglu et al., 2008): in these studies Giaccone and Gonullu's groups confirmed that tumor patients treated with bortezomib (i.e. a pharmacological proteasome inhibitor used for triggering accumulation of unfolded proteins and therefore death of the metabolically hyperactive cancer cells) develop HF. This process has been successfully attenuated in vitro by Fu et al., who showed that the overexpression of endoplasmic reticulum-resident chaperone GRP78 in rat neonatal cardiomyocytes protects from the damages induced by proteasome inhibitors (Fu et al., 2008).

Further crucial observations associating protein folding and cardiac failure derive from the work of J. Robbins and colleagues, which demonstrated the active role of proteins prone to the formation of amyloid structure in the degeneration of the organ to a failing condition (Pattison et al., 2008). In particular the authors showed the deleterious effects of an exogenous pro-amyloigenic peptide (poly-Q Huntintin) on the cardiac function in transgenic mice. These results generate the intriguing hypothesis for the findings of Li et al (Li et al., 2006), which reported the presence of mutations in the PS1 and PS2 genes in families affected by the genetic forms of DCM. In fact, alterations in the γ-secretase complex may produce degeneration of the APP processing pathways, leading to increased production of pro-amyloigenic $A\beta_{42}$.

Based on these previous studies, we hypothesize that in idiopathic DCM the subnormal post-translational processing of proteins may lead to the accumulation of unfolded species in the cardiomyocytes and, eventually, to cell damage and death.

To verify our hypothesis we propose the following specific aims:

1. Verify the presence of unfolded proteins in idiopathic DCM samples.

2. Characterize the unfolded protein response in these samples.

3. Investigate the levels of AD-related proteins.

4. Identify the protein(s) involved in the formation of the aggregates.

5. Identify the pathways specifically altered in idiopathic DCM using high throughput analysis

CHAPTER 2

MATERIAL AND METHODS

2.1 Human samples

The diseased human heart samples used in this study were collected at Massachusetts General Hospital with patient informed consent under a protocol approved by the Institutional Review Board. The organs were explanted from patients undergoing cardiac transplantation at the time of the operation and immediately stored in ice-cold low-potassium University of Wisconsin cardioplegic solution (100 mM potassium lactobionate, 25 mM KH_2PO_4, 5 mM $MgSO_4$, 30 mM raffinose, 5 mM adenosine, 3 mM glutathine, 1 mM allopurinol, 5% w/v hydroxyethyl starch, 8 mg/l dexamethasone, 40 U/l insulin, $2x10^5$ U/l penicillin, pH 7.4 (Desrois et al., 1999)).

The hearts classified as non-failing were instead obtained under family approval from the National Disease Research Interchange (NDRI) program. These organs only included hearts considered not suitable for transplantation because of age of the donor, blood transfusion while in the emergency room or absence of compatible recipient within reasonable distance from the site of explant. The organs were delivered in cold University of Wisconsin cardioplegic solution for the transport.

Upon arrival in the lab the hearts were immediately dissected and processed with different protocols compatible with the downstream analysis planned. In particular, approximately 1 cm^3 of myocardium from the anterior wall of the left ventricle was saved for RNA isolation and immediately snap frozen to prevent RNA degradation and 1 mm^3 was stored in a 2.5% solution of grade II glutaraldehyde (Sigma, MO - Cat # G6257) for electron microscopy analysis. For these two critical applications we carefully selected areas with no macroscopic presence of adipose and/or fibrotic tissue. An additional part of the front wall (2-3 cm^3) surrounding a branch of the left anterior descending coronary artery was isolated, washed with phosphate-buffered saline (PBS, 137 mM NaCl, 2.7 mM KCl, 4.3 mM Na_2HPO_4, 1.47 mM KH_2PO_4 pH 7.4) + heparin and perfused with PLP solution (4% paraformaldehyde- 75 mM lysine - 10 mM sodium metaperiodate in 0.1M Na_2PO_4). The remaining tissue was instead divided in the four chambers, cut in small pieces and snap frozen as above.

Biopsy samples for early-stage DCM were instead collected with patient informed consent and directly stored in glutaraldehyde 2.5%.

All the cardiac samples collected were catalogued in a database including information such as age, gender, race, diagnosis or cause of brain death, clinical history, medications at the time of tissue harvesting, heart functional assessment, pathological analysis of the explanted organ, etc. This allowed us to divide the individuals used in these studies basing our selection, when possible, on sex, age and race for matching case and controls.

Strict confidentiality on all the information and data was maintained to protect the privacy of all donors and patients.

2.2 Congo red staining

Snap-frozen cardiac tissue was cut with a cryostat (temperature of the chamber: -18° C, temperature of the piece holder adjusted between -18° and -23° C to obtain wrinkle-free, non-cracked sections) at 8 μm thickness. The slices were collected on superfrost plus glass slides (Fisher Scientific, GA) and immediately stored at -80° C. The slides were then processed using a commercial congo red staining kit (Sigma, MO – Cat # HT60) based on Puchtler's modification of the original protocol (DC Sheenhan, 1980). Briefly, the samples were fixed in paraformaldehyde 4% for 10 min, washed 3 times in ddH$_2$O (10 min each wash) and counterstained in hematoxilin for 3 min (Gill #3 formulation). The excess of dye was washed as above and the slides were incubated in alkaline sodium chloride solution (NaCl-saturated SD 3A alcohol 80%:NaOH 1% 1:100) for 20 min and stained in alkaline congo red solution (0.2% congo red in NaCl-saturated SD 3A alcohol 80%:NaOH 1% 1:100) for 20 min. The slides were then washed three times in ethanol 100%, clarified in xylene and mounted in xylene-based mounting media. The samples were then analyzed in polarized and bright light.

2.3 Thioflavin-S staining

Tissue slides were prepared as described in chapter 2.2. The frozen sections were fixed in paraformaldehyde 4% for 10 min, washed 3 times in ddH$_2$O (10 min each wash) and immersed for 5 min in thioflavin-S staining solution (1% thioflavin-S in H$_2$O) as previously described (Guntern et al., 1992). Starting from this step, the entire procedure was performed in controlled light conditions to avoid the degradation of the

fluorochrome and photobleaching effect. The slides were then differentiated for 5 min in ethanol 70%, rinsed in ddH$_2$O twice (5 min each) and mounted using a fluorescence-compatible mounting media (DAKO, Denmark). The slides were then imaged on a confocal microscope (Leica TCS) using an excitation wavelength of 430 nm and detection at 550 nm.

2.4 Electron microscopy

The samples were processed and analyzed by the PMB Microscopy Core at MGH following a modification of a previously described protocol (Burghardt and Droleskey, 2006). Briefly, 1 mm^3 fragments of cardiac tissue were fixed in glutaraldehyde 2.5% solution for at least 2 hours. The excess of fixative was removed by three 5 min washes with tyrodes-cacodylate buffer (0.1 M NaCl, 2.5 mM KCl, 5 mM MgCl$_2$·6 H$_2$O, 12 mM NaHCO$_3$, 5 mM glucose, 10 mM Na(CH$_3$)$_2$AsO$_2$·3 H$_2$O 0.2 mM CaCl$_2$·2 H$_2$O pH 7.4) and the tissue fragments were dehydrated in crescent concentration of ethanol (25%, 50%, 75%, 95%, 100%, 100%, 5 min each) and incubated in two changes of propylene oxide (respectively 50% in ethanol and 100%) for 10 min. The specimens were then infiltrated with Epon 812 resin (50% in propylene oxide for 1 h and two changes of 100% respectively for 1 h and 24 h at 60°C) and polymerized for 7 h. The polymerized blocks were cut in 100 nm slices with an ultramicrotome and collected on formvar-coated grids. The samples were post stained in uranyl acetate for 5 min followed by immersion in lead citrate for 5 min. The excess of staining solution was removed by washing the grid in NaOH 20 mM and water. The samples were then observed in a transmission electron microscope at 80 kV.

2.5 Immunofluorescence

Snap frozen cardiac tissue was cut at 5 μm thickness and stored as described in paragraph 2.2. The samples were then fixed in paraformaldehyde 4% w/v for 15 min, washed 3x (10 min each) in PBS and blocked in PBS + bovine serum albumin (BSA) 5% w/v for 1 h at RT. The primary antibody was diluted in PBS + BSA and incubated on the slides for 90 min at RT. Specific dilutions and conditions for the antibodies used are summarized in Table 2.1 and will be listed in the relative chapters. The

Table 2.1. Commercial antibodies and conditions.

Antigen	Source	Cat #	Application (dilution)
19S rpt 3	Biomol Int.	PW8765	Wb (1:1000)
19S rpt 5	Biomol Int.	PW8770	Wb (1:1000)
20S α6	Biomol Int.	PW8100	Wb (1:1000)
20S β2	Biomol Int.	PW8895	Wb (1:1000)
20S β5	Biomol Int.	PW8210	Wb (1:1000)
Aβ	Covance	SIG-39300	IF (1:200)
APP	Abeta	W02	Wb (1:1000)
	Sigma	A8717	Wb (1:1000), IF (1:1000)
ATF6	Imgenex	IMG-273	Wb (1:500)
Calsequestrin	Thermo	PA1-9*13	Wb (1:1000)
Caspase 12	Abcam	AB18766	Wb (1:1000)
Chop	Biolegend	643601	Wb (1:500)
E2Fα-P	Cell Sygnaling	119A11	Wb (1:1000)
GADPH	Zymed	39-8600	Wb (1:1000)
IgG (Gt) Alexa 633-conjugated	Invitrogen	A-21082	IF (1:200)
IgG (Ms) Alexa 633-conjugated	Invitrogen	A-21050	IF (1:200)
IgG (Ms) Alexa 633-conjugated	Invitrogen	A-21070	IF (1:200)
IgG (Ms) HRP-conjugated	GE Lifescience	RPN4201	Wb (1:2000)
IgG (Rb) HRP-conjugated	GE Lifescience	RPN4301	Wb (1:2000)
Oligomers	Invitrogen	AHB0052	EM (1:400), IF (1:400), IP (1:100)
PS1	Millipore	A5308	IF (1:200), Wb (1:1000)
PS2	Thermo	MA1754	IF (1:200), Wb (1:750)
PS2-P	Calbiochem	PC235	IF (1:200)
Serca 2a	Abcam	AB3625	IP (1:100), Wb (1:1000)
Ubiquitin	Sigma	U5379	Wb (1:500)
XBP-1	Santa Cruz	SC7160	Wb (1:200)

Abbreviations: Wb: Western blot, IF: immunofluorescence, EM: electron microscopy-immunogold

samples were then washed twice in high salt PBS (PBS + NaCl 2.7 g/L), rinsed in PBS and incubated 45 min at room temperature with fluorochrome-conjugated secondary antibody in dark conditions (Invitrogen, CA, Alexa 633-cojugated anti-mouse, anti-rabbit or anti-goat 1:1000 in PBS+BSA). All the following steps were conducted in controlled light to avoid degeneration of the fluorescent signal. The slides were washed as described above and incubated in PBS + DAPI (1 µg/ml). The excess of DAPI was removed by two washes with PBS. The slides were finally

mounted using fluorescence-compatible mounting media (DAKO, Denmark), sealed and observed with a confocal microscopy (Leica TCS).

2.6 Immunogold staining

1 mm^3 of PLP-fixed cardiac samples was dehydrated in crescent serial ethanol solutions (25%, 50%, 75%, 95%, 100%, 100% v/v, 5 min each) and embedded in inclusion resin – medium grade (EMsciences, PA) at 50° C overnight. The polymerized blocks were cut in 100 nm slices with a Reichter Ultracut E ultramicrotome and collected on formvar-coated grids. The samples were then rehydrated to PBS with ethanol serial dilutions (100%, 95%, 75%, 50%, 25%, 5 min each) and processed the PMB Microscopy Core at MGH as previously described (Burghardt and Droleskey, 2006). Briefly, the sections were blocked in PBS+5% normal goat serum (NGS). The primary antibody (anti-oligomers A11 produced in rabbit, Invitrogen AHB0052 1:400) was labeled with colloidal gold (10 nM in DAKO antibody diluent) for 1 h at RT and applied to the slides. The hybridization was performed for 1 h at RT in continuous agitation. The unbound antibody was removed with 3x PBS washes (5 min each) and the grids were counterstained with 2% aqueous uranyl acetate for 5 minutes. The excess of staining solution was removed by washing the samples in NaOH 20 mM and water. The slides were then dried and observed in a transmission electron microscope (JEOL 1011) set at 80 kV.

2.7 Laser capture microdissection

Snap frozen cardiac tissue was cut as described in chapter 2.2 and collected on different types of slides. These included:

- Regular glass (Fisher Scientific, GA)
- Positively charged glass (Fisher Scientific, GA)
- Plastic (Fisher Scientific, GA)
- Plastic film-coated glass (Alphametrix Biotech, Germany)
- Polyethylene terephthalate membrane frame slides (Alphametrix Biotech, Germany)

The frozen sections were rehydrated in PBS 1x for 5 min, stained with thioflavin-S (5 min in thioflavin-S 1% in PBS followed by a differentiation step in ethanol 70% for 5 min, ethanol 95% for 5 min, two 5 min incubations in absolute ethanol and a final 5 min step in xylene) and dried o.n. at RT (Burghardt and Droleskey, 2006). This protocol was slightly modified by removing the final xylene step for the slides containing plastic material due to the solvent incompatibility of the support.

Three different instruments were tested for this the laser microdissection:

- Leica LMD 6000
- Zeiss P.A.L.M.
- Leica LMD 7000

In particular the polyethylene terephthalate membrane frame slides were exclusively used with the last system.

In all the cases the controlling software was programmed to automatically detect the Thioflavin-S signal (excitation 430 nm-detection 550 nm) and to isolate the positive fibers with a UV laser pulsed microbeam. The cell dissected on the Leica LMD 6000 apparatus were collected on CapSure collection cups (Invitrogen, CA) and transferred to regular 1.5 ml tubes, while the samples excised on the Zeiss P.A.L.M. were transferred directly to the tube by pressure catapulting. The cell selected with the Leica LMD 7000, instead were dropped by gravity directly in a 1.5 ml tube.

The collected Thioflavin-S positive material was resuspended in lysis buffer (tris HCl 10 mM, 7M urea, 2M thiourea, 2% chaps, 2% chapsO, 1% NP-40, 10% glycerol, 0.1% C_8E_{12}, 7 µg/ml calpain inhibitor, 1x Roche Complete proteinase inhibitor cocktail, pH 7.4) before further analysis.

2.8 Sarcoplasmic reticulum isolation

SR membrane-enriched isolation was performed as described by Hajjar et al. (Hajjar et al., 1997). 30 g of frozen of tissue in small chunks were resuspended in 300 ml of 0.3 M sucrose, 1 mM phenylmethylsulfonyl fluoride, 20 mM pipes pH 7.4 and homogenized at 4° C with a polytron PT10-35 homogenizer. The homogenates were clarified by centrifugation (500 g for 20 min at 4° C). The resulting supernatant was

collected and centrifuged at high speed (25000 g) for 60 min at 4° C to pellet the SR-enriched membrane fractions. The supernatant from this step was disposed and the pellet was incubated in 5 ml of 600 mM KCl, 30 mM sucrose, 20 mM pipes on ice for 30 min. The reconstituted material was homogenized as above, aliquoted and snap-frozen in liquid N_2.

2.9 Western blot

~500-1000 mg of cardiac tissue were lysed and quantified as described in paragraph 2.5. 50 μg of protein lysate were mixed with 6x Laemmli loading buffer (380 mM tris HCl, 60% v/v glycerol, 12% w/v sodium dodecyl sulfate (SDS), 0.015 % w/v bromophenol blue), denatured at 55° C for 10 min and loaded on 4-20% poly acrylamide gel (PAGE) and run at 34 mA for 1.5 h in 25 mM tris, 192 mM glycine, 0.1%. At the end of the electrophoresis step, the proteins were transferred at 400mA to a Hybond-ECL nitrocellulose membranes (supported, 0.22 μm pore) for 1.25 h at 4° C in 25 mM tris, 192 mM glycine, 20% methanol, pH 8.3,. The membranes were quickly rinsed in tris-buffered saline-tween 20 (TBS-T, 150 mM NaCl, 25 mM Tris-HCl, pH 7.6 + Tween 20 0.1%), blocked in TBS-T + non-fat dry milk 5% w/v for 1 h at room temperature and incubated over night at 4° C using unlabelled primary antibodies diluted in TBS-T + non-fat dry milk 5% w/v. Specific dilutions and conditions for the antibodies used are summarized in Table 2.1 and will be listed in the relative chapters. The membrane were washed 3x in TBS-T (5 min each) and hybridized with horseradish peroxidase-labeled secondary antibodies (DAKO anti-mouse, rabbit or goat IgG 1:2000) for 1 h at RT in TBS-T + non-fat dry milk 5% w/v. The membrane was detected with ECL reagent (GE lifescience, NJ) following the guidelines indicated by the manufacturer. The results were standardized to the content of GADPH (Zymed, 1:1000) for cytosolic proteins or calsequestrin (Upstate, 1:1000) for SR proteins using ImageJ software (NIH) and MS Excel for data analysis.

2.10 Immuno-precipitation

~500-1000 mg of cardiac tissue were crushed in liquid nitrogen and homogenized in RIPA buffer (50mM tris-cl pH 7.4, 150mM NaCl, 1% NP40, 0.25% w/v Na-deoxycholate, 1mM phenylmethanesulfonylfluoride (PMSF), 1x Roche complete mini

protease inhibitor, 1x Sigma phosphatase inhibitor). The lysates were centrifuged 10 minutes at 14000 rpm in a tabletop microcentrifuge at 4° C to eliminate detergent-insoluble fractions, the supernatant was collected and the protein content was quantified using a commercial Bradford protocol (Biorad, CA)(Bradford, 1976). 500 μg of protein were diluted in tris-buffered saline (TBS, 150 mM NaCl, 25 mM Tris-HCl, pH 7.6) and incubated with continuous agitation for 1 h at 4° C with 5 μg of antibody (see Table 2.1 for a complete list of sources and dilutions) to allow the formation of the immunocomplexes. Following the incubation 20 μl of protein G-coated sephadex G100 suspension (GE Bioscience, NJ) were added to capture the immunocomplexes and incubated overnight at 4 C in gentle continuous agitation. The next day the sephadex-immunocomplex particles were pelleted for 5 min at 14000 rpm in a tabletop microcentrifuge at 4° C, the supernatant removed and the pellet was resuspended in IP washing buffer (150 mM NaCl, 50 mM hepes, 0.1% triton X-100, pH 7.6 + proteinase inhibitors). This step was repeated three times to remove contaminations from unbound and aspecific proteins; the pellet was then resuspended in 30μl of 1x Laemmli loading buffer and denatured at 95° C for 3 min to promote the dissociation of the sephadex-immunocomplex bonds. The released Sephadex was removed by pelleting for 3 min at 14000 in a tabletop microcentrifuge, while the supernant (~25 μl) was loaded on 4-20% PAGE and processed as described in chapter 2.9.

2.11 DADT/PAGE

Snap frozen cardiac tissue was cut on a cryostat (temperature of the chamber: -18° C, temperature of the piece holder: variable between -18° and -23° C) at 20 μm thickness and collected in staining baskets. The basket containing 20-30 slices were immersed in PBS for 5 min and then incubated for 5 min in 1% thioflavin-S; the tissue was then differentiated in EtOH 70% for 5 min and rehydratated with two 5 min washes of PBS. The slides were transferred to a 1.5 ml tube and centrifuged at full speed for 30 s. The excess of PBS was removed and replaced with RIPA buffer (50 mM Tris-cl pH 7.4, 150 mM NaCl, 1% v/v NP40. 0.25% w/v Na-deoxycholate, 1mM PMSF, 1x Roche Complete mini protease inhibitor, 1x Sigma phosphatase inhibitor). The lysates were incubated on ice for 30 min and centrifuged 10 min at 14000 rpm in a tabletop

microcentrifuge at 4° C to eliminate detergent-insoluble fractions, the supernatant was collected and the protein content was quantified using the Bradford protocol. 50 μg of whole cell protein lysate were mixed with 6x Laemmli loading buffer, denaturated at 37° C for 1 h and loaded on a DADT/PAGE gel composed by a stacking portion (2.56% acrylamide, 0.45% diaminedithiol (DADT), 0.1 M tris pH 6.8, 10% glycerol, 0.1% SDS, 0.06% ammonium persulfate, 0.5% tetramethylethylenediaminide) overlaid on the separating gel (10% w/v acrylamide, 0.5% w/v bis-acrylamide, 0.375 M tris HCl pH 8.6, 10% v/v glycerol, 0.1% w/v SDS, 0.067% w/v ammonium persulfate, 0.067% w/v tetramethylethylenediaminide) (Fritz et al., 1989). The gel was run at 15 mA for 2 h and then the thioflavin-S signal was detected on a Typhoon 9400 high-resolution gel laser scanner (GE lifescience, NJ) set at 430/550 nm (excitation/detection).

2.12 Agarose gel for protein separation

1 g of frozen cardiac tissue was ground in liquid nitrogen and homogenized in RIPA buffer (50 mM tris-HCl pH 7.4, 150 mM NaCl, 1% v/v NP40. 0.25% w/v Na-deoxycholate, 1mM PMSF, 1x Roche complete mini protease inhibitor, 1x Sigma phosphatase inhibitor). The lysates were centrifuged 10 minutes at 14000 rpm in a tabletop microcentrifuge at 4° C to eliminate detergent-insoluble fractions. The supernatant was collected and the protein content was quantified using the Bradford protocol (Bradford, 1976). 500 μg of protein lysate were mixed in a 1:1 ratio with 2x tris-glycine loading buffer (125 mM tris HCl pH 6.8, 15% v/v glycerol, 4% w/v SDS, 0.002% w/v bromophenol blue, 1.25 M β-mercaptoethanol), denaturated at 95° C for 5 min and loaded on 2% SeaPlaque GTG agarose gel (Lonza, ME) prepared in 1x running buffer (90 mM tris base, 90 mM boric acid, 0.1% SDS) and placed in a horizontal submarine apparatus. No stacking gel was present. The gel was run at 80 V for 2 h and stained in Sypro Ruby® gel stain (Invitrogen, CA) following the instructions suggested by the manufacturer (Berggren et al., 2002). In particular, we selected to proceed following the longer basic protocol due to the higher thickness of the gel compared to a acrylamide one. Briefly, the gel was fixed in 50% v/v methanol, 7% v/v acetic acid (2 changes of 100 ml, 30 min each), stained with the staining solution o.n. and washed for 30 min in 100 ml of 10% v/v methanol, 7% v/v acetic

acid. All the steps were performed at RT in continuous agitation and, after the addition of the Sypro reagent, in controlled light conditions. Particular attention was focused on avoiding keratin contamination from the operator by using disposable sterile containers and tools for this step and the following. At the end of the staining process the gel was stored in fresh wash solution and imaged on a Typhoon 9400 high-resolution gel laser scanner (GE lifescience, NJ) with excitation set at 450 nm, emission at 650 nm and photomultiplier at 500 V.

2.13 Detergent extraction of amyloid fibers

The separation of hydrophobic amyloid structures was based on a modification of the protocol previously described by Ramsby et al. (Ramsby and Makowski, 1999). Snap-frozen cardiac tissue (~1 g) was crushed in liquid nitrogen and immediately transferred in TBS 1x + 1x Complete® proteinase inhibitor cocktail (Roche, CH) in round bottom 14 ml tubes. The samples were homogenized with a PT10-35 Polytron homogenizer with 3 cycles of 30 s each intercalated with 1 min of incubation on ice to prevent excessive protein degradation. The suspension was processed with a Branson 250 sonicator at 40% of power for 10 times for 10 s each. Each sonication cycles was followed by 1 min on ice to prevent overheating of the samples. 1 ml of sample was transferred to an Eppendorf tube and ~100 μl of glass beads (500 μm in diameter) were added. The tubes were vortexed at full speed for 1 min and centrifuged at 14000 g for 10 min at 4° C to remove the insoluble debris and the beads. The protein content of the supernatant was evaluated with a commercial Bradford protocol (Biorad, CA) and saved for SDS-PAGE analysis. The insoluble residue from the centrifugation was resuspended in 200 μl of TBS 1x + triton-X 1% v/v + 1x Complete® proteinase inhibitor cocktail (Roche, CH), vortexed, incubated on ice for 30 min and centrifuged as above. The Triton-X-soluble phase was collected and the protein concentration was evaluated using a Lowry method-based commercial kit (RC-DC, Biorad, CA)(Lowry et al., 1951). The triton-X-insoluble material was resuspended in 200 μl 1x TBS+ SDS 2% w/v + 1x Complete® proteinase inhibitor cocktail (Roche, CH) and processed as above. The supernatant was loaded on a SDS-PAGE 4-20% and stained with coomassie blue at the end of the run (Meyer and Lamberts, 1965).

The insoluble residue from the SDS extraction was resuspended in 1 ml of 1x TBS + formic acid 70%, vortexed, incubated 30 min at RT and centrifuged to remove the insoluble material. The supernatant was transferred to a new tube and the pH was neutralized by slowly adding ~120 μl of 1 N NaOH while incubating on ice. The pH of the solution was tested on pH paper and the solution was dialyzed with 3 kDa-pore centrifuge concentrators (Millipore, MA).

2.14 Oligomer immunoprecipitation and PAGE separation

Snap-frozen cardiac tissue (~1 g) was processed and quantified as in paragraph 2.20 and 500 μg of total proteins were used for the following analysis. The lysates were diluted with TBS + 1x Complete© proteinase inhibitor cocktail to 500 μl and incubated with the anti-oligomer antibody A11 (Invitrogen, CA – AHB0052 1:100) for 1 h at 4° C in continuous agitation. The immunocomplexes were isolated using 20 μl of protein G-coated sephadex G100 particles (GE lifesciences, NJ), which were incubated overnight in the solution in continuous agitation at 4 C. The sephadex-immunocomplex particles were precipitated by centrifugation for 5 min at 14000 g at 4° C, the supernatant removed and the pellet was resuspended in TBS + 1x Complete© proteinase inhibitor cocktail. This step was repeated three times; the pellet was then resuspended in 30 μl of 1x Laemmli loading buffer and denaturated at 95° C for 3 min to promote the dissociation of the sephadex-immunocomplex bounds. The released sephadex was removed by pelleting for 3 min at 14000 rpm in a tabletop microcentrifuge at RT, while the supernant (~25 μl) was loaded on 4-20% PAGE and run at 34 mA for 1.5 h in 25 mM tris, 192 mM glycine, 0.1% SDS. The gel was removed form the cassette and stained in Sypro Ruby® gel stain (Invitrogen, CA) as described in chapter 2.12. The acquired image of the gel was transferred to a Non-Linear workstation and analyzed using the TotalLab v.2005 software to automatically identify the bands in each lane. The automatic recognition was manually monitored and, when necessary, corrected by analyzing the densitometry profile of the lane. The bands showing statistically different intensity between DCM and non-failing ($p<0.05$) were isolated by band excision on a regular UV transilluminator and stored for subsequential analysis in 10% v/v methanol, 7% v/v acetic acid.

2.15 Differential sedimentation of unfolded structures

Density-based separation of amyloid fibers was performed by modification of a previously described protocol for protein aggregates extraction from *E. Coli* (Schrodel and de Marco, 2005). 1 g of frozen tissue was ground in liquid nitrogen using a pestle and collected in a 15 ml tube on ice. The sample was stained with 5 ml of thioflavin-S solution (0.125% thioflavin-S, 1% triton-X) and homogenized 60 s with a PT10-35 Polytron homogenizer at full speed. The tube was incubated 10 min on ice to allow the thioflavin-S to infiltrate the amyloid structure of the unfolded proteins. The excess of dye was removed by centrifuging the sample for 10 min at 15,000 g at 4° C and the pellet was washed by resuspending in ethanol 50% v/v and centrifuging 10 min at 15,000 g at 4°C. The ethanol was eliminated and the pellet was washed in deionized H_2O and recentrifuged in the same conditions. The supernatant was removed and the pellet was resuspended in lysis buffer (150 mM NaCl, 20 mM Tris pH 7.6, 1 mM $CaCl_2$, 1% NP-40, 1% triton-X, 10% glycerol, 1% SDS, Complete proteinase inhibitors (Roche, CH)) and sonicated with a Branson 250 apparatus at 40% power with 15 cycles of 10 s sonications/1 min on ice. The sample was centrifuged 10 min at full speed at 4° C in a regular tabletop centrifuge. The soluble and insoluble phases were separated and loaded on different sucrose step gradients (0%, 30%, 50%, 70%, 80% in 20 mM tris pH 8.0). The tubes were centrifuged for 18 h at 4° C at 180,000 g and the thioflavin-positive bands were detected by using a UV light source and isolated by needle aspiration. Each band was then loaded on appropriate continuous gradients (25→60%, 45→75% or 60→80% depending on the level where the band was isolated) and centrifuged 18 h at 180,000 g at 4° C. The tubes were unloaded and observed under UV line to identify thioflavin-positive bands that were collected by needle aspiration and saved for further analysis. A small aliquot of each band was separated to evaluate the relative aggregation index. This parameter was calculated as ratio between Abs_{280} and Abs_{340}, accordingly to what has been previously described (Schrodel and de Marco, 2005).

2.16 Mass spectrometry

The protein extracts were analyzed by ion trap - liquid chromatography tandem mass spectrometry (LC-MS/MS) by the Proteomics Resource Center at the Harvard School of Public Health (Boston, MA). Briefly, the samples were desalted using Centricon concentrators (Millipore, MA – membrane cutoff size 5 KDa) and re-constituted in 0.1% formic acid. The extracts were transferred in Eppendorf tubes, denatured with 6 M guandine hydrochloride, 50 mM NH_4HCO_3 at RT for 30 min and concentrated with Centricon concentrator. The guanidine hydrochloride was diluted by refilling the top cup with 50 mM NH_4HCO_3 and the sample was re-concentrated. This step was repeated three times to achieve almost complete removal of guanidine HCl (<15 μM final). The samples were collected from the concentrator and reduced in dithiothreitol (DTT) 10 mM final at 37° C for 15 min, followed by addition of iodoacetamide 50 mM final at RT in dark. DTT and iodoacetamide were removed by concentrator as described for guanidine HCl. The samples were digested by adding 50 U/ml trypsin (1/50 of the total volume) and incubating overnight at 37° C. The reaction was stopped with formic acid (0.2% v/v final), loaded on the liquid chromatography apparatus and finally transferred to the MS instrument (LTQ Orbitrap, Thermo Scientific), which was controlled by the Xcalibur software. The results were analyzed using Bioworks 3.0 (Thermo Scientific).

2.17 Oligomer in-vitro production

Oligomer solution was obtained using $A\beta_{42}$ purified peptide (Sigma, MO) as described by Kayed et al. (Kayed et al., 2003). The lyophilized peptide was reconstituted with a mix of H_2O:acetonitrile 1:1 and diluted to a final concentration of 2 mM in hexafluoroisopropanol. The diluted solution was sonicated for 30 s and added to ddH_2O in a siliconized container. The hexafluoroisopropanol was removed by evaporation and the water-based solution was continuously stired for 96 h. Aliquots were sampled at 6 and 12 h and every 12 h afterwards in order to verify the correct formation of the pre-amyloid molecular species. This process was monitored by blotting the samples on a sheet of Hybond-ECL nitrocellulose membrane (supported, 0.22 μm pore). The membrane was dried, quickly rinsed in TBS-T, and processed as described in chapter 2.9 using a primary antibody specifically

recognizing the three-dimensional structure of oligomers (Invitrogen, CA – AHB0052). This protocol produces mostly oligomers in the spherical conformation. More complex structures (annular protofibrils and pores) were instead obtained adding 5% of hexane.

At the end of the process the mature fibrils were separated from the solution by centrifugation (14000 g at 4° C for 20 min) and their conformation was verified by electron microscopy analysis.

2.18 Cardiomyocyte isolation

Murine cardiomyocytes were isolated as previously described by Liao et al. (Liao and Jain, 2007). B6 normal mice (Charles River Labs, MA, age: 4-8 weeks) were injected with 0.2 ml of heparin (2 mg/ml) and sacrificed by cervical dislocation; the heart was immediately removed and placed in ice-cold sterile saline. The heart was cannulated through the aortic valve, secured to the catheter with 3.0 silk suture, connected to a perfusion pump and placed in a thermostated glass jacket set to maintain the temperature of the organ around 37° C during the perfusion process. The heart was perfused for 3 min at 3 ml/min with Ca^{2+}-free perfusion buffer (137 mM NaCl, 4 mM KCl, 1 mM $MgCl_2$, 10 mM hepes, 0.33 mM NaH_2PO_4, 10 mM glucose, 5 mM taurine, 10 mM 2,3-Butanedione monoxime (BDM) pH 7.4) and then perfused with enzyme buffer (perfusion buffer + 360 mg/L collagenase B (Roche, CH), 480 mg/L collagenase D (Roche, CH), 60 mg/L protease XIV (Sigma, MO)) until the tissue was soft (7-10 min). Both the solutions were equilibrated at 37° C before use and continuously oxygenated during the whole process to prevent ischemic degeneration of the tissue. The heart was removed from the perfusion apparatus and placed in a sterile Petri dish containing transfer buffer (perfusion buffer + bovine serum albumin 0.5 mg/ml), in which the tissue was mechanically dissociated using two sets of forceps. The cell suspension was filtrated through strainers and pelleted by gravity in transfer buffer with increasing concentration of Ca^{2+} (0.06 mM, 0.24 mM, 0.6 M, 1.2 mM, 15 min each). The cell pellet obtained from the 1.2 mM Ca^{2+} was isolated and used for the following experiments.

2.19 Cardiomyocyte contractility analysis

Mouse cardiomyocytes isolated as described above were incubated 5 min in Fura-2AM (Invitrogen, CA) at RT and seeded in a flow chamber placed on an inverted microscope as previously described (del Monte et al., 1999). The cells were allowed to attach to the surface of the chamber for 5 min without any flow and successively superfused with Tyrode solution (137 mM NaCl, 4 mM KCl, 1 mM $MgCl_2$, 10 mM hepes, 0.33 mM NaH_2PO_4) at 37° C. External stimulation was applied with a biphasic pulse (frequency: 50 Hz, V: 50% above threshold). Due to the presence of damaged cells in the suspension, the myocytes used in this study were selected based on their aspect: cells without a clear striation pattern and showing presence of sarcolemmal blebs or granulation were excluded. The cells characterized by acceptable appearance were analyzed up to 12 h after the isolation. After obtaining stable contraction and Ca^{2+} transient, the baseline was recorded. The cardiomyocytes were then exposed to 0.5 or 5 μg of oligomers by rapid cell-focused administration of the solution through an Octaflow apparatus (ALA Scientific, NY).

Control cells were treated in the same conditions replacing the oligomer solution with plain PBS. The cardiomyocyte contraction amplitude and rate of contraction were monitored using a camera and a system equipped with Ionoptix software (Ionoptix, MA), which has embedded edge detection. The intracellular Ca^{2+} content of the cells was monitored in real time by recording the excitation ratio of fura-2 at 340 and 380 nm with a dual-excitation spectrophotometer. All these experiments were performed in controlled light environment to minimize external interference from ambient light.

2.20 Genetic analysis

Genomic DNA was extracted from 200 mg of frozen cardiac tissue using Qiagen DNeasy kit (Qiagen, Germany) according to the guidelines suggested by the manufacturer. The genomic DNA was eluted in 30 μl and quantified with a Nanodrop spectrophotometer (Nanodrop, DE). In order to sequence the entire codifying and promoter regions, we used sets of primers selected at a distance of at least 20-30 bp from the extremity of each exon or of the promoter. The primers were kindly provided by the Genetic and Aging Research Unit at Massachusetts General Hospital.

The PCR was performed using Phusion® polymerase (NEB, MA). The following conditions were used for the amplification of each primer set:

Genomic DNA	100 μg
Buffer HF 5x	10 μl
Primer mix 10 μM each	2.5 μl
dNTPs 2.5 mM each	4 μl
ddH$_2$O	Up to 50 μl
Enzyme 2 U/μl	0.5 μl

Initial denaturation: 98° C for 30 s

35 cycles: 98° C for 15 s

        annealing[†] for 15 s

        72° C for 20 s

Final extension: 72° C for 7 min

[†]: the annealing temperature (T_a) for each primer set was obtained calculating the annealing temperature of each primer (= [(a+t) x 2 + (g+c) x 4] − 4) and setting the lower temperature of the pair as T_a for the reaction.

An aliquot (5 μl) of the PCR products was verified on an agarose gel and the remaining was purified by spin-column (PCR purification kit, Qiagen, Germany) following the instructions suggested by the manufacturer. The purified products were sequenced and the resulting electropherograms from DCM samples were compared to gene sequences published in Genebank (http://www.ncbi.nlm.nih.gov/, NCBI Build 36.1), in the University of California-Santa Cruz Human Genome Database (http://genome.ucsc.edu, The March 2006 Human Reference Sequence) and to a database of genomic sequences isolated form lymphoblasts of AD patients and normal controls and conserved at the Genetic and Aging Research Unit at Massachusetts General Hospital. The analysis was performed using Genecode Sequencher 4 (Genecode, MI).

2.21 PSEN1 Promoter variant expression level evaluation

Genomic DNA was extracted from normal and mutated samples and quantified as above. The promoter regions 72672641-72673058 and 72673065-72673530 of the *PSEN1* gene (including respectively the mutation position -92 and -21) were amplified by PCR using Phusion® polymerase (NEB, MA) and the following primer sets, which included restriction enzyme-recognized sequences for easier cloning and a short poly-a to facilitate the restriction enzyme processing (in parenthesis):

- *PSEN1*-92 FWD: 5'-(AAAGCTAGC)GCCTCTAGGCAAGCAATTTTG T_m 62° C
- *PSEN1*-92 REV: 5'-(AAACTCGAG)TATGTCCATCTTTCCATGT GAATAC T_m 66° C

- *PSEN1*-21 FWD: 5'-(AAAGCTAGC)TGTTACCTGGAAGAAGC T_m 60° C
- *PSEN1*-21 REV: 5'-(AAACTCGAG)AAATCTCATCTTGAATTGATTG T_m 58° C

The following conditions were used for the amplification:

Genomic DNA	100 μg
Buffer HF 5x	10 μl
Primer mix 10 μm each	2.5 μl
dNTPs 2.5 mM each	4 μl
ddH$_2$O	Up to 50 μl
Enzyme 2 U/μl	0.5 μl

Initial denaturation: 98° C for 30 s

35 cycles: 98° C for 15 s

       58° C (PSEN1-92) or 54° C (PSEN1-21) for 15 s

       72° C for 20 s

Final extension: 72° C for 7 min

The normal and mutated fragments (-92C, -92delC, -21G and -21A) were purified by spin-column (PCR purification kit, Qiagen, Germany) following the instructions suggested by the manufacturer and digested o.n. with NheI and XhoI (NEB, MA). The digested fragments were separated on a 0.8% w/v agarose gel, excised, gel purified with a gel extraction kit (Qiagen, Germany) and ligated into the promoterless vector (Promega, WI, Figure 2.1) preventively digested with the same restriction enzyme set and gel purified. The following conditions were used for the ligation:

Insert	90 fmol
Backbone	30 fmol
Ligase 1 U/µl (Invitrogen, Ca)	1 µl
Ligase buffer 5x	4 µl
ddH$_2$O	Up to 20 µl

The reaction was performed for 1 h at RT and the ligase was inactivated at 65° C for 15 min. The ligated product was diluted 1:10 in ddH$_2$O and 2 µl of the dilution were used to transform 40 µl of electrocompetent One Shot *E.Coli* (Invitrogen, CA)
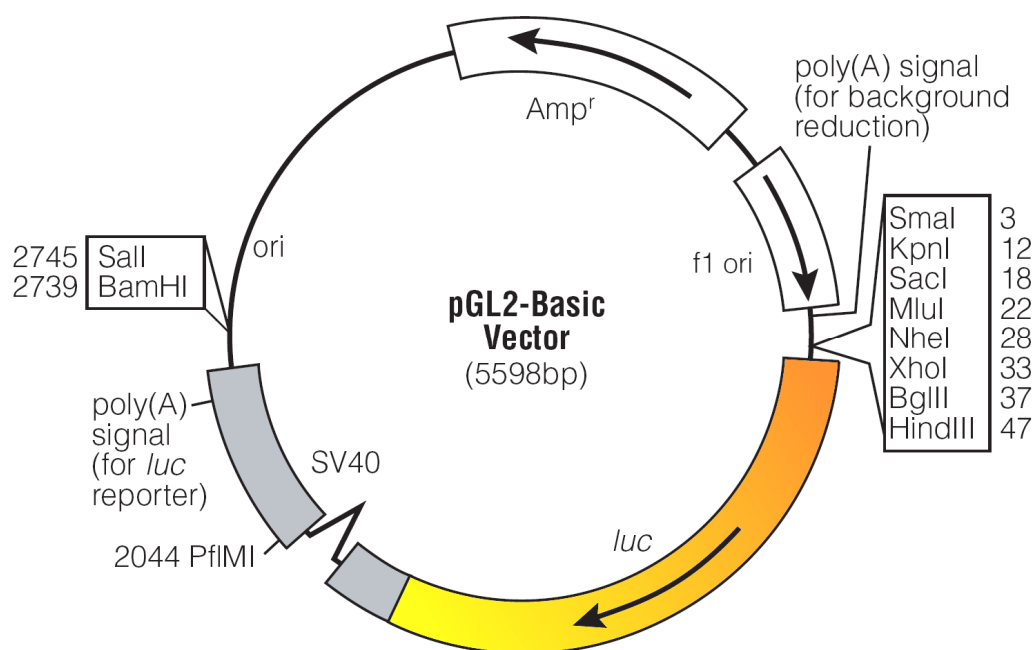
Figure 2.1. Map of pGL2-basic. (From: http://www.promega.com)

at 1800 V. The bacteria were allowed to express the ampicillin resistance gene for 1 at 37° C in super optimal broth with catabolite expression media (2% w/v bacto-tryptone, 0.5% w/v bacto-yeast extract, 8.56 mM NaCl, 2.5 mMKCl) and then plated on Luria broth (LB)-agar plates (1% w/v tryptone, 0.5% v/w yeast extract, 1% w/v NaCl, 1.2% v/w agar) + 75 µg/ml of ampicillin. The colonies were screened by restriction analysis and then sequenced to verify the correct amplification using the same primers used for the initial amplification (*PSEN1*-92 FWD and REV and *PSEN1*-21 FWD and REV). The clones matching the desiderated sequence were selected for the following experiments.

To verify the activity of the promoter fragments cloned, we plated $8x10^4$ H4 naïve neuroglioma cells (gift of Dr. Tanzi at Massachusetts General Hospital) in 24-well tissue culture plates using 500 µl/well of Dulbecco's modified Eagle's medium 4.5 g/L glucose (Sigma, MO) supplemented with 9% heat-inactivated fetal calf serum (Sigma, MO), 100 units/ml penicillin (Sigma, MO), 100 µg/ml streptomycin and 2 mM L-glutamine (Sigma, MO). The day following the plating the cells were transiently transfected with lipofectamine-2000 (Invitrogen, CA) following the protocol suggested by the manufacturer. As an internal control for the efficiency of transfection a second plasmid constitutively expressing *Renilla* luciferase (pRL-CMV, Promega, WI) was co-trasfected with the different forms of pGL2-PSEN promoter under investigation as previously described (Yang et al., 2004). Briefly, 0.4 µg of endotoxin-free pGL2 and 0.4 µg of pRL-CMV were diluted in 50 µl of Optimem media (Invitrogen, CA). In a different tube 2 µl of lipofectamine 2000 were mixed to 50 µl of Optimem media and incubated at RT. After 10 min the two tubes were mixed, incubated for 20 min at RT and distributed on a well. After 48 h the cells were washed and the expression levels of the two reporter genes activity was assayed using a dual luciferase reporter assay (Promega, WI) as indicated by the manufacturer. Briefly, each well was harvested in 65 µl of passive lysis buffer 1x, the cell debris removed by centrifugation in a tabletop microcentrifuge (5 min at 14000 rpm at RT) and 10 µl of the supernatant were dispensed into a black 96-well assay plate. The plate was analyzed with a Victor 5 plate reader (Perkin-Elmer, MA) equipped with automated dual injector and programmed to dispense 100 µl of LARII reagent buffer (Promega, WI), followed by 2 s incubation and 5 s of firefly luciferase-emitted light detection.

The firefly luciferase reaction was blocked by addition of 100 μl of freshly prepared Stop and Glow reagent, which also provides the substrate for *Renilla* luciferase. Incubation and detection for this second step was performed as above. The activity of the promoter was calculated as the ratio between the Firefly and *Renilla* activities. pGL2 promoterless activity was used to estimate the background of the process. The result for each variant was indicated as percentage of the wild-type construct. Each comparison was performed in triplicate and statistical significance was calculated using Student's t-test.

2.22 Population analysis

The single nucleotide polymorphisms (SNP) identified by sequence analysis were compared with the allele frequency and heterozygosity for the Caucasian normal population collected in the International HapMap database (http://www.hapmap.org) and in the NCBI SNP database, using the CEPH collection, which includes genomic information from Utah residents with Northern and Western European ancestors (Murray et al., 1994, Frazer et al., 2007).

Allele frequency for AD patients was kindly provided by Genetic and Aging Research Unit at Massachusetts General Hospital.

2.23 RNA purification

RNA from patient samples was prepared as recommended by Affymetrix guidelines Rev. 5. 500 mg of frozen tissue was crushed using a mortar and a pestle in liquid nitrogen and collected in a round bottom 14 ml tube. 5 ml of cold TRIzol (Invitrogen, CA) were added and the suspension was homogenized with a Polytron homogenizer for 30 s at full speed keeping the tube on ice. The tube was placed on ice for 1 minute before repeating the procedure to avoid overheating the sample. The Polytron probe was rinsed after each sample with diethylpyrocarbonate (DEPC) water, cleaned with ethanol and rinsed again in fresh DEPC water. The excess of DEPC water was removed using sterile gauze before processing the next sample. Each sample was divided in 5 RNAse-free 1.5 ml microcentrifuge tubes and centrifuged 10 min at 12,000 g at 4°C to remove remaining insoluble material. The supernatant was transferred to a new microcentrifuge tube, incubated at RT for 5 min and mixed with

200 µl of chloroform. The organic and the aqueous phases were mixed by vortexing 1 minute at full speed, incubated 3 min at RT and centrifuged 15 min at 12,000 g at 4°C. After this spin the aqueous phase formed a clear layer on top of the pink organic phase. The aqueous phase was transferred to a fresh tube trying not to perturb the organic phase in order to avoid carryover and contamination that could compromise the downstream reactions. 500 µl of cold RNAse-free isopropanol were added to precipitate the nucleic acids, the tubes were incubated 10 min on ice and the nucleic acids were pelleted at 12,000 g for 10 min at 4°C. The isopropanol was removed and the pellets were washed with 75% v/v RNase-free ethanol. The tubes were re-centrifuged as above and the ethanol was totally removed by aspiration. The pellets were dried on ice for 10 min to allow complete evaporation of the residual ethanol and resuspended in nuclease-free non DEPC-treated water (Sigma-Aldrich, MO). Total RNA was further purified from protein contaminations using RNeasy Mini Kit colums (Qiagen, CA) following the guidelines suggested by the manufacturer and eluted in a total volume of 50 µl. 1.5 µl of the samples were analyzed on a Nanodrop (Nanodrop, DE) spectrophotometer to evaluate concentration and purity (i.e., Abs 260/280 ratio). The integrity of the RNA and presence of RNase contamination were then assayed using a 2100 Bioanalyzer microfluidistic station (Agilent Technologies, CA) equipped with RNA nano chips.

2.24 cRNA preparation

Only the RNA samples showing no signs of degradation, appropriate 260/280 ratio (>1.8) and with concentration higher than 1 µg/µl were selected for further analysis as described in the Affymetrix guidelines Rev. 5. 20 µg of total RNA from each sample were mixed with 2 µl of T7-Oligo(dT) primer (50 µM) and with a combination of exogenous PolyA mRNA. The reaction controls included a set of polyadenylated RNA messengers for *B. subtilis* genes that are absent in eukaryotic samples: *lys, phe, thr* and *dap*. The volume was adjusted to 11 µl with RNase-free non DEPC-treated water. The secondary structures of the RNA were resolved by incubating the reaction mixes at 70° C for 10 minutes and then cooled to 4° C for 2 min. The RNA was reverse transcribed to cDNA by adding 2 µl of DTT 0.1 M, 1 µl of dNTPs (10 mM each) and 4 µl of 5x 1st strand reaction mix (Invitrogen, CA). The reaction mix was

preincubated 2 minutes at 42°C before adding 2 μl of Superscript II reverse transcriptase and incubating for 1 h at 42° C. The reverse transcription was stopped by incubating at 4° C for 2 min. The second strand of cDNA was synthesized by adding 91 μl of RNAse-free non DEPC-treated water, 30 μl of 5x 2nd strand reaction mix, 3 μl of dNTPs (10 mM each), 1 μl of *E. coli* DNA ligase, 4 μl of *E. coli* DNA polymerase I. The RNA present in the reaction mix was degraded by adding 1 μl of RNAse H. The samples were incubated at 16° C for 2 hours before adding 2 μl of T4 DNA polymerase and incubating 5 min at 16° C. The reaction was stopped by adding 10 μl of 0.5 M EDTA and the double stranded cDNA was purified using cDNA cleanup spin columns (Qiagen, CA). The samples were mixed to 600 μl of cDNA binding buffer. The pH was checked using the pH indicator present in the binding buffer before loading the solution in the column. The column was spinned at full speed for 1 min and the flow-through was discarded. The column was washed by adding 750 μl of cDNA wash buffer and spun at 8,000 g for 1 min. The flow-through was discarded and the column was centrifuged for 5 min at full speed to remove any contamination from the ethanol present in the wash buffer. The cDNA was then eluted in a fresh tube by pipeting 14 μl of cDNA elution buffer directly on the membrane, incubating 1 min in upright position and centrifuging at full speed for 1 min.

6 μl of the eluate were transcribed *in vitro* and labeled with biotin by adding 4 μl of 10x *in-vitro* transcription (IVT) labeling buffer, 12 μl of IVT labeling NTP mix and 4 μl of IVT labeling enzyme mix. The volume of the reaction was adjusted to 40 μl with RNase-free non DEPC-treated water (14 μl) and the samples were incubated for 16 hours at 37° C. The biotinylated cRNA was purified using cRNA cleanup spin columns (Qiagen, CA). 60 μl of RNase-free non DEPC-treated water, 350 μl of IVT cRNA binding buffer and 250 μl of ethanol were added to the IVT reaction mix. The solution was loaded in a column and centrifuged at 8,000 g for 15 s. The flow-through was discarded and the filter was washed with 500 μl of wash buffer. The column was re-centrifuged as above and the flow-through was discarded. This step was repeated with a final wash of 500 μl of 80% ethanol. The flow-through was discarded and the residual ethanol removed by centrifuging for 5 min at full speed (14000 rpm in a tabletop centrifuge). 21 μl of RNAse-free non DEPC-treated water was added to the

membrane and the labeled cRNA was eluted in a fresh tube by spinning at full speed for 1 min.

The cRNA was quantified using a Nanodrop spectrophotometer and diluted to a final concentration between 0.5 and 1 μg/μl.

2.25 Hybridization

The biotinylated cRNA was fragmented to 50-200 nucleotide fragments using a protocol based on a metal-induced reaction. 20 μg of cRNA were adjusted to 32 μl and mixed to 8 μl of 5x fragmentation buffer (Affymetrix, CA). The solution was incubated at 94°C for 35 min and then kept at 4° C. An aliquot (1 μl) of the reaction was assayed on an Agilent Bioanalyzer 2100 using a Pico RNA chip in order to verify the fragmentation pattern of the samples.

The fragmented cRNA (20 μg in 39 μl) was mixed with 150 μl of 2x hybridization buffer (Affymetrix, CA, pre-equilibrated at RT), 3 μl of herring sperm DNA (10 mg/ml prewarmed at 40°C), 3 μl of BSA (50 mg/ml pre-warmed at 40°C), and two exogenous controls: oligonucleotide B2 (Affymetrix, CA, 5 μl of 3 nM solution pre-warmed at 40°C) and a 20x solution of *bioB. bioC, bioD, cre*. The hybridization cocktail was heated at 99°C for 5 min, cooled to 45°C for 3 min and centrifuged at full speed for 5 min to remove any insoluble material. In the meantime the U133 plus 2.0 microchip arrays (Affymetrix, CA, one per sample) were equilibrated at room temperature for 15 min, preconditioned with 1x hybridization buffer and incubated at 45°C for 10 min in a rotation oven. The preconditioning solution in the chips was removed and replaced with the hybridization cocktail. The cartridges were placed in the hybridization oven and incubated for 16 h at 45°C with rotation.

After the incubation the chips were washed and stained on a Genechip Fluidistic Station 450 (Affymetrix, CA) according to the following protocol: 42 min in buffer A (300 μl of 2x stain buffer, 24 μl of BSA (50 mg/ml), 6 μl of phycoerythrin-conjugated streptavidin (Molecular Probes, CA), 270 of RNase-free non DEPC-treated water), 10 min in Buffer B (300 μl of 2x stain buffer, 24 μl of BSA (50 mg/ml), 6 μl of goat IgG (Sigma-Aldrich), 3.6 of biotinylated anti-goat IgG Ab (Vector Laboratories) and 266 of RNase-free non DEPC-treated water), followed by 27 min in Buffer A.

The cartridges were analyzed by eye to confirm the absence of bubbles in the reading area and scanned on a Genechip Scanner 3000 (Affymetrix, CA).

2.26 Microarray analysis

The data were exported as .cel file and normalized by global scaling. All the quality control parameters were calculated by the Affymetrix GeneChip Operating Software (Dumur et al., 2004). In addition the scanned images were examined to verify the absence of spotted, bleached or damaged area on the hybridization plates (Quackenbush, 2002). Data from different chips were normalized using the GeneChip Robust MultiChips Analysis algorithm (GCRMA), performed with R in Bioconductor (Cope et al., 2004, Wu and Irizarry, 2004).

2.27 Statistical analysis and selection of differentially expressed probes

A probe was considered absent in a group when the absolute intensity recorded for all the patients belonging to that group was lower than 8 fluorescence units as suggested by the manifacturer. This threshold was selected based on previous experience from the consultants that collaborated in this study. The expression of a particular probe in a determined group was indicated as the average of all the samples belonging to that group. Statistical significance was calculated using Spotfire DecisonSite 8.0 software by applying ANOVA and 2-tail unpaired t-test for unknown variance and multiclass analysis (Golub et al., 1999). mRNA levels were considered altered when either their content between two different groups was at least 2 (arbitrary value) fold up- or down-regulated. Any difference in expression was considered statistically significant only when the p value calculated by ANOVA and t-test was lower or equal to 0.05. The differentially expressed genes matching the parameters mentioned above were grouped in the following three categories:

- DCM-specific genes: concurrently significantly up- or down-regulated both in DCM vs. controls and DCM vs. amyloidosis, but not significantly altered between amyloidosis and controls.
- Amyloidosis-specific genes: concurrently significantly up- or down-regulated both in amyloidosis vs. controls and DCM vs. amyloidosis, but not significantly altered between DCM and controls.

- Failing-related genes: concurrently significantly up- or down-regulated both in amyloidosis vs. controls and DCM vs. controls.

2.28 Clustering and self organizing maps

K-means clustering and Self-organizing maps were used to group the genes identified as altered by similarity of profiles on the normalized average of the subgroups of samples (Tamayo et al., 1999). Hierarchical clustering on median normalized samples was performed on all samples using SpotFire DecisionSite 8.0 for Functional Genomics. The analysis was performed applying cosine correlation with complete linkage (Eisen et al., 1998, Datta, 2003).

2.29 Functional analysis

The genes which were significantly differentially expressed from the microarray analysis were further examined to identify specific pathways involved in the diseases considered as previously described (Huang da et al., 2009a, Huang da et al., 2009b). The data were respectively submitted to the Database for Annotation, Visualization and Integrated Discovery (DAVID, http://david.abcc.ncifcrf.gov/home.jsp), to the Kyoto Encyclopedia of Genes and Genomes (KEGG, http://www.genome.jp/kegg) and to the Biocarta database (http://www.biocarta.com) using the EASE software. The results from the algorithms were limited to association involving at least 2 genes with p<0.05.

2.30 Data validation

The data from the microarray analysis were confirmed by selecting a limited number of altered probes and evaluating their alteration by quantitative real-time PCR (qRT-PCR).

cDNA for the reaction was obtained by reverse transcribing 2 μg of total RNA from the same preparations used for the Genechip analysis using Omniscript RT Kit (Qiagen, CA).

The RNA was mixed with 4 μl of 10x reverse-transcriptase buffer, 4 μl of dNTP mix (5 mM each dNTP), 4 μl of oligo-dT$_9$ primer (10 μM), 20 units of RNAseOut RNAse inhibitor (Invitrogen, CA) and 8 units of Omniscript reverse transcriptase. The

volume was adjusted to 40 μl with RNAse-free non DEPC-treated water. The reaction mix was incubated 1 h at 37° C and the obtained cDNA was aliquoted in 3 μl single use aliquots to avoid repeated freeze/thaw cycles which could compromise the quality of the samples.

The qRT-PCR was performed using an ABI Prism 7000 Thermocycler (Applied Biosystems, CA). Each sample was assayed in triplicate to minimize the experimental error. 1 μl of cDNA was mixed in 10 μl of QuantiTect SYBR Green PCR Kit (Qiagen, CA), 1 μl of primer mix containing 10 μM of the forward and reverse gene-specific primers and 8 μl of PCR grade water. The following gene-specific primer sets were used in the reactions:

- *ApoE* F: 5'-CCAATCACAG GCAGGAAGAT-3'; R: 5'-CTGTCTCCAC CGCTTGCT-3'.

- *ANP* F: 5'-GCCTAGGGAC AGACTGCAAG-3'; R: 5'-ATCACAACTC CATGGCAACA-3'.

- *BNP* F: 5'-CCGCCTTTGA AGTGACTCAT-3'; R: 5'-ACCGTGGAAA TTTTGTGCTC-3'.

- *DSCR1* F: 5'-AGGGGCCACT CTCTACTGGT-3'; R: 5'-TTGCTGCTGT TTTCACAACC-3'.

- *Nestin* F: 5'-CACCCTCAGA AAAGGAGGAG-3'; R: 5'-CAGGAAGAAA AGGTGCCTCA-3'.

- *RARRES1* F: 5'-CAACTGAAAA ACCCCTTGGA-3'; R: 5'-GAAAGCCAAA TCCCAGATGA-3'.

- *STNC* F: 5'-ATTCCCACCA ACAAAATCCA-3'; R: 5'-GGAAAAACAT GGCAGAGGAA-3'.

- *TNN1* F: 5'-GTGAGCATG GTGTGTATGC-3'; R: 5'-AGAGCATCTG GGAGGCACTA-3'.

Each primer set was designed using Primer3 (http://frodo.wi.mit.edu/primer3/) using specific settings to minimize the possibility of hairpin secondary structures and primer dimer formation (maximum self complementarity = 8.00, maximum 3' self

complementarity = 3.00). The optimal T_m for each primer was set at 60° C. The total length of the amplicons was 200±25 bp. When possible the primers were designed to match a junction region between 2 exons in order to minimize the possibility of amplification of genomic DNA contaminating the samples.

The thermocycler was set to perform an initial step (2 min) at 50° C to allow the uracyl-N-glycosylase degradation of carryover DNA contamination from previous reactions. The *Taq* Polymerase was then activated for 15 min at 95° C before starting the cycling step consisting of denaturation at 94° C for 15 s, annealing at 60° C for 30 s and extension at 72° C for 30 s. The data were acquired during the last step. The cycling step was repeated 40 times and was followed by a melting protocol to confirm the absence of secondary structures and/or dimerization of the primers. Only one gene was assayed on a single plate containing the cDNAs from all the patients simultaneously in order to minimize the experimental variability. Contamination from genomic DNA was evaluated performing an additional reaction using a set of intronic primers (F: 5'-CTGTCCTCCA ACTGTCAGCA-3'; R: 5'-CTCTTCCAAG GGGATCATCA-3')

The data were analyzed with the 7000 SDS 1.1 RQ application (Applied Biosystems, CA). The threshold for each gene was automatically calculated by the software. The automatic analysis was manually corrected in case the threshold was located in a non-linear segment of the amplification trace. The C_T of each gene was automatically calculated and the content of messenger RNA was standardized to the level of 18S rRNA (evaluated by qPCR using the primer set F: 5'-TCATGTGGTGTTGAGGAAGC -3'; R: 5'- GGCGTGGATTCTGCATAATG -3').

2.31 Statistical analysis

Statistical analysis was generally performed by Student's t-test using Excel software (Microsoft, WA). Results were considered significant when $p < 0.05$. Specific statistical methods used for particular sets of data are described in the relevant Material and Methods sections.

CHAPTER 3

IDENTIFICATION OF PROTEIN AGGREGATES AND ACTIVATION OF THE UNFOLDED PROTEIN RESPONSE IN IDIOPATHIC DILATED CARDIOMYOPATHY

3.1 Introduction

In the last decade increasing attention has been focused on the role of unfolded protein material in the etiology and the progression of several diseases even traditionally non related to the presence of amyloid fibers, including Parkinson's disease, Creuzfeldt-Jacob disease, diabetes, obesity and cancer (Hosoi and Ozawa).

The first report showing correlation between a pathological condition and the presence of unfolded protein dates back to the beginning of last century when Alois Alzheimer presented to the scientific community a case of early age onset dementia characterized by the presence of aggregates resulting positive to silver staining. Later characterization of these aggregates allowed the identification of two distinct types of deposits, which are referred as senile plaques (extracellular) and neurofibrillar tangles (intracellular) and are respectively due to the accumulation of amyloid β (Aβ) and tau (Tanzi and Bertram, 2005).

This condition (later named after its discoverer) is characterized by a large majority of sporadic cases with no clear genetic inheritance (~95%) (Bertram and Tanzi, 2004). However, several genetic studies performed on the remaining portion of the patients led to the identification of a significant number of fully penetrant mutations that are inherited following the classical Mendelian rules (Blacker and Tanzi, 1998). These mutations are all related to three specific genes codifying the Amyloid precursor protein (APP), presenilin 1 (PS1) and presenilin 2 (PS2) and mapping respectively on chromosome 21, 1 and 14.

These three genes have been extensively characterized in the central nervous system, mainly due to their association with Alzheimer's Disease (AD). However, a recent study suggested the presence of a correlation between heart failure and the presenilin genes by performing a linkage analysis on early-onset familial forms of dilated cardiomyopathy (DCM) (Li et al., 2006). In particular, Li et al reported two unknown mutations (D333G in PSEN1 and S130L in PSEN2) which where present in 0.9% of the families included in the study (3/325). PS1 and PS2 are highly conserved

polytopic proteins which are considered the catalytic core of the γ-secretase complex, an enzymatic complex that is involved in the cleavage of several cellular proteins such as *notch* (Zhao et al.) and, mainly, of APP with consequent production of Aβ (De Strooper, 2003).

The function of these proteins in the heart hasn't been completely elucidated. However studies conducted on knock-out mice for the presenilins showed their importance at a cardiac level even at very early developmental stages (Donoviel et al., 1999, Nakajima et al., 2004). An interesting function of the γ-secretase complex that has been observed in the brain is related to its capacity of interacting with sorcin, one of the major inhibitors of the ryanodine receptor (Lokuta et al., 1997, Pack-Chung et al., 2000, Farrell et al., 2003).

If this last regulatory mechanism is confirmed in the cardiac muscle, PS1 and PS2 could represent important molecules in the excitation-contraction coupling.

The mentioned observations by Hershberger's group on familial DCM (Li et al., 2006) open an innovative and interesting field of investigation for better understanding the non-familial forms of the disease. Only 35% of the cases of DCM can be directly correlated to genetic causes including in particular sarcomeric and cytoskeletal components as well as proteins associated to the regulation of the Ca^{2+} homeostasis (Schonberger and Seidman, 2001, Olson, 2004). The majority of DCM cases are instead related epigenetic causes including exposure to toxic substances, infection or underlying presence of autoimmune diseases; however in a significant number of patients the disease cannot be associated to a specific causative agent. Therefore it is possible that some of these cases can be related to malfunction of the γ-secretase complex which may lead to dysfunction in Ca^{2+} homeostasis and eventually creates appropriate conditions for the accumulation of misfolded peptides. In general alterations in Ca^{2+} homeostasis in DCM lead to the extensively described contractility impairment typically observed in cardiomyocytes deriving from subjects affected by this condition. However, Ca^{2+} has several other important roles in eukaryotic cells beside the regulation of the contraction, including regulation of the apoptotic process, signaling and protein folding. This last process, in particular, occurs mostly in the ER/SR, involving several proteins which are considered Ca^{2+}-dependent. Therefore

124

the depletion of sarcoplasmic Ca^{2+} characterizing late-stage DCM cardiomyocytes might produce impairment on the post-translational folding of the polypeptide chains, leading to the progressive accumulation of unfolded peptides forming β-sheeted structures.

At the moment only three forms of cardiac degenerative conditions leading to heart failure have been related to the accumulation of unfolded protein fibers: light chain amyloidosis, transthyretin (TTR) cardiomyopathy (Kelly and Strauss, 1994) and desmin cardiomyopathy (Bova et al., 1999, Li et al., 1999). However, only the latest is specifically related to folding dysfunction in the cardiac cells. Amyloidosis and TTR cardiomyopathy, instead, originate in the immune system and in the liver respectively as consequences of immunoglobulin-overexpressing lymphomas (Buxbaum, 2004) or expression of mutated insoluble forms of prealbumin (Hesse et al., 1993). The presence of unfolded insoluble fibers in the circulation and their deposition in the cardiac muscle leading to increased stiffness and impaired contractility of the organ has been considered the only reason for cardiac dysfunction for several years (McCarthy and Kasper, 1998). On the other side, recent findings suggest that the devastating effects of unfolded protein accumulation in the heart may be also mediated at least in part by the presence of soluble precursors of the amyloid fibers which do not have any effect on the alteration of the mechanical property and stiffness of the organ. These molecules, called oligomers, are β-sheeted protein aggregates formed by a limited number of peptides (3 to 12) commonly detectable in all the form of foldopathies and usually present in large amount in the proximity of mature fiber formations. This hypothesis is supported by several studies conducted on isolated neurons suggesting that the deleterious effects of the accumulation of Aβ in AD are not mediated (at least totally) by the presence of the insoluble amyloid fibers but are instead related to the presence of the intermediates of the fibrillogenesis process (Gong et al., 2003, Klyubin et al., 2004, Walsh and Selkoe, 2004, Cleary et al., 2005).

In this chapter we will focus our attention on the determination of the role of AD-related proteins in the etiology of idiopathic DCM: our results show interesting

dysregulation of the levels of APP, PS1 and PS2 that can be related to the altered calcium homeostasis commonly observed in late-stage DCM. Additionally, we report and characterize two novel mutations in the promoter regions of PS1 and PS2, which led to significant decreased expression of the two proteins.

Because of the role that PS1 and PS2 have in the regulation of the RyR and calcium release from the sarcoplasmic reticulum, we will evaluate the impairment in the protein folding process. According to our data DCM cardiomyocytes show intracellular deposits of β-sheeted fibers and high levels of oligomers, which exhibit the capacity of impairing the mechanical property of the cell.

In addition we will address the effects that the accumulation of unfolded peptide has on the cell by evaluating the levels of key components of the unfolded protein response (UPR).

3.2 Results

3.2.1 Detection of Protein Aggregates

The detection of β-sheeted aggregates is normally achieved in clinical practice for the diagnosis of AD or other amyloid-related diseases using histochemical approaches based on the use of dyes such as Congo Red and Thioflavin-S (Figure 3.1). These
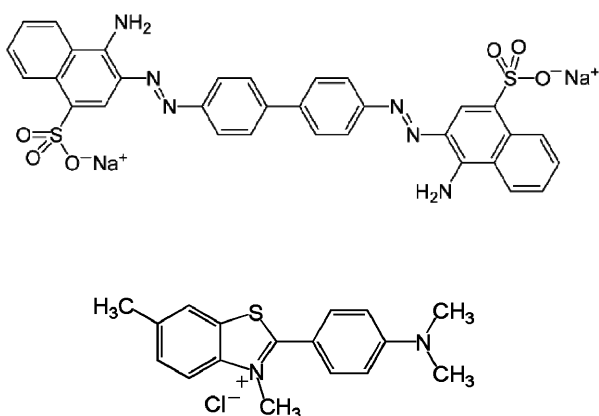
3.1. Molecular structure of Congo Red (top) and thioflavin-S (bottom).
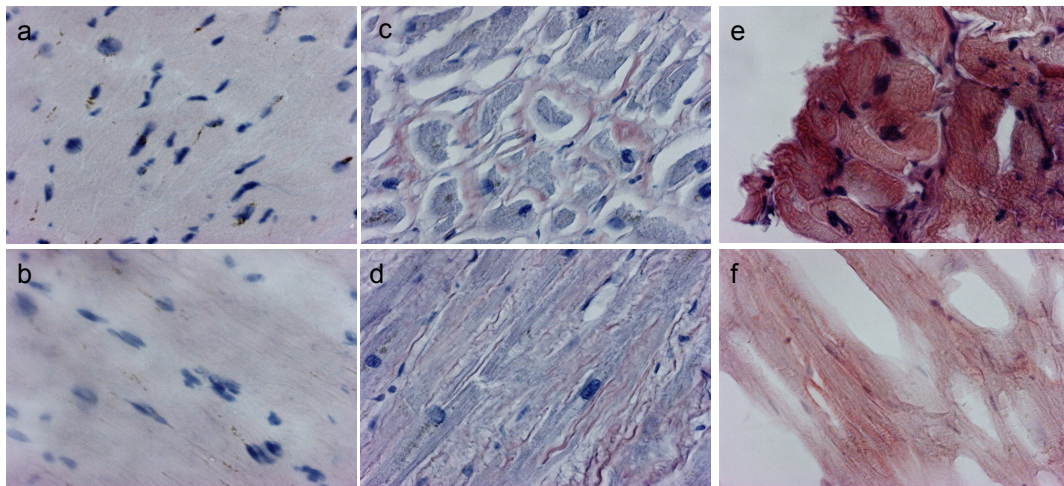
3.2. Congo red staining of non-failing (a: transversal, b: longitudinal), amyloid (c: transversal, d: longitudinal) and DCM (e: transversal, f: longitudinal) samples. Congo red analysis shows the presence of congophilic materials in the cytoplasm of DCM cardiomyocytes. This observation is in contrast to what observed in systemic amyloidosis, in which the deposition of congophilic material is diffused in the extracellular matrix.

dyes are characterized by the capacity of specifically binding β-sheeted deposits independently of the amino-acid sequence, respectively giving red-orange staining in bright light associated with apple-green birefringence under polarized light (Congo Red) and intense fluorescence in the green spectrum after UV exposure (Thioflavin-S).

Samples from idiopathic DCM hearts (n=23) and non-failing donors (n=14) were stained using Congo Red. The staining protocol was validated using cardiac muscle samples from systemic amyloidosis (n=6) as positive controls. As expected all the positive controls showed diffused red-orange staining in the extracellular matrix, while no signal was detectable in the cardiomyocyte fibers. 17 out of 23 (74%) of the idiopathic DCM samples we tested showed intense signals (Figure 3.2). However, the distribution of the dye was significantly different from what observed in the amyloidosis samples: the staining signal was concentrated within the cardiomyocytes, while no evident staining was observed in the extracellular matrix. Instead, most of the donor samples didn't show any Congo Red positivity, except for 2 out of 14 (14%). Interestingly both these two samples derived from 75 year-old subjects, which were the oldest included in the donor group.

These data were confirmed using thioflavin-S staining as an alternative protocol in order to minimize the possibility of false positives due to the unspecific binding of
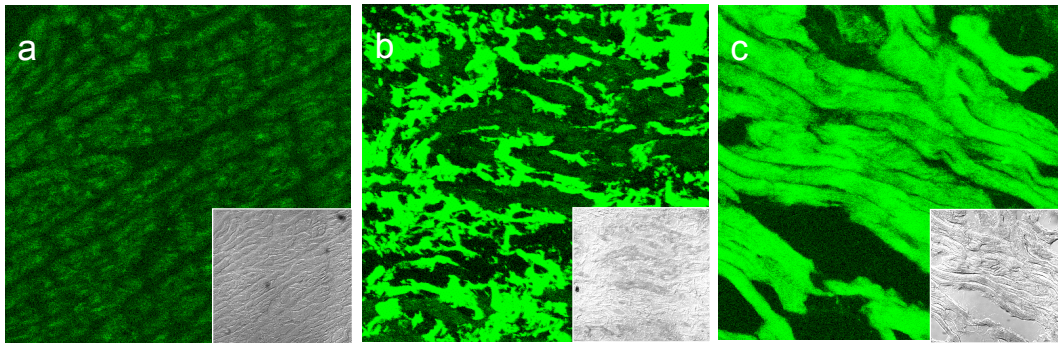
3.3. Thioflavin-S staining. Thioflavin staining of non-failing (a), amyloid (b) and DCM patients (c) clearly showed the presence of intracellular amyloid aggregates in the DCM samples, while the amyloid patient used as positive control showed the presence of aggregates in the extracellular matrix.

Congo Red to proteins characterized by periodic structure such as collagen (Figure 3.3).

Further verification of the findings deriving from the histochemical staining was obtained from the ultrastructural evaluation of the idiopathic DCM hearts (n=5). The samples analyzed were specifically selected in order to avoid interference and presence of false positives associated to the severe degeneration of the cellular functions in late-stage DCM and the physiological accumulation of aggregates observed in the aging process. Early-stage idiopathic DCM sample were obtained from explanted organs (n=5) from subjects with an average age of 52 years old (range 31-65) or from biopsies (n=2) deriving form subjects with an average age of 45 (range 24-65). The electron microscopy analysis of these samples clearly showed the presence of large areas of disorganized high-contrast material of proteic nature mainly in the cytoplasm and partially in the extracellular compartment (Figure 3.4), resembling the distribution of tau-originated tangles and β-amyloid plaques in AD (Kayed et al., 2003). These aggregates don't present any similarity with physiological fibers such as collagen. In addition they seem to be more abundant in proximity of the myofilaments and appear to induce a disorganizing effect on the filament itself (arrows). The deposits were observed in all the subjects analyzed, which included biopsies from early-stage DCM (Figure 3.5, arrows). This suggests the presence of strong relationship between the presence of these structures and the onset and progression of idiopathic DCM.
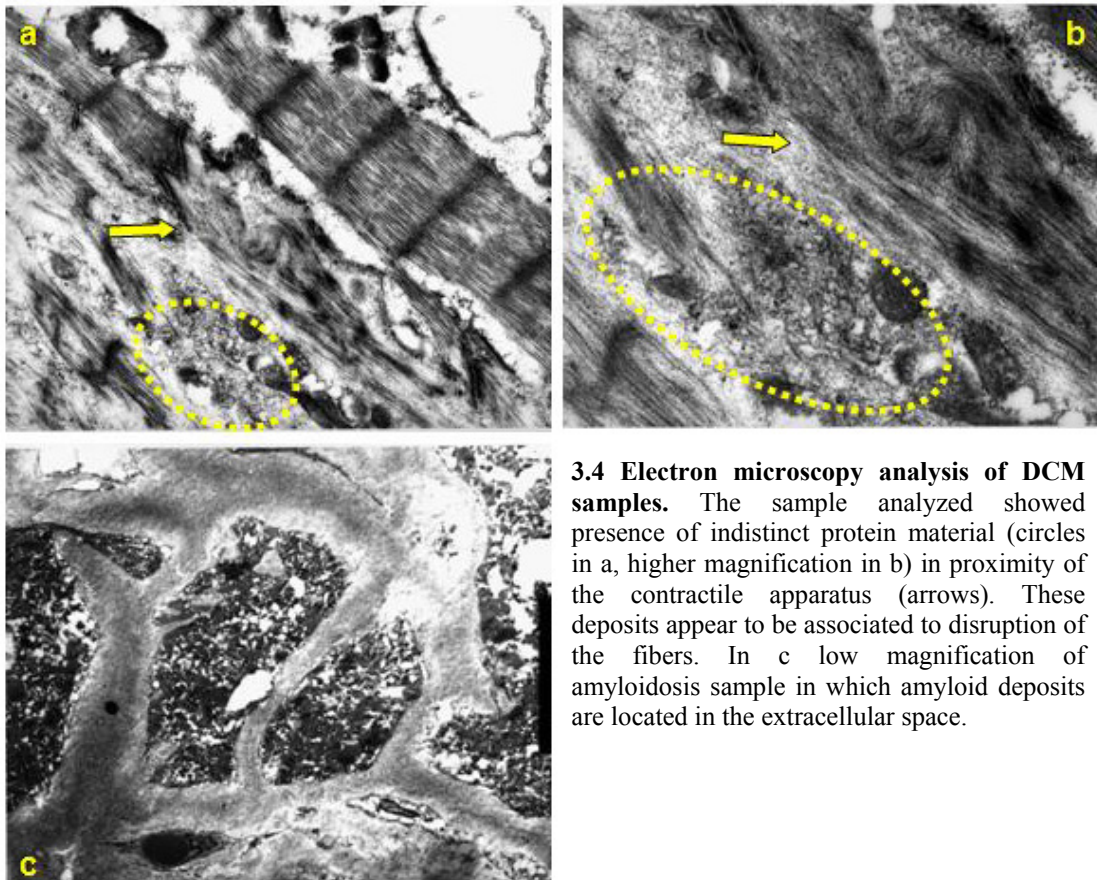
3.4 Electron microscopy analysis of DCM samples. The sample analyzed showed presence of indistinct protein material (circles in a, higher magnification in b) in proximity of the contractile apparatus (arrows). These deposits appear to be associated to disruption of the fibers. In c low magnification of amyloidosis sample in which amyloid deposits are located in the extracellular space.

3.2.2 Evaluation of the levels of AD-related proteins

In the last decade increasing interest has been focused on the relationship between γ-secretase and the regulation of Ca^{2+} content in the cell. This process is apparently mediated by several mechanisms including direct (Hayrapetyan et al., 2008) and sorcin-mediated (Lokuta et al., 1997, Pack-Chung et al., 2000, Farrell et al., 2003) modulation of the RyR and direct interactions between presenilins and SERCA (Jin et al.). To elucidate the role of presenilins in the regulation of the cardiac isoform of SERCA, we first evaluated the presence of interaction between the two molecules by coimmunoprecipitation. As expected SERCA2a behaves similarly to SERCA2b and coimmunoprecipitated with PS1 in almost all the samples analyzed (SERCA2a antibody: Thermo, MA dil 1:1000, α-PS1: for IP: Millipore, MA dil 1:100, for WB: Millipore, MA, dil 1:1000, Figure 3.6). These data suggest that alterations of the
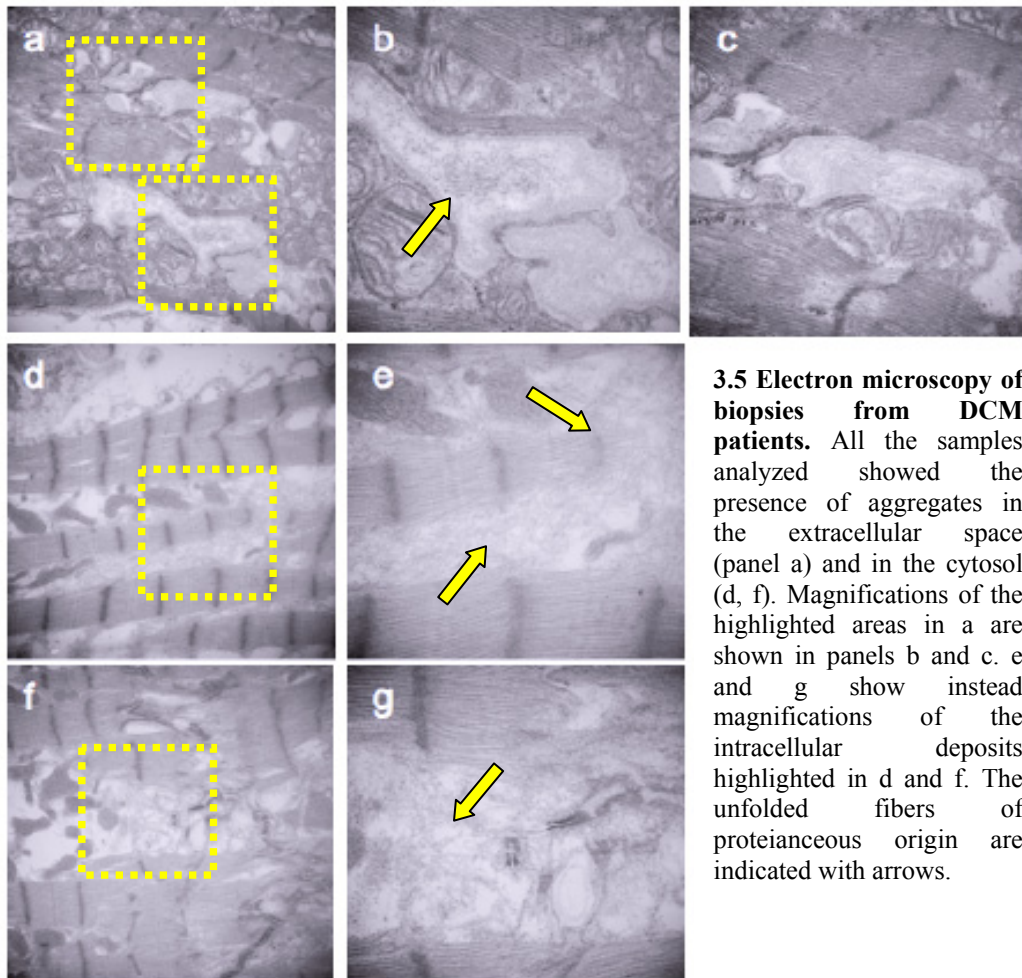
3.5 Electron microscopy of biopsies from DCM patients. All the samples analyzed showed the presence of aggregates in the extracellular space (panel a) and in the cytosol (d, f). Magnifications of the highlighted areas in a are shown in panels b and c. e and g show instead magnifications of the intracellular deposits highlighted in d and f. The unfolded fibers of proteianceous origin are indicated with arrows.

content or of the activity of the components of the γ-secretase complex might be sufficient to generate anomalies in the calcium homeostasis that can lead to the formation of the unfolded peptide deposits previously described and can contribute to the development of a failing condition at least in part.

In order to verify whether our observations were related to altered content of the γ-secretase components, we evaluated the levels of the catalytic subunit of the complex (i.e., presenilin 1 and presenilin 2) by performing Western blots on pooled sarcoplasmic reticulum preparations from non-failing and DCM samples (antibodies: α-PS1: Millipore, MA dil 1:1000, α-PS2, Thermo, MA dil 1:750). Interestingly, our results showed undetectable levels of PS2 in DCM samples (Figure 3.7) associated with a moderate increase of the content of full length PS1 (50 kDa band), which averaged 46% according to densitometry ratio quantification. As presenilins are

C+   Non-   DCM
            Failing

Serca2a

PS1
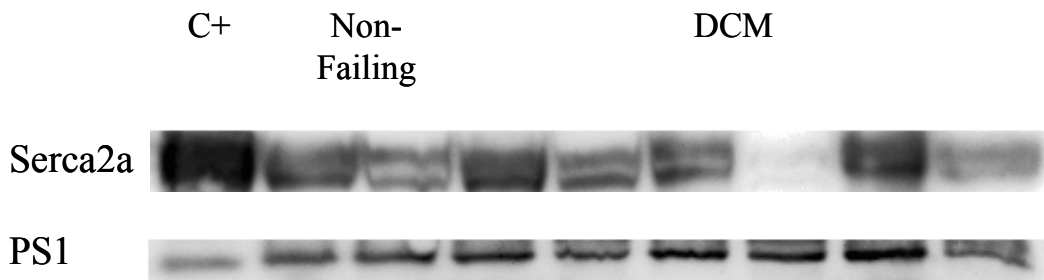
3.6 Detection of Serca2a following immunoprecipitation of PS1. PS1 and Serca2a co-precipitate, suggesting direct interaction between the two proteins. C+ = PS1-overexpressing CHO cells.

usually synthesized as full-length inactive proteins, they need to undergo an endoproteolytic step to reach the functional state. During this process the amino- and carboxyl-termini are cleaved by a complex including nicastrin, anterior pharynx defective 1 and presenilin enhancer 2, in order to create a substrate docking region inbetween the two subunits (Xia, 2008). The primary antibody we used for detecting PS1 was developed against an epitope mapping in the amino-terminus of the protein, thus allowing the visualization of the cleaved fraction by western blot as a band with molecular weigh of 28-30 kDa. Our results showed no significant alteration of this fragment in DCM compared to non-failing (Figure 3.7, lower band).

The alteration of PS levels was confirmed by immunofluorescence analysis in which DCM cardiac samples were compared to non-failing and AD hearts were used as reference (Figure 3.8). As expected, PS1 showed increased content in DCM (+377%). Instead we couldn't observe any significant variation in the levels of PS2, although

3.7. Presenilin1 and 2 levels in SR preps from DCM (n=6) and non-failing (n=4) hearts. Left panels show Western blot analysis of the content of PS2 (top) and PS1 (bottom). Interestingly, PS2 shows massive decrease in DCM patients, while PS1 shows moderate increase of the full length form. An additional band relative to the N-terminus of the protein after proteolytic activation was visible around 30 kDa, with no significant difference between normal and DCM samples. Right panel shows the densitometric analysis of the full length forms of the two proteins tested. CS= calsequestrin.

DCM   NOR

PS2   50 KDa

PS1   50 KDa
                       36 KDa

CS   64 KDa
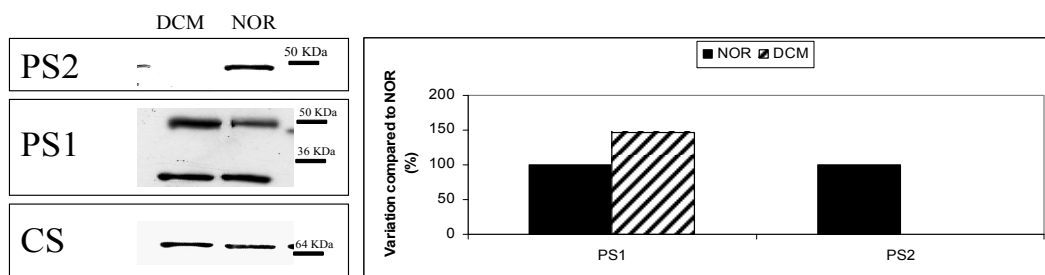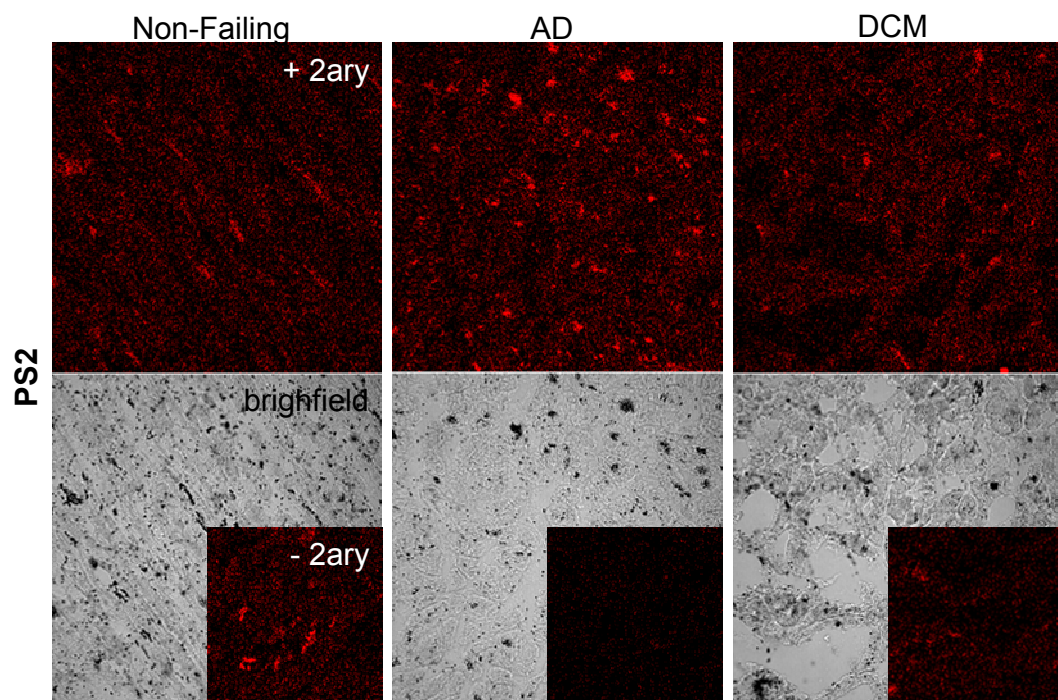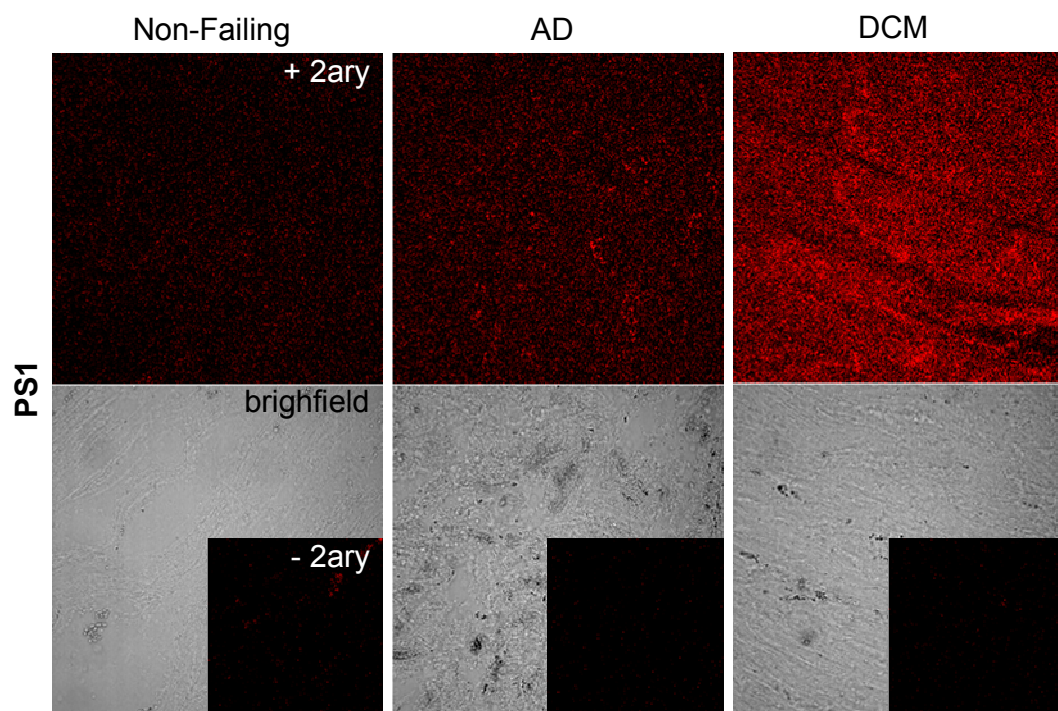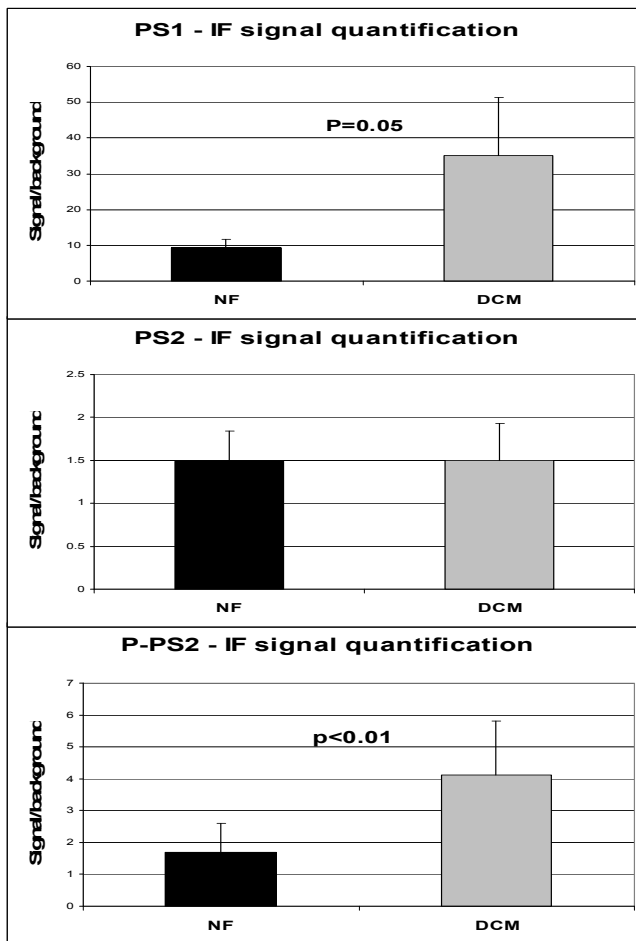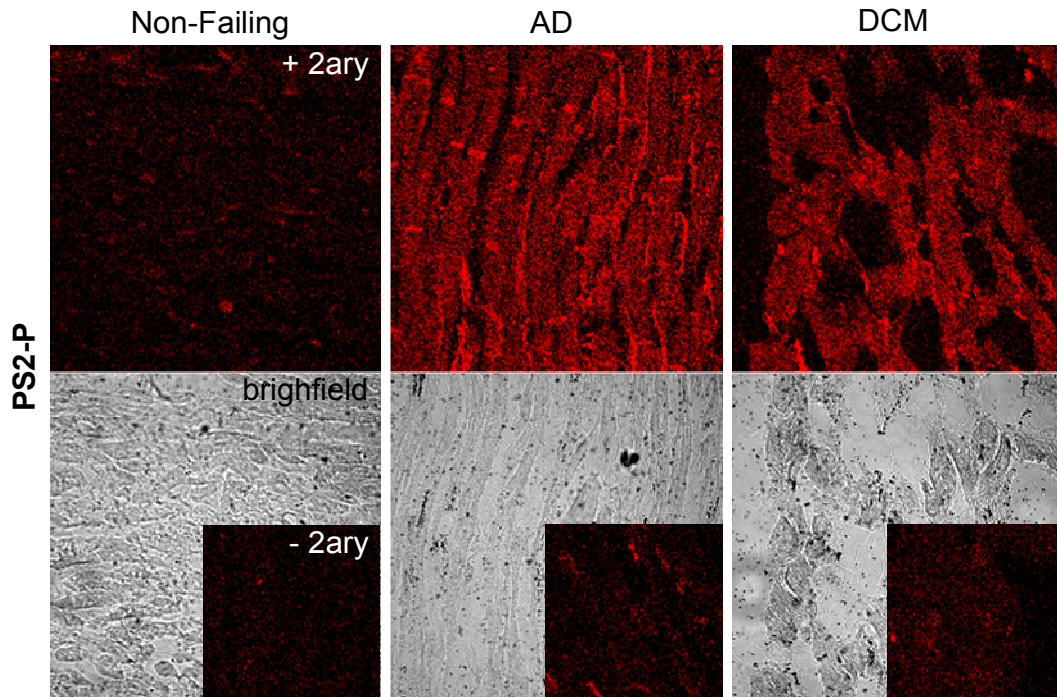
3.8. Immunofluorescence detection of PS1 and PS2 in Non-failing (n=4), Alzheimer (n=2) and DCM (n=6) heart sections. The DCM samples in average showed an increased signal/noise ratio for PS1 and for the phospshorylated form of PS2 (PS2-P). No significant difference was instead observed in the PS2 content between non-failing and DCM. Alzheimer samples showed increased content for all the proteins assayed. In order to determine the autofluorescence of each sample, the small panel on the bottom right corner of each picture shows a mirror sample treated following the same protocol with the exclusion of the secondary antibody incubation. The quantification of the signal of each sample examined was calculated as signal/background ratio. The graphs represent the averages of each group.
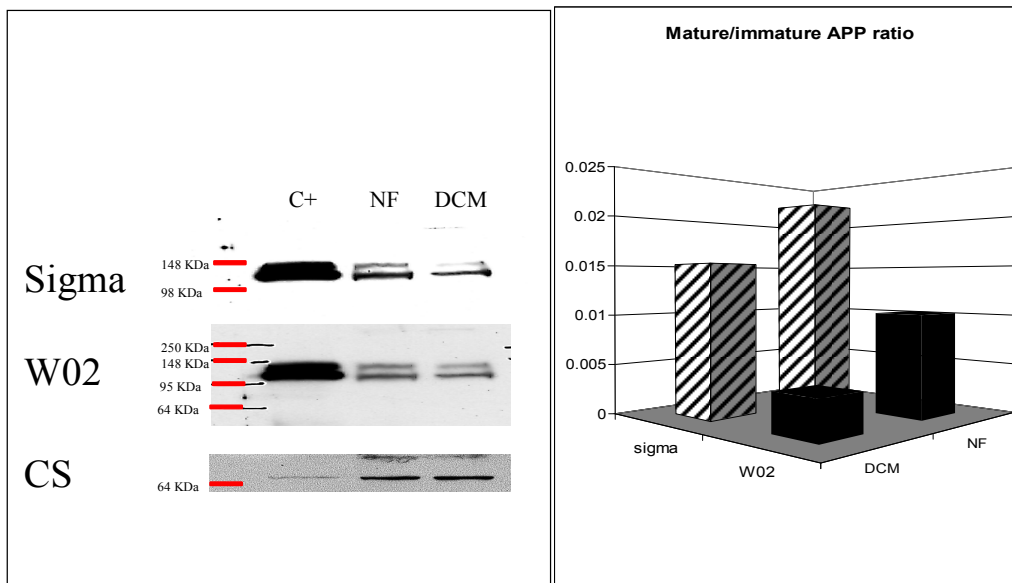
3.9. APP levels in non-failing (n=4) and DCM hearts (n=6). Left panel shows Western blots probed for APP using two different commercial antibodies. In the right panel, densitometric analysis of the amount of mature and immature APP. C+ = APP overexpressing CHO cells. CS= calsequestrin.

we were able to detect a significant increase of its phosphorylated form (antibodies: α-PS1: Millipore, MA dil 1:200, α-PS2: Thermo, MA dil 1:200, α-Phospho-PS2: Calbiochem, MA 1:200, secondary: Alexa 655, Invitrogen, CA dil 1:200). We attributed our incapacity of detecting any change in these last proteins due to a technical limit of the technique or of the antibodies used.

Although γ-secretase interacts and cleaves several proteins, the main substrate of the enzyme complex is APP. In order to verify any alteration of the levels of APP in DCM, we performed Western blot analysis of APP in pooled sarcoplasmic reticulum-enriched preparations. These experiments showed decreased content of APP in DCM samples, both in the native and mature forms (Figure 3.9). The results were confirmed using two different commercially available antibodies (α-APP: Sigma, MD dil 1:2000, Abeta, Germany dil 1:1000). However, these findings resulted in contrast with our analysis based on immunofluorescence, in which we could observe an increased signal/noise ratio in DCM samples compared to non-failing (+ 214%, antibodies: α-APP Sigma, MD dil 1:1000, secondary: Alexa 655, Invitrogen, CA dil 1:200, Figure 3.10). This discrepancy can be attributed to the presence of APP in several cellular
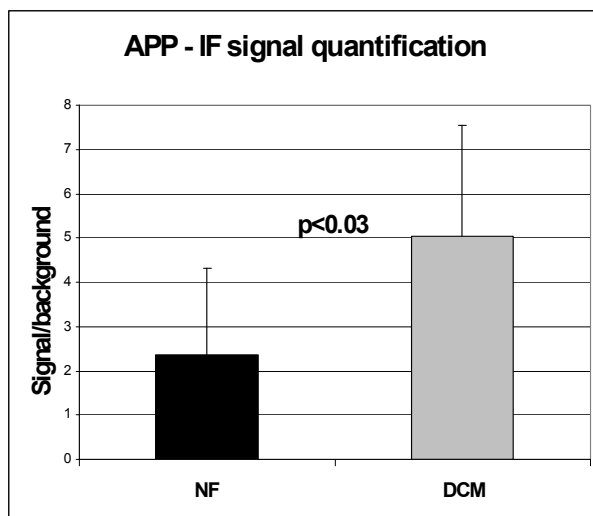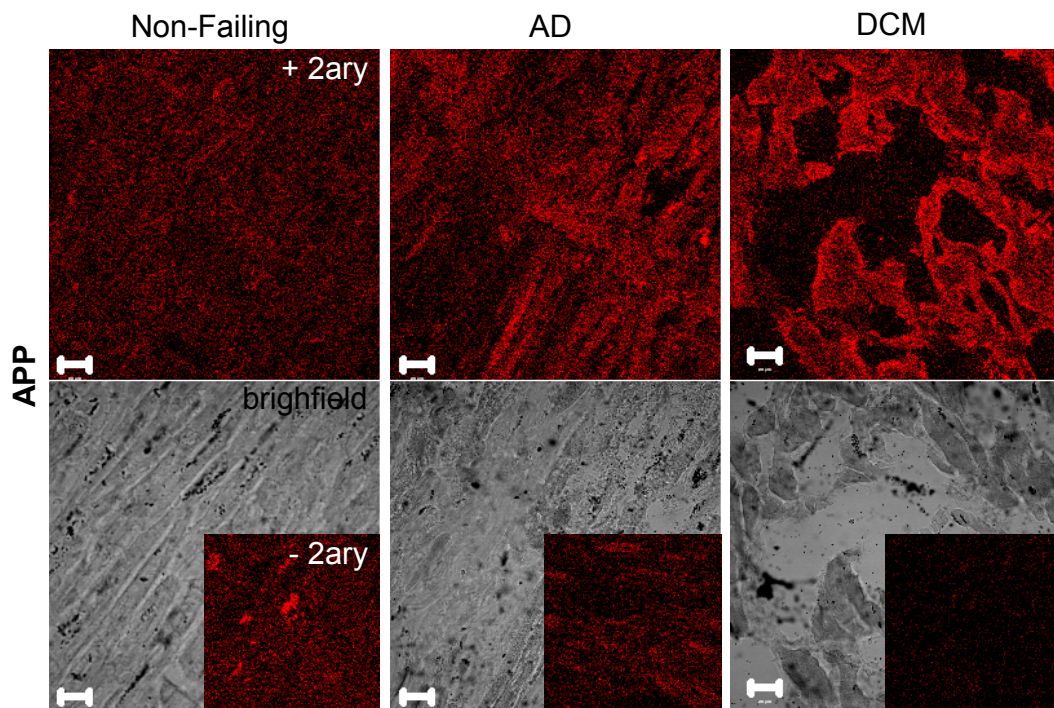
3.10. Immunofluorescence detection of APP on Non-failing (n=4), Alzheimer (n=2) and DCM (n=6) heart slices. DCM samples in average showed an increased signal/noise ratio, while AD samples didn't show any alteration. In order to determine the autofluorescence of each sample, the small panel on the bottom right corner of each picture shows a mirror sample treated following the same protocol with the exclusion of the secondary antibody incubation. The quantification of the signal of each sample examined was calculated as signal/background ratio. The graph represents the averages of each group.

compartments such as the plasma/sarcolemma, which are not included in the sarcoplasmic reticulum preparations used for Western blots.

As Aβ is considered the final product of APP after presenilin-operated processing, we assayed the levels of the peptide by immunofluorescence (antibodies: α- Aβ 6E10 Covance, secondary Alexa 655 α-Rb, Invitrogen, CA dil 1:1000, Figure 3.11). Our results didn't show any significant difference between non-failing and DCM patients. No additional confirmation of the Aβ levels by Western blot was possible due to the unsatisfactory performance of the antibody for this technique.
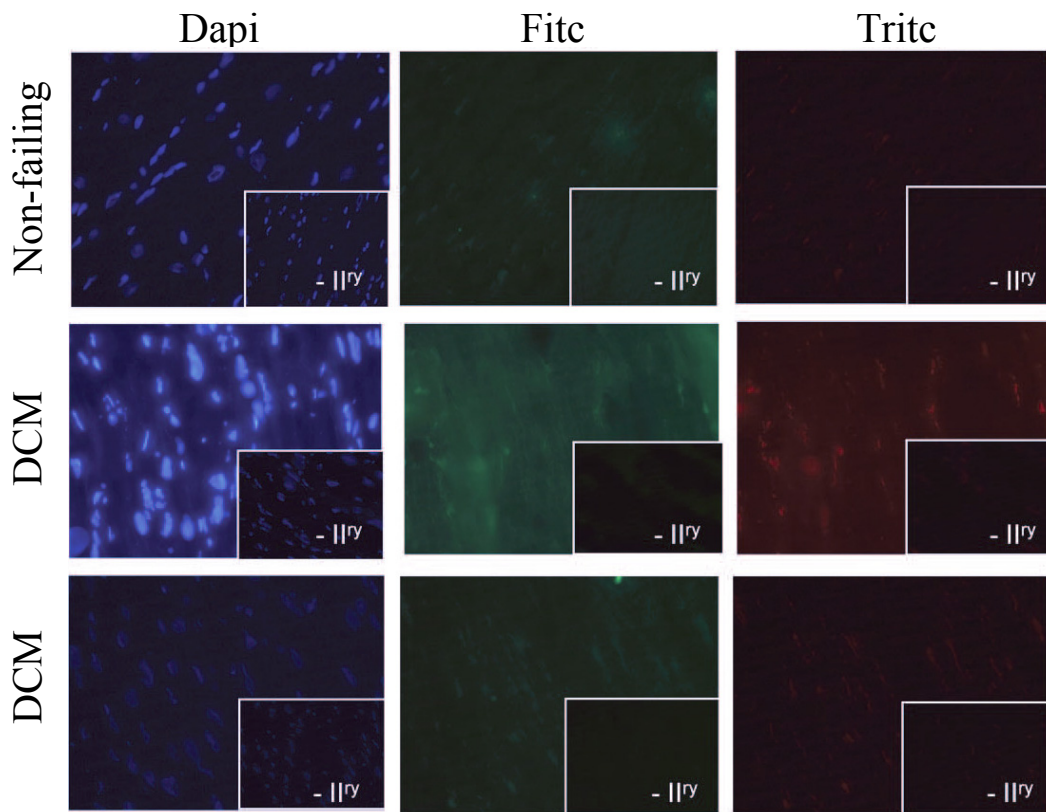
3.11 Immunodetection of Aβ in DCM samples. DCM patients (n=23) do not seem to have increased content of Aβ compared to non-failing samples (n=14). This limits the possibility that Aβ is actively involved in the formation of protein deposits detected by histological and EM-based analysis. The analysis was confirmed with two different fluorochromes to limit the interference due to autofluorescence of the tissue.

3.2.3 Genetic analysis of PSEN1 and PSEN2

Most of the alterations of the levels and activity of the γ-secretase complex in AD patients have been related to specific mutations in the genes encoding PS1 (*PSEN1*) and PS2 (*PSEN2*) (Tanzi and Bertram, 2001). We therefore analyzed the promoter and the coding exons of the two genes in order to identify anomalies that can be associated to the anomalies reported above. Genomic DNA isolated from 20 idiopathic DCM cases was sequenced and compared to the corresponding fragments deposited in public databases. This analysis led to the identification of two unpublished and two previously reported mutations (Table 3.1). In particular patient 14 carried a deletion in position -92 (-92delC) upstream of the alternative transcription initial exon 1A (Rogaev et al., 1997) (corresponding to position

3.1 Presenilin mutations detected in iDCM patients.
The genotype frequency is relative to the total number of DCM cases analyzed (n=20).

Gene	Mutation	UCSC Genome Sequence Database Position	Minor allele Frequency	Genotype Frequency	
PSEN1	-92delC	Chr14:72672839	0.025	CC (95%)	C- (5%)
PSEN1	-21G→A	Chr14:72673257	0.025	GG (95%)	GA (5%)
PSEN1	A953G/E318G	Chr14:72742931	0.025	AA (95%)	AG (5%)
PSEN2	G185A/R62H	Chr1:225138072	0.05	GG (90%)	GA (10%)

72672839 on the University of Califorria – Santa Cruz (UCSC) Genome Chr 14 Database); a different mutation (-21G→A, corresponding to position 72673257 on UCSC Genome Chr 14 Database) was instead found in patient 4 upstream of the alternative transcription initial exon 1B. Patient 4 showed an additional previously reported missense mutation in the coding region of PSEN1 in position 953 (A→G) (Sandbrink et al., 1996), leading to the substitution of glutamate$_{318}$ with a glycine residue. A second previously reported mutation (Cruts et al., 1998) was instead observed in the coding region of PSEN2 (G185A, corresponding to position 225138072 in the UCSC Chr 1 Database and leading to a substitution of an arginine residue with a histidine in position 62 of the polypeptidic sequence) in patients 1 and 14. It is interesting to observe that the three patients showing mutations in the regions analyzed (#1, 4, 14) were female with Caucasian background.

The two novel mutations were characterized *in vitro* to evaluate their functional effects on the expression of PS1. We cloned the regions of the PS1 promoter ranging from 72672641 to 72673058 and 72673065 to 72673530 (according to UCSC Genome Chr 14 Database), which respectively include the two mutations -92delC and -21G→A and the corresponding TATA boxes. The DNA fragments were cloned upstream to the coding region in a vector containing a reporter gene (*Renilla* Luciferase, FLuc) and transfected into H4 human neuroglioma cells to verify the expression of luciferase. Our results showed a significant reduction (75%, p=10^{-7}) of the FLuc activity for the construct containing the -92delC mutation when compared to the wild type allele (Figure 3.12, left). Similarly, we observed a decrease (32%,
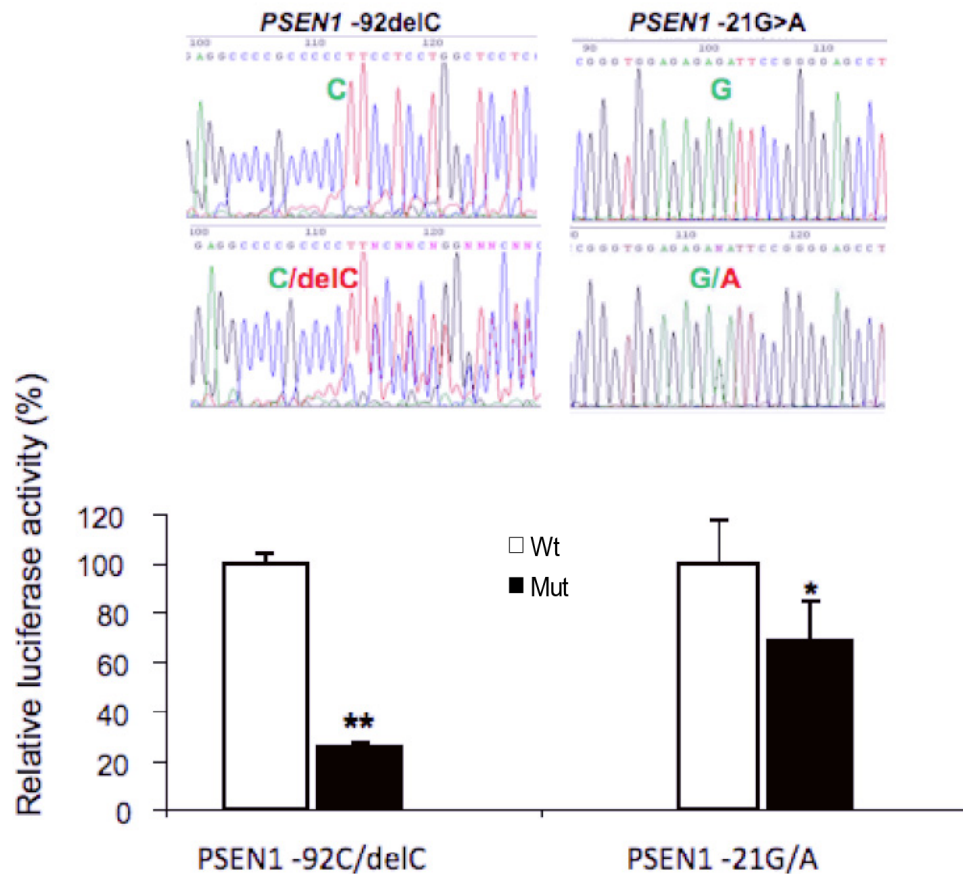
3.12 Analysis of the two novel mutations identified in the PS1 promoter. The activity of the mutated promoter was assayed using *Renilla* luciferase as a reporter gene. Both the alterations showed significantly impaired expression (-92delC: -75%, $p<0.003$; -21G→A: -32%, $p<0.05$).

$p=0.015$) of the luciferase activity in the comparison between the -21G→A mutation and the wild type allele (Figure 3.12, right).

Interestingly, the wild type variant of the promoter showed significantly increased expression for exon 1A versus exon 1B (5-fold).

Further confirmation of the inhibited transcriptional activity associated to the mutations in the *PSEN1* promoter derived from the evaluation of PS1 levels by Western blot (Figure 3.13). Although we observed increased PS1 levels in all the DCM samples, the three patients carrying the mutations (marked by squares) showed decreased PS1/SERCA ratios compared to the average of the DCM group. Because of the central role of the presenilin in APP processing, we investigated whether this alteration was producing modifications in the content of Aβ by immunohistochemistry.
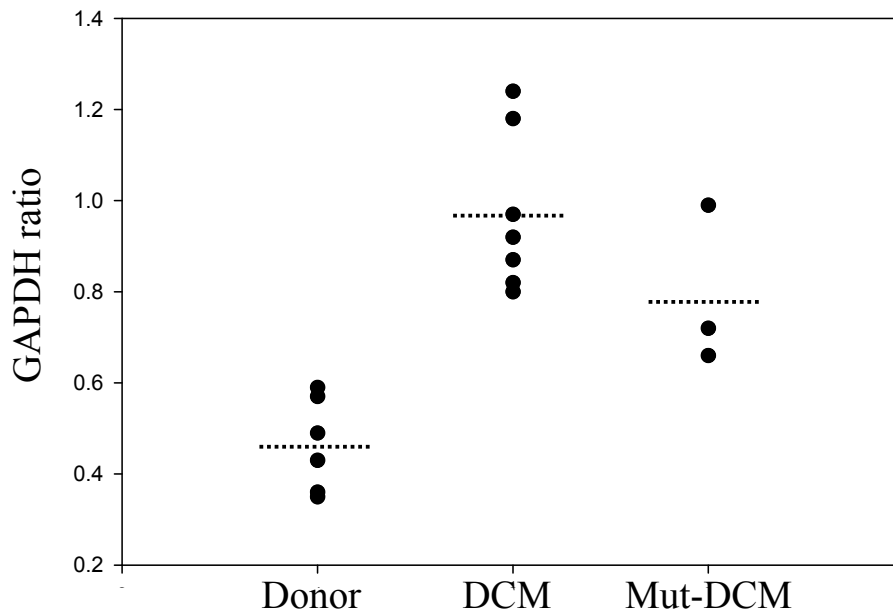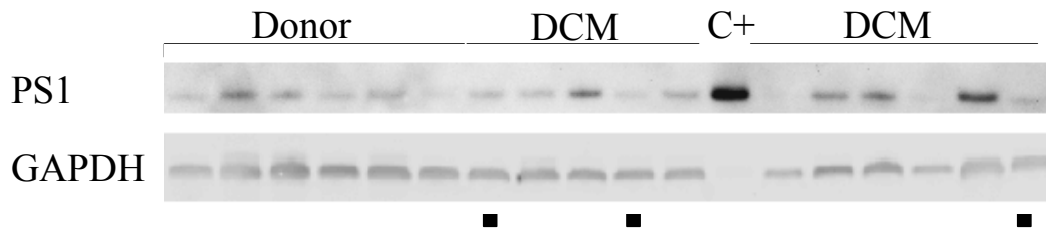
3.13 Analysis of PS1 levels in DCM samples. The content of PS1 appeared increased in DCM samples when compared to non-failing controls (0.93 ± 0.25 vs. 0.56 ± 0.24, p=0.01 from Krustal-Wallis test). The carriers of the newly identified mutations (marked by an arrow in the Western blot) showed lower levels of PS1 than the patients without any variants (0.79 ± 0.18), although our results didn't reach statistical significance. All the values were standarized to GAPDH content. C+= PS1-overexpressing CHO cells.

Our results didn't show any significant change between the mutation carriers and the other DCM patients (Figure 3.14). No additional information regarding the content of Aβ is available due to the unsatisfactory performance of the antibody used for Western blot application.

3.2.4 Population analysis

It is possible that the mutations we describe in this chapter are not specifically involved in idiopathic DCM and they can be associated to other diseases and, in
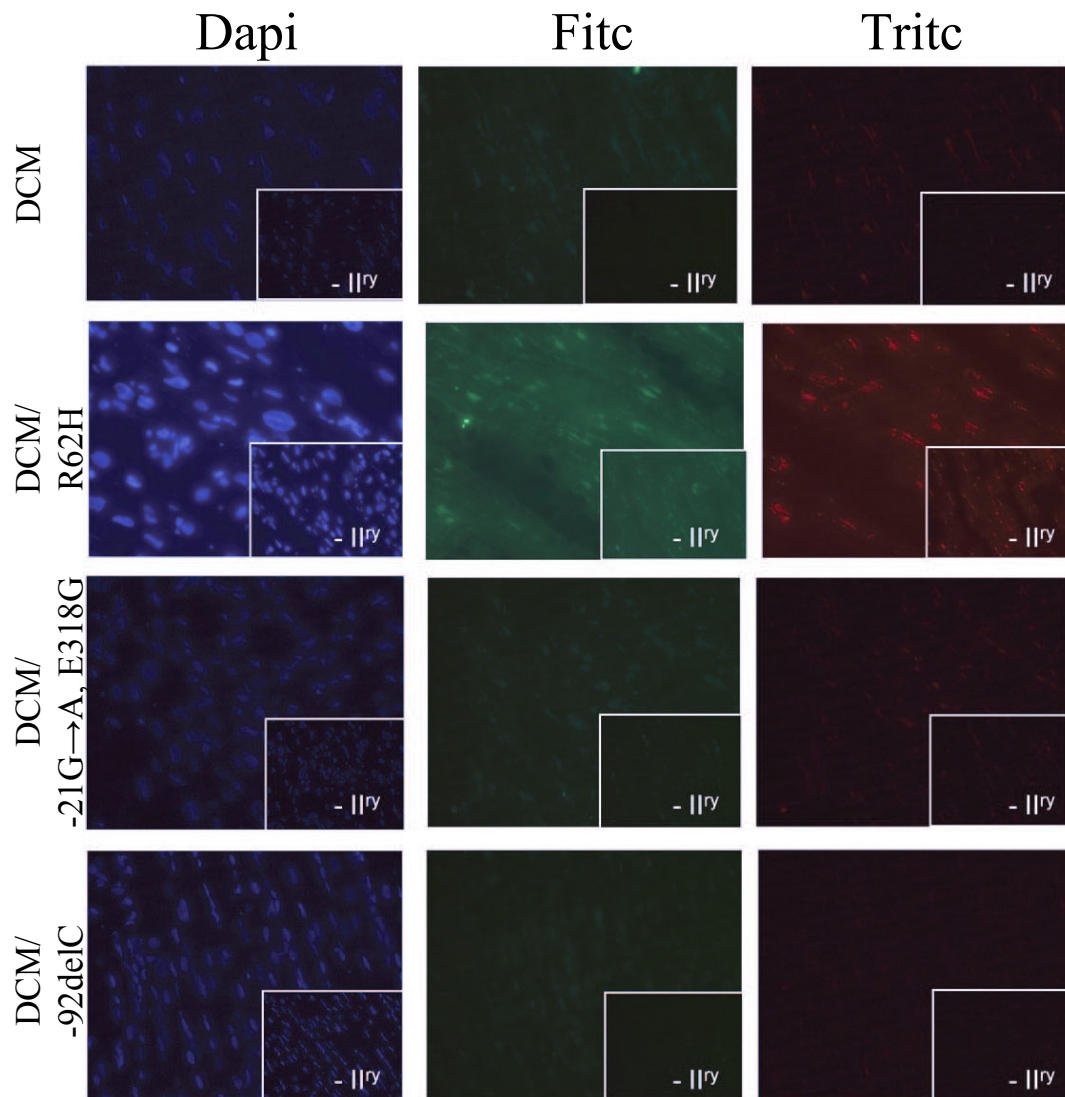
3.14. Immunodetection of Aβ in patients carryng mutations in the Presenilin genes. The alterations of the presenilin genes we described did not induce any significant detectable alteration of the Aβ processing pathway compared to regular DCM samples. The analysis was confirmed with two different fluorochromes to limit the interference due to autofluorescence of the tissue.

particular, AD. In order to investigate this aspect we performed single nucleotide polymorphism (SNP) analysis on existing sequencing data from genomic DNA isolated from AD patients stored in the Massachusetts General Hospital Institute for Neurodegenerative Disorders.

Our analysis showed that none of the AD patients analyzed was showing the mutation -21G→A in PSEN1(Table 3.2); the second mutation in the PSEN1 promoter (-92delC) was instead found in 8 out of 1632 chromosomes analyzed (allele frequency 0.005).

3.2 Population analysis of the mutations detected in DCM samples.

Gene	Mutation	Frequency	Chromosomes analyzed
PSEN1	-21G→A	0	1632
PSEN1	-92delC	0.005	1632
PSEN1	E318G	0.02	596
PSEN2	R62H	0.016	320

The two mutations we found in the coding regions of PSEN1 and PSEN2 were respectively showing allele frequency equal to 0.02 (PSEN1 E318G, found in 12/596 chromosomes) and 0.016 (PSEN2 R62H, 5 chromosomes out of 320 analyzed). The data relative to these last two alterations were in line with previous reported analyses (Sandbrink et al., 1996, Cruts and Van Broeckhoven, 1998, Albani et al., 2007). The evaluation of the segregation of these mutations in identified AD families didn't show any significant association between these mutations and the development of the neurodegenerative condition.

3.2.5 Effects of oligomers on cardiomyocyte function

In the past the presence of amyloid fibers has been closely related to cytotoxicity. However, recent discoveries in the AD field are limiting and reevaluating the role of mature fibers in the perpetration of adverse effects on the cell: according to the most recent theories oligomers have a major role in this process, while the deposition of amyloid fibers could simply represent a defensive mechanism to limit the accumulation of the toxic soluble species in the neurons (Walsh and Selkoe, 2004, Cleary et al., 2005). These observations raised the possibility that similar properties of the oligomers may be valid also in non-neural cell types, including the cardiomyocytes.

The mechanism(s) involved in the cytotoxic effect has still not been completely elucidated: some groups proposed that the presence of oligomers alters the Wnt pathway ultimately leading to significant decrease of the content of β-catenin (Hedgepeth et al., 1997, Inestrosa et al., 2005). Other theories, instead, suggested a direct involvement of the oligomers in the formation of unregulated cation channel in
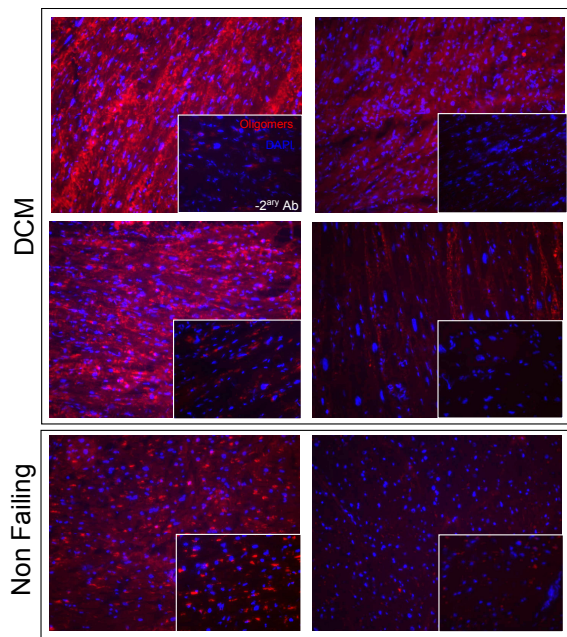
3.15. Oligomer immunofluorescence. Immunofluorescence analysis of DCM (n=23) and non-failing n=14) samples showed a significant difference in the content of oligomers between the two groups analyzed. The small box in the lower right corner of each image shows the background level obtained on mirror slices not incubated with the secondary antibody.

the membrane, eventually leading to the activation of the apoptotic cascades and induction of oxidative stress (Demuro et al., 2005).

We first evaluated whether the accumulation of unfolded β-sheeted protein fibers in the cardiomyocytes was associated to the presence of other species characterized by lower molecular complexity, such as oligomers. We based our experimental approach on the use of a structural antibody developed by Dr. Glabe's group, characterized by the capacity of specifically recognizing the three-dimensional structure of oligomers with no cross reactivity with mature amyloid fibers. This antibody has been proven to bind most of the oligomeric species described to date independently from their amino-acidic sequence (Kayed et al., 2003).

We examined 23 cases of idiopathic DCM and compared them with 14 non-failing samples by immunohistochemistry. As expected all the DCM showed higher intensity staining than non-failing (antibodies: α-oligomers Invitrogen, CA dil 1:400, Figure 3.15). Of note some of the non-failing samples showed some levels of positive signal to this analysis. However the signal/background ratio was significantly higher in the DCM group.

In addition we investigated the presence of oligomeric species in early-stage DCM cases before evident unfolded protein deposits were detectable in the cardiomyocytes. Due to the limited amount of material, biopsies from the patients (n=2) were stained
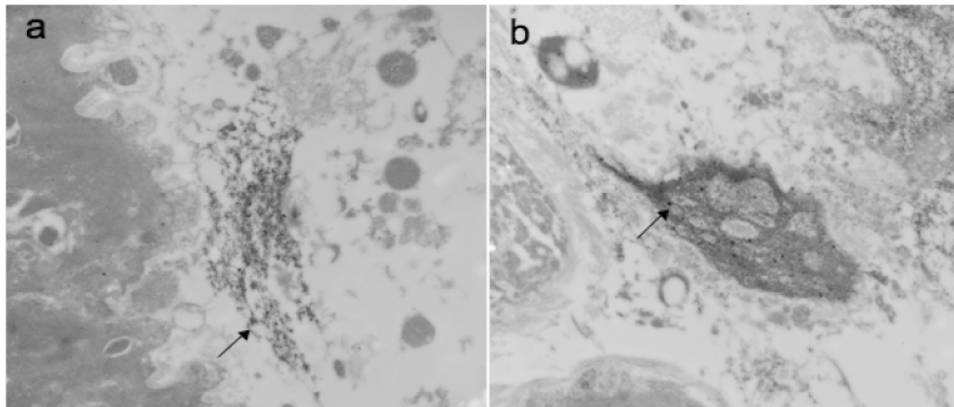
3.16 Electron microscopy analysis of DCM samples. Staining with antibodies conjugated with colloidal gold particles showed the presence of oligomers in the myocardium (arrows). a = early stage DCM, b = end stage DCM before LVAD implantation.

with the immunogold technique using the structural antibody previously mentioned and analyzed by electron microscopy (antibody: α-oligomers, Invitrogen, CA dil 1:400, secondary: gold-conjugated DAKO, DK dil 1:20). In addition this technique presented the advantage of a higher sensibility compared to the immunofluorescence approach previously adopted. Interestingly, early-stage DCM showed diffused presence of oligomers, similarly to what was observed in the core of myocardium deriving from an end stage idiopathic DCM patient removed for left ventricular assist device (LVAD) implantation (Figure 3.16).

This evidence regarding the presence of oligomers in idiopathic DCM heart does not necessarily correlate to a toxic effect of the β-sheeted structure on cardiomyocytes leading to degeneration of ventricular function. To assess this question we exposed isolated adult mouse cardiomyocytes to oligomers generated *in vitro* from commercially available lyophilized Aβ (Figure 3.17a), supporting this choice with recent findings suggesting that the adverse effects of oligomer species are exclusively mediated by their three-dimensional structure independently of their amino-acid sequence (Demuro et al., 2005). Different concentrations of oligomers (0.5-5 μg/ml) were administered to the cardiomyocytes while contractility and Ca^{2+} transient were recorded. Our results showed that the release of oligomers on the cell surface produced significant increase of peak systolic content of Ca^{2+} and of the velocity of Ca^{2+} release (Figure 3.17b). These alterations produced consistent anomalies in the cell contractility (Figure 3.17c).

3.17 Effects of oligomers on murine isolated cardiomyocytes. The preparations used in the experiments were tested by dot-blot at different time points to identify the peak in oligomer content (A, top panel). In addition the oligomers were tested by EM for their capacity of forming fibers after exposure to hexane (bottom panels, left: insoluble pellet, right: oligomers-containing supernatant). The preparations were administered to isolated cardiomyocytes producing alteration of the contractility (B, top left panel) and impairment of Ca^{2+} handling (B, bottom left panel) compared to PBS - treated cardiomyocytes (B, right panels). The quantification of the alterations in Ca^{2+} content showed significant reduction of the systolic concentration (C, left panel) and of the velocity of release (right panel). For statistical purposes we repeated the experiment in presence of oligomers on cardiomyocytes derived from three different animals. As control we instead used cardiomyocytes from two animals, which were exposed to PBS instead of the PBS/oligomers solution. Three cells/animal were recorded.

C
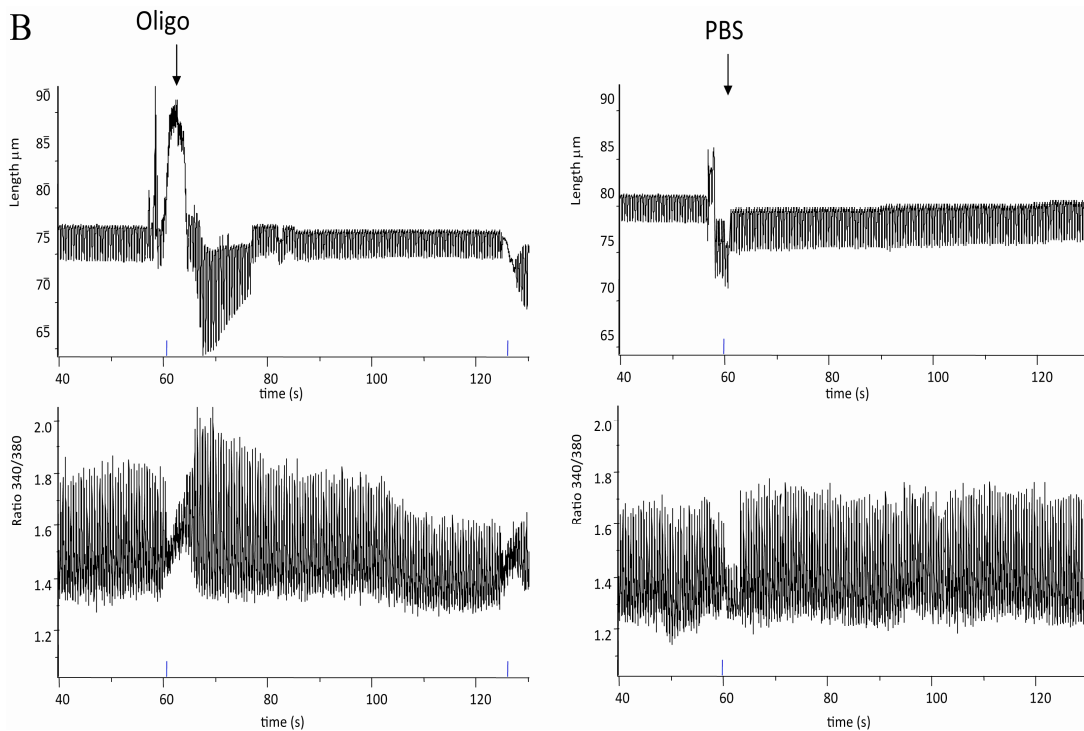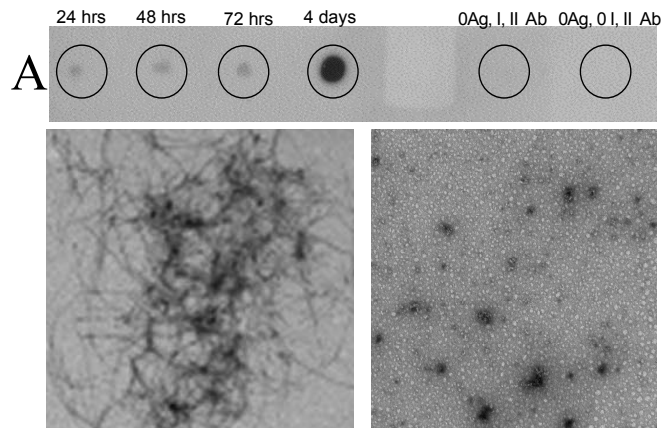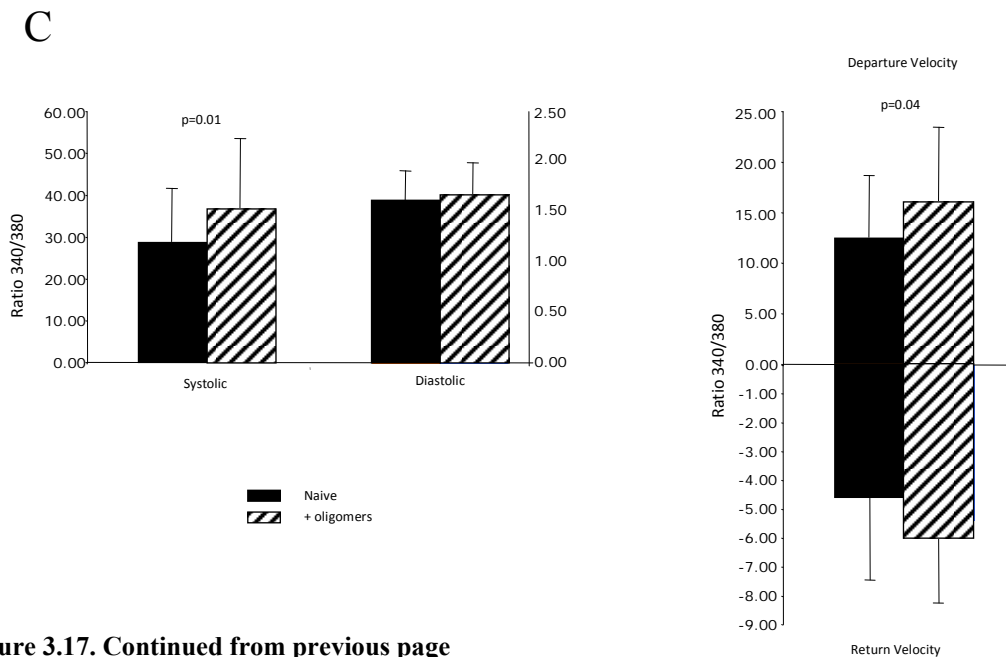
Figure 3.17. Continued from previous page

3.2.6 Evaluation of UPR-component levels

As the accumulation of β-sheeted unfolded species has toxic effect on the cell, eukaryota evolved mechanisms to prevent the formation of oligomers and amyloid fibers, which have been grouped as unfolded protein response (UPR).

In our analysis we selected several key components of the UPR in order to identify which pathways are activated following the events we described in this chapter. In particular we focused on proteins involved in the control of the folding process (chaperones GRP78 and 94), peptides related to the ubiquitin/proteasome pathway (Ubiquitin, RTP3 and RTP5 of the proteasome 19S subunit, β2, β5 and α6 of the 20S subunit), transcription factors induced or modified during an unfolded protein shock response (ATF6, eIF2αP, Chop, XBP1) and a protein regulating the apoptotic process (Caspase12). We analyzed the content of the mentioned peptides by Western blot using SR-enriched preparations (for SR peptides such as GRP78 and GRP94) or whole cell lysates (Figure 3.18). As expected, our results showed significant increase in DCM samples for the chaperones GRP78 and GRP94 (respectively +198% and +273%, antibodies: not commercially available - generous gift of Dr. A.M. Lompré,

dil 1:500), the transcription factors Chop (+134%, antibody: BioLegend, dil 1:500) and ATF6 (both in the native (+162%) and active (+158%) forms, antibody: Imgenex, dil 1:500) and for Caspase 12 (+165%, antibody: Abcam, dil 1:1000). No significant differences were instead observed between non-failing controls and DCM patients for ubiquitin (antibody: Sigma dil 1:500), α6 (antibody: Biomol International, dil 1:1000), β2 (antibody: Biomol International, dil 1:1000), RPT3 (antibody: Biomol

3.18 Analysis of UPR-related protein content in DCM (n=9) and non-failing (n=6) samples. DCM samples showed significantly decreased levels of 20S-β_5 (-60%) and increased content of ATF6 (active, +158%, and native, +162%, forms), Caspase 12 (+165%) and Chop (+134%).

No alterations were instead observed for the phosphorylated form ofE2IFα, XBP1, Native ATF6, Ubiquitin, 19S-Rtp3, 19S-Rtp5, 20S-α_6 and 20S-β_2. All the levels were calculated as ratios of GADPH content. (Continued on next page)
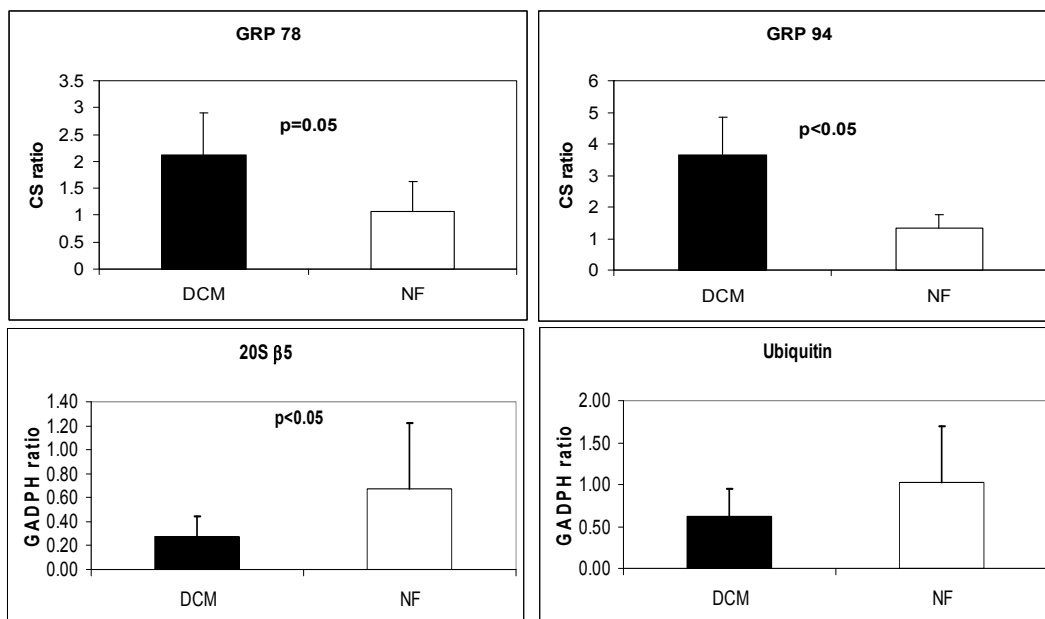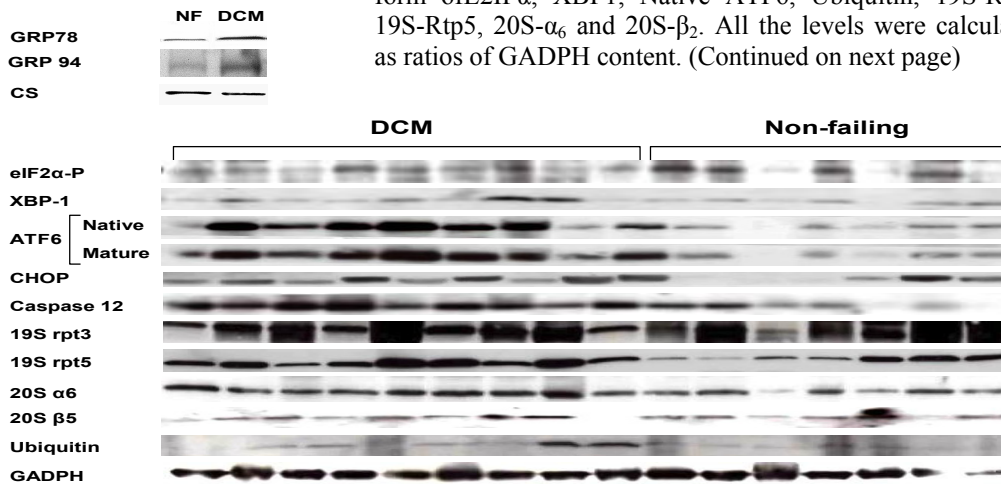
Figure 3.18. Continued from previous page
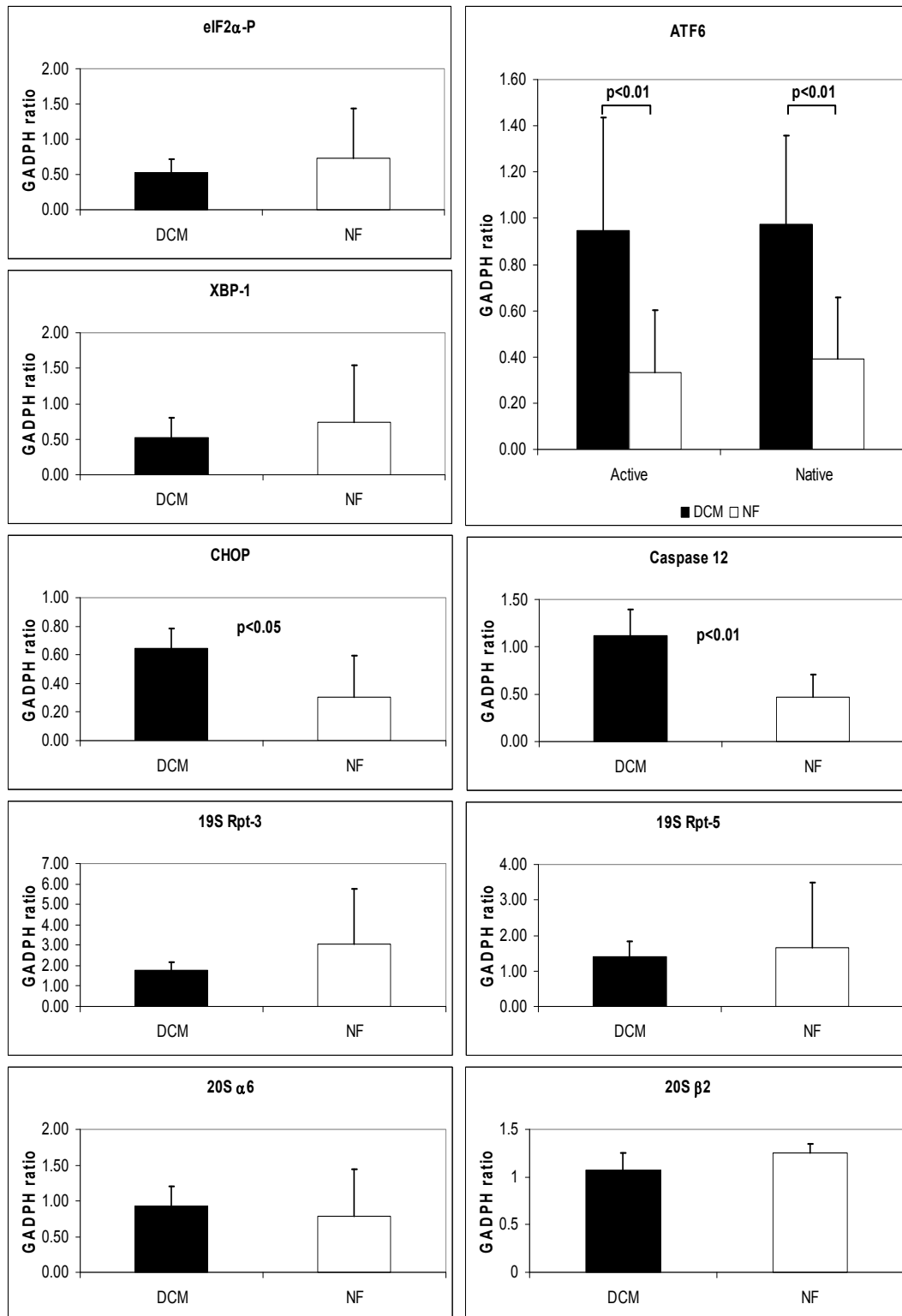
International, dil 1:1000), RTP5 (antibody: Biomol International, dil 1:1000), XBP1 (antibody: Santa Cruz, dil 1:200) and eIF2αP (antibody: Cell Signaling dil 1:1000). Of note, DCM samples showed lower content of one of the catalytic subunits of the 20S proteasome (20S β5, -60%, antibody: Biomol International, dil 1:1000).

3.3 Discussion

In this chapter we focused on the determination of the etiology of idiopathic DCM, a common cause of heart failure. The mechanisms responsible for the development of this condition and its evolution to heart failure are currently obscure. Our analysis allowed us to identify a series of unknown molecular mechanisms which are summarized in Figure 3.19. In particular, we described the presence of consistent amounts of unfolded protein material in DCM hearts, which were characterized by the β structure typically observed in amyloid fiber, as confirmed by staining with amyloid-specific dyes such as Congo Red and thioflavin-S. Ultrastructural observation of these deposits showed preferential distribution in the cytoplasm of cardiomyocytes and no apparent correlation with any known form of aggregates. As expected the formation of amyloid fibers was also associated with the presence of intermediates still characterized by the β-sheeted structure but with lower molecular complexity. In particular we were able to identify a diffuse presence of oligomers in the diseased heart of both early and late stage patients.

The presence of unfolded peptides assuming β-sheeted structures has been associated to negative effects on the metabolism of the cell for many years. Therefore, the findings we report strongly suggest the existence of substantial relationships between the presence of this structurally disorganized material of proteic origin within the cardiomyocytes and the development and progression of idiopathic DCM. This hypothesis is supported by our results deriving form normal isolated murine cardiomyocytes exposed to increasing concentration of artificial oligomers, which showed limited tolerance of the cell to these molecules. In particular our observations
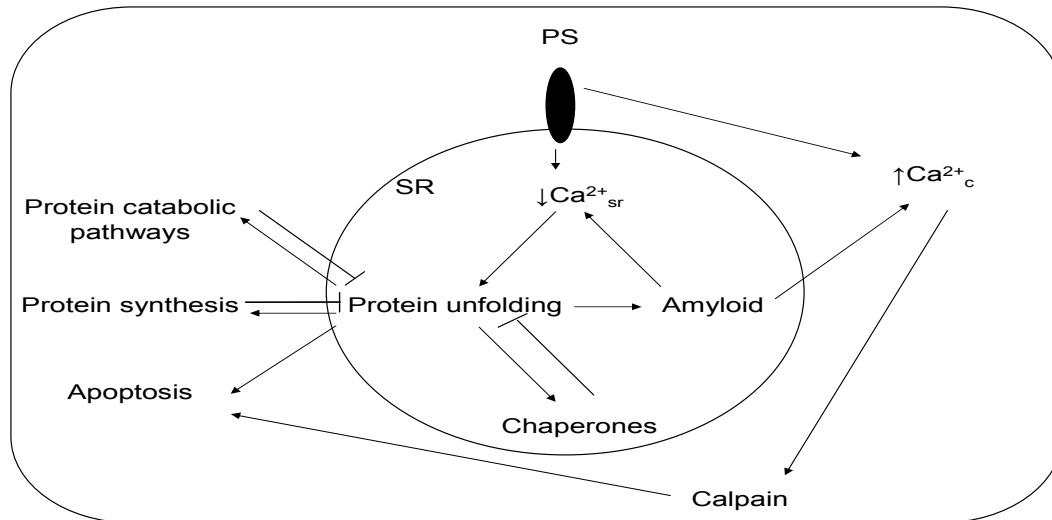
Figure 3.19. Schematic representation of the mechanisms described.

demonstrated severe alterations in the contractility of the cell and in Ca^{2+} handling, which, eventually, produced cell death.

In addition our study focused on the characterization of proteins involved in the etiology of foldopathies and that have been reported to be related to Ca^{2+} regulation, such as PS1, which showed interaction with SERCA by co-immunoprecipitation. In particular we analyzed the levels of PS1, PS2 and Phospho-PS2 in DCM-affected hearts, showing critical increase of the first associated with a significant drop in the expression of PS2 (that instead appeared to be present mostly in the phosphorylated form). Our findings also showed that the principal substrate of the presenilin (i.e., APP) was increased as resulted form immunofluorescence analysis of the protein on cardiac tissue, although the levels in the SR membranes appeared decreased by Western blot. These contrasting observations may be attributed in first place to the distribution of APP in the cell (as the molecule processing follows a complex pathway involving different cellular compartments than the SR), but also to an artifact due to the preferential localization of the transmembrane peptide in lipid rafts, which are detergent-resistant structure and, therefore, are removed as insoluble material during the preparation of the samples. Further characterization of the γ-secretase system in DCM patients showed a series of mutation in the genomic sequence of *PSEN1* and *PSEN2* genes. In particular we were able to identify two previously reported alterations in the cds of the genes and two unknown mutations in the promoter region

of *PSEN1* (-92delC and -21G→A), which were characterized in vitro and resulted able to induce significant decrease of the expression of the downstream ORF.

A last interesting group of observation we reported in this chapter was related to the characterization of the UPR. In particular our experiments showed increased levels of the SR chaperones GRP78 and GRP94 and of the pro-apoptotic factors Chop and Caspase 12.

One of the prominent features of idiopathic DCM is the impairment of Ca^{2+} re-uptake in the sarcoplasmic reticulum. This defect leads to increased concentration of the ion in the cytosol, followed by activation of the sarcolemma Ca^{2+} transport systems (including Na^+-Ca^{2+} exchanger and Ca^{2+} ATPase) and, eventually, by progressive depletion in the cellular storage compartments and in particular in the SR. As the SR is one of the most important locations for protein folding and post-translational modification, any major alteration of the microenviroment of the organelle produces significant outcomes on several cell functions. In particular, the accumulation of unfolded proteins has been largely related to severe impairment of relevant cellular functions in several neurodegenerative disorders and other chronic diseases (Gething and Sambrook, 1992, Ross and Poirier, 2004, Gorza and del Monte, 2005). In this study we report the presence of unfolded protein deposits in cardiac samples deriving from idiopathic DCM patients, suggesting the existence of common underlying etiologies between this cardiac condition and other amyloid-related pathologies. Although we didn't specifically address the consequences of the presence of β-sheeted peptides on human cardiomyocytes, we were able to determine the devastating effects of unfolded fibers on the mechanical and Ca^{2+} handling properties of cardiac cells isolated from normal adult mice. This evidence considerably supports the hypothesis that analogous effects may occur in idiopathic DCM.

The accumulation of unfolded protein is a common characteristic of the aging process in several tissues and organs. In the heart these deposits are present as senile plaques and are characterized by an amyloid-like structure. Senile plaques have been described in normal non-diseased individuals over 60 years old (de Exel Nunes et al., 2006, Steiner and Hajkova, 2006), with a peak of incidence of 25% in the population

over the 8th decade of age (Cornwell et al., 1983). For the first time we report the presence of β-sheeted species in relatively younger patients affected by idiopathic DCM. Of note, our analysis included a limited number of biopsies deriving from subjects in the early stages of the disease that showed results comparable to the data obtained in late stage DCM individuals. These findings represent an important confirmation of the fact that the unfolded proteins may have an active role in the etiology of idiopathic DCM and, additionally, they significantly exclude the possibility that their presence is a mere consequence of the aging process or of the devastating effects of the late-stage failing condition. Thus, our results propose an alternative vision of the idiopathic form of DCM as a premature aging process of the cardiac muscle, similarly to how early-occurring neurodegenerative diseases such as AD compare to senile dementia.

The presence of β-sheeted protein fibers has been directly associated to negative effects on the cell metabolism for a long time. However these insoluble aggregates represent only the endpoint of a process during which a monomeric unfolded protein reaches progressively higher levels of molecular complexity including oligomers, protofibrils and fibrils. The most recent findings in the AD field showed that soluble oligomers are the most prominent mediators of the β-amyloid-associated toxicity on neurons (Cleary et al., 2005, Lansbury and Lashuel, 2006). In the current study we demonstrated the presence of oligomers in the myocardium of idiopathic DCM patients. In addition, we report the effect of this form of molecular aggregates on cardiomyocytes, showing for the first time a significant spike in the systolic Ca^{2+} concentration after administration of oligomers to cells, which may lead to metabolic alterations and eventually to death (Stevens and Argon, 1999, Chandrashekhar and Narula, 2003, Del Monte and Hajjar, 2008). Although our results contribute to the improvement of our knowledge about the pathological mechanism associated to the degeneration of DCM cardiomyocytes, these data introduce new and intriguing hypotheses on the role of these molecule in the etiology of the disease. In fact, we can not exclude that the presence of oligomers might be a pre-existing condition to the Ca^{2+} homeostasis alteration mainly associated to non-fully penetrant mutations or to the age-related degeneration of the catalytic pathways of the cell. Consequently, the

progressive accumulation of these molecular species might be able to produce Ca^{2+} handling alterations which might lead to the well-known alteration of the cell but, in addition, also exacerbate the process of formation of oligomers. Although extremely interesting, this hypothesis require further investigations that could be performed for example on animal models once the protein(s) involved in the formation of the oligomers are identified.

It is interesting to observe that alterations in Ca^{2+} handling have been investigated also in AD in the last decade (LaFerla, 2002). Indeed several studies have reported that γ-secretase have multiple roles in the regulation of the intracellular Ca^{2+}. These include the capacity of forming a cation permeable channel responsible for the vast majority of passive Ca^{2+} leaks from the ER (Tu et al., 2006) and the modulation of the RyR by direct interation (Hayrapetyan et al., 2008) or by cleaving sorcin (Pack-Chung et al., 2000). In addition, the proteins forming the catalytic core of γ-secretase seem to have significant interactions with SERCA –one of the key proteins in the excitation-contraction coupling process-, attenuating its function when the presenilins are downregulated (Green et al., 2008). According to our results significant interaction is present between the cardiac-specific isoform of SERCA (2a), suggesting that the regulation mechanism observed by Green et al. may be valid even in the heart (Green et al., 2008). As a consequence, the increase of PS1 we observed in DCM samples may be explained not only as a compensatory process to balance the drop in PS2 but also as a protective mechanism initiated by cells in order to indirectly stimulate SERCA2a activity to prevent Ca^{2+} accumulation in the cytosol.

The genomic characterization of the presenilin genes led to the identification of two novel alterations of the *PSEN1* promoter in three patients (-92delC and -21G→A), both related to severe downregulation of the expression of the relative genes, decreased content of the relative protein compared to other idiopathic DCM samples and, most likely, inhibition of SERCA2a activity. Our analysis allowed also the identification of two previously described mutations in the coding region of *PSEN1* and P*SEN2*. In particular *PSEN1* E318G produced the modification of a polar acidic (glutamate) into a neutral residue (glycine) in the large cytoplasm loop between the transmembrane domains 6 and 7. This domain is considered a "hot spot" of the

molecule due to the large number of AD-related mutations identified: indeed, alterations in this region have been related to altered cleavage of the N- and C-termini of PS1 (Thinakaran et al., 1996) with consequent reduced capacity of docking the target proteins (Mah et al., 2000, Xia, 2008). Instead, the mutation found in PSEN2 (R62H) maps in a different "hot spot" located in the N-terminus of the molecule. This alteration has been related to increased degradation of the molecule, reduced stability and impaired Notch processing in both AD (Cruts et al., 1998) and breast cancer (To et al., 2006).

Although PS1 and PS2 are characterized by high homology, it is interesting to observe that the two mutations in the coding sequence we detected map in two of the most diverse domains. This suggests that these two regions may have an important role in modulating different functions of the proteins in the heart, that, according to our results are neither related to alterations in the APP processing nor to altered levels of Aβ.

One of the most common cellular responses to the accumulation of unfolded peptides consists in the activation of a large array of mechanisms aimed to eliminate the amyloid produced and to prevent the formation of new fibers. These mechanisms are grouped in the unfolded protein response (UPR). Several studies have described the alteration of several components of this system in foldopathies (Lindholm et al., 2006). In particular, the presence of Aβ in AD-affected neurons seems to trigger the expression of important components of the UPR such as GRP78 and PERK (Hoozemans et al., 2005) (which reflects a neuroprotective activity), and, eventually, activation of the apoptotic pathway mediated by Caspase 12 (Nakagawa et al., 2000).

Our characterization of the key components of the UPR revealed a significant increase in the levels of several of the tested proteins as an expected cardioprotective reaction to the accumulation of β-sheeted deposits. However the substantial increase in Chop and Caspase 12 levels suggests that the cardiomyocytes are mostly prone to apoptosis, especially in late stage DCM such as the samples we used for this analysis.

In addition it was interesting to observe that the catalytic subunit β_5 of the 20S proteasome showed significantly lower expression. As the proteasome seems to be actively involved both in processing and degrading presenilin 1 (Honda et al., 1999),

we can speculate that the alteration we are reporting may have an primary role in determining the increase in PS1 we described in this chapter. This hypothesis is supported by several recent clinical observations on the use of the proteasome inhibitor bortezomid for different forms of tumors: indeed, administration of this chemotherapic agent in patients resulted in the development of severe acute heart failure (Voortman and Giaccone, 2006, Hacihanefioglu et al., 2008), which was reverted by interruption of the treatment.

In conclusion, the data we present in this chapter considerably support the hypothesis of an active role of protein misfolding in the pathogenesis of idiopathic DCM. Our results show that the formation of oligomers induces alteration of the Ca^{2+} handling and toxicity for the cell. In addition alterations of the genes encoding the presenilins produces modification in the structure and in the expression of the proteins, which may lead to exacerbation of Ca^{2+} mishandling due to the proven interactions of these peptides with key elements of the excitation-contraction coupling.

However, our findings did not completely elucidate whether the aggregates we describe have a primary active role in the etiology of the condition leading to the well-described Ca^{2+} alterations or they are merely a consequence of pre-existing Ca^{2+} handling anomalies with deleterious effects on the progression of the disease. As a result of these observations, a better elucidation of the proteins involved in the formation of unfolded species is critical to the development of early diagnosis marker and new approaches for the treatment of DCM.

3.3.1 Limitations

Although our results open new and intriguing perspectives in the determination of the etiology of DCM, we should consider some technical limitations related to the experiments presented in this chapter.

First, the determination of the toxic effects of the oligomers on isolated cardiomyocytes was determined administering pre-formed oligomers to the cells in the extracellular space. In this chapter we extensively demonstrated the presence of intracellular oligomers amyloid deposits in DCM samples, but we obtained only marginal evidences of the presence of unfolded proteins in the extracellular space.

154

Therefore, the use of exogenous pre-formed oligomers should be seen as a model in which the effects of the intracellular oligomeric species are not specifically investigated. However, we consider this approach the best model to our knowledge for this type of study. In fact, a solution for this issue could be obtained from the use of regulated promoters for the intracellular expression of amylogenic peptides, but the technologies currently available for this purpose are still showing consistent limitations in terms of elimination of background expression. In addition, the kinetics of the activation of these promoters might be incompatible with *in vitro* studies on isolated cardiomyocytes due to the limited survival of these cells.

A second limitation derives from the incomplete characterization of some of the samples used in the experiments. In fact the use of SR preps in some of the Western blots presented in this chapter would have required a preliminary evaluation of the contamination with membranes deriving from the sarcolemma and other organelles. This could have been estimated performing assays for proteins belonging to the SR (such as SERCA2a) and for proteins usually non present in the SR (such as Na^+/K^+ ATPase and 5' nucleotidase) as previously described (Jaqua-Stewart et al., 1979).

An additional group of limitations of the study we presented is instead associated to the possibility of unspecific binding in the techniques involving the use of antibodies. Although we tried to control this issue with preliminary blocking steps to saturate unspecific binding sites, it is crucial to exclude the possibility that our conclusions might derive from erroneous data interpretation. In this regards, the confidence in our results might have been improved by adding a series of positive and negative controls. For example, the co-immunoprecipitation experiments might have beneficed form the evaluation of the capacity of the proteins tested to unspecificallly bind the protein G-coated sephadex beads in absence of the antibody and/or in presence of a non-specific immunoglobulin belonging to the same isotype. Similarly, it would have been important to determine the role of unspecific binding in the immunofluorescence experiments by verifying the intensity of the signal in absence of the primary antibody, while our negative controls were only focused to determine the interference deriving from autofluorescence of the tissue.

CHAPTER 4

ISOLATION AND IDENTIFICATION

OF UNFOLDED PEPTIDES IN

IDIOPATHIC DILATED

CARDIOMYOPATHY

4.1 Introduction

Protein aggregation is a common characteristic of several degenerative diseases usually affecting the central nervous system (Kopito and Ron, 2000). In the heart the formation of amyloid fibers has been related to the occurrence of conduction disturbances and deterioration of the contractile function associated to a progressively increased stiffness of the cardiac tissue known as restrictive cardiomyopathy (Nihoyannopoulos and Dawson, 2009). This process is usually related to alterations in plasma proteins such as serum amyloid A (SAA), transthyretin (TTR) or light chain immunoglobulins which are not normally synthesized in the heart, but are transported to the organ from a remote location by the plasma. More recently, the formation of intracellular cardiac-specific amyloid fibers has been described as a result of the accumulation of unfolded desmin due to a mutation in the molecular chaperone α-β crystallin (CryAB) (Sanbe et al., 2004).

In the previous chapter we documented the presence of intracellular non-CryAB-related unfolded protein aggregates in late-stage iDCM samples and we demonstrated their deleterious effects on the normal activities of the cardiomyocyte and, in particular, on the contractile function. In addition, we showed a general upregulation of several proteins involved in controlling the accumulation of unfolded proteins. However, the molecular mechanisms leading to the accumulation of protein aggregates in cardiomyocytes remain still obscure.

In the past, the characterization of protein(s) implicated in the formation of amyloid complexes represented a critical step in elucidating the pathogenesis of the related diseases (Khan and Falk, 2001). One of the most commonly used methods was based on the genetic identification of the gene(s) involved by linkage analysis in individuals affected by the familial form of the pathological conditions (Tanzi et al., 1987). However, this approach has several limitations mainly related to the influence of epigenetic factors or to incomplete penetrance of the genetic defects. Therefore the purification and biochemical analysis of the amyloid structures represents a valid alternative to the genetic characterization for the identification of amyloigenic

proteins in those pathologies in which no clear evidence of familial inheritance is available, such as iDCM.

The major obstacle related to the biochemical characterization of amyloid consists in the remarkable heterogeneity of the peptides forming the structures. To date at least 20 amyloigenic proteins have been identified with highly different amino-acid sequence but with comparable capacity of producing similar three-dimensional β-sheeted fibers. This leads to significant differences in the chemical and physical properties of the amyloid fibers, including different density and different sensibility to detergents, reducing and denaturing agents (Kaplan et al., 2003).

All the successful protocols for isolating amyloid fiber described to date are based on several methods which have been developed since the beginning of last century. These methods can be classified in four large groups:

- Methods based on surface characteristics (such as solubility);
- Methods based on structural properties (such as size and shape);
- Methods based on bioproperties (such as affinity);
- Methods based on net charge.

In this chapter we will develop different biochemical approaches for the purification of the unfolded peptides that we localized in the intracellular space of cardiomyocytes. As the accumulation of insoluble amyloid fiber is always associated to the presence of soluble oligomers with different biochemical characteristics (Glabe, 2008), we designed distinct and parallel experimental plans focused on the isolation of either the soluble or the insoluble species.

Most of the experiments presented in this chapter are meant to be considered as pilot tests performed on limited numbers of samples mainly because of the uniqueness of the samples and the large amount of starting material required by the purification steps.

One of the major challenges for this study is represented by the elevated number of proteins expressed in cardiac tissue such as the components of the contractile

apparatus, which can easily confuse the interpretation of high throughput analysis for the identifications of proteins. In addition, the ER stress conditions of the DCM cardiomyopathy may produce further degeneration of the ER folding machinery, leading to the accumulation of a large variety of unfolded proteins. In order to enrich the content of our sample in the oligomeric species or in the mature fiber content, our strategy included a preliminary separation conducted with both well-established techniques such as gel electrophoresis, immunoprecipitation, solubility fractionation, density gradient separation and more recently developed techniques such as laser capture microscopy. The samples obtained from this first step were then processed by mass spectrometry to identify the purified proteins. In particular, we gradually increased the stringency of our analysis starting from protocols requiring low amounts of starting material and progressively moving to approached producing more purified material, which also required high amounts of cardiac tissue.

A second problem associated with this study and, more specifically, to the isolation of oligomers is related to the total absence of data regarding their compatibility to solvents. This aspect introduces a major limit to the number of protocols that can be applied to the identification of this molecular species, since the use of an aggressive detergent may lead to the dissociation of the oligomer structure and, consequently, to our incapacity of detection. To overcome this issue we tried to work in non-denaturating conditions when possible.

Our work did not result in the isolation of any specific protein with an active role in the formation of unfolded molecular species. However, the characterization of the unfolded "bodies" described in the previous chapter still remains an objective of primary importance for understanding the molecular mechanisms involved in the protein aggregation in the failing heart and, eventually, for the development of new diagnostic and therapeutic approaches in the following paragraphs. We will therefore analyze in detail the limitations which prevented a successful identification using our experimental plan and techniques, as a reference for future characterization of the aggregasomes.

4.2 Results

4.2.1 High molecular weight protein-optimized gel separation

Gel separation is a common technique for separating proteins based on their size. This approach is usually based on the use of polyacrylamide gel electrophoresis, which in general achieves successful separation of polypeptides ranging from 4-5 kDa to 250-300 kDa. However, in our specific case, we expected to identify insoluble fibers with higher molecular weight, which can't easily migrate through this type of gel matrix. Our analysis was therefore focused on the use of two different techniques optimized for the separation of large proteins.

The first protocol was based on the use of horizontal agarose gels that were loaded with tissue lysate and stained with Sypro-Ruby. Our results showed poor separation of the cellular proteins and no specific bands were identifiable for MS analysis (Figure 4.1).

The second technique we adopted was instead based on the addition of diaminedithiol (DADT) in vertical acrylamide gels to help the generation of a large-pore matrix. In our pilot experiment we were able to obtain a good resolution of the cellular proteins and we could isolate 4 bands that appeared differentially present in DCM and non-failing samples (Figure 4.2). However this protocol was not appropriate for the use in combination with MS apparatuses because DADT was not efficiently removed from the sample and generated several problems to the equipment including the occlusion of the sample loading lines.
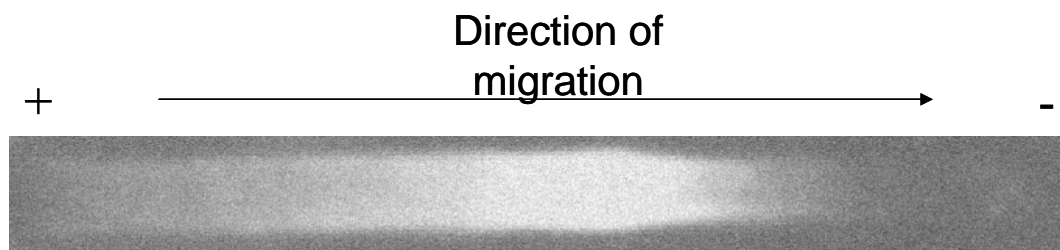
Figure 4.1. Agarose gel electrophoresis of protein extracts. The protein extract from one cardiac amyloidosis sample was loaded on an agarose gel to in-gel migration of large molecular weight such as amyloid aggregates and fibers. However the scarce resolution of the gel did not allow the visualization of any specific band to isolate for further processing.
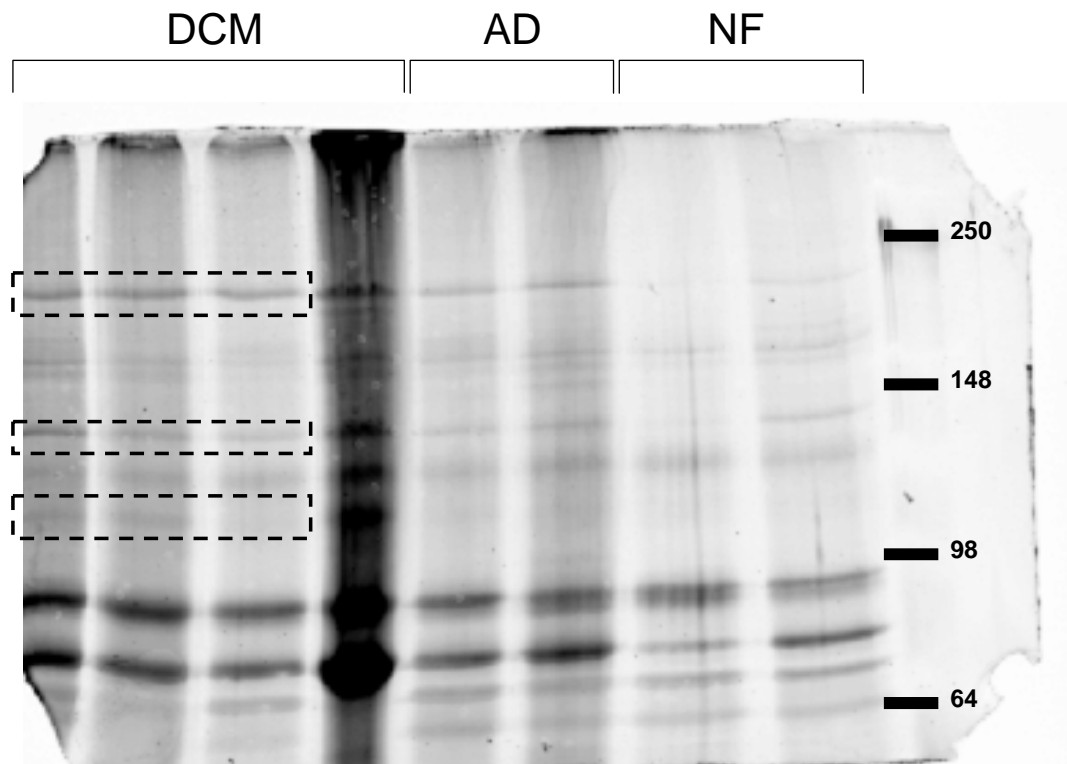
Figure 4.2. DADT-PAGE. Lysate from 4 DCM, 2 AD and 2 NF samples were loaded on a DADT gel. The box indicates the bands that were considered overexpressed and that were excised for further analysis. The sample in the 4th lane from the left resulted overloaded and no bands were isolated for the following experiments.

4.2.2 Laser capture microdissection (LCM)

A second type of approach we tested was focused on enriching the tissue lysates for MS in amyloid-positive cardiomyocytes with concomitant elimination of extracellular matrix protein contamination. In the past LCM has been frequently and successfully used for the isolation of specific areas/cells from tissue slices for genomic analysis and, more recently, the technique has been applied also to the proteomic characterization of amyloid plaques in AD. However in our specific case, the collection of the isolated cells from the remaining tissue was highly problematic due to the high strength-bonds that cardiac tissue appears to produce with the charges on the glass surface of the slides. According to our observations, the best slide for LCM of cardiomyocytes was the plain, no charge glass slide (Table 4.1), which allowed the recovery of 40-60% of the laser-isolated thioflavin-S-positive cardiomyocytes (Figure 4.3).

Table 4.1. Comparison between different slides for LCM

Slide	LCM apparatus	Pros	Cons
Regular glass, no charge	Leica LMD 6000 Zeiss P.A.L.M.	• Best recovery of the captured cells	• Tissue adhesion was sometimes unsatisfactory
Regular glass, charged	Leica LMD 6000 Zeiss P.A.L.M.	• Good tissue adhesion	• High strength of the tissue/glass interaction leading to difficult recovery of the captured cells
Plastic	Leica LMD 6000 Zeiss P.A.L.M.	• Good tissue adhesion	• Low resistance to solvents • Deformation during collection
Plastic film-coated glass	Leica LMD 6000 Zeiss P.A.L.M.	• Good tissue adhesion • Easy recovery of the captured cells	• Low resistance to solvents • Plastic film was carried over
Polyethylene terephthalate membrane frame slides	Leica LMD 7000	• Easy recovery of the captured cells	• Extremely low resistance to solvents • Plastic film was carried over

Unfortunately our results showed that the amount of proteins collected with this protocol was extremely low, leading to the necessity of large amounts of starting material to allow the subsequential MS analysis.

4.2.3 Differential sedimentation

Differential sedimentation has been successfully used in the past for the isolation of exogenous proteins produced in *E.Coli*, which in general are stored in the prokaryotic cell as unfolded insoluble structures called inclusion bodies. This protocol is normally based on the centrifugation of the whole cell lysate on a single multi-step sucrose gradient, but in our specific case we added a second step of centrifugation based on a linear gradient due to the higher complexity of eukaryotic cells.

As expected, unbound thioflavin-S was overlaying the gradients at the end of each step of centrifugation (Figure 4.4). However, we were able to observe multiple thioflavin-S-positive bands both in DCM and non-failing samples. In addition, the
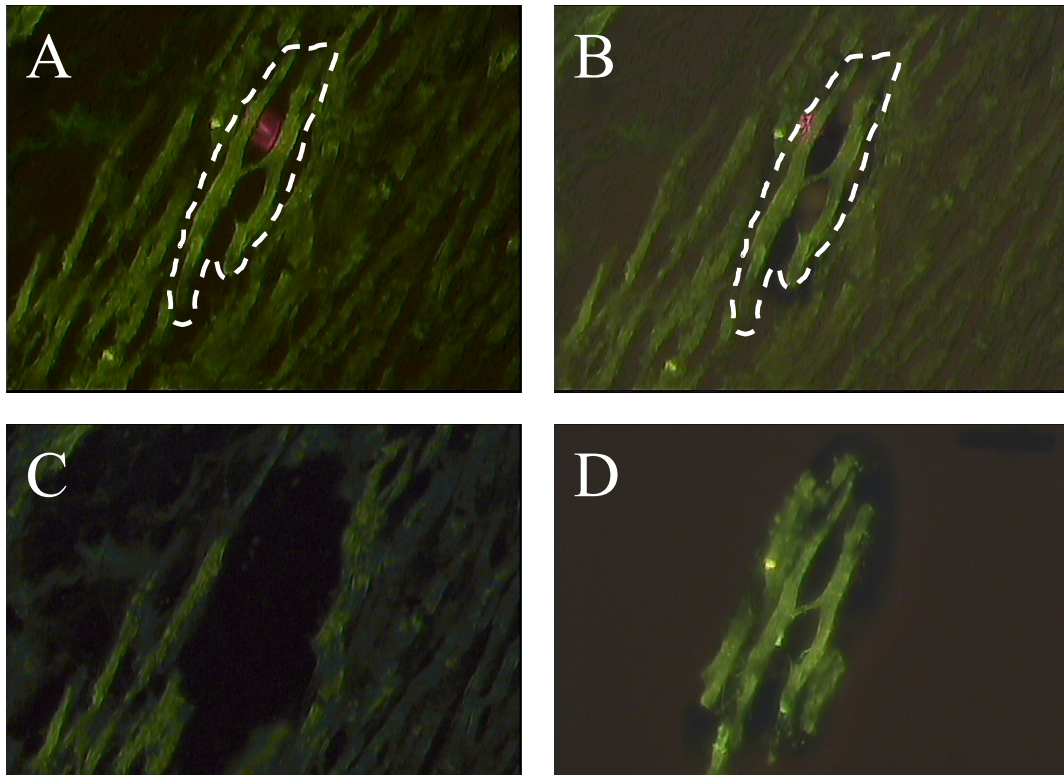
Figure 4.3. LCM of Thioflavin-stained cardiac tissue on Leika LMD 6000. The area of interest was delimited manually or recognized automatically by the software of the system (A). After confirmation of the area, the apparatus cut around the region with a focused laser beam (red dot) (B). The excised fibers were removed (C) by adhesion of a collecting cup (D). This particular sequence shows the isolation of two cardiomyocytes.

distribution pattern of the bands on the gradients was not consistent in the two groups analyzed.

The bands characterized by higher aggregation index (Abs 280/340, Table 4.2) were selected for a pilot MS analysis, but the complexity of the samples still resulted in a limiting step for the appropriate identification of peptides.

4.2.4 Detergent extraction of amyloid fibers

Amyloid fibers are generally characterized by low solubility in water-based solutions. However in the past the aggregates have been successfully solubilized using high concentration of detergents. Based on this background, we performed several steps of solubilization using increasing concentrations of detergents to eliminate the water-soluble material and progressively extract the molecules in the insoluble pellets. Our experimental design was based respectively on the use of TBS, followed by TBS+Triton-X 1% v/w and TBS+SDS 2% v/w.

A
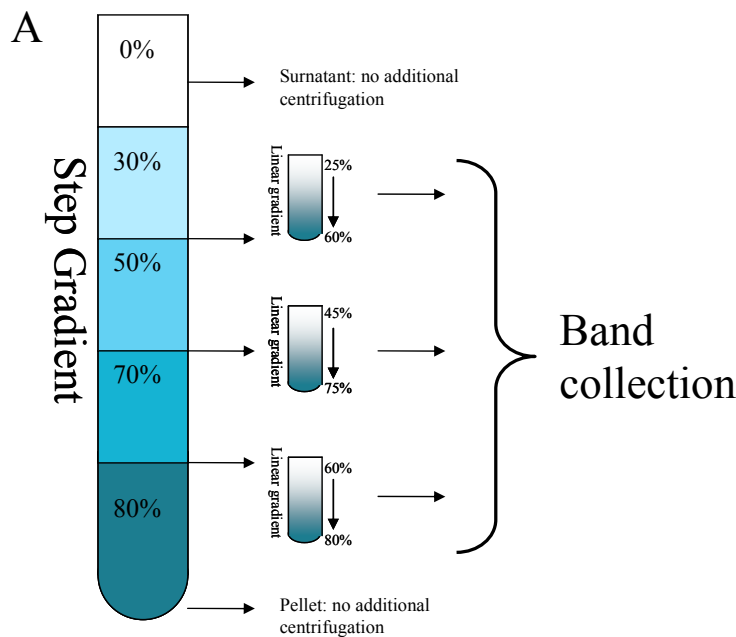
Figure 4.4. Density-based separation on sucrose gradients. Tissue lysates were loaded on a step gradient to separate the thioflavins-S positive material based on its density. The supernatant (mostly containing unbound thioflavin-S) and any eventual thioflavin-S pellet were collected and stored without further processing (A). The bands lying between each step of the gradient were loaded on linear higher resolution gradients in order to obtain a better separation of the unfolded fibers. A total of 7 DCM and 2 non-failing samples were processed with this protocol. 2 amyloid samples were added to the analysis as positive control. The thioflavin-positive bands collected at the end of each linear gradient are summarized in B. The protocol did not show any consistency of the distribution of the bands across samples belonging to the same group. The shaded samples were selected for further pilot characterization. Abbreviations: Amy: amyloidosis.

B

Diagnosis	Starting tissue (mg)	Thio-S+ Pellet	25-60%	45-75%	60-80%
Amy	350	x			1 band
Amy	960		1 band	1 band	2 bands
DCM	1500				1 band
DCM	500	x			1 band
DCM	650			1 band	1 band
DCM	1260		3 bands	1 bands	4 bands + diffuse signal along the tube
DCM	780			2 bands	1 band
DCM	950	x			1 band
DCM	650				1 band
NF	270			1 band	
NF	270				1 band

After the extraction, the samples were concentrated and loaded on a SDS-PAGE gel. As illustrated in Figure 4.5 our results show abnormal gel migration of the samples, which is probably due to interference of residual detergents, as the migration pattern seem to be significantly worse in the SDS-treated fractions.

Table 4.2. Aggregation index of the Thioflavin-S bands isolated from the linear sucrose gradient-based separation. The band characterized by the highest aggregation index (i.e. 280/340 ratio – shaded) among the bands isolated from the DCM and the amyloid samples analyzed were selected for further analysis. This experiment represented a validation of the protocol for the extraction of amyloid fibers. In fact as AL systemic amyloidosis is due to the overproduction of light immunoglobulin chains, we expected to obtain this protein ID from the MS analysis performed on the amyloid sample.

Sample	Gradient range	Band Id	Abs_{280}	Abs_{340}	Ratio
Amyloid	25-60%	1	0.009	0.004	2.657
	45-75%	1	0.035	0.005	6.509
	60-80%	1	0.102	0.057	1.801
	60-80%	2	0.078	0.035	2.259
DCM	25-60%	1	0.112	0.082	1.356
	25-60%	2	0.038	0.025	1.508
	25-60%	3	0.030	0.009	3.333
	45-75%	1	0.037	0.016	2.357
	60-80%	1	0.072	0.034	2.114
	60-80%	2	0.182	0.110	1.645
	60-80%	3	0.020	0.002	9.714
	60-80%	4	0.035	0.006	5.721

In addition, we tried to dissolve the insoluble residual material from the TBS+SDS extractions using formic acid 70%. However this approach resulted incompatible with the downstream analysis because of the impossibility of efficiently removing the formic acid without precipitating the molecules in solution.

4.2.5 Oligomer immunoprecipitation

Immunoprecipitation (IP) is a common technique to enrich a solution in particular protein using the specificity of antibodies. Our strategy was based on the use of oligomer-targeting immunoglobulins in order to eliminate the vast majority of cellular proteins present in the lysates and to obtain samples more compatible with the resolution limitations of MS.

The antibody (Invitrogen, CA, AHB0052) was used at a final dilution of 1:100 in a total volume of 500 µl; due to the limited information available on the biochemical
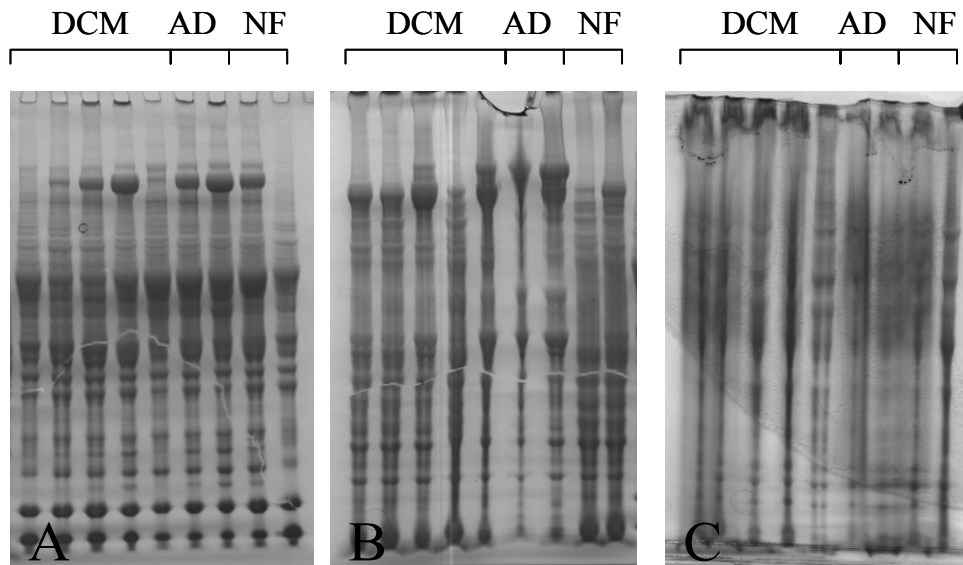
Figure 4.5. Detergent extraction of amyloid material. Cardiac tissues from DCM (n=4), AD (n=2) and NF (n=2) samples were homogenized in sequential steps using progressively increasing detergent strength. The supernatants obtained from each step were run on a SDS-PAGE gel and the migration of the different size proteins was visualized by Coomassie Blue staining. While the resolution of the gel was satisfactory for the native extraction (TBS, panel A), no satisfactory results were observed in the detergent-containing phases (Triton-X 100, panel B and SDS, panel C).

characteristics of DCM-related oligomers, the IP was performed in native conditions to inhibit the dissociation of the oligomeric structures. A pilot MS analysis of these samples didn't significantly recognize any specific peptide probably due to the incapacity to achieve a significant dissolution of the unspecific bonds and removal of the proteins not specifically recognized by the antibody during the wash steps.

We tried to address this problem by adding a second separation step based on a regular SDS-PAGE. The gel was stained to perform a densitometry analysis (Figure 4.6). We were able to identify 8 bands resulting differentially expressed between the DCM and non-failing groups, which were analyzed by MS.

This analysis led to the significant identification of a peptide belonging to the ankyrin repeat domain-containing protein 18A in band G (GI: 283549153), for which no biological function has been reported so far. Further database analysis showed that the peptide does not belong to the ankyrin repeat domain within the protein, but instead belongs to a region with unknown function (Figure 4.7).
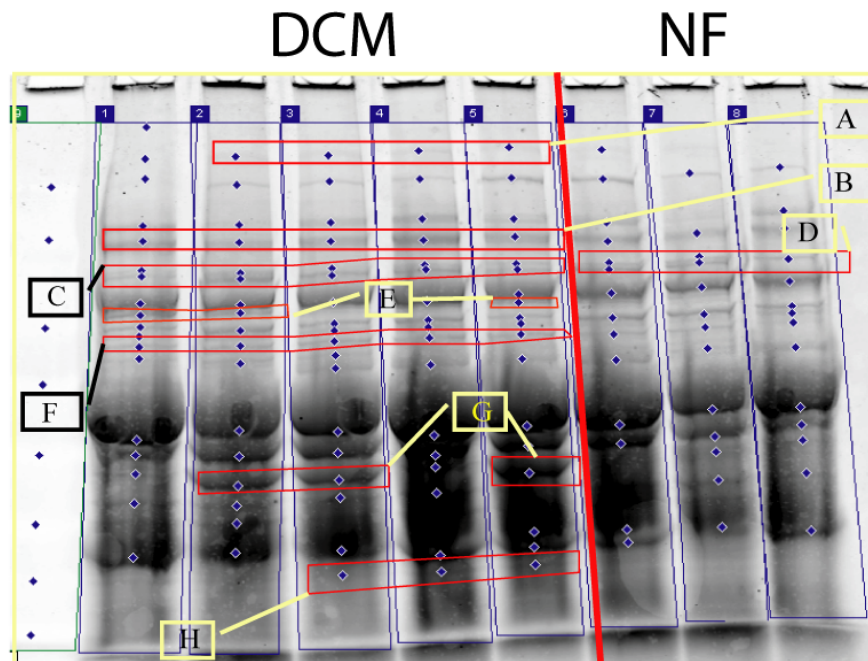
Figure 4.6. Isolation of soluble unfolded aggregates (oligomers) by immunoprecipitation.
Oligomers from DCM (n=5) and non-failing (NF, n=3) samples were immunoprecipitated in non-denaturing conditions and loaded on a SDS-PAGE. The band pattern generated by each sample was standardized and analyzed (next page, top panel shows an exemplificative densitometry profile obtained from a DCM sample). The bands showing significant increase in DCM (identified as A, C, D, E, F, G, H in the table) were excised for further processing.

4.3 Discussion

The assumption that every polypeptide chain can always reach its own functional state had been a paradigm in biochemistry and molecular biology for several decades; however in the last fifteen years a significant quantity of studies illustrated the importance of the protein folding process in the etiology of several degenerative diseases.

In the past the study of genetic transmission in affected families and linkage analysis in sporadic cases proved to play a critical role in the identification of most of the proteins currently known to be associated to foldopathies (Bertram and Tanzi, 2005, Bertram and Tanzi, 2009). However, in some diseases such as idiopathic DCM, the presence of genetic aberrations may be of secondary importance to the occurrence of particular epigenetic and environmental conditions, resulting in the inability to identify the specific cause underlying the pathological condition.
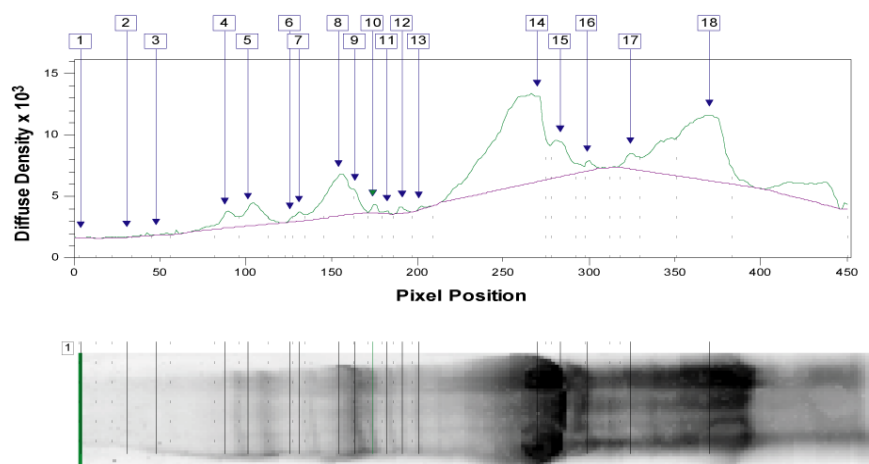
Ref Band	DCM1	DCM2	DCM3	DCM4	DCM5	NF1	NF2	NF2		Average DCM	Average NF	Stdev DCM	stdev NF	pVal	ID
1	3.16E+04	0.00E+00	0.00E+00	0.00E+00	0.00E+00	0.00E+00	0.00E+00	0.00E+00		6.32E+03	0.00E+00	1.41E+04	0.00E+00	0.187	
2	3.64E+04	1.11E+05	1.18E+05	1.81E+05	1.24E+05	7.74E+04	0.00E+00	0.00E+00		1.14E+05	2.58E+04	5.16E+04	4.47E+04	0.026	A
3	4.23E+04	1.58E+05	1.80E+05	1.55E+05	5.15E+05	4.77E+05	1.58E+05	1.33E+05		2.10E+05	2.56E+05	1.79E+05	1.92E+05	0.377	
4	1.03E+06	1.26E+05	3.56E+05	8.51E+05	3.27E+05	4.60E+05	0.00E+00	5.62E+05		5.37E+05	3.41E+05	3.81E+05	2.99E+05	0.227	
5	1.83E+06	6.33E+05	9.21E+05	1.66E+06	9.51E+05	8.30E+05	4.78E+05	9.78E+05		1.20E+06	7.62E+05	5.17E+05	2.57E+05	0.082	B
6	3.47E+04	2.05E+05	1.05E+05	8.75E+04	1.73E+05	4.15E+04	2.96E+04	0.00E+00		1.21E+05	2.37E+04	6.80E+04	2.14E+04	0.015	C
7	3.68E+05	8.72E+05	5.68E+05	6.45E+05	5.29E+05	6.62E+05	5.67E+05	3.95E+05		5.97E+05	5.41E+05	1.85E+05	1.35E+05	0.322	
9	3.97E+06	2.79E+06	4.67E+06	5.38E+06	4.01E+06	3.54E+06	2.92E+06	3.09E+06		4.16E+06	3.18E+06	9.61E+05	3.19E+05	0.044	D
10	7.17E+05	5.71E+05	0.00E+00	0.00E+00	3.71E+05	0.00E+00	0.00E+00	0.00E+00		3.32E+05	0.00E+00	3.27E+05	0.00E+00	0.043	E
11	2.39E+05	6.79E+05	2.53E+05	4.02E+05	1.74E+05	5.45E+05	6.03E+05	4.10E+05		3.49E+05	5.19E+05	2.02E+05	9.93E+04	0.082	F
12	9.23E+04	0.00E+00	1.47E+05	1.83E+05	8.26E+04	0.00E+00	0.00E+00	2.08E+05		1.01E+05	6.92E+04	6.97E+04	1.20E+05	0.353	
13	1.95E+05	2.37E+05	2.46E+05	1.76E+05	1.72E+05	1.23E+05	1.31E+05	6.01E+04		2.05E+05	1.05E+05	3.44E+04	3.90E+04	0.011	G
14	9.64E+04	1.87E+05	4.77E+04	0.00E+00	0.00E+00	0.00E+00	7.30E+04	0.00E+00		6.62E+04	2.43E+04	7.83E+04	4.22E+04	0.182	
15	0.00E+00	0.00E+00	2.01E+05	2.12E+05	9.73E+04	3.13E+05	0.00E+00	3.66E+05		1.02E+05	2.26E+05	1.03E+05	1.98E+05	0.198	
16	2.07E+07	1.06E+07	1.39E+07	2.45E+07	1.41E+07	1.72E+07	1.02E+07	1.42E+07		1.68E+07	1.39E+07	5.67E+06	3.50E+06	0.203	
17	2.71E+06	4.06E+06	4.00E+06	5.80E+06	2.64E+06	5.18E+06	3.21E+06	1.57E+06		3.84E+06	3.32E+06	1.29E+06	1.81E+06	0.344	
18	3.51E+05	2.16E+06	1.83E+06	2.48E+06	3.08E+06	0.00E+00	4.01E+05	6.41E+04		1.98E+06	1.55E+05	1.02E+06	2.15E+05	0.007	H
19	8.05E+05	7.49E+05	6.70E+05	3.14E+06	0.00E+00	0.00E+00	1.37E+06	5.38E+05		1.07E+06	6.37E+05	1.20E+06	6.93E+05	0.270	
20	0.00E+00	2.39E+06	0.00E+00	0.00E+00	0.00E+00	0.00E+00	0.00E+00	0.00E+00		4.78E+05	0.00E+00	1.07E+06	0.00E+00	0.187	
21	1.16E+07	8.23E+06	1.37E+07	2.16E+07	1.37E+07	2.36E+07	8.92E+06	1.25E+07		1.38E+07	1.50E+07	4.94E+06	7.64E+06	0.411	
22	0.00E+00	0.00E+00	0.00E+00	0.00E+00	1.66E+06	1.93E+06	0.00E+00	0.00E+00		3.31E+05	6.44E+05	7.41E+05	1.12E+06	0.347	
23	0.00E+00	0.00E+00	4.28E+05	3.43E+04	5.87E+04	0.00E+00	0.00E+00	0.00E+00		1.04E+05	0.00E+00	1.83E+05	0.00E+00	0.136	

Figure 4.6 –continued from previous page

An alternative approach to avoid these limitations and identify a putative candidate responsible for the development of iDCM consists in the direct characterization of the proteins involved in the unfolded protein deposits we described.

Our approach was based on a first phase of extraction of the proteins, followed by a second step focused on the analysis of the extract, based on tandem mass spectrometry.

Tandem mass spectrometry has been considered for several years the best approach for the accurate identification of peptides in a complex solution (Gozal et al., 2006). In particular increasing attention has been focused on this technique in amyloid research due to the interesting perspective of characterizing the peptides involved in

170

Ankyrin repeat
domain

```
ORIGIN
     1 mrklfsfgrr lgqallssmd qeyagpgydi rdwelrkihr aaikgdaaev ercltrrfrd
    61 ldardrkdrt vlhlacahgr vqvvtlllhr rcqidicdrl nrtplmkavh sqeeacaivl
   121 lecganpnie diygntalhy avynkgtsla erllshhani ealnkegntp llfainsrrq
   181 hmvefllknq anihavdnfk rtalilavqh nlssivtlll qqnirissqd mfgqtaedya
   241 lcsdlrsirq qilehknkml knhlrndnqe taamkpanlk krkerakaeh nlkvaseekq
   301 erlqrsenkq pqdsqsygkk kdamygnfml kkdiamlkee lyaikndslr kekkyiqeik
   361 siteinanfe ksvrlnekmi tktvarysqq lndlkaenar lnselekekh nkerleaeve
   421 slhsslatai neyneiverk dlelvlwrad dvsrhekmgs nisqltdkne llteqvhkar
   481 vkfntlkgkl retrdalrek tlalgsvqld lrqaqhrike mkqmhpngea kesqsigkqn
   541 sleerirqqe lenlllerql edarkegdnk eivinihrdc lengkedlle ernkelmkey
   601 nylkekllqc ekekaerevi vrefqeelvd hlktfsises plegtshchi nlnetwtskk
   661 klfqveiqpe ekheefrklf elisllnyta dqirkknrel eeeatgykkc lemtinmlna
   721 fanedfschg dlntdqlkmd ilfkklkqkf ndlvaekeav ssecvnlakq nevlhqells
   781 mrnvqekcek lekdkkmlee evlnlkthme kdmvelgklq eykseldera vqeiekleei
   841 hlqkqaeyek qleqlnkdnt aslkkkeltl kdveckfskm ktayeevtte leefkeafag
   901 avkannsmsk klmksdkkia vistklftek qrmkyflstl ptrpepelpc venlnsieln
   961 rkyipktair iptsnpqtsn ncknfltevl lc
```

Region recognized by
MS with p<0.05

Figure 4.7. Ankyrin repeat domain-containing protein 18A amino acid sequence and location of the peptide recognized by MS.

plaques for diagnostic purposes and to develop more effective therapeutic approaches (Murphy et al., 2006). However, our results show a substantial incapacity of significantly recognizing any known peptide in the protein extract analyzed. We can hypothesize that this issue was related to a series of limitations in the extraction methods we developed. In particular our strategy was based on several different protocols designed to progressively increase the stringency of the protein isolation. Although we were aware that low-stringency isolation techniques such as LCM might have produced protein extracts excessively complex to be analyzed by mass spectroscopy, we considered this step-based approach critical to increase the probability of identifying the specific proteins involved in the aggregates. In fact the total absence of biochemical information for the deposits such as stability and solubility limited our possibilities to use the more aggressive extraction methods previously described for the isolation of moderately and strongly detergent-resistant fibers (Rostagno and Ghiso, 2009).

In our opinion, the last protocol we described has the highest potential to isolate the proteins involved in the aggregates among the different extraction techniques tested

in this chapter. However, some optimization steps are still required to enrich the immunoprecipitates with oligomers and to efficiently remove unspecific contaminants. We suppose that this goal can be achieved by modifying the immunoprecipitation phase of the process: our experiments were performed using a non-denaturating washing buffer to preserve the native conformation of proteins and the interactions between them. The use of a mild detergent during the washing process could have promoted the dissociation of unspecific binding peptides, resulting in a less complex protein extract for the downstream analysis. The most critical step for this approach is represented by the choice of a safe detergent for the oligomeric structures, which should be selected empirically due to the lack of biochemical characteristics as mentioned above. This could have been achieved by incubating tissue slides in different washing buffer formulations, followed by immunohistochemistry staining for oligomeric structures as described in chapter 3.

This detergent-resistance screening would have improved our knowledge of the aggregate properties and addressed us towards more compatible techniques of separation. In particular the agarose gel separation we attempted has been previously used for the analysis of large proteins or SDS-stable high molecular weight complexes (Bagriantsev et al., 2006), since agarose gels are characterized by larger matrix pores than acrylamide (Kryndushkin et al., 2003). However, DCM aggregates don't seem to be as SDS-resistant as other amyloid fibers, which in general maintain their three-dimensional structures and dissociate from non-amyloid proteins after exposure to the detergent.

Beside these limitations, this protocol allowed us to identify a fragment of the ankyrin repeat domain-containing protein 18A as an iDCM-specific peptide. At the moment the presence in the cell of this protein has been predicted only by analysis of large cDNA clone libraries (Strausberg et al., 2002, Kimura et al., 2006). Therefore, the available information about this protein is very limited and represents a major issue for further characterization. An additional limitation in the determination of the role of this protein in iDCM also derives from the fact that the ankyrin repeat domain (which maps in a different region of the polypeptidic chain than the fragment recognized by our analysis) is one of the most common motifs found in proteins and is apparently related to large variety of biological activity (Sedgwick and Smerdon,

1999). Interestingly the ankyrin repeat domain has been recently identified in CARP, a small nuclear factor that seems to be mutated in a small subset of DCM patients (Moulik et al., 2009). The alteration of this gene in particular produces altered stretch-induced gene expression and impaired interaction with the mechanosensory system of the cell. We can therefore speculate that ankyrin repeat domain-containing protein 18A may have similar role in the cardiomyocytes, but unfortunately, the absence of specific commercial antibodies for the protein restricts the possibility of further characterization, including the validation of the data obtained by MS, and prevents more informative analysis such as the electromicroscopy-based immunocolocalization of the oligomers and the protein. A possible alternative for the validation of these results is represented by the evaluation of the transcript by qRT-PCR, although the data obtained with this technique do not necessarily correlate with the actual protein content.

The remaining approaches we considered are instead affected by substantial issues. For example, the use of DADT has been applied in the past for the electrophoretic separation of large proteins and proteic complexes. However no communications of successful combination of this technique and mass spectrometry have been reported to our knowledge. This is probably due to an incompatibility between the two protocols due to the incapacity of completely eliminating gel residues from the samples loaded in the mass spectroscopy apparatus, which in our hand led to occlusion of the sample loading lines.

The progressive sedimentation method we propose in this chapter, instead, represents an adaptation of a protocol previously described for the purification of unfolded inclusion body resulting from overexpression of exogenous proteins in *E.coli* (Schrodel and de Marco, 2005). In order to enhance the separation of the thioflavin-S-positive fibers and to improve the resolving capacity of the first gradient, we modified the protocol by performing an additional sucrose gradient separation for each band extracted from the first step. We decided to generate this second gradient as linear and we selected the light and heavy solution to mix based on the position of each band in the first gradient. However we think that the considerably higher complexity

of a eukaryotic cell lysate represented a limiting step for obtaining an appropriate separation form this approach specifically developed for prokaryotes. Therefore, in our opinion a decrease of the complexity of the initial protein lysate might be beneficial for a successful identification of the unfolded peptides. For example, the elimination of background generated by the extracellular matrix components could be achieved by using cardiomyocytes isolated from DCM cases; however this alternative, although attractive, was not feasible at the time when the study was performed mainly because of the large amount of starting material required.

The second protocol we proposed for amyloid fiber purification using the biochemical properties of the molecules was based on the scarce solubility in water-based buffers of the aggregates, which can be improved with the addition of detergents to the sample buffer. However our findings suggest that the methodologies applied are incompatible with the downstream analysis, since our SDS-PAGEs show a progressive deterioration of the resolving capacity of the gel with the increase of detergent strength and concentration. We hypothesize that this limitation is primarily related to large amounts of residual detergents in the samples which interferes with the electrophoretic run. To overcome this issue, we considered the possibility to dialyze the samples before loading them on the SDS-PAGE. However this process could allow the recreation of large insoluble aggregates which are unable to migrate through the gel matrix.

The concept of eliminating as many interfering impurities as possible was also the rationale behind the LCM-based approach we proposed. However, our observations suggest that also the isolation of the single cardiomyocytes does not lead to the generation of lysate compatible with the downstream analysis.

The combination of LCM and mass spectrometry has been successfully employed to characterize the peptides involved in Alzheimer's disease in the past (Gozal et al., 2006). However we should consider than the studies reported to date focus on large extracellular aggregates characterize by low complexity, since the plaques mostly contains the amyloigenic peptide. These structures are usually easily isolated from the rest of the tissue using conventional LCM protocols. Instead, as we observed in the

previous chapter, the distribution of the aggregates in DCM is intracellular, affects the vast majority of the cardiomyocytes and is not related to specific structures. Therefore the isolation of the thioflavin-S positive aggregates doesn't allow significant enrichment in the proteins specifically involved in the fiber formation and a second purification step would be necessary. This represents an important limitation especially for the amount of material required for the analysis, although the latest MS apparatuses can produce high-quality results even from a very low starting amount of material (Craven and Banks, 2001, Mustafa et al., 2008).

An additional problem we encountered in all the analysis presented derived from the fact that the samples used in this study were obtained from late-stage iDCM. We can speculate that the long-term exposure to the unfolded peptides we described in the previous chapter leads to progressive saturation of the unfolded protein response systems and, eventually, to a degeneration of the capacity of the cell to resolve the accumulation of existing unfolded peptides and prevent the misfolding of newly synthesized proteins. Therefore, it this plausible that in this context the aggregates are not just formed by a single protein or by a limited number of peptides, but they include every cellular protein that fails to reach its functional state due to the lack of a properly functioning folding apparatus. This hypothesis is supported by recent finding in pancreatic β-cells showing that the process of molecular crowding (i.e., the continuous accumulation of unfolded toxic proinsulin in the ER) exacerbates the defect in protein folding in diabetes (Despa).

In conclusion, the identification of the proteins involved in the intracellular deposits in iDCM represents an open challenge for a better understanding of the disease and to generate new diagnostic and therapeutic tools. In particular our approach was characterized by a series of technical limitations that might be circumvented by using early stage-DCM samples in the first place. Additional possible solutions might derive from the combination of some of the isolation techniques we proposed in this chapter, although we should consider that extensive manipulation are highly impractical due to the limited amount of starting material usually available.

CHAPTER 5

GENE EXPRESSION PROFILING OF DILATED CARDIOMYOPATHY

5.1 Introduction

In the previous chapters we described the presence of insoluble protein aggregates in cardiac tissue derived from patients diagnosed with DCM. In addition, we demonstrated that these deposits and in particular their soluble intermediate molecular precursors can produce impairment of the cardiomyocyte activity and alterations in the UPR pathway that can lead potentially to apoptosis. The identification of peptides specifically involved in the formation of these amyloid fibers still represents a challenging procedure for the technologies currently available for proteomics analysis. Therefore in this chapter we will approach the characterization of altered cellular pathways in DCM by evaluating the alterations in the messenger RNA (mRNA) levels performing a high throughput analysis based on the microarray technology. This technique present several advantages compared to the traditional approaches for the identification of proteins and genes related to a certain pathological condition. In particular, the last generation of microarray allows the analyses of thousands of genes at the same time with high reliability and reproducibility. In addition, microarrays represent a faster and technically easier alternative compared to other genomic and proteomic techniques (Asakura and Kitakaze, 2009).

In the past decade a considerable number of studies have been based on the use of microarray to elucidate new genes and pathways related to the etiology of DCM.
In 2000 a paper from Yang et al (Yang et al., 2000) reported alteration of a total of 17 genes from a limited number of patients (2 non-failing, 1 DCM, 1 ischemic cardiomyopathy). Among these messengers, 12 mRNA showed differential expression between non-failing and failing samples and 5 instead were expressed only in DCM hearts. The authors categorized these genes in 5 main gene ontology groups: structural, metabolic, cell stress-related, protein synthesis-related and related to the degradation of myocardial proteins.
The main limitation of this study consisted in the limited number of patients analyzed. Different publications appeared in the following years with larger pools of samples

included in each study group (Barrans et al., 2002, Hwang et al., 2002, Tan et al., 2002, Grzeskowiak et al., 2003, Steenman et al., 2003, Kaab et al., 2004, Yung et al., 2004, Kittleson et al., 2005, Colak et al., 2009). In addition, these studies could take advantage of technological improvements in the microarray technology, which led to increased number of messengers analyzed in a single chip and to higher reliability of the data. In these papers the authors generally showed alterations in several genes encoding for sarcomeric and cytoskeletal proteins, transcription factors, stress response proteins and Ca^{2+} handling, extracellular matrix components, proteins related to fatty acid metabolism, and apoptosis.

Additional interesting data on the transcriptosome of DCM heart have become available from other groups that investigated specific aspects of DCM: Haddad et al (Haddad et al., 2008) focused on the determination of genre-specific transcriptional alterations, showing differential deregulation of genes related to contractility (specifically deregulated in male patients), energy metabolism and transcription and translation (specifically altered in female samples). Dr. Léger's group, instead, determined chamber-specific differences in DCM samples, detecting a relatively limited number of alterations between left and right ventricles (Steenman et al., 2003). An alternative approach to the determination of the molecular pathways altered in DCM was instead explored in a paper by Hannenhalli et al (Hannenhalli et al., 2006): the authors analyzed the promoter regions of the genes found to be deregulated in order to determine which transcription factor binding sites were over-represented.

It is interesting to observe that neither of these publications showed results overlapping similar studies performed by different authors. Factors that may contribute to the discrepancies include the quality of the samples (and therefore of the RNA) and the limited availability of age and sex-matched samples. Further variability can also arise from the use of terminal heart failure patients as source of samples for these studies: in 2003 Grzeskowiak et al were successfully able to obtain a homogeneous fingerprinting of early stage DCM patients (Grzeskowiak et al., 2003), showing deregulation of genes related to intracellular signaling at early stages, while

in the late stages of the disease deregulation of apoptosis and cell cycle regulation gene levels seem to be predominant.

Additional obstacles for successful comparison of the previously published data are related to the fact that all the analyses published to date were performed using different chips and/or different platforms for the analysis. A study from Barth et al (Barth et al., 2006) recently showed the integration of 4 independently-run microarray datasets, leading to the identification of a set of 27 genes and minimizing the overinterpretation of each single set of data.

The majority of the microarray profiling for DCM published to date were performed comparing normal non-failing with failing DCM hearts. However in some cases the authors introduced ischemic hearts as an additional group of study in order to isolate the gene specifically modified by ischemia (Yang et al., 2000, Hwang et al., 2002, Steenman et al., 2003, Kittleson et al., 2005).

The present study, instead, is focused on the identification of a subset of messengers that are specifically altered in DCM and not related to the adverse remodeling commonly occurring in failing heart independently of the etiology. Our approach is based on an innovative three-way comparison of the transcriptome in non-failing, DCM and systemic amyloidosis. Amyloidosis is a systemic pathology affecting several organs and, in particular, kidney, liver and heart (Selkoe, 2003). The most common form of systemic amyloidosis is associated with multiple myelomas and malignant lymphomas, which are often characterized by uncontrolled overexpression and secretion of immunoglobulin chains in B lymphocytes. These proteins are delivered to the peripheral organs where they form amyloid deposits that affect the correct organ functions (Van Geluwe et al., 2006). The presence of these unfolded molecular species in the heart produces a restrictive cardiomyopathy that eventually leads to a failing condition. The most interesting aspect of this disease for our study consists in the localization of the etiology of the disease: although systemic amyloidosis doesn't originate directly in the heart, it is characterized by devastating cardiac effects producing activation of the remodeling pathways similarly to what is observed in other forms of HF.

In addition, the presence of immunoglobulin deposits in the extracellular matrix produces alterations of the redox state of the cardiomyocytes leading to impaired contractile function and Ca^{2+} handling (Brenner et al., 2004). As the unfolded light chain immunoglobulins assume a β-sheeted three-dimensional structure, we expect them to produce effects similar to what we observed in chapter 3 with Aβ oligomers on the cardiomyocytes. Therefore, we hypothesize that the inclusion of hearts affected by amyloidosis in our study will allow distinguishing the genes involved in the etiology and initial phases of DCM from the genes related to the evolution of the disease and related to the toxic consequences of the accumulation of unfolded products.

The analytical approach we propose resulted in the identification of 10 DCM-specific and 41 amyloidosis-specific genes and a total of 118 failing-related genes. While the latter were associated to a large array of biological processes, DCM- and amyloidosis-specific genes mainly clustered in two specific pathways: nervous system development and skeletal and tissue remodeling respectively.

5.2 Results

This study is based on the comparison between cardiac samples obtained from three different groups: patients affected by idiopathic DCM (n=6), patients affected by systemic amyloidosis (n=5) and non-failing donor hearts (n=6, Table 5.1). We structured our data processing in order to obtain a three-way comparison leading to the identification of DCM-specific genes (i.e., significantly altered in the DCM-amyloidosis and DCM-non failing comparisons, but not altered between amyloidosis and non-failing) and amyloidosis-specific genes (i.e., significantly altered in the DCM-amyloidosis and amyloidosis-non failing comparisons, but not altered between DCM and non-failing). Our analysis also produced the identification of a third subset of genes common to amyloidosis and DCM; this group includes the genes that are involved in the development of heart failure, independently from the etiology of the condition.

Table 5.1 Clinical data of the samples used for the microarray analysis

Pt	Diagnosis	age	Gender	Cause of death	Other diseases	Medications
1	Non-failing	56	Male	ICH		
2	Non-failing	35	Male	GSW (head)		
3	Non-failing	56	Male	ICH		
4	Non-failing	62	Female	CVA	HTN, mild LV hypertrophy	
5	Non-failing	57	Female	N/A	Legioneer Disease, Choliestomy, HTN	
6	Non-failing	75	Female	N/A	HTN, hypothyroidism, varicous veins	
1	DCM	56	Male	N/A	NIDDM, pulm HTN, AF, CRI	
2	DCM	57	Male	N/A	CM, HTN, AF, hyperlipemia, hyperthyroidism post Amio,Obesity	Diuretics, antiarrhythmics, anticoagulants, nitrates, lipid lowering, PDE inhibitors
3	DCM	25	Male	N/A	Anemia, asthma	Beta-blockers, antinflammatory
4	DCM	31	Female	N/A	Asthma	Diuretics, beta-blockers, digoxin, ACE inhibitors, anticoagulants
5	DCM	65	Female	N/A	COPD, AF ETOH, hypothyroidism	Diuretics, digoxin, ACE inhibitors, antiarrhythmics, lipid lowering, levothyroxine
6	DCM	43	Female	N/A	Anoxyc brain injury	Diuretics, beta-blockers, alpha-blockers, Ca2+ anthagonists
1	Amyloidosis	61	Male	N/A		Antidepresants, 5HT blockers
2	Amyloidosis	58	Male	N/A	Sleep apnea, NSvT, AF, obstructive sleep apnea, Hyperlipemia	Diuretics, Ca2+ anthagonists, albuterol, lipid lowering
3	Amyloidosis	67	Male	N/A	MI	
4	Amyloidosis	37	Female	N/A	Hypothyroidism, kidney stones	Diuretics, antiarrhythmics, PDE inhibitors
5	Amyloidosis	55	Female	N/A	Acute renal failure, NSVT	Diuretics, colchicine

List of abbreviation used: NIDDM = Non insulin dependent diabetes mellitus, AF = atrial fibrillation, Pulm HTN = pulmonary hypertension, HTN = systemic hypertension, CRI = chronic renal insufficiency, COPD+ chronic obstructive pulmonary disease, ETOH= alcohol consumption, MI = myocardial infarction, NSVT= non sustained ventricular tachycardia, GSW = gun shot wound, ICH=intracranial hemorragia
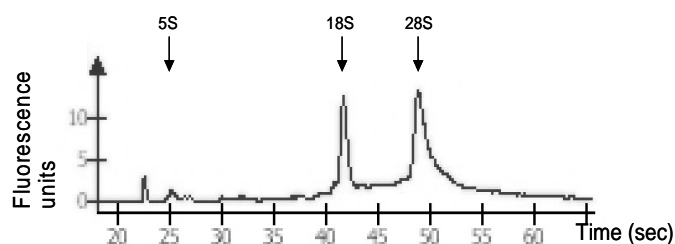
Figure 5.1. Bioanalyzer profiles of a representative RNA sample. The graph shows the modification of units of fluorescence (FU) of the sample with the progression of the run. This RNA preparation showed insignificant presence of degradation and neat peaks for the tRNAs 5, 18 and 28S, which were detected respectively at 22, 41 and 50 sec after the beginning of the run.

5.2.1 RNA extraction

The RNA samples were quantified on a spectrophotometer by reading the absorbance at 260 nm. The concentrations were ranging between 250 and 650 ng/µl. The contamination with protein was evaluated by reading the absorbance at 280 nm and analyzing the Abs_{260}/Abs_{280} ratios: all the samples showed values ranging from 1.7 and 2.0. The quality and the integrity of the RNA were tested by microcapillary electrophoresis. The Abs_{260} profile of each run showed distinct peaks for the tRNAs 5S, 18S and 28S (Figure 5.1). No signs of accumulation of low molecular weight-degradation fragments were detected in the area surrounding the 5S tRNA peak. In addition the integration of the peaks relative to the 18S and 28S tRNAs showed ratios close to 1:2. These results were considered compatible with the Affymetrix guidelines for the quality of RNA for the microarray analysis.

5.2.2 Microarray preparation

The quality of the cRNA prepared was evaluated before the fragmentation process. The profile of the samples showed no tRNA peaks and correct distribution of the RNAs of different length, consisting in considerable amount of short-medium molecules (over 200-250 bases) gradually declining for longer molecules (Figure 5.2a). The analysis was repeated after performing a random metal-catalyzed fragmentation reaction. The Abs_{260} profile showed a wide peak shifted to the beginning of the run and corresponding to 50-200 base-long molecules (Figure 5.2b). No evidence of unfragmented cRNA was observed.
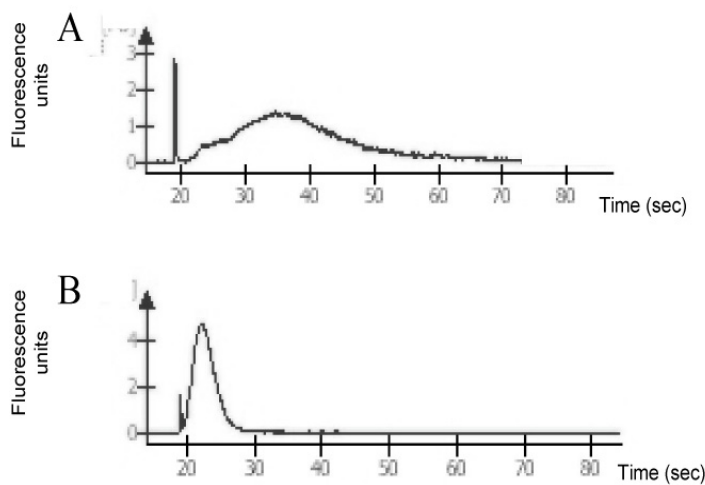
Figure 5.2. Bioanalyzer profile of a representative cRNA sample before (a) and after (b) fragmentation. The graphs show the alterations of the fluorescence units (FU) against time. The wide bump showed in (a) between 21 and 55 seconds is correlated to the presence of several cRNA of different length, which were successfully disrupted to 50-200 base-long fragments as indicate by the narrow peak present between 20 and 27 sec in (b).

5.2.3 Microarray analysis

Quality control of the scanned chip images was performed before further analysis of the data. All the normalized images were characterized by comparable high quality. The percentage of present calls on each chip ranged between 40.6% and 47.8%, with an average of 44%±2.17% (27,125±1,338 probes, Figure 5.3). The overall pre-normalization variability across the samples did not exceed 15% in term for all the following parameters: background, noise, spike-ins, levels of exogenous controls and housekeeping genes. A total of 19,357 probe sets (=31.4% of all the probes on the chip surface) were identified as present or marginally present in all the 17 samples in the study, while 22,316 (=36.2%) were considered absent, i.e. not represented in any of the samples. The presence/absence similarity across the samples and the different groups considered was equal to 67.6%, indicating good consistency of the results obtained.

The data were processed considering as differentially expressed all the probes showing difference in post-normalization signal intensity of at least 2 fold. Preliminary 2-group analyses indicated analogue differentially expressed probe distribution in the DCM-non failing and amyloidosis-non failing comparisons with the majority of the probes significantly up-regulated (DCM-non failing: 312 upregulated and 272 downregulated; amyloidosis-nonfailing: 558 upregulated and 215 downregulated, Table 5.2). The DCM-amyloidosis comparison, instead, showed 197 probe underexpressed and 40 overexpressed. In addition we observed that most of the
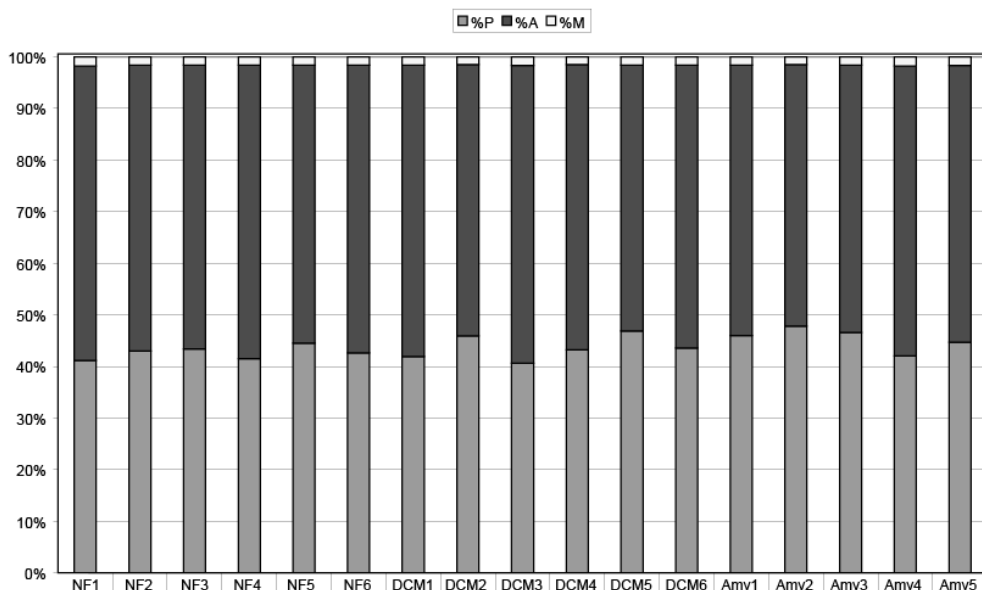
Figure 5.3. Amount of probe sets in each microchip image considered present (i.e. characterized by normalized intensity higher than 8, labeled as P) or absent (labeled as A). All the samples showed comparable number of present probes ranging between 40.6% and 47.8%. On average the number of present probes was of 27,125±1,338 or 44%±2.17% of the total. M represents the exogenous positive controls introduced during the cRNA syntesis.

altered probes in the DCM-non failing comparison showed changes between and 0.08 and 6 fold, while the alterations between amyloidosis and non failing groups were distributed within a larger interval (0.04 and 32 folds, Figure 5.4).

Table 5.2. Number of probes altered in each 2-group comparison.

	Non-failing		Amyloidosis	
	Over-expressed	Under-expressed	Over-expressed	Under-expressed
Amyloidosis	558	215	-	-
DCM	312	272	197	40
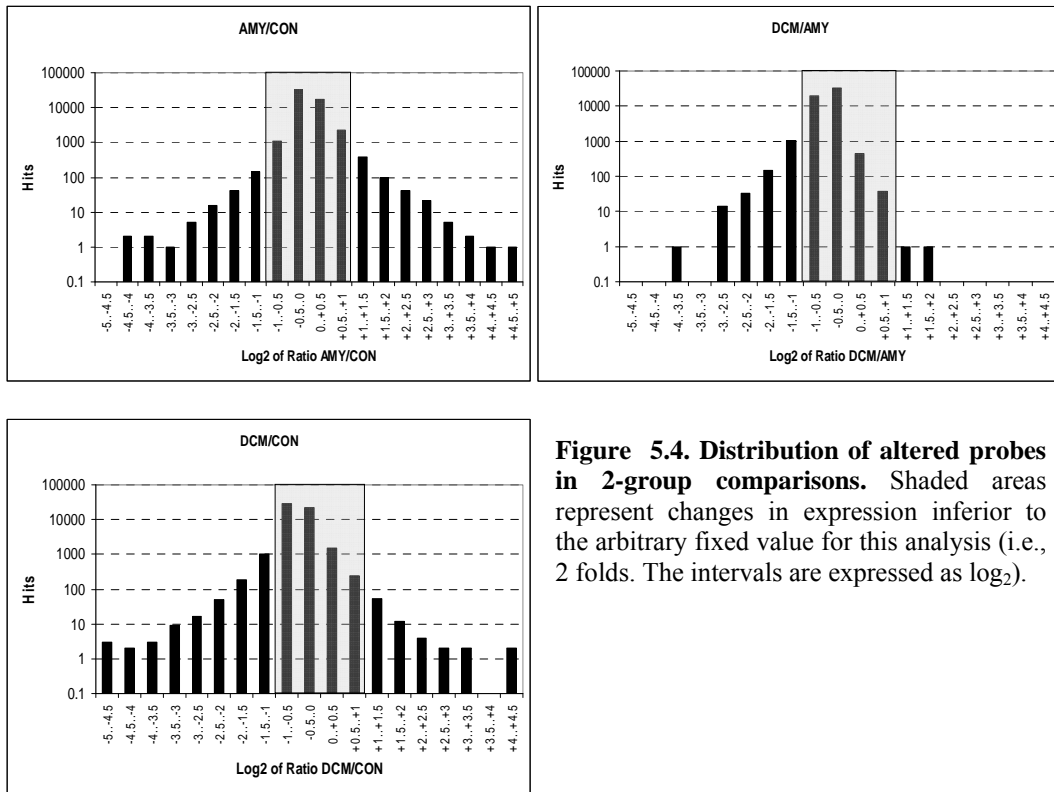
Figure 5.4. Distribution of altered probes in 2-group comparisons. Shaded areas represent changes in expression inferior to the arbitrary fixed value for this analysis (i.e., 2 folds. The intervals are expressed as $\log_2$).

5.2.4 Group comparison

The probes that were differentially expressed in our 2-group analysis represent a combination of genes specific for the disease and genes that instead contribute to the progressive degeneration in the failing process or are altered as an adaptive mechanism (Figure 5.5). In order to efficiently discriminate these two categories of genes we introduced a more complex analysis based on simultaneous comparison of the three different groups used in this study. This analysis allowed the recognition respectively of amyloidosis and DCM-specific genes and the separation from the
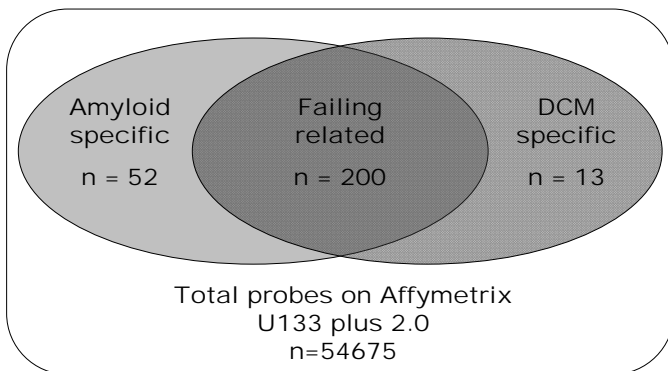
Figure 5.5. Representation of the rationale behind the use of our three-group analysis. The probes that are commonly altered in DCM and Amyloidosis were separated from the disease-specific and considered failing-associated.

187

genes commonly altered in the two diseases, which were labeled as "failing-associated".

Our approach led to the identification of limited DCM-specific probes (6 upregulated and 7 downregulated, Table 5.3) representing a total of 10 known genes (4 increased and 6 decreased). The probes specifically altered in amyloidosis totaled 52 overexpressed sets and none underexpressed (Table 5.4), representing 41 known genes. The failure-related probes (i.e., significantly differentially expressend in DCM and amyloidosis) included a total of 200 EST (118 increased and 82 decreased, listed in Table 5.5) representing 138 known genes (82 increased and 56 decreased).

The probes resulting DCM-specific, amyloidosis-specific or failing-related were organized by hierarchical clustering (Figure 5.6). In particular the DCM-specific probes distinctly grouped all the DCM patients and clearly separated them from non-failing samples (Figure 5.6a), with the exception of the sample indicated as donor 1 (red arrow), that instead clustered within the DCM group. The amyloidosis samples, instead, were randomly interspersed between both DCM and non-failing. The
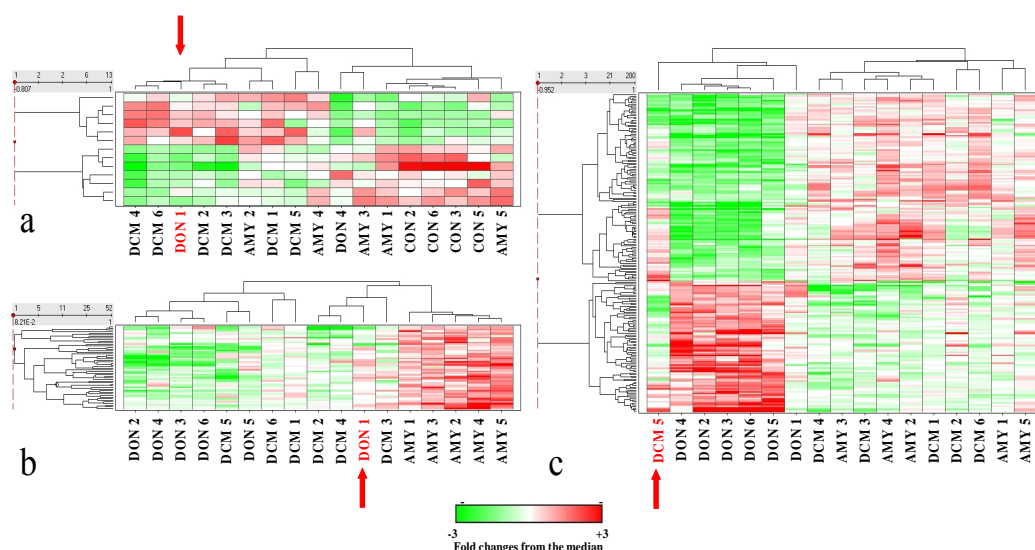
Figure 5.6. Hierarchical clustering of DCM- (panel a), amyloidosis (panel b) and failing specific (panel c) genes in the 17 samples analyzed. The samples were distributed on the x axis according to their similarities in the expression profile for the probe considered, i.e., samples with similar expression profile are close to each other. The color of each probe for each samples indicate the variation relative to the median value of all the samples considered. The red arrow indicates samples showing dissociation from their respective groups.

Table 5.3. List of genes significantly different in DCM vs AMY and non-failing samples (p<0.05). Column 5 and 7 represent the ratio between the average expression respectively in DCM vs CON and DCM vs AMY.

Probe Set ID	Accession	Gene Title	Gene Symbol	DCM\CON	p	DCM/AMY	p
downregulated							
230161_at	BF513346	CD99 molecule	CD99	0.443	0.021	0.441	0.002
208451_s_at	NM_000592	complement component 4A/ complement component 4B	C4A /// C4B	0.476	0.033	0.305	0.001
1555758_a_at	AF213040	cyclin-dependent kinase inhibitor 3 (CDK2-associated dual specificity phosphatase)	CDKN3	0.423	0.038	0.464	0.046
205404_at	NM_005525	hydroxysteroid (11-beta) dehydrogenase 1	HSD11B1	0.465	0.002	0.364	0.003
229498_at	AI197932	MRNA; cDNA DKFZp779M2422 (from clone DKFZp779M2422)	---	0.328	0.036	0.419	0.031
203649_s_at	NM_000300	phospholipase A2, group IIA (platelets, synovial fluid)	PLA2G2A	0.078	0.009	0.249	0.032
202075_s_at	NM_006227	phospholipid transfer protein	PLTP	0.498	0.029	0.454	0.030
Upregulated							
214985_at	AF070571	Clone 24739 mRNA sequence	---	3.020	0.003	2.081	0.037
215253_s_at	AL049369	Down syndrome critical region gene 1	DSCR1	3.850	0.001	2.147	0.029
203184_at	NM_001999	fibrillin 2 (congenital contractural arachnodactyly)	FBN2	2.331	0.041	2.468	0.036
231963_at	BG111938	Homo sapiens, clone IMAGE:3869276, mRNA	---	3.703	0.007	2.618	0.039
229346_at	AW028075	nestin	NES	3.119	0.004	2.225	0.035
228121_at	AU145950	Transforming growth factor, beta 2	TGFB2	3.226	0.033	2.159	0.040

189

Table 5.4. List of genes showing significant difference in AMY versus DCM and non-failing samples (p<0.05). Column 5 and 7 represent the ratio between the average expression respectively in AMY vs CON and AMY vs DCM.

Probe Set ID	Accession	Gene Title	Gene Symbol	AMY/CON	p	AMY/DCM	p
209309_at	D90427	alpha-2-glycoprotein 1, zinc	AZGP1	2.586	0.006	2.470	0.004
217014_s_at	AC004522	alpha-2-glycoprotein 1, zinc	AZGP1	2.144	0.009	2.039	0.006
219962_at	NM_021804	angiotensin I converting enzyme (peptidyl-dipeptidase A) 2	ACE2	4.880	0.004	2.218	0.011
222257_s_at	AK026461	angiotensin I converting enzyme (peptidyl-dipeptidase A) 2	ACE2	3.743	0.011	2.030	0.027
207173_x_at	D21254	cadherin 11, type 2, OB-cadherin (osteoblast)	CDH11	4.217	0.007	2.425	0.003
206227_at	NM_003613	cartilage intermediate layer protein, nucleotide pyrophosphohydrolase	CILP	3.088	0.039	2.431	0.028
205713_s_at	NM_000095	cartilage oligomeric matrix protein	COMP	11.467	>0.001	9.467	0.001
206545_at	NM_006139	CD28 molecule	CD28	2.021	0.038	2.021	0.039
229121_at	BE857553	CDNA FLJ44441 fis, clone UTERU2020242	----	2.449	>0.001	2.030	0.002
231993_at	AK026784	CDNA: FLJ23131 fis, clone LNG08502	----	3.248	0.008	3.383	0.012
227443_at	AI972386	chromosome 9 open reading frame 150	C9orf150	2.351	0.009	2.176	0.001
225681_at	AA584310	collagen triple helix repeat containing 1	CTHRC1	12.111	0.005	3.670	0.003
232458_at	AU146808	Collagen, type III, alpha 1	COL3A1	3.096	0.001	2.862	0.001
221729_at	AL575735	collagen, type V, alpha 2	COL5A2	3.318	>0.001	2.128	0.030
213800_at	X04697	complement factor H	CFH	3.378	0.001	3.454	0.001
201313_at	NM_001975	enolase 2 (gamma, neuronal)	ENO2	5.312	0.002	3.059	0.002
205174_s_at	NM_012413	glutaminyl-peptide cyclotransferase (glutaminyl cyclase)	QPCT	3.376	0.000	2.079	0.004
224646_x_at	BF569051	H19, imprinted maternally expressed untranslated mRNA	H19	4.388	0.008	5.318	0.005
205422_s_at	NM_004791	integrin, beta-like 1 (with EGF-like repeat domains)	ITGBL1	5.368	0.002	4.315	0.019
214927_at	AL359052	Integrin, beta-like 1 (with EGF-like repeat domains)	ITGBL1	4.058	0.002	4.183	0.002
1557080_s_at	AI753143	Integrin, beta-like 1 (with EGF-like repeat domains)	ITGBL1	4.455	0.005	4.594	0.027
221558_s_at	AF288571	lymphoid enhancer-binding factor 1	LEF1	2.525	0.008	2.895	0.005
238481_at	AW512787	matrix Gla protein	MGP	4.108	>0.001	4.381	0.033
202016_at	NM_002402	mesoderm specific transcript homolog (mouse)	MEST	3.377	0.016	2.249	0.018
219773_at	NM_016931	NADPH oxidase 4	NOX4	3.150	0.014	2.242	0.021
210809_s_at	D13665	periostin, osteoblast specific factor	POSTN	7.990	0.003	3.724	0.001
214981_at	AW137148	Periostin, osteoblast specific factor	POSTN	3.323	0.007	3.062	0.015
228481_at	BG541187	Periostin, osteoblast specific factor	POSTN	6.551	0.000	3.404	0.012

Continued.

Table 5.4. Continued from previous page.

1555778_a_at	AY140646	periostin, osteoblast specific factor	POSTN	10.773	0.003	4.665	0.001
201860_s_at	NM_000930	plasminogen activator, tissue	PLAT	2.127	0.034	2.208	0.012
234103_at	AU145191	Potassium channel, subfamily T, member 2	KCNT2	2.640	0.005	2.930	0.009
213791_at	NM_006211	proenkephalin	PENK	7.534	0.006	3.710	0.006
204223_at	NM_002725	proline/arginine-rich end leucine-rich repeat protein	PRELP	2.846	0.005	2.736	0.022
220005_at	NM_023914	purinergic receptor P2Y, G-protein coupled, 13	P2RY13	4.269	>0.001	3.054	0.005
209496_at	BC000069	retinoic acid receptor responder (tazarotene induced) 2	RARRES2	2.214	0.037	2.544	0.017
232231_at	AL353944	runt-related transcription factor 2	RUNX2	3.254	0.000	2.262	>0.001
204035_at	NM_003469	secretogranin II (chromogranin C)	SCG2	3.387	0.017	3.107	0.028
212190_at	AL541302	serpin peptidase inhibitor, clade E (nexin, plasminogen activator inhibitor type 1), member 2	SERPINE2	5.665	0.008	2.286	0.006
219197_s_at	AI424243	signal peptide, CUB domain, EGF-like 2	SCUBE2	2.899	0.001	2.484	0.002
1554195_a_at	BC021680	similar to AVLV472	MGC23985	2.787	0.002	2.563	0.033
240890_at	AA041298	similar to Caspase-4 precursor (CASP-4) (ICH-2 protease) (TX protease) (ICE(rel)-II)	LOC648470	2.504	0.009	2.133	0.030
213139_at	AI572079	snail homolog 2 (Drosophila)	SNAI2	2.038	0.008	2.141	0.037
226444_at	AI700476	Solute carrier family 39 (zinc transporter), member 10	SLC39A10	3.012	0.010	2.839	0.016
204595_s_at	AI300520	stanniocalcin 1	STC1	2.895	0.036	4.315	0.015
204597_x_at	NM_003155	stanniocalcin 1	STC1	2.850	0.031	4.694	0.015
230746_s_at	AW003173	Stanniocalcin 1	STC1	3.136	0.003	4.244	0.020
208850_s_at	AL558479	Thy-1 cell surface antigen	THY1	2.753	0.016	2.378	0.046
213285_at	AV691491	transmembrane protein 30B	TMEM30B	2.141	0.013	2.002	0.022
219410_at	NM_018004	transmembrane protein 45A	TMEM45A	2.152	0.015	2.462	0.001
1563655_at	AL832707	troponin T type 2 (cardiac)	TNNT2	2.558	0.022	2.158	0.012
203868_s_at	NM_001078	vascular cell adhesion molecule 1	VCAM1	2.148	0.038	2.486	0.006
204534_at	NM_000638	vitronectin	VTN	2.659	0.004	2.171	0.029

Table 5.5. List of genes showing significant and similar difference both in amyloidosis and DCM versus non-failing samples (p<0.05). Column 5 and 7 represent the ratio between the average expression respectively in DCM vs CON and AMY vs CON.

Probe Set ID	Accession	Gene Title	Gene Symbol	DCM/CON	p	AMY/AMY	p
downregulated							
215014_at	AL512727	---	---	0.391	0.001	0.399	0.001
1556989_at	AF086069	ADAM metallopeptidase with thrombospondin type 1 motif, 9	ADAMTS9	0.407	0.032	0.402	0.049
220287_at	NM_020249	ADAM metallopeptidase with thrombospondin type 1 motif, 9	ADAMTS9	0.421	0.034	0.374	0.042
205083_at	NM_001159	aldehyde oxidase 1	AOX1	0.169	0.002	0.182	0.006
205082_s_at	AB046692	aldehyde oxidase 1	AOX1	0.268	0.004	0.293	0.010
39248_at	N74607	aquaporin 3 (Gill blood group)	AQP3	0.309	0.003	0.430	0.007
219464_at	NM_012113	carbonic anhydrase XIV	CA14	0.428	0.026	0.448	0.048
1557326_at	BC041938	CDNA clone IMAGE:5301138	---	0.293	0.001	0.299	0.008
229004_at	AI970797	CDNA FLJ26557 fis, clone LNF01992	---	0.416	0.030	0.347	0.012
238718_at	BF382322	CDNA FLJ37816 fis, clone BRSSN2003093	---	0.479	0.006	0.462	0.007
235117_at	AI191897	ChaC, cation transport regulator-like 2 (E. coli)	CHAC2	0.419	0.043	0.290	0.002
222542_x_at	BF724826	chaperone, ABC1 activity of bc1 complex like (S. pombe)	CABC1	0.382	0.005	0.391	0.008
218168_s_at	NM_020247	chaperone, ABC1 activity of bc1 complex like (S. pombe)	CABC1	0.428	0.004	0.470	0.008
223987_at	AF332891	chordin-like 2	CHRDL2	0.365	0.043	0.336	0.048
217767_at	NM_000064	complement component 3 /// similar to Complement C3 precursor	C3 /// LOC653879	0.256	0.002	0.383	0.036
205382_s_at	NM_001928	complement factor D (adipsin)	CFD	0.464	0.010	0.489	0.017
228796_at	BE645967	copine IV	CPNE4	0.204	0.003	0.370	0.001
239260_at	AI338960	corin, serine peptidase	CORIN	0.158	0.002	0.243	0.012
239261_s_at	AI338960	corin, serine peptidase	CORIN	0.307	0.011	0.336	0.035
230915_at	AI741629	dehydrogenase/reductase (SDR family) member 7C	DHRS7C	0.142	0.008	0.124	0.011
209560_s_at	U15979	delta-like 1 homolog (Drosophila)	DLK1	0.099	0.001	0.049	0.004
226573_at	AI829795	DIRAS family, GTP-binding RAS-like 1	DIRAS1	0.486	0.015	0.447	0.014
228176_at	AA534817	endothelial differentiation, sphingolipid G-protein-coupled receptor, 3	EDG3	0.337	0.015	0.361	0.029
231741_at	NM_005226	endothelial differentiation, sphingolipid G-protein-coupled receptor, 3	EDG3	0.462	0.027	0.437	0.033
223895_s_at	BC001038	epsin 3	EPN3	0.449	0.013	0.452	0.013
223859_at	AF153416	erythrocyte membrane protein band 4.1 like 4B	EPB41L4B	0.313	0.001	0.398	0.007
240065_at	AI769413	family with sequence similarity 81, member B	FAM81B	0.156	0.025	0.157	0.024

Continued.

Table 5.5. Continued from previous page.

232267_at	AL162032	G protein-coupled receptor 133	GPR133	0.365	0.001	0.424	0.030
206204_at	NM_004490	growth factor receptor-bound protein 14	GRB14	0.445	>0.001	0.466	0.034
208886_at	BC000145	H1 histone family, member 0	H1F0	0.446	0.015	0.427	0.021
222921_s_at	AF232238	hairy/enhancer-of-split related with YRPW motif 2	HEY2	0.370	0.008	0.390	0.033
209398_at	BC002649	histone 1, H1c	HIST1H1C	0.443	0.003	0.437	0.006
1559929_at	AL700385	Homo sapiens, clone IMAGE:4042121	---	0.378	0.002	0.304	0.001
1553797_a_at	NM_153011	hypothetical locus FLJ30594	FLJ30594	0.225	0.016	0.245	0.032
1562921_at	BC040700	Hypothetical protein LOC646927	LOC646927	0.259	0.006	0.202	0.003
221321_s_at	NM_014591	Kv channel interacting protein 2	KCNIP2	0.125	0.018	0.188	0.046
223727_at	AL136722	Kv channel interacting protein 2	KCNIP2	0.156	0.013	0.219	0.039
214460_at	NM_002338	limbic system-associated membrane protein	LSAMP	0.333	0.019	0.365	0.049
224918_x_at	AI220117	microsomal glutathione S-transferase 1	MGST1	0.215	0.003	0.321	0.006
1565162_s_at	D16947	microsomal glutathione S-transferase 1	MGST1	0.220	0.006	0.339	0.016
231736_x_at	NM_020300	microsomal glutathione S-transferase 1	MGST1	0.245	0.003	0.320	0.006
218251_at	NM_021242	MID1 interacting protein 1 (gastrulation specific G12-like (zebrafish))	MID1IP1	0.255	0.003	0.317	0.015
233482_at	AL360257	MRNA full length insert cDNA clone EUROIMAGE 51148	---	0.394	0.022	0.262	0.002
213832_at	AA530995	MRNA; cDNA DKFZp547P042 (from clone DKFZp547P042)	---	0.386	0.001	0.456	0.004
214650_x_at	AL050328	myelin oligodendrocyte glycoprotein	MOG	0.370	0.011	0.339	0.013
203814_s_at	NM_000904	NAD(P)H dehydrogenase, quinone 2	NQO2	0.445	0.008	0.488	0.028
205577_at	NM_005609	phosphorylase, glycogen; muscle	PYGM	0.471	0.013	0.476	0.002
225726_s_at	AB033026	pleckstrin homology domain containing, family H (with MyTH4 domain) member 1	PLEKHH1	0.468	0.017	0.471	0.025
231740_at	NM_000525	potassium inwardly-rectifying channel, subfamily J, member 11	KCNJ11	0.481	0.005	0.430	0.005
1555167_s_at	BC020691	pre-B-cell colony enhancing factor 1	PBEF1	0.404	0.046	0.384	0.024
217739_s_at	NM_005746	pre-B-cell colony enhancing factor 1	PBEF1	0.430	0.021	0.482	0.037
217738_at	BF575514	pre-B-cell colony enhancing factor 1	PBEF1	0.439	0.018	0.487	0.038
235129_at	BF510098	protein phosphatase 1, regulatory (inhibitor) subunit 1A	PPP1R1A	0.475	0.032	0.436	0.026
231040_at	AW512988	RAR-related orphan receptor B	RORB	0.313	0.001	0.417	0.027
242385_at	R18374	RAR-related orphan receptor B	RORB	0.482	0.024	0.499	0.045
214369_s_at	AI688812	RAS guanyl releasing protein 2 (calcium and DAG-regulated)	RASGRP2	0.485	0.002	0.482	0.002
221872_at	AI669229	retinoic acid receptor responder (tazarotene induced) 1	RARRES1	0.046	0.018	0.059	0.035
206392_s_at	NM_002888	retinoic acid receptor responder (tazarotene induced) 1	RARRES1	0.048	0.011	0.064	0.021
206391_at	NM_002888	retinoic acid receptor responder (tazarotene induced) 1	RARRES1	0.179	0.020	0.170	0.028
223468_s_at	AL136826	RGM domain family, member A	RGMA	0.395	0.004	0.458	0.022

Continued.

193

Table 5.5. Continued from previous page.

Probe set	Accession	Value 1	p 1	Value 2	p 2	Gene symbol	Gene name
229839_at	AI799784	0.194	>0.001	0.366	>0.001	SCARA5	Scavenger receptor class A, member 5 (putative)
235849_at	BE787752	0.194	>0.001	0.372	>0.001	SCARA5	scavenger receptor class A, member 5 (putative)
236717_at	AI632621	0.258	0.005	0.203	0.002	LOC165186	similar to RIKEN cDNA 4632412N22 gene
230475_at	AI368415	0.454	0.006	0.460	0.003	LOC388135	similar to RIKEN cDNA 6030419C18 gene
229730_at	AI193973	0.313	0.042	0.206	0.002	SMTNL2	smoothelin-like 2
1559977_a_at	AL832282	0.392	0.002	0.322	0.017	SLC25A34	solute carrier family 25, member 34
232245_at	AU151211	0.465	0.003	0.426	0.010	SLC25A34	solute carrier family 25, member 34
206628_at	NM_000343	0.458	0.018	0.445	0.042	SLC5A1	solute carrier family 5 (sodium/glucose cotransporter), member 1
201349_at	NM_004252	0.383	0.002	0.494	0.022	SLC9A3R1	solute carrier family 9 (sodium/hydrogen exchanger), member 3 regulator 1
219911_s_at	NM_016354	0.269	0.029	0.319	0.034	SLCO4A1	solute carrier organic anion transporter family, member 4A1
218424_s_at	NM_018234	0.231	0.004	0.198	0.001	STEAP3	STEAP family member 3
1554830_a_at	AF262322	0.281	0.007	0.255	0.001	STEAP3	STEAP family member 3
226086_at	AB037848	0.400	0.018	0.446	0.024	SYT13	synaptotagmin XIII
226408_at	AA905942	0.407	0.001	0.475	0.001	TEAD2	TEA domain family member 2
238323_at	AA337048	0.431	0.019	0.491	0.020	TEAD2	TEA domain family member 2
227236_at	AI743596	0.409	0.009	0.490	0.004	TSPAN2	tetraspanin 2
226117_at	AA195074	0.497	0.001	0.346	0.010	TIFA	TRAF-interacting protein with a forkhead-associated domain
237858_s_at	AI291290	0.176	0.005	0.279	0.012	---	Transcribed locus
229954_at	AI025415	0.328	0.010	0.350	0.008	---	Transcribed locus
239297_at	BE932011	0.409	0.021	0.357	0.010	---	Transcribed locus
204731_at	NM_003243	0.494	0.016	0.477	0.019	TGFBR3	transforming growth factor, beta receptor III (betaglycan, 300kDa)
227899_at	AI817458	0.257	0.011	0.336	0.015	VIT	vitrin
Upregulated							
244755_at	AI243681	3.324	0.006	2.765	0.003	---	---
242093_at	AW263497	4.080	0.008	2.385	0.042	---	---
234082_at	AU146017	2.193	0.009	2.631	0.015	---	---
209460_at	AF237813	2.064	0.002	2.306	0.019	ABAT	4-aminobutyrate aminotransferase
209459_s_at	AF237813	2.222	0.027	2.367	0.025	ABAT	4-aminobutyrate aminotransferase
226925_at	AW069729	2.032	0.002	2.473	0.019	ACPL2	acid phosphatase-like 2
228342_s_at	AA843297	2.364	0.035	2.453	0.001	ALPK3	alpha-kinase 3
214846_s_at	AB037751	2.038	0.043	2.290	0.002	ALPK3	alpha-kinase 3
217073_x_at	X02162	7.968	0.002	6.522	0.001	APOA1	apolipoprotein A-I

Continued.

Table 5.5. Continued from previous page.

Probe	Accession	Description	Symbol		>0.001		
204450_x_at	NM_000039	apolipoprotein A-I	APOA1	4.198	>0.001	5.238	0.014
219558_at	NM_024524	ATPase type 13A3	ATP13A3	3.637	0.004	3.684	0.042
212297_at	BF218804	ATPase type 13A3	ATP13A3	2.625	0.002	2.705	0.049
209735_at	AF098951	ATP-binding cassette, sub-family G (WHITE), member 2	ABCG2	5.459	0.011	5.854	>0.001
218332_at	NM_018476	brain expressed, X-linked 1	BEX1	3.588	0.003	4.881	>0.001
209618_at	U96136	catenin (cadherin-associated protein), delta 2 (neural plakophilin-related arm-repeat protein)	CTNND2	3.221	0.003	2.484	0.021
1557256_a_at	AA879409	CDNA FLJ37672 fis, clone BRHIP2012059	---	4.484	0.003	5.632	0.001
238455_at	AA329676	CDNA FLJ45742 fis, clone KIDNE2016327	---	2.272	0.013	2.605	0.001
236297_at	AI420817	CDNA FLJ45742 fis, clone KIDNE2016327	---	2.272	0.006	2.630	0.003
225244_at	AA019893	chromosome 1 open reading frame 142	C1orf142	2.589	0.001	2.618	0.015
230424_at	AU144860	chromosome 5 open reading frame 13	C5orf13	3.837	0.004	2.991	0.046
225817_at	AB051536	cingulin-like 1	CGNL1	4.498	0.006	3.991	0.001
204363_at	NM_001993	coagulation factor III (thromboplastin, tissue factor)	F3	2.498	0.008	2.941	0.001
202311_s_at	AI743621	collagen, type I, alpha 1	COL1A1	2.436	0.005	6.758	0.002
202310_s_at	K01228	collagen, type I, alpha 1	COL1A1	3.250	0.034	10.105	0.012
1556499_s_at	BE221212	collagen, type I, alpha 1	COL1A1	2.760	0.023	5.606	0.018
202404_s_at	NM_000089	collagen, type I, alpha 2	COL1A2	3.709	0.009	9.450	0.004
215076_s_at	AU144167	collagen, type III, alpha 1	COL3A1	2.583	0.021	5.785	0.001
211161_s_at	AF130082	collagen, type III, alpha 1	COL3A1	2.719	0.016	6.884	0.004
201852_x_at	AI813758	collagen, type III, alpha 1	COL3A1	2.553	0.035	6.355	0.049
213110_s_at	AW052179	collagen, type IV, alpha 5	COL4A5	2.759	0.040	3.276	0.039
212489_at	AI983428	collagen, type V, alpha 1	COL5A1	2.229	0.018	5.101	0.039
212488_at	N30339	collagen, type V, alpha 1	COL5A1	2.708	0.025	6.633	0.009
226237_at	AL359062	Collagen, type VIII, alpha 1	COL8A1	2.784	0.008	3.762	0.043
214587_at	BE877796	collagen, type VIII, alpha 1	COL8A1	2.294	0.007	3.041	0.000
204345_at	NM_001856	collagen, type XVI, alpha 1	COL16A1	2.106	0.012	4.050	0.028
208096_s_at	NM_030820	collagen, type XXI, alpha 1	COL21A1	2.444	0.023	2.538	0.005
216235_s_at	S81545	endothelin receptor type A	EDNRA	2.660	0.001	2.444	0.001
204464_s_at	NM_001957	endothelin receptor type A	EDNRA	2.755	0.001	2.911	0.002
204463_s_at	AU118882	endothelin receptor type A	EDNRA	3.047	0.001	3.205	0.001
206070_s_at	AF213459	EPH receptor A3	EPHA3	2.235	0.005	3.389	0.004
241457_at	AI821935	F-box and leucine-rich repeat protein 7	FBXL7	2.012	0.004	2.052	0.006
233276_at	AU146390	F-box and leucine-rich repeat protein 7	FBXL7	2.058	0.031	2.144	0.006

Continued.

Table 5.5. Continued from previous page.

209955_s_at	U76833	fibroblast activation protein, alpha	FAP	2.369	0.049	6.527	>0.001
231382_at	AI798863	Fibroblast growth factor 18	FGF18	3.462	0.010	2.875	0.002
211485_s_at	AF211188	fibroblast growth factor 18	FGF18	2.861	0.010	2.024	0.023
206987_x_at	NM_003862	fibroblast growth factor 18	FGF18	3.866	0.007	3.012	>0.001
211029_x_at	BC006245	fibroblast growth factor 18 /// fibroblast growth factor 18	FGF18	3.416	0.011	2.570	0.003
242586_at	H07986	Fibronectin type III and SPRY domain containing 1-like	FSD1L	2.167	0.001	2.315	0.009
204452_s_at	AF072872	frizzled homolog 1 (Drosophila)	FZD1	2.288	0.005	2.365	0.002
204451_at	NM_003505	frizzled homolog 1 (Drosophila)	FZD1	2.971	0.004	3.258	0.009
233437_at	AF238869	gamma-aminobutyric acid (GABA) A receptor, alpha 4	GABRA4	7.522	0.010	7.681	0.004
208463_at	NM_000809	gamma-aminobutyric acid (GABA) A receptor, alpha 4	GABRA4	6.321	0.008	7.758	0.003
207010_at	NM_000812	gamma-aminobutyric acid (GABA) A receptor, beta 1	GABRB1	8.095	0.002	9.590	0.013
205488_at	NM_006144	granzyme A (granzyme 1, cytotoxic T-lymphocyte-associated serine esterase 3)	GZMA	2.695	0.013	2.431	0.001
238227_at	AI698001	GTPase activating Rap/RanGAP domain-like 3	GARNL3	2.951	0.025	2.727	0.003
205543_at	NM_014278	heat shock 70kDa protein 4-like	HSPA4L	2.045	0.019	2.289	0.021
203903_s_at	NM_014799	hephaestin	HEPH	2.218	0.006	3.240	>0.001
205523_at	U43328	hyaluronan and proteoglycan link protein 1	HAPLN1	4.744	0.020	4.084	0.042
229669_at	AA166965	hypothetical gene supported by BC072410	LOC440416	2.870	0.024	3.200	>0.001
202718_at	NM_000597	insulin-like growth factor binding protein 2, 36kDa	IGFBP2	2.292	0.041	4.061	>0.001
203424_s_at	AW157548	insulin-like growth factor binding protein 5	IGFBP5	2.123	0.010	2.541	0.005
204439_at	NM_006820	interferon-induced protein 44-like	IFI44L	2.639	0.023	3.035	0.044
228462_at	AI928035	iroquois homeobox protein 2	IRX2	3.692	0.046	2.449	0.026
205842_s_at	AF001362	Janus kinase 2 (a protein tyrosine kinase)	JAK2	2.643	0.046	2.155	0.003
205841_at	NM_004972	Janus kinase 2 (a protein tyrosine kinase)	JAK2	2.656	0.027	2.267	0.002
237733_at	AA846804	KIAA0564 protein	RP11-125A7.3	2.252	0.026	2.295	0.023
223690_at	AF113211	latent transforming growth factor beta binding protein 2	LTBP2	3.228	0.011	5.521	0.001
204682_at	NM_000428	latent transforming growth factor beta binding protein 2	LTBP2	2.317	0.020	4.272	0.001
205381_at	NM_005824	leucine rich repeat containing 17	LRRC17	2.543	0.006	4.115	0.001
203434_s_at	AI433463	membrane metallo-endopeptidase (neutral endopeptidase, enkephalinase, CALLA, CD10)	MME	2.693	0.049	3.887	>0.001
206201_s_at	NM_005924	mesenchyme homeobox 2	MEOX2	2.179	0.014	2.997	0.008
1564733_at	BC013931	Microtubule-associated protein, RP/EB family, member 2	MAPRE2	2.030	0.021	2.294	0.008
1559942_at	BC040713	MyoD family inhibitor domain containing	MDFIC	2.733	>0.001	2.410	0.004
211675_s_at	AF054589	MyoD family inhibitor domain containing	MDFIC	2.071	0.001	2.122	0.004
209957_s_at	M30262	natriuretic peptide precursor A	NPPA	8.322	0.019	5.948	0.043

Continued.

Table 5.5. Continued from previous page.

Probe	Accession	Description	Symbol				
206801_at	NM_002521	natriuretic peptide precursor B	NPPB	13.050	0.006	17.154	0.017
224774_s_at	AK022622	neuron navigator 1	NAV1	2.082	0.026	2.053	0.010
224773_at	N57538	neuron navigator 1	NAV1	2.479	0.010	2.012	0.050
224772_at	AB032977	neuron navigator 1	NAV1	2.614	0.009	2.120	0.005
224770_s_at	AI937060	neuron navigator 1	NAV1	2.743	0.002	2.055	0.007
228723_at	AL360198	Neuroplastin	NPTN	2.275	0.005	2.030	0.001
227971_at	AI653107	Nik related kinase	NRK	3.552	0.015	7.438	0.003
204749_at	NM_004538	nucleosome assembly protein 1-like 3	NAP1L3	5.139	0.006	6.127	0.005
226140_s_at	AI934347	OTU domain containing 1	OTUD1	3.002	0.014	3.032	0.001
207808_s_at	NM_000313	protein S (alpha)	PROS1	2.009	0.023	4.047	0.005
216456_at	AL162044	Protocadherin 9	PCDH9	2.132	0.014	2.163	0.003
203096_s_at	BF439282	Rap guanine nucleotide exchange factor (GEF) 2	RAPGEF2	2.027	0.016	2.754	0.002
202035_s_at	AI332407	secreted frizzled-related protein 1	SFRP1	3.343	0.040	4.156	0.001
230071_at	AI333326	Septin 11	38971	2.611	0.023	2.739	>0.001
212413_at	D50918	septin 6	38966	2.002	0.014	2.662	0.008
212414_s_at	D50918	septin 6 /// cytokine-like nuclear factor n-pac	SEPT6 /// N-PAC	2.328	0.047	3.395	0.037
230660_at	AU146709	SERTA domain containing 4	SERTAD4	2.580	0.040	3.231	>0.001
241872_at	AI149963	SH3-domain GRB2-like (endophilin) interacting protein 1	SGIP1	2.648	0.028	5.036	>0.001
205751_at	NM_003026	SH3-domain GRB2-like 2	SH3GL2	15.924	>0.001	6.363	0.002
228141_at	AA173223	Similar to RIKEN cDNA 2310016C16	LOC493869	2.160	0.008	3.261	0.003
227628_at	AL571557	similar to RIKEN cDNA 2310016C16	LOC493869	2.072	0.020	3.044	0.009
210363_s_at	AF107028	sodium channel, voltage-gated, type II, beta	SCN2B	2.845	0.040	3.389	0.006
228181_at	AI553933	solute carrier family 30 (zinc transporter), member 1	SLC30A1	2.179	0.034	2.176	0.024
228486_at	AW165999	solute carrier family 44, member 1	SLC44A1	2.005	0.018	2.856	0.006
237285_at	BF056896	sorbin and SH3 domain containing 2	SORBS2	2.033	0.011	2.690	0.001
233720_at	AK000782	Sorbin and SH3 domain containing 2	SORBS2	2.309	0.009	3.135	0.001
220858_at	NM_014133	sorbin and SH3 domain containing 2	SORBS2	2.485	0.002	2.868	0.028
223235_s_at	AB014737	SPARC related modular calcium binding 2	SMOC2	2.334	0.031	2.455	0.004
209437_s_at	AB051390	spondin 1, extracellular matrix protein	SPON1	2.002	0.044	2.150	0.001
230836_at	AI422986	ST8 alpha-N-acetyl-neuraminide alpha-2,8-sialyltransferase 4	ST8SIA4	2.248	0.004	2.237	0.006
203373_at	NM_003877	suppressor of cytokine signaling 2	SOCS2	2.663	0.001	2.201	0.043
203372_s_at	AB004903	suppressor of cytokine signaling 2	SOCS2	3.163	>0.001	2.245	0.006
209890_at	AF065389	tetraspanin 5	TSPAN5	2.494	>0.001	2.093	>0.001

Continued.

197

Table 5.5. Continued from previous page.

239239_at	W58601	Transcribed locus	---	31.130	0.001	11.025	0.006
231035_s_at	AI697976	Transcribed locus	---	2.770	0.023	2.853	0.002
238429_at	AI342543	transmembrane protein 71	TMEM71	3.332	0.031	5.563	0.002
205177_at	NM_003281	troponin I type 1 (skeletal, slow)	TNNI1	28.949	>0.001	25.785	0.001
213201_s_at	AJ011712	troponin T type 1 (skeletal, slow)	TNNT1	3.210	0.012	3.039	0.001
226921_at	AV715153	ubiquitin protein ligase E3 component n-recognin 1	UBR1	2.041	0.002	2.132	0.003
203798_s_at	NM_003385	visinin-like 1	VSNL1	2.168	0.010	2.122	0.001
230643_at	BE220265	Wingless-type MMTV integration site family, member 9A	WNT9A	5.811	>0.001	6.672	0.007
222581_at	AF089744	xenotropic and polytropic retrovirus receptor	XPR1	2.177	>0.001	2.002	0.005
241793_at	BE674227	zinc finger, MYND-type containing 17	ZMYND17	3.610	0.036	5.109	0.004

hierarchical clustering of the amyloidosis-specific probes resulted in a very clear distinction between the amyloidosis, DCM and non-failing samples (Figure 5.6b), with the exception of donor 1 that showed again an expression profile closer to DCM than to non-failing samples. The hierarchical clustering of failing-associated genes showed clear separation of the non-failing samples from DCM and amyloidosis patients. Only the DCM sample designated as DCM 5 was (red arrow) showed a transcriptosome profile closer to non-failing samples.

The two samples clustering outside of their respective groups were further investigated with a more detailed clinical history analysis in order to find the cause of the abnormal transcriptome profile. This revealed presence of mild hypertrophy in donor 1 and history of increased alcohol consumption in DCM 5.

With these post-analysis considerations, we can conclude that the results form the hierarchical clustering suggested consistency of the analysis performed and clear specificity of the EST identified.

5.2.5 PCR validation

RNA microarrays are based on an extremely powerful technology which allows the determination of the levels of thousands of transcripts at the same time. However, this expression profiling method is also characterized by high occurrence of false positive and false negative due to several causes including cross hybridization of cRNAs with similar sequences, artifacts deriving from the preparation of the samples leading to preferential enrichment of a subset of transcripts or simply deriving from technological limitations of the detection systems. Therefore it is of primary importance to validate the data obtained from microchips analyses using alternative methods. Currently the most accurate and trusted method for microarray data validation is the quantitative real-time-PCR (qRT-PCR).

qRT-PCR was used in our study to confirm the expression levels of randomly selected genes showing differential expression in the groups we analyzed. In particular we assayed the levels of nestin (NES) and Down Syndrome Critical Region 1 (DSCR1) for the DCM-specific genes and apolipoprotein E (APOE) and stanniocalcin (STNC) for the amyloidosis-specific genes (Figure 5.7). In addition we verified four failing-related genes: atrial natriuretic peptide (ANP), brain natriuretic peptide (BNP), slow-
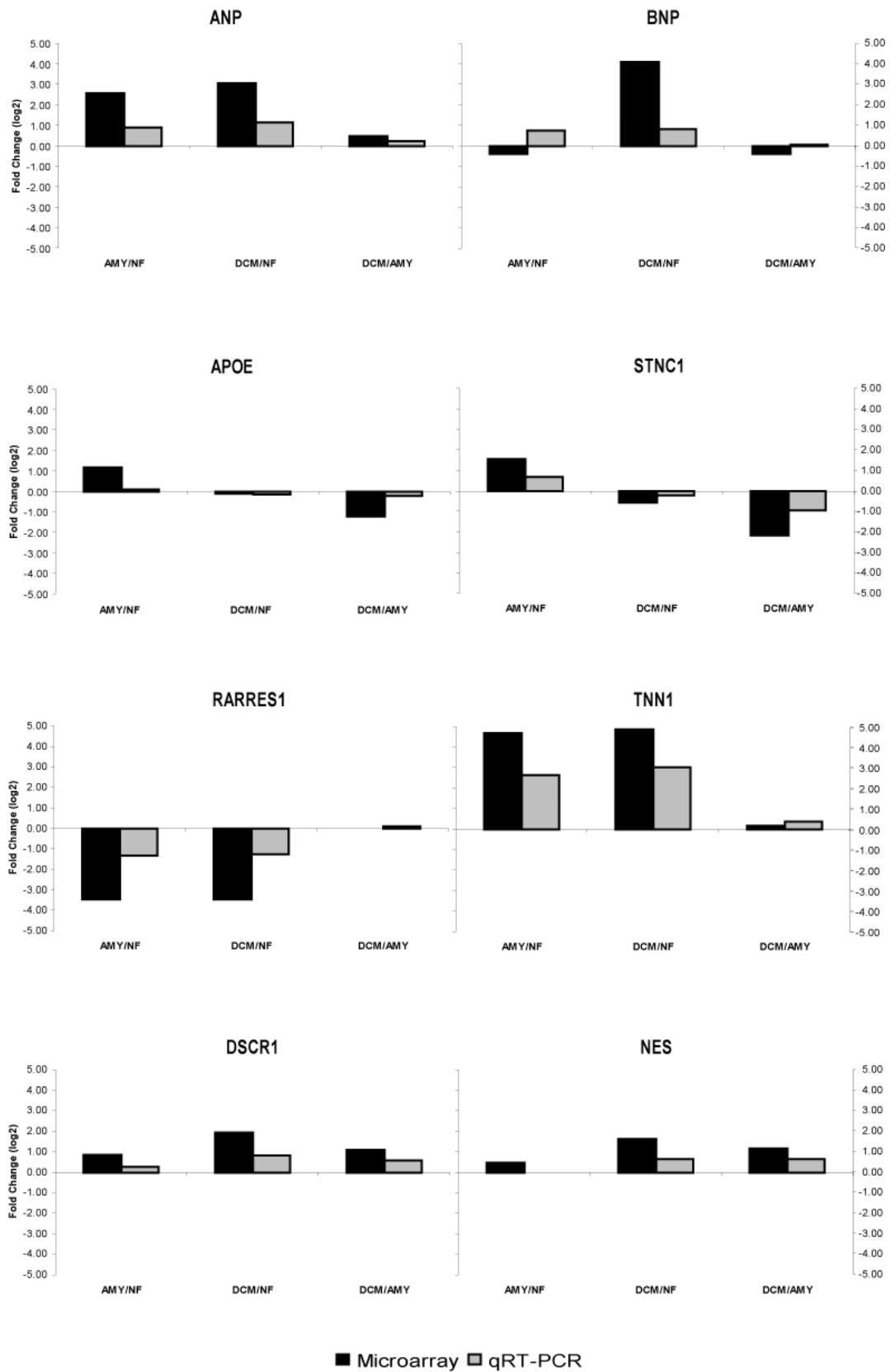
A

B

Gene		Microarray	qRT-PCR
ANP	Amyloidosis/Control	5.94	1.86
	DCM/Control	8.32	2.17
	DCM/Amyloidosis	1.4*	1.17*
BNP	Amyloidosis/Control	0.76	1.69
	DCM/Control	17.15	1.76
	DCM/Amyloidosis	0.76*	1.04*
RARRES1	Amyloidosis/Control	0.09	0.39
	DCM/Control	0.09	0.41
	DCM/Amyloidosis	1*	1.05*
TNN1	Amyloidosis/Control	25.85	6.19
	DCM/Control	28.95	8.07
	DCM/Amyloidosis	1.12*	1.3*
APOE	Amyloidosis/Control	2.23	1.06*
	DCM/Control	0.93*	0.9*
	DCM/Amyloidosis	0.42	0.85*
STNC1	Amyloidosis/Control	2.96	1.61
	DCM/Control	0.67*	0.85*
	DCM/Amyloidosis	0.22	0.52
DSCR1	Amyloidosis/Control	1.79*	1.2*
	DCM/Control	3.84	1.77
	DCM/Amyloidosis	2.14	1.48
NES	Amyloidosis/Control	1.4*	1*
	DCM/Control	3.11	1.58
	DCM/Amyloidosis	2.22	1.57

*=not statistically significant

Figure 5.7. qRT-PCR validation of microchip results. The levels of four failing-related genes (atrial natriuretic peptide (ANP), brain natriuretic peptide (BNP), retinoic acid receptor responder 1 (RARRES1), slow-twitch skeletal troponin 1 (TNN1)), 2 DCM-specific (DSCR1), nestin (NES)) and 2 amyloidosis-specific (apolipoprotein E (APOE), stanniocalcin 1 (STNC1)) were analyzed by qRT-PCR and standardized to the content of 18S tRNA. Panel a compares the averages of each gene for each group analyzed in the study. Statistically significance between two groups ($p<0.05$) is indicated by the presence of a horizontal bar. In b the data from qRT-PCR are compared to what was generated from the microarray analysis.

twitch skeletal troponin 1 (TNN1) and retinoic acid receptor responder 1 (RARRES1). The results were standardized to the content of 18S tRNA of each sample. Our results showed accuracy between the microarray and qRT-PCR data in 7 transcripts out of 8 (87.5%). Only the amyloidosis-specific gene APOE did not show expression levels matching with the microchip results.

5.2.6 Gene Ontology analysis

Microarray studies generate a large amount of data that often becomes excessively difficult to analyze in order to identify the pathways involved in certain phenotypes. A valid contribution to the analysis of these results and to understand their biological meaning derives from the use of Gene Ontology databases. These databases collect all the known molecular functions, cellular localization and interactions of gene products.

For our study we submitted the lists of significantly altered probes we identified from our 3-group analysis to the Database for Annotation, Visualization and Integrated Discovery (DAVID).

According to the database, 123 of the 200 failing-related EST deriving from our analysis were significantly associated to biological processes (summarized in Table 5.6a and visualized in Figure 5.8). No specific correlation was instead detected for the remaining 77 probes. The analysis performed using the KEGG database showed significant alteration in the complement/coagulation cascades and in the extracellular matrix-receptor interaction (Table 5.6b). The biocarta database, instead, suggested presence of alterations in the activin like kinase pathway (Table 5.6c).

Table 5.6. List of biological processes and pathways associated to the failing process according to DAVID (a), Kyoto encyclopedia of genes and genomes (KEGG) (b) and biocarta databases (c). Only processes involving at least 2 genes and p<0.05 were included. Abbreviations: Wnt: wingless-type mouse mammary tumor virus integration site ECM: Extra-cellular matrix ALK: Activin receptor-like kinase (Bone morphogenetic protein receptor type IA precursor).

A

Process	Count	p value
Establishment of localization	38	0.001
Localization	38	0.001
Transport	35	0.001
Cell communication	35	0.037
Development	31	>0.001
Ion transport	20	>0.001
Inorganic anion transport	11	0.000
Anion transport	11	0.000
Morphogenesis	11	0.012
Phosphate transport	10	>0.001
Circulation	6	0.001
Regulation of cell growth	5	0.012
Regulation of growth	5	0.015
Cell growth	5	0.028
Regulation of cell size	5	0.028
Wnt receptor signaling pathway	4	0.038
Blood pressure regulation	3	0.024
Osmoregulation	2	0.043
Not classified	77	

B

Process	Count	p value
Complement and coagulation cascades	4	0.018
ECM-receptor interaction	4	0.039
Not classified	130	

C

Process	Count	p value
ALK in cardiac myocytes	4	0.012
Not classified	134	

The application of the DAVID algorithm to the 13 DCM-specific probes indicated the presence of a group (n=3) of EST involved in the system maturation and, in particular, in the nervous system development, while 10 probes were not significantly classified in any category (Table 5.7). The consultation of the KEGG and Biocarta database could not associate any specific pathway to the identified DCM-specific ESTs.
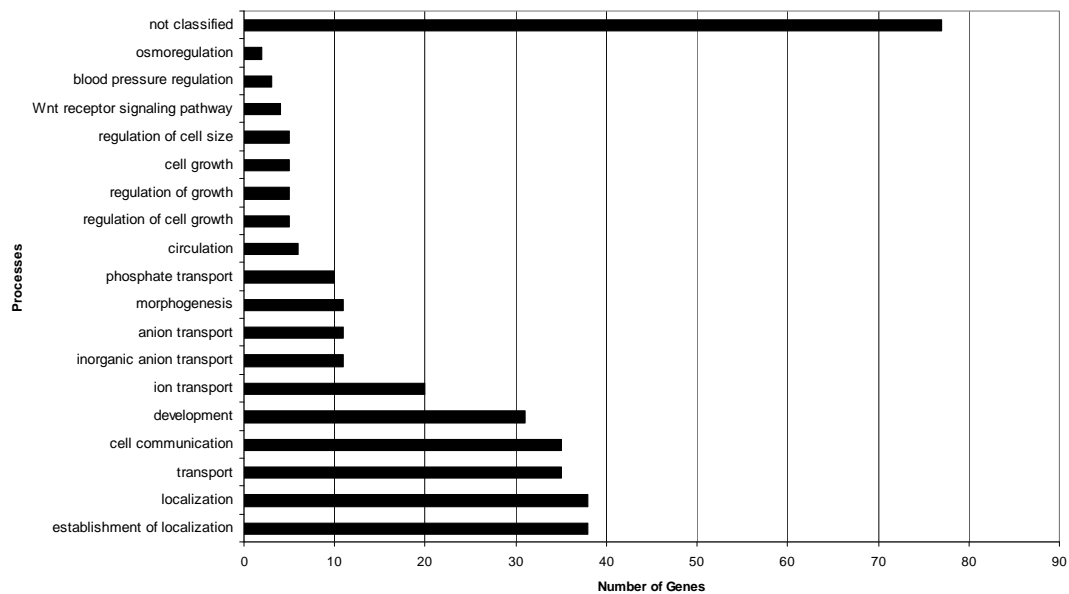
Figure 5.8. Biological processes associated to the failing-specific genes according to the Database for Annotation, Visualization and Integrated Discovery (DAVID).

203

The amyloidosis-specific probes resulted involved mostly in processes such as development, cell adhesion and tissue remodeling (Table 5.8 and Figure 5.9). No significant classification was instead indicated for 20 EST out of the 52 identified by our analysis. According to the KEGG database, the amyloidosis-specific probes resulted related to cell communication, focal adhesion and extracellular matrix-receptor interaction pathways (Table 5.8b). In addition, the biocarta database identified a cluster of probes involved in the maturation of T lymphocytes from their naïve state (Table 5.8c): Thy-1 and CD28.

5.3 Discussion

In the previous chapter we attempted to identify unknown myocardial alterations involved in the etiology of idiopathic DCM using a proteomic-based approach such as mass spectrometry. Unfortunately, several technical limitations associated to the technique restricted the possibility of obtaining significant results. In this study we propose the use of a second high throughput technique to investigate new causes of DCM. In particular we decided to develop a comprehensive picture of the transcriptosome of the failing tissue using the microarray technology, which allows the detection of the levels of thousand of ESTs. Several limitations have been described in the past in relationship to this technique, including the biological variability of the samples (especially when deriving from human patients), stochastic variability or the incapacity of detecting alterations in the post-translational

Table 5.7. List of biological processes associated to DCM according to DAVID database. No pathways resulted significantly related to DCM according to KEGG and biocarta databases. Only processes involving at least 2 genes and p<0.05 were included.

Process	Count	p value
Nervous system development	3	0.032
System development	3	0.032
Not classified	10	

Table 5.8. List of biological processes and pathways associated to amyloidosis according to DAVID (a), KEGG (b) and biocarta databases (c). Only processes involving at least 2 genes and p<0.05 were included.

A

Process	Count	p value
Organismal physiological process	12	>0.001
Development	11	>0.001
Cell adhesion	8	0.001
Organ development	8	0.001
Skeletal development	6	0.004
Tissue development	5	0.005
Regulation of organismal physiological process	4	0.005
Biomineral formation	3	0.005
Bone remodeling	3	0.005
Ossification	3	0.005
Phosphate transport	3	0.015
Tissue remodeling	3	0.022
Positive regulation of T cell activation	2	0.050
Not classified	20	

B

Process	Count	p value
Cell communication	5	>0.001
Focal adhesion	4	0.022
ECM-receptor interaction	3	0.028
Not classified	36	

C

| Process	Count	p value
T Cytotoxic Cell Surface Molecules	2	0.037
T Helper Cell Surface Molecules	2	0.037
Not classified	39	

Amyloidosis-specific
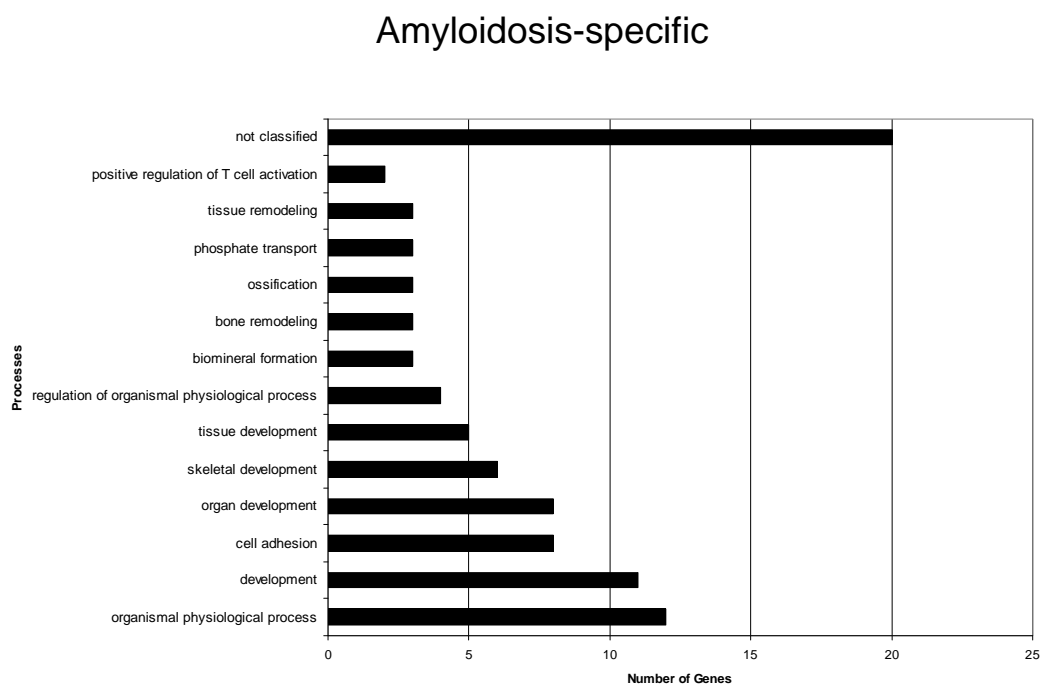
Figure 5.9. Biological processes associated to the amyloid-specific genes according to the Database for Annotation, Visualization and Integrated Discovery (DAVID).

modification pathways. However, microarrays are nowadays commonly considered a valid and efficient method to analyze multiple pathways simultaneously, significantly reducing the problems associated to the inter-experimental variability.

Our analysis was performed with the most complete human chip available (Affymetrix Human Genome U133 Plus 2.0), which contains more than 54,000 EST and allowed one of the most detailed characterization of the DCM transcriptome up to date.

The rationale supporting this study consists in separating the transcripts specifically expressed in DCM from the messengers involved in the progression of the failing condition and, at least in part, from the effects produced by the pharmacological treatment of the disease. We therefore propose a 3-group analysis including two different causes of HF, idiopathic DCM and systemic-light chain amyloidosis, and a control group of non-failing samples. Light chain amyloidosis is a systemic disorder associated to malignant lymphomas or myelomas. The uncontrolled expansion of B lymphocyte clones in these forms of liquid tumors often produces overexpression of immunoglobulin chains, leading to their accumulation in the circulation and,

eventually, to the aggregation in amyloid fibers. The deposition of this molecular species in the heart gradually increases the stiffness of the organ and reduces the elasticity of the tissue, leading to a restrictive cardiomyopathy and to heart failure. In addition, the presence in the extracellular space of β-plated unfolded structures can directly impair the cardiomyocyte contractility by altering the redox state and the Ca^{2+} handling of the cell (Brenner et al., 2004). As we demonstrated in Chapter 3, idiopathic DCM samples show strong evidences of unfolded proteins not associated to any known amyloigenic alteration (Sanbe et al., 2004). We assume that the presence of these aggregates produces effects on the cardiomyocytes, which may include modifications of the transcription profile of the cell. As systemic amyloid is associated with deposition of amyloid aggregates in the whole body, here we hypothesize that the exposure to circulating amyloid may be able to produce at least part of the transcriptosome alterations normally due to the formation of intracellular amyloid fibers in cardiomyocytes. Based on this assumption, we think that the direct comparison between systemic amyloidosis and DCM samples also allows increased precision in determining a subset of DCM-specific genes by permitting the identification of the modifications of the transcriptome due to the potential effects of amyloid fibers on the cells.

Our data from gene-ontology analysis show that the genes that we identify as failure-related mainly group in 4 categories: metabolism (Sack and Kelly, 1998, Tan et al., 2002, Oyama and Chittur, 2005), ion transport and localization (Barrans et al., 2001, Barrans et al., 2002, Hwang et al., 2002, Yung et al., 2004), fibroblast grow and activation (Reiss et al., 1995) and extracellular matrix components (categorized as response to wounding and development in Table 5.8). We can hypothesize that this indicates the activation of a series of mechanisms to counteract the progressive loss of cardiac function during the failing process. Although they have beneficial effects in the short term by providing structural support and resilience to the organ, these mechanisms eventually produce deleterious maladaptive results consisting in excessive stiffness of the organ, electromechanical uncoupling and further decompensation (Sharma et al., 2005).

Some of the genes that we identified as failing-related have been previously proven to be associated to the progression of the disease and are currently used as clinical markers (Rademaker and Richards, 2005). The detection of overexpression of genes such as the atrial natriuretic peptide (ANP) and the brain natriuretic peptide (BNP) in both amyloidosis and DCM samples is a confirmation of the validity of our results, which demonstrate to be in line with previous studies. ANP and BNP in the past have been associated to a compensatory activity aimed to oppose the increasing inefficiency in cardiac activity typically observed during the progression of heart failure. These genes are acquiring increasing interest both as diagnostic and prognostic indicators as well as potential target for the development of alternative therapeutic approaches, even if they can not be classified as initial cause of the failing process.

Considering the significant differences between amyloidosis and DCM both in term of etiologies and features of the diseases, it is interesting to observe that the two groups we analyzed share a large majority of common altered genes and are instead characterized by relatively small groups of disease-specific messengers (amyloidosis: 41, DCM: 10).

The analysis of the amyloidosis-related transcripts showed significant alterations in genes related to mechanical stress -including the detection of mechanical stress-, skeletal development, tissue remodeling, cell-to-cell and cell-to matrix adhesion. The continuous accumulation of light immunoglobulin chains produces major alterations to the elasticity of the heart that lead to increased pressure on the cardiac walls and deposition of extracellular matrix components characterized by higher resistance to mechanical stress. Although this process is aimed to protect the cardiac tissue from being damaged, in the long term it accelerates the development of restrictive cardiomyopathies and the occurrence of heart failure.

In addition our data suggest the presence of increased levels of two surface markers involved in the maturation of T-cells (Thy-1 and CD28), which may be related to the presence of lymphocyte T infiltrates in the cardiac tissue or, alternatively, may

represent a consequence of the immunosuppressive therapeutic approach involved in the treatment of systemic AL amyloidosis.

Within the amyloidosis-specific genes, *STC1* was overexpressed in all the amyloidosis samples analyzed. This gene codify for Stanniocalcin 1 (Stc1), an highly conserved homodimer glycoprotein involved in the regulation of Ca^{2+} homeostasis and transportation in the intestine (Madsen et al., 1998). The role of Stc1 in the myocardium, instead, seems related to the protection of the cardiomyocytes during diastole by regulating the Ca^{2+} currents in order to prevent overload of the ion and hypercontracture of the cell (Koizumi et al., 2007). Previous data from Hamad et al (Sheikh-Hamad et al.) show no alteration of Stc1 mRNA levels in failing hearts; however the authors detected significant increase of the protein levels that can apparently be reverted by cardiac unload mediated by left ventricular assist device (LVAD).

In addition to the protective role on Ca^{2+} overload, that is a common feature of heart failure independently from the etiology, *STC1* gene overexpression in cardiac amyloidosis might relate to the response of cardiac tissue to the accumulation of unfolded β-pleated protein fibers in the extracellular space. Stc1 shares 61% homology with stanniocalcin 2 (Stc2), a protein shown to be overexpressed following the administration of β-amyloid fibers in the culture media in isolated neuroblastoma cells (Kim et al., 2003). Stc2 is also activated following endoplasmic reticulum stress by ATF4 and PERK, two molecules of the unfolded protein response pathway (Ito et al., 2004). The activation of *STC1* in stress condition seems to be achieved independently of ATF4 and PERK. However we can not exclude overlapping functional roles of these two peptidic hormones and *STC1* activation mediated by other components of the UPR.

The gene-ontological classification of the DCM-specific genes identified showed a limited number of messengers which have ever been related to DCM and which were characterized by clear involvement in the development processes and, more specifically, in the development of nervous system.

Among the genes that were overexpressed we considered of particular interest the presence of nestin. Nestin is a protein belonging to the family of the intermediate filaments normally expressed in the nervous system during neurogenesis in the embryonic development. In adult subjects nestin expression has been observed in the pituitary gland and in the subventricular zone of the brain (Kukekov et al., 1999, Leonard et al., 2009, Weiss et al., 2009) and, at lower levels, in several stem cell niches including the bone marrow (Kachinsky et al., 1995, Fukuhara et al., 2005, Wagner et al., 2006). Interestingly, some of these studies also reported the presence of nestin positive cells in the cardiac tissue. Different hypotheses have been formulated to explain the function of nestin in the myocardium: nestin positive cells can develop from neural types normally present in the heart (neural fiber (El-Helou et al., 2005) or cells deriving from the activation of dormant multipotent precursors homed in the heart but originated from the neural crest during embryogenesis (Tomita et al., 2005)) or can relocate to the heart from other tissues such as bone marrow as a protective and reparative response to injury or prolonged stress condition (Fukuhara et al., 2005). Alternatively, the overexpression of nestin we observed can be related to a compensatory process specific to the cardiomyocytes to replace cytoskeletal elements previously described to be progressively lost in late stage cardiomyopathies (Hein et al., 2000, Kostin et al., 2000) and to increase the mechanical resistance of the cardiomyocytes (Capetanaki et al., 1997).

A second DCM-specific messenger we considered interesting was a gene relate to Down Syndrome (SD), Down Syndrome Critical Region 1 (*DSCR1*). This gene was identified in 1997 on the chromosome 21 in a highly conserved region (q22.1-2) in all the patients affected by Chr 21 trysomy (Fuentes et al.). Although no clear biological role for this gene has been described to date, functional analyses classified *DSCR1* as an "adaptive response stress gene" (Crawford et al., 1997, Leahy et al., 1999).
DSCR1 encodes for calcipressin, a proline-rich protein normally found at high levels in the brain and in the heart at developmental stage. During adulthood this protein seems instead to be constitutively overexpressed in pathological conditions such as DS (as a result of polyploidy of the region 21q22.1-2) and Alzheimer's Disease (Fuentes et al., 1995, Fuentes et al., 2000, Casas et al., 2001, Porta et al., 2007).

Several groups investigated the presence of correlation between the two diseases, collecting interesting results: in fact it seems that DS patients develop increased cognitive impairment during the 4th decade of life. These forms of dementia are similar to what has been observed in AD. In addition *post mortem* analysis of DS brain samples clearly show markers typically associated to AD, such as diffuse presence of amyloid plaques (Lemere et al., 1996, Liu et al., 2006). Of note these alterations are apparently not related to the presence of an additional copy of the *APP* gene (that maps closely to *DSCR1* in region 21q21), since they appear to be present even in partial trisomic subjects in which *DSCR1* is present in 3 copies, while *APP* is diploid (Korenberg et al., 1989).

The role of calcipressin in AD, instead, seems related to protecting the cell from the oxidative stress that is commonly observed in the disease as suggested by the elevated levels of oxidized proteins in *post-mortem* examinations (Subbarao et al., 1990, Balazs and Leon, 1994, Lovell et al., 1995, Sayre et al., 1997). Several studies showed that calcipressin has beneficial effects in the short term in presence of stress conditions originated from accumulation of oxygen radicals (Ermak et al., 2002). However the chronic expression of the protein seems to induce irreversible damage and therefore to the progression of the degenerative condition (Ermak et al., 2001, Ermak and Davies, 2002, Ermak et al., 2002, Ermak and Davies, 2003).

The DSCR1-mediated cellular response to oxidative stress in AD seems to activated by release of Ca^{2+} in the cytoplasm (Crawford et al., 1997, Leahy et al., 1999). Therefore we can hypothesize that the well-described accumulation of Ca^{2+} in DCM hearts triggers the expression of DSCR1 to achieve a transient protective effect for the cardiomyocytes. In particular calcipressin seems to directly inhibit the calcineurin signal transduction pathway, by blocking the capacity of the protein to allocate in the Ca^{2+}-calmodulin-dependent serine/threonine phosphatase holoenzyme (PP2B), in which it represents the catalytic subunit (Fuentes et al., 2000).

The calcineurin A pathway is a highly conserved transduction system in eukaryotes (Liu et al., 1991) and seems to have an important function in triggering cellular reactions in response to several extracellular stimuli. In neurons the pathway appears to be related to the creation of memory (Barinaga, 1998, Zhuo et al., 1999) and to

apoptosis (Asai et al., 1999, Honig and Rosenberg, 2000). The role and the effects of the activation of this pathway in the heart are still debated: some reports associated calcineurin to cellular growth and to hypertrophy (Molkentin et al., 1998, De Windt et al., 2001), while other groups demonstrated the capacity of the protein to induce apoptosis of the cardiomyocytes by dephosphorylating BAD (Saito et al., 2000, Wang et al., 2002).

Overexpression of *DSCR1* has also been detected in the adult heart as a response to mechanical stress conditions such as pressure overload-induced hypertrophy. This suggests that *DSCR1* might have a role as a negative feedback mechanism regulating the activity of calcineurin (Dorn, 2001, Rothermel et al., 2001, Wang et al., 2002, Ni et al., 2006). In fact, transgenic murine models overexpressing *DSCR1* showed reduced hypertrophic response to exercise and adrenergic stimulation and, in the long term, significantly lower probability of progression towards a failing condition. In *DSCR1*(-/-) knockout mice, instead, the absence of the calcipressin aggravated the hypertrophic response to the activation of the calcineurin pathway and no significant alteration of the development of hypertrophy was observed as consequence of chronic adrenergic stimulation and of pressure overload.

According to several studies the cardioprotective role of *DSCR1* might be related to a chaperon-like function associated to calcipressin (Crawford et al., 1997, Leahy et al., 1999). Interesting observations on the analysis of the amino acid sequence of the protein showed the presence of regions highly homologous to chaperones belonging to the glucose-regulated protein (*grp*) class, which, similarly to *DSCR1*, have been extensively described to be induced by alterations of Ca^{2+} homeostasis (Leahy et al., 1999). In addition, calcipressin has been showed to share the same localization pattern of *grp78*, the most abundant of the *grp*s: in absence of stress stimuli the protein is concentrated in the perinuclear area and in the cytosol, while during stress conditions the protein is translocated to the endoplasmic reticulum, where calcipressin can accomplish its hypothetical chaperon activity (Leahy and Crawford, 2000).

Other investigators reported involvement of calcipressin in the regulation of the cell cycle and proliferation: the overexpression of DSCR1 has been described to be

associated to an arrest in the cell cycle in G1-phase (Leahy and Crawford, 2000) which might be mediated by direct action of calcipressin on the proteins involved in the progression of cell cycle, i.e., cyclins and cyclin-dependent kinases (CDKs).

In our specific case the upregulation of DSCR1 specifically observed in DCM samples might be part of an adaptive response to chronic stress conditions including alterations of Ca^{2+} homeostasis or the accumulation of unfolded peptides we described in chapter 3. Alternatively, we can speculate that the upregulation of DSCR1 is a low-penetrance genetic alteration that produces inhibition of the hypertrophic remodeling of the heart normally mediated by calcineurin and downregulation of CDKs in presence of stress conditions or other genetic factors. This last hypothesis is supported by our experimental data in which we could observe a significant decrease of the cyclin-dependent kinase inhibitor 3 (CDKN3), a dual-specificity phosphatase that interacts with both cdc2 and CDK2 (Hannon et al., 1994). These two proteins control the progression of the cell cycle respectively from G2 to M phase and from G1 to S phase (Liao et al., 2001). Their levels are usually elevated during cardiac development in the embryonic and neonatal stages; however their expression progressively decreases to basal levels during adulthood (Kang et al., 1997) and their role in terminally differentiated non-proliferating cell is still unclear. Results obtained from different *in vitro* models including neonatal cardiomyocytes suggested that cdc2 and CDK2 are involved in the initiation of the apoptotic process (Meikrantz et al., 1994, Hiromura et al., 1999). However other studies reported that CDK activity is required in neonatal cardiomyocytes for the hypertrophic response to serum stimulation (Tamamori et al., 1998). These data are supported by the analysis of cardiac tissue deriving from transgenic mice overexpressing CDK2, in which the heart showed an increase in mononucleated cardiomyocytes and exacerbated hypertrophic response to pressure overload with no change in the proportion of mononucleated cells. Interestingly, the CDK2-mediated apoptosis initiation seems to be related to the activation of caspase 3, with no participation of the calcineurin pathway. Therefore the downregulation of the CDK2 inhibitor we observed in our results in DCM samples might be compatible to increased apoptotic signals that lead to further degeneration of the cardiac tissue.

An additional interesting observation on the function of DSCR1 was recently reported by Dr. Ryeom's group (Baek et al., 2009). DS patients seem to have lower incidence of tumors than the normal population and the cancer protection activity seems to be specifically achieved by the overexpression of calcipressin. The occurrence of cardiac tumors is usually a rare event. Therefore we can speculate that DSCR1 is overexpressed in the heart during the aging process in order to prevent the formation of tumor masses in the organ. However the long term overexpression of the gene combined with other still unknown factors might lead to the alterations leading to DCM.

In conclusion, in the vast majority of the cases DCM is a multi-factorial disease in which multiple genetic defects and environmental factors combine producing progressive dilatation of the heart and contractile dysfunction. The identification of specific factors involved in the etiology of this condition represents an important goal for understanding the alterations in that portion of patients that are still categorized as idiopathic. This will lead to considerable advancements in the recognition of risk factors as well as in early detection of the disease and in the development of new therapeutic approaches. The study we performed used high throughput technologies to obtain a complete picture of the expression pattern of DCM, focusing in particular on the determination of those aspects that specifically characterize DCM from other cardiomyopathies. Our results show interesting involvement of genes related to neurodegenerative diseases and to the development of the nervous system and suggest new intriguing therapeutic possibilities to explore in the future.

5.3.1 Limitations

Although microarrays represent an attractive method for obtaining the most complete and detailed picture of the transcriptome available with current technologies, we have to consider some limitations of the technique. First, the alterations detected by microarray do not always correspond to actual alteration in protein levels since a considerable number of regulatory steps are present between the mRNA maturation and the functional protein. These include translational regulation, folding, post-

translational modification, transport to the correct subcellular location and stability of the protein.

A second limitation of microarrays derives from the significant occurrence of false negative and false positive detection. It has been estimated that a good quality microarray analysis is biased by at least a 5% intrinsic error due to technological limits (Firestein and Pisetsky, 2002, Hindmarch et al., 2006). This percentage is even higher in the case when low amount of starting material is available and the investigators are forced to introduce an RNA amplification step that might preferentially amplify particular subsets of messengers. It is therefore important to validate the results obtained from RNA chips using more reliable techniques such as qRT-PCR. However the amount of data generated by a microarray analysis is usually extensive and the validation step is usually limited to selected genes of interest. In our specific study we could confirm 87.5% of the selected genes, even if we obtained confirmation of the quality of the analysis from the hierarchical clustering of the samples for the genes that we defined as amyloidosis-, DCM- and failing- specific, in which we showed a clear separation of the patients in the 3 different groups analyzed.

Of note our analysis could not confirm the majority of expression alterations previously described by other authors in heart failure, with the exception of ANP and BNP (Barrans et al., 2002, Chen et al., 2002). This discrepancy might be attributed to several factors including the use of different genechip platforms and the strict cut-off threshold (2-folds) we adopted for processing the data. The adoption of less restrictive parameters (cut-off threshold=1.5 fold) on a limited number of messengers previously described allowed the confirmation of earlier reported HF-related genes such as lumican. This approach would allow the identification of larger numbers of messenger for each group we analyzed, although it would also introduce several technical difficulties in term of validation and analysis of the results.

Further inconsistencies between different microarray-based studies also arises from the biological variability between the individuals analyzed and their stage of the disease. This represents a major limitation not only for the meta-comparisons, but also for the analysis of the data of a single study. To minimize this error we specifically selected samples that were matched for the age, gender and, when possible, for ethnicity. However further variability was introduced by other factors which we

couldn't verify especially for the non-failing samples, of which limited clinical history was available. These include the presence of concomitant pathological conditions and social habits such as diet and smoking (Bristow, 2003).

A final limitation affecting microarray-based analyses as well as other high throughput studies is related to the extensive statistical processing that is normally applied to this type of data (Storey and Tibshirani, 2003). This complex issue, which has been referred as multiple testing problem, derives from the intrinsic probability that the statistical analysis applied to every gene represented on the microarray chip can lead to an erroneous conclusion (Pounds, 2006). While this probability has minimal effects on traditional approaches due to the limited amounts of genes analyzed, significant issues arise when instead one or more entire pathways are considered without the possibility of analyzing multiple biological replicates because of the limited material available or the costs associated to the analysis. Although this problem can be partially addressed by introducing stricter significance cutoff thresholds for each gene considered, the occurrence of false positives and false negatives still can not be ignored and several analytic methods have been developed to estimate the robustness of a study. Based on these considerations, the results obtained from high throughput studies such as the observation we report in this chapter should be seen as preliminary data regardless of the statistical method used for the analysis and should be followed by more focused functional validation.

CHAPTER 6

FINAL CONSIDERATIONS

Final considerations

In some cases cardiovascular diseases can be prevented, but in some others our knowledge of the detailed molecular aspects and involved pathways is still fragmentary and requires further investigation.

In the last five years a significant number of publications describing the involvement of the UPR in several cardiac conditions have appeared, confirming this pathway as a common alteration for a continuously increasing number of human pathologies.

Evidences of activation of the UPR including increased *XBP-1* mRNA splicing and overexpression of GRP78 have been clearly demonstrated after inducing hypoxia in isolated rat neonatal cardiomyocytes as well as general increased expression of several UPR components have been described in cardiomyocytes derived form the peri-infarcted area both in humans and in murine models of ischemic heart disease. These observations have been related to a protective role of the UPR components against the ischemic insult. In particular, recent studies show that the ATF6 arm of the UPR seems to have significant effect on the expression of GRP78 and GRP94, with consequent beneficial effects on the cardiomyocyte. However, other reports showed that longer exposures to the hypoxia activate other pathways of the UPR such as the CHOP- and caspase 12-mediated apoptosis and that the survival of the cell depends almost completely on the intensity and duration of the ischemic event.

Similar observations have been reported also for heart failure and DCM, including the increase of GRP78 levels and morphological modifications of the ER, which suggest the presence of an overload process. Interestingly, studies conducted on mice after aortic banding showed the activation of the CHOP signaling pathway only in the failing hearts but not in the hypertrophic, which confirms the hypothesis that the UPR-induced apoptosis is initiated by persistent ER stress conditions and UPR activation.

It is interesting to observe that the heart seems to be one of the most sensitive organs to the negative effects of prolonged activation of the UPR. In fact, animal studies showed that the induction of alterations of the normal vescicular traffic leads to the accumulation of ubiquitinated proteins in the ER, producing a situation of stress and,

eventually, DCM with no obvious alterations in other organs. Similarly, clinical reports showed that the administration of proteasome inhibitors such as bortezomib (which are normally used in the treatment of cancer and systemic amyloidosis) produce toxic effects on the heart and leads to the development of a severe acute failing condition similar to DCM.

Additional confirmation of the role of the protein folding control has been reported in desmin-related cardiomyopathy, in which the work of J. Robbins and collaborators elucidated the presence of electron-dense granulofilaments characterized by the β-sheeted structure typically observed in other amyloid-related pathologies. These deposits were associated to anomalies of α-β crystallin, eventually leading to the incapacity of this chaperone to control the appropriate folding of desmin and progressive impairment in degradation of the aberrant peptides.

In the previous chapters we described our findings related to idiopathic dilated cardiomyopathy, one of the main causes of heart failure. In particular our results show for the first time the presence of thioflavin-S-positive and electron-dense aggregates of proteinaceous material in the cytosol of cardiomyocytes affected by the disease, which formed intracellular fibers similar to the structures normally observed in the amyloid deposits of several conditions related to the accumulation of unfolded proteins. Our experiments demonstrated that the presence of these structures is associated to a general activation of the cellular mechanisms involved in the control of the accumulation of unfolded peptides including transcription factors (ATF6), chaperones (GRP78 and GRP94) and peptides involved in the activation of the apoptotic cascade (CHOP and Caspase 12), which may explain the diffuse apoptotic process normally observed in late-stage DCM cardiac samples.

Although in the past the expression of pro-amyloigenic peptides such as polyQ-huntintin has been positively associated to the development of heart failure, our study demonstrated the presence of mature amyloid structures and pre-amyloid precursors (oligomers) of endogenous nature, which seem able to produce devastating effects on the cardiomyocytes and on the contractile function. Our results from isolated murine cardiomyocytes showed that this toxicity seems to be mediated through significant alterations in Ca^{2+} handling, which led to increased velocity of Ca^{2+} release from the

SR and systolic cytoplasmatic Ca^{2+} content. These data reflect what has been observed in amyloid-associated neurodegenerative diseases such as Alzheimer's disease. In fact, several studies in the AD research field demonstrated the presence of several interactions between the γ-secretase complex and cardinal molecules involved in the intracellular Ca^{2+} regulation, such as RyR and SERCA. In our study we confirmed the presence of direct interaction between the cardio-specific form of SERCA and Presenilin 1 by co-immunoprecipitation. In addition, we were able to show significant alterations of the presenilin levels in DCM-affected hearts, which might be correlated to genomic alterations leading to altered expression levels, instability or defective function. In particular the genomic analysis of our sets of patients identified two previously described AD-related mutations in the codifying sequence (A953G in PS1 and G185A in PS2) and two new polymorphisms in the promoter region of the PSEN1 gene (-92delC and -21G→A). We characterized these two new SNIPs using an *in vitro* reporter assay and our results showed that the presence of either of these two alterations produces dramatic reduction of the expression of the protein encoded downstream (respectively 75% for -92delC and 32% for -21G→A).

These observations represent interesting and innovative findings in the DCM field. Nonetheless, the identification of the protein(s) forming the amyloid species is still of primary importance. In this regard our strategy was based on a series of different methods to obtain tissue lysates enriched in insoluble aggregates (fibers) or in soluble oligomers. Our analysis was structured to start from relatively simple techniques involving the analysis of the whole tissue lysates on gels optimized for the separation of large protein complexes (DADT-PAGE and agarose). However, this approach did not produce any significant result. Therefore, our experiment focused on the elaboration of new protocols to isolate amyloid fibers (by taking advantage of the specific density of these structures) and oligomers (by co-immunocoprecipitating the aggregates with antibodies recognizing their specific three-dimensional structure). These techniques were ultimately paired to a mass-spectrometry analysis to identify the peptides present in the purified products. In particular the immunoprecipitation of the oligomeric forms allowed the identification of a peptide called ankyrin repeat

domain-containing protein 18A, which, at the moment, has not been associated to any recognized significant biological role. Therefore, additional investigation on the functions of this protein in the normal heart needs to be conducted to understand its involvement in DCM.

Although we were not able to specifically identify the protein(s) directly involved in the amyloid deposition process through biochemical analysis, our findings opened new and intriguing perspectives for the analysis of DCM. For example, we proposed an innovative analytical approach in which we attempted to focus on DCM-specific genes by comparing the DCM transcriptome with the transcriptional profile of restrictive heart failure associated to systemic amyloidosis. This analysis led to the identification of a limited set of purely DCM-specific genes which are not altered by the deposition of amyloid products and are not related to the development and progression of the failing condition.

For this study we adopted a high-throughput method such as RNA microchip, using the most comprehensive array currently on the market, which recognized the levels of expression of over 50,000 ESTs. The analysis of this vast amount of data led to the identification of a very limited set of iDCM-specific ESTs (13 in total, which were associated to 10 known genes) and, in parallel, to the identification of 200 failing-associated EST (representing 138 known genes) and 52 amyloidosis-specific sequences (representing 41 known genes).

Interestingly, the gene-ontological analysis of the DCM-specific ESTs showed that the only significantly recognizable cluster of genes included sequences normally correlated to the neuro-developmental process, such as nestin and DSCR-1. The latter, in particular, seems related to a chaperone-like activity that might be evoked by the intracellular Ca^{2+} dysregulation and by the toxicity produced by the accumulation of unfolded peptides. However, several studies showed that overexpression of DSCR-1 in the long term could have deleterious effects by inhibiting hypertrophy and by initiating the degeneration towards the failing process.

Of note, in this study we were able to observe significant and intriguing common features between Alzheimer's disease and iDCM, which included the deposition of

amyloid, the alterations in the APP processing pathway and the overexpression of DSCR-1. These findings can be interpreted as a consequence of the exponential increase in the lifespan of human beings in the last century associated to the progressively ameliorating conditions of life. In fact, the occurrence and progression of degenerative disease such as AD or DCM might be considered as a degeneration of the cellular aging process, which normally become manifest as defects in the cellular catabolic processes and accumulation of senile plaques. In fact it is commonly accepted that the proteosomal function consistently decreases with age, especially in tissues rich in terminally differentiated cells with low regenerative capacity such as the CNS and the heart. This process seems to be associated to alterations in the subunit composition of the proteasome and/or to post-transtlational modifications, with correlates with the progressive accumulation of oxidized proteins. Similar age-depending degeneration has been observed also in the lysosome, the other major catabolic apparatus of the cell. This process seems to be totally due to unknown epigenetic reasons and appears to be totally independent from the presence of defective lysosomal enzymes. As the lysosome seems to have a significant role in the removal of aberrant proteins and, in particular, of proteins prone to the formation of aggregates, the progressive degeneration of the organelle activity can produce reduction of the autophagy process and gradual accumulation of oligomeric species with deleterious effects on the cell. A significant confirmation of this concept in cardiomyocytes derives from Nakai et al. recent work, in which the authors showed that perturbation of the autophagy process by inhibiting proteins of the Atg family produces severe cardiac alterations in animal models eventually leading to the development of DCM.

The degeneration of the lysosomal activity has been visually associated to the accumulation of lipofuscin, which are degradation-resistant pigments of heterogeneous nature containing portion of proteins linked by aldehyde bridges originating from lipid-derive peroxides. However, at the moment several theories are still debated regarding whether these molecules have any significant impact on any cell function or are completely inert.

The role of the catabolic pathways in the heart has been also shown in a series of hereditary disease involving lysomal defects, such as Fabry, Pompe or Danon, in which heart insufficiency has been described to occur earlier.

Unfortunately, at the moment our knowledge of the mechanisms involved in these processes is very limited although several groups are already investigating these different aspects of the aging process in order to find useful clues for deciphering the etiology of several diseases that are still not completely understood. However we consider that this topic will receive even more attention in the next decades as the world population's life expectancy is supposed to increase even further and aging-related disease will represent a major social problem in the developed countries.

In conclusion, we can say that our work has shed new light on the etiology of idiopathic dilated cardiomyopathy by linking the disease to the accumulation of intracellular amyloid species, a process that seems to be involved in several other degenerative diseases. Although we were not able to identify a specific candidate as a target for an innovative therapeutic approach, our study opens new and intriguing topics in DCM-related research. Among these we consider of particular importance for future studies the determination of the causative nature of the accumulation of unfolded proteins: although our data clearly show the significant degenerative effects of oligomer accumulation on cardiomyocytes, we were not able to clarify whether the presence of these molecular forms just reflects a general cellular dysfunction due to the pre-existence of a different pathological state and/or molecular alteration.

6.1 Limitations and future directions

Although we were able to report some innovative findings in the iDCM field, we are aware that our analysis is characterized by major limitations mainly due to the typology of the samples used in the study and to technical limits of the technologies currently available.

226

In fact, during the interpretation of the results presented in this book we should consider with particular attention that the samples used for the experiments described were mostly derived from late-stage iDCM patients, in which the cellular functions are usually significantly compromised. Thus, we can't exclude that impairment in the Ca^{2+} handling in the cell may be a pre-existing condition with deleterious effects on the folding apparatus, eventually leading to the formation of the aggregates we reported. Therefore, it would be of interest to investigate the presence of these anomalies in early-stage DCM that, unfortunately, were not available in the tissue bank from which we obtained our samples. Additional confirmations of the possible role of cellular Ca^{2+} anomalies on the generation of ER stress, activation of the UPR and, eventually, formation of amyloid forms may derive from the analysis of resections obtained from hypertrophic hearts and chronic valve diseases, which also present Ca^{2+} handling impairment.

We also consider that further significant information on the etiology of DCM and on the role of the APP processing machinery in the heart could derive from the analysis of cardiac samples from AD patients, as our observations support previous data showing DCM-related alterations in the presenilin genes. In fact, no clinical reports describing the cardiac characteristics of AD patients have been published to date to our knowledge, mostly because the aggravation of the health conditions of these subjects is generally clinically associated to the degeneration of the neural function. In particular, it would be interesting to evaluate the cardiac function of late-stage patients to determine the presence of cardiac alterations and DCM signs, while post-mortem analysis of the cardiac tissue will reveal the presence of amyloidosis and UPR activation.

In addition, several observations of UPR activation and ER stress have been reported in the last few years in patients and animal models of ischemic heart disease and cardiac hypertrophy. Therefore, it will be of relevant interest to verify whether any of the phenomena we reported in DCM is present in different cardiac conditions or it is peculiar to the disease we examined.

A second limitation to our study derives from our incapacity to identify the peptides involved in the intracellular aggregates mainly due to technical difficulties. We still believe that a better understanding of the causes underlying idiopathic DCM could be achieved though characterization of the protein(s) involved in the amyloid deposits in cardiomyocytes. Therefore, we consider this step a primary goal for future developments of the work described in this volume.

The experimental protocols we investigated showed several technical limitations mainly related to the large variety of proteins expressed in the myocardium, which could not be resolved by enriching the lysates in the oligomeric and amyloid species. In addition, we should consider that the use of late stage-DCM samples implies the presence of a terminally compromised folding and quality control processes in the cardiomyocytes and, consequently, the accumulation of unfolded protein deposits composed by peptides not necessarily amyloidogenic.

A second major technical limitation derives from our complete lack of information regarding the solubility of the peptides involved in the aggregates and their resistance to detergents. In fact we think that the high background we obtained from the mass spectrometry-based analysis of our lysates is mainly due to the presence of contaminants not characterized by amyloid structures, which could have been removed form the solution with the use of mild detergents. An alternative approach to obtain better resolution of the different proteins present in our lysates is represented by the use of 2D gel instead of the linear PAGE we adopted. However at the moment this strategy is still highly inconvenient for the large requirements in starting material and the costs associated to the post-separation analysis.

Besides the development of methods to resolve the issues we encountered during our experimental process, our results opened a new interesting field of investigation which will be useful for a more detailed comprehension of iDCM and the aging process in the heart and will facilitate the generation of new diagnostic tools and therapeutic approaches.

In particular, one of the major limitations currently limiting iDCM research consists in the absence of convenient spontaneous animal models, which still represent critical tools for basic and translational research.

In the past three decades, several investigators have developed a large number of rodent and large animal models which mimic the signs typically observed in the human condition. One of the most common models currently available for rodents consists of inducing pressure overload by surgical banding of the ascending aortic tract, which leads to compensated hypertrophy that eventually degenerates into dilated cardiomyopathy. Alternatively, a large number of transgenic and knock-out models has been developed and characterized especially in mice.

Although these models provided invaluable support for increasing our knowledge on several aspects and molecular mechanisms involved in iDCM, they represent good models only for the study of the clinically manifest phases of iDCM, due to the scarce information regarding the etiology of the disease currently available.

As the results we report in this thesis enhance our knowledge of the possible mechanisms involved in the development of iDCM, it will be interesting to evaluate the effects of the alterations we report in transgenic models. In particular a large array of transgenic mice carrying alterations related to APP processing has been developed for Alzheimer's disease research. The characterization of the cardiac function and UPR system in these animals may be able to provide significant confirmation of our results and, at the same time, provide new useful tools for iDCM research.

The complete delineation of the molecular mechanisms related to a specific pathological condition is a critical step for designing more efficient diagnosis protocols and more effected and targeted therapeutic approaches. In particular the study we described suggests novel and interesting aspects of iDCM which appear to have significant importance for the etiology and the development of the disease.

More detailed analysis of these characteristics will lead to the identification of new non invasive protocols for early diagnosis of DCM and therefore to the possibility of early and more effective treatments. In particular the identification of a larger subset of DCM-specific mutations such as the PSEN alterations we described in chapter 3 will allow the development of easy genetic screening, which, as we expect the number of mutations to grow, will be excellent candidates for the development of high throughput diagnosis techniques such as single nucleotide polymorphism microarrays.

In addition, we consider that critical improvements to early diagnosis of DCM will also derive from the identification of the specific proteins(s) involved in the formation of oligomers and fibers. In fact this will allow the development of ligands which specifically bind the aggregating species and which will be of significant utility for non-invasive imaging analysis such as magnetic resonance or positron emission tomography.

A second important perspective deriving from the identification of the pro-amyloid protein(s) consists of the possibility of developing assays for the detection of the involved peptides in the body fluids, as we can speculate that the accumulation of the proteins(s) involved in the formation of the oligomeric and amyloid species may be associated to the release in the circulation of specific amyloigenic peptides similarly to what is currently under debate for plasma Aβ in AD.

Other interesting perspectives deriving from the observations we report in this thesis are related to the development of new therapies aimed to limit the accumulation of oligomers, by directly downregulating the protein(s) involved in the formation of the amyloid prefibrillar forms or by stimulating and enhancing the activation of the cellular mechanisms related to the resolution of unfolded protein-induced stress conditions. Alternatively, a different approach for the identification of new therapeutic approaches could be based on a more detailed characterization of the mechanisms involved in the manifestation of the toxic effect related to the accumulation of unfolded proteins, in order to identify specific targets to inhibit the activation of the UPR cascade steps that lead to cell dysfunction and, eventually, to apoptosis.

As we demonstrated that iDCM presents several common aspects with other forms of amyloidosis, we can speculate that the therapeutic approaches in development for this group of diseases may present some relevant effects also on iDCM. Unfortunately, no efficient therapy is available for most amyloid-based conditions at the moment; however the recognition of the molecular mechanisms generating the accumulation of oligomers and involved in the toxicity of these molecular species will allow a process currently largely adopted by pharmaceutical companies for fast identification of

potential new drugs, which is based on the screening of large libraries of small molecules to identify the compounds that interfere with specific processes.

Alternatively, other innovative therapeutic approaches may arise from applications of interesting studies emerged in the last few years and showing the importance of cutting-edge technologies such as gene silencing for the downregulation of overexpressed protein using small interfering (si) RNA. However, at the moment this approach is still affected by significant limitations, including the efficiency and specificity of the *in vivo* delivery of the siRNA molecules and the variable silencing effect.

In summary, the study we presented shows the critical role of unfolded proteins in the development of DCM and, in particular, the deleterious effects of the accumulation of oligomers on contractility and Ca^{2+} handling. This process eventually leads to severe impairment of the folding apparatus of the cardiomyocyte which appears to activate the Chop- and Caspase 12-mediated apoptotic pathway. In addition we identified two novel mutations in the presenilin 1 promoter which seem to induce alteration of the expression of the gene with possible effects on the recently proposed regulation of this protein on SERCA2a.

On the basis of these observations, we developed an innovative 3-group analysis of the global transcriptosome which analyzed simultaneously the expression levels in DCM, non-failing and amyloidosis-affected individuals. This approach allowed the identification of a very limited number of DCM-specific messengers by distinguishing them from transcripts related to the progression of the failing process and mRNA induced by the accumulation of unfolded proteins. Interestingly these included DSCR1 and Nestin, two genes normally associated to the development of the neural system.

Although these findings creates new and intriguing fields of investigation, further analyses are still required to identify the protein(s) involved in the formation of the aggregates we reported and to elucidate whether these unfolded structures are causative of the Ca^{2+} dysregulation observed in DCM or if they simply represent a consequence of it.

CITED LITERATURE

Albani, D., Roiter, I., Artuso, V., Batelli, S., Prato, F., Pesaresi, M., Galimberti, D., Scarpini, E., Bruni, A., Franceschi, M., Piras, M. R., Confaloni, A. and Forloni, G., 2007. Presenilin-1 mutation E318G and familial Alzheimer's disease in the Italian population. Neurobiol Aging. 28, 1682-1688.

Argon, Y. and Simen, B. B., 1999. GRP94, an ER chaperone with protein and peptide binding properties. Semin Cell Dev Biol. 10, 495-505.

Arimura, T., Hayashi, T., Terada, H., Lee, S. Y., Zhou, Q., Takahashi, M., Ueda, K., Nouchi, T., Hohda, S., Shibutani, M., Hirose, M., Chen, J., Park, J. E., Yasunami, M., Hayashi, H. and Kimura, A., 2004. A Cypher/ZASP mutation associated with dilated cardiomyopathy alters the binding affinity to protein kinase C. J Biol Chem. 279, 6746-6752.

Asai, A., Qiu, J., Narita, Y., Chi, S., Saito, N., Shinoura, N., Hamada, H., Kuchino, Y. and Kirino, T., 1999. High level calcineurin activity predisposes neuronal cells to apoptosis. J Biol Chem. 274, 34450-34458.

Asakura, M. and Kitakaze, M., 2009. Global gene expression profiling in the failing myocardium. Circ J. 73, 1568-1576.

Back, S. H., Schroder, M., Lee, K., Zhang, K. and Kaufman, R. J., 2005. ER stress signaling by regulated splicing: IRE1/HAC1/XBP1. Methods. 35, 395-416.

Baek, K. H., Zaslavsky, A., Lynch, R. C., Britt, C., Okada, Y., Siarey, R. J., Lensch, M. W., Park, I. H., Yoon, S. S., Minami, T., Korenberg, J. R., Folkman, J., Daley, G. Q., Aird, W. C., Galdzicki, Z. and Ryeom, S., 2009. Down's syndrome suppression of tumour growth and the role of the calcineurin inhibitor DSCR1. Nature. 459, 1126-1130.

Baglioni, S., Casamenti, F., Bucciantini, M., Luheshi, L. M., Taddei, N., Chiti, F., Dobson, C. M. and Stefani, M., 2006. Prefibrillar amyloid aggregates could be generic toxins in higher organisms. J Neurosci. 26, 8160-8167.

Bagriantsev, S. N., Kushnirov, V. V. and Liebman, S. W., 2006. Analysis of amyloid aggregates using agarose gel electrophoresis. Methods Enzymol. 412, 33-48.

Bahrudin, U., Morisaki, H., Morisaki, T., Ninomiya, H., Higaki, K., Nanba, E., Igawa, O., Takashima, S., Mizuta, E., Miake, J., Yamamoto, Y., Shirayoshi, Y., Kitakaze, M., Carrier, L. and Hisatome, I., 2008. Ubiquitin-proteasome system impairment caused by a missense cardiac myosin-binding protein C mutation and associated with cardiac dysfunction in hypertrophic cardiomyopathy. J Mol Biol. 384, 896-907.

Balazs, L. and Leon, M., 1994. Evidence of an oxidative challenge in the Alzheimer's brain. Neurochem Res. 19, 1131-1137.

Bales, K. R., Du, Y., Dodel, R. C., Yan, G. M., Hamilton-Byrd, E. and Paul, S. M., 1998. The NF-kappaB/Rel family of proteins mediates Abeta-induced neurotoxicity and glial activation. Brain Res Mol Brain Res. 57, 63-72.

Bar, H., Strelkov, S. V., Sjoberg, G., Aebi, U. and Herrmann, H., 2004. The biology of desmin filaments: how do mutations affect their structure, assembly, and organisation? J Struct Biol. 148, 137-152.

Barinaga, M., 1998. Is apoptosis key in Alzheimer's disease? Science. 281, 1303-1304.

Barrans, J. D., Allen, P. D., Stamatiou, D., Dzau, V. J. and Liew, C. C., 2002. Global gene expression profiling of end-stage dilated cardiomyopathy using a human cardiovascular-based cDNA microarray. Am J Pathol. 160, 2035-2043.

Barrans, J. D., Stamatiou, D. and Liew, C., 2001. Construction of a human cardiovascular cDNA microarray: portrait of the failing heart. Biochem Biophys Res Commun. 280, 964-969.

Barth, A. S., Kuner, R., Buness, A., Ruschhaupt, M., Merk, S., Zwermann, L., Kaab, S., Kreuzer, E., Steinbeck, G., Mansmann, U., Poustka, A., Nabauer, M. and Sultmann, H., 2006. Identification of a common gene expression signature in dilated cardiomyopathy across independent microarray studies. J Am Coll Cardiol. 48, 1610-1617.

Behl, C., Davis, J. B., Klier, F. G. and Schubert, D., 1994. Amyloid beta peptide induces necrosis rather than apoptosis. Brain Res. 645, 253-264.

Bennett, M. J., Sawaya, M. R. and Eisenberg, D., 2006. Deposition diseases and 3D domain swapping. Structure. 14, 811-824.

Berggren, K. N., Schulenberg, B., Lopez, M. F., Steinberg, T. H., Bogdanova, A., Smejkal, G., Wang, A. and Patton, W. F., 2002. An improved formulation of SYPRO Ruby protein gel stain: comparison with the original formulation and with a ruthenium II tris (bathophenanthroline disulfonate) formulation. Proteomics. 2, 486-498.

Bertolotti, A., Zhang, Y., Hendershot, L. M., Harding, H. P. and Ron, D., 2000. Dynamic interaction of BiP and ER stress transducers in the unfolded-protein response. Nat Cell Biol. 2, 326-332.

Bertram, L. and Tanzi, R. E., 2004. Alzheimer's disease: one disorder, too many genes? Hum Mol Genet. 13 Spec No 1, R135-141.

Bertram, L. and Tanzi, R. E., 2005. The genetic epidemiology of neurodegenerative disease. J Clin Invest. 115, 1449-1457.

Bertram, L. and Tanzi, R. E., 2009. Genome-wide association studies in Alzheimer's disease. Hum Mol Genet. 18, R137-145.

Bienengraeber, M., Olson, T. M., Selivanov, V. A., Kathmann, E. C., O'Cochlain, F., Gao, F., Karger, A. B., Ballew, J. D., Hodgson, D. M., Zingman, L. V., Pang, Y. P., Alekseev, A. E. and Terzic, A., 2004. ABCC9 mutations identified in human dilated cardiomyopathy disrupt catalytic KATP channel gating. Nat Genet. 36, 382-387.

Birks, E. J., Latif, N., Enesa, K., Folkvang, T., Luong le, A., Sarathchandra, P., Khan, M., Ovaa, H., Terracciano, C. M., Barton, P. J., Yacoub, M. H. and Evans, P. C., 2008. Elevated p53 expression is associated with dysregulation of the ubiquitin-proteasome system in dilated cardiomyopathy. Cardiovasc Res. 79, 472-480.

Blacker, D. and Tanzi, R. E., 1998. The genetics of Alzheimer disease: current status and future prospects. Arch Neurol. 55, 294-296.

British Heart Foundation. Heartstats.2001.

Bova, M. P., Yaron, O., Huang, Q., Ding, L., Haley, D. A., Stewart, P. L. and Horwitz, J., 1999. Mutation R120G in alphaB-crystallin, which is linked to a desmin-related myopathy, results in an irregular structure and defective chaperone-like function. Proc Natl Acad Sci U S A. 96, 6137-6142.

Bradford, M. M., 1976. A rapid and sensitive method for the quantitation of microgram quantities of protein utilizing the principle of protein-dye binding. Anal Biochem. 72, 248-254.

Braunwald, E., 1996. Heart Disease: A Textbook of Cardiovascular Medicine. W.B. Saunder Company.

Brenner, D. A., Jain, M., Pimentel, D. R., Wang, B., Connors, L. H., Skinner, M., Apstein, C. S. and Liao, R., 2004. Human amyloidogenic light chains directly impair cardiomyocyte function through an increase in cellular oxidant stress. Circ Res. 94, 1008-1010.

Bristow, M. R., 2003. Microarray measurements of gene expression before and after left ventricular assist device placement. J Am Coll Cardiol. 41, 1107-1108.

Burghardt, R. C. and Droleskey, R., 2006. Transmission electron microscopy. Curr Protoc Microbiol. Chapter 2, Unit 2B 1.

Buxbaum, J. N., 2004. The systemic amyloidoses. Curr Opin Rheumatol. 16, 67-75.

Calfon, M., Zeng, H., Urano, F., Till, J. H., Hubbard, S. R., Harding, H. P., Clark, S. G. and Ron, D., 2002. IRE1 couples endoplasmic reticulum load to secretory capacity by processing the XBP-1 mRNA. Nature. 415, 92-96.

Cannell, M. B., Crossman, D. J. and Soeller, C., 2006. Effect of changes in action potential spike configuration, junctional sarcoplasmic reticulum micro-architecture and altered t-tubule structure in human heart failure. J Muscle Res Cell Motil. 27, 297-306.

Capell, A., Beher, D., Prokop, S., Steiner, H., Kaether, C., Shearman, M. S. and Haass, C., 2005. Gamma-secretase complex assembly within the early secretory pathway. J Biol Chem. 280, 6471-6478.

Capetanaki, Y., Milner, D. J. and Weitzer, G., 1997. Desmin in muscle formation and maintenance: knockouts and consequences. Cell Struct Funct. 22, 103-116.

Carrascosa, J. L., Llorca, O. and Valpuesta, J. M., 2001. Structural comparison of prokaryotic and eukaryotic chaperonins. Micron. 32, 43-50.

Casas, C., Martinez, S., Pritchard, M. A., Fuentes, J. J., Nadal, M., Guimera, J., Arbones, M., Florez, J., Soriano, E., Estivill, X. and Alcantara, S., 2001. Dscr1, a novel endogenous inhibitor of calcineurin signaling, is expressed in the primitive ventricle of the heart and during neurogenesis. Mech Dev. 101, 289-292.

Caughey, B. and Lansbury, P. T., 2003. Protofibrils, pores, fibrils, and neurodegeneration: separating the responsible protein aggregates from the innocent bystanders. Annu Rev Neurosci. 26, 267-298.

Cechetto, D. F., Hachinski, V. and Whitehead, S. N., 2008. Vascular risk factors and Alzheimer's disease. Expert Rev Neurother. 8, 743-750.

Chan, S. L., Mayne, M., Holden, C. P., Geiger, J. D. and Mattson, M. P., 2000. Presenilin-1 mutations increase levels of ryanodine receptors and calcium release in PC12 cells and cortical neurons. J Biol Chem. 275, 18195-18200.

Chandrashekhar, Y. and Narula, J., 2003. Death hath a thousand doors to let out life. Circ Res. 92, 710-714.

Chang, A. N. and Potter, J. D., 2005. Sarcomeric protein mutations in dilated cardiomyopathy. Heart Fail Rev. 10, 225-235.

Chapman, D., Weber, K. T. and Eghbali, M., 1990. Regulation of fibrillar collagen types I and III and basement membrane type IV collagen gene expression in pressure overloaded rat myocardium. Circ Res. 67, 787-794.

Chen, F., Yu, G., Arawaka, S., Nishimura, M., Kawarai, T., Yu, H., Tandon, A., Supala, A., Song, Y. Q., Rogaeva, E., Milman, P., Sato, C., Yu, C., Janus, C., Lee, J., Song, L., Zhang, L., Fraser, P. E. and St George-Hyslop, P. H., 2001. Nicastrin binds to membrane-tethered Notch. Nat Cell Biol. 3, 751-754.

Chen, Q., Liu, J. B., Horak, K. M., Zheng, H., Kumarapeli, A. R., Li, J., Li, F., Gerdes, A. M., Wawrousek, E. F. and Wang, X., 2005. Intrasarcoplasmic amyloidosis impairs proteolytic function of proteasomes in cardiomyocytes by compromising substrate uptake. Circ Res. 97, 1018-1026.

Chen, X., Piacentino, V., 3rd, Furukawa, S., Goldman, B., Margulies, K. B. and Houser, S. R., 2002. L-type Ca2+ channel density and regulation are altered in failing human ventricular myocytes and recover after support with mechanical assist devices. Circ Res. 91, 517-524.

Chong, Z. Z., Li, F. and Maiese, K., 2005. Stress in the brain: novel cellular mechanisms of injury linked to Alzheimer's disease. Brain Res Brain Res Rev. 49, 1-21.

Cleary, J. P., Walsh, D. M., Hofmeister, J. J., Shankar, G. M., Kuskowski, M. A., Selkoe, D. J. and Ashe, K. H., 2005. Natural oligomers of the amyloid-beta protein specifically disrupt cognitive function. Nat Neurosci. 8, 79-84.

Colak, D., Kaya, N., Al-Zahrani, J., Al Bakheet, A., Muiya, P., Andres, E., Quackenbush, J. and Dzimiri, N., 2009. Left ventricular global transcriptional profiling in human end-stage dilated cardiomyopathy. Genomics. 94, 20-31.

Connell, P., Ballinger, C. A., Jiang, J., Wu, Y., Thompson, L. J., Hohfeld, J. and Patterson, C., 2001. The co-chaperone CHIP regulates protein triage decisions mediated by heat-shock proteins. Nat Cell Biol. 3, 93-96.

Coombs, G. S., Covey, T. M. and Virshup, D. M., 2008. Wnt signaling in development, disease and translational medicine. Curr Drug Targets. 9, 513-531.

Cope, L. M., Irizarry, R. A., Jaffee, H. A., Wu, Z. and Speed, T. P., 2004. A benchmark for Affymetrix GeneChip expression measures. Bioinformatics. 20, 323-331.

Cornwell, G. G., 3rd, Murdoch, W. L., Kyle, R. A., Westermark, P. and Pitkanen, P., 1983. Frequency and distribution of senile cardiovascular amyloid. A clinicopathologic correlation. Am J Med. 75, 618-623.

Correia, B. E., Loureiro-Ferreira, N., Rodrigues, J. R. and Brito, R. M., 2006. A structural model of an amyloid protofilament of transthyretin. Protein Sci. 15, 28-32.

Craven, R. A. and Banks, R. E., 2001. Laser capture microdissection and proteomics: possibilities and limitation. Proteomics. 1, 1200-1204.

Crawford, D. R., Leahy, K. P., Abramova, N., Lan, L., Wang, Y. and Davies, K. J., 1997. Hamster adapt78 mRNA is a Down syndrome critical region homologue that is inducible by oxidative stress. Arch Biochem Biophys. 342, 6-12.

Cruts, M. and Van Broeckhoven, C., 1998. Presenilin mutations in Alzheimer's disease. Hum Mutat. 11, 183-190.

Cruts, M., van Duijn, C. M., Backhovens, H., Van den Broeck, M., Wehnert, A., Serneels, S., Sherrington, R., Hutton, M., Hardy, J., St George-Hyslop, P. H., Hofman, A. and Van Broeckhoven, C., 1998. Estimation of the genetic contribution of presenilin-1 and -2 mutations in a population-based study of presenile Alzheimer disease. Hum Mol Genet. 7, 43-51.

Cupers, P., Bentahir, M., Craessaerts, K., Orlans, I., Vanderstichele, H., Saftig, P., De Strooper, B. and Annaert, W., 2001. The discrepancy between presenilin subcellular localization and gamma-secretase processing of amyloid precursor protein. J Cell Biol. 154, 731-740.

Currie, S. and Smith, G. L., 1999. Enhanced phosphorylation of phospholamban and downregulation of sarco/endoplasmic reticulum Ca2+ ATPase type 2 (SERCA 2) in cardiac sarcoplasmic reticulum from rabbits with heart failure. Cardiovasc Res. 41, 135-146.

Daehmlow, S., Erdmann, J., Knueppel, T., Gille, C., Froemmel, C., Hummel, M., Hetzer, R. and Regitz-Zagrosek, V., 2002. Novel mutations in sarcomeric protein genes in dilated cardiomyopathy. Biochem Biophys Res Commun. 298, 116-120.

Dally, S., Monceau, V., Corvazier, E., Bredoux, R., Raies, A., Bobe, R., del Monte, F. and Enouf, J., 2009. Compartmentalized expression of three novel sarco/endoplasmic reticulum Ca2+ATPase 3 isoforms including the switch to ER stress, SERCA3f, in non-failing and failing human heart. Cell Calcium. 45, 144-154.

Datta, S., 2003. Comparisons and validation of statistical clustering techniques for microarray gene expression data. Bioinformatics. 19, 459-466.

Davidoff, A. J. and Gwathmey, J. K., 1994. Pathophysiology of cardiomyopathies: Part I. Animal models and humans. Curr Opin Cardiol. 9, 357-368.

DC Sheenhan, B. H., 1980. Theory and Practice of Histotechnology. In: Mosby (Ed.), St Louis (MO), pp. 177-178.

de Exel Nunes, L. M., Salge, A. K., de Oliveira, F. A., Teixeira Vde, P. and Dos Reis, M. A., 2006. Cerebral and cardiac amyloidosis in autopsied elderly individuals. Clinics (Sao Paulo). 61, 113-118.

De Ferrari, G. V. and Moon, R. T., 2006. The ups and downs of Wnt signaling in prevalent neurological disorders. Oncogene. 25, 7545-7553.

De Strooper, B., 2003. Aph-1, Pen-2, and Nicastrin with Presenilin generate an active gamma-Secretase complex. Neuron. 38, 9-12.

De Windt, L. J., Lim, H. W., Bueno, O. F., Liang, Q., Delling, U., Braz, J. C., Glascock, B. J., Kimball, T. F., del Monte, F., Hajjar, R. J. and Molkentin, J. D., 2001. Targeted inhibition of calcineurin attenuates cardiac hypertrophy in vivo. Proc Natl Acad Sci U S A. 98, 3322-3327.

DeKosky, S. T., Scheff, S. W. and Markesbery, W. R., 1985. Laminar organization of cholinergic circuits in human frontal cortex in Alzheimer's disease and aging. Neurology. 35, 1425-1431.

Del Monte, F. and Hajjar, R. J., 2008. Intracellular devastation in heart failure. Heart Fail Rev. 13, 151-162.

del Monte, F., Harding, S. E., Schmidt, U., Matsui, T., Kang, Z. B., Dec, G. W., Gwathmey, J. K., Rosenzweig, A. and Hajjar, R. J., 1999. Restoration of

contractile function in isolated cardiomyocytes from failing human hearts by gene transfer of SERCA2a. Circulation. 100, 2308-2311.

Demuro, A., Mina, E., Kayed, R., Milton, S. C., Parker, I. and Glabe, C. G., 2005. Calcium dysregulation and membrane disruption as a ubiquitous neurotoxic mechanism of soluble amyloid oligomers. J Biol Chem. 280, 17294-17300.

Despa, F., Endoplasmic reticulum overcrowding as a mechanism of beta-cell dysfunction in diabetes. Biophys J. 98, 1641-1648.

Desrois, M., Sciaky, M., Lan, C., Cozzone, P. J. and Bernard, M., 1999. Metabolic and functional effects of low-potassium cardioplegic solutions for long-term heart preservation. Magma. 8, 77-82.

DeWitt, M. M., MacLeod, H. M., Soliven, B. and McNally, E. M., 2006. Phospholamban R14 deletion results in late-onset, mild, hereditary dilated cardiomyopathy. J Am Coll Cardiol. 48, 1396-1398.

Dillmann, W. H., 1999. Small heat shock proteins and protection against injury. Ann N Y Acad Sci. 874, 66-68.

Dobson, C. M., 2003. Protein folding and misfolding. Nature. 426, 884-890.

Donoviel, D. B., Hadjantonakis, A. K., Ikeda, M., Zheng, H., Hyslop, P. S. and Bernstein, A., 1999. Mice lacking both presenilin genes exhibit early embryonic patterning defects. Genes Dev. 13, 2801-2810.

Dorn, G. W., 2nd, 2001. Calcineurin inhibition in hypertrophy: back from the dead! Circulation. 104, 9-11.

Dumur, C. I., Nasim, S., Best, A. M., Archer, K. J., Ladd, A. C., Mas, V. R., Wilkinson, D. S., Garrett, C. T. and Ferreira-Gonzalez, A., 2004. Evaluation of quality-control criteria for microarray gene expression analysis. Clin Chem. 50, 1994-2002.

Eisen, M. B., Spellman, P. T., Brown, P. O. and Botstein, D., 1998. Cluster analysis and display of genome-wide expression patterns. Proc Natl Acad Sci U S A. 95, 14863-14868.

Elam, J. S., Taylor, A. B., Strange, R., Antonyuk, S., Doucette, P. A., Rodriguez, J. A., Hasnain, S. S., Hayward, L. J., Valentine, J. S., Yeates, T. O. and Hart, P. J., 2003. Amyloid-like filaments and water-filled nanotubes formed by SOD1 mutant proteins linked to familial ALS. Nat Struct Biol. 10, 461-467.

El-Helou, V., Dupuis, J., Proulx, C., Drapeau, J., Clement, R., Gosselin, H., Villeneuve, L., Manganas, L. and Calderone, A., 2005. Resident nestin+ neural-like cells and fibers are detected in normal and damaged rat myocardium. Hypertension. 46, 1219-1225.

Ellgaard, L. and Helenius, A., 2003. Quality control in the endoplasmic reticulum. Nat Rev Mol Cell Biol. 4, 181-191.

Ellis, R. J. and van der Vies, S. M., 1991. Molecular chaperones. Annu Rev Biochem. 60, 321-347.

Engelhardt, S., Bohm, M., Erdmann, E. and Lohse, M. J., 1996. Analysis of beta-adrenergic receptor mRNA levels in human ventricular biopsy specimens by quantitative polymerase chain reactions: progressive reduction of beta 1-adrenergic receptor mRNA in heart failure. J Am Coll Cardiol. 27, 146-154.

Enjeti, A. K., Walsh, M. and Seldon, M., 2005. Spontaneous major bleeding in acquired factor X deficiency secondary to AL-amyloidosis. Haemophilia. 11, 535-538.

Ermak, G. and Davies, K. J., 2002. Calcium and oxidative stress: from cell signaling to cell death. Mol Immunol. 38, 713-721.

Ermak, G. and Davies, K. J., 2003. DSCR1(Adapt78)--a Janus gene providing stress protection but causing Alzheimer's disease? IUBMB Life. 55, 29-31.

Ermak, G., Harris, C. D. and Davies, K. J., 2002. The DSCR1 (Adapt78) isoform 1 protein calcipressin 1 inhibits calcineurin and protects against acute calcium-mediated stress damage, including transient oxidative stress. Faseb J. 16, 814-824.

Ermak, G., Morgan, T. E. and Davies, K. J., 2001. Chronic overexpression of the calcineurin inhibitory gene DSCR1 (Adapt78) is associated with Alzheimer's disease. J Biol Chem. 276, 38787-38794.

Esler, W. P., Stimson, E. R., Jennings, J. M., Vinters, H. V., Ghilardi, J. R., Lee, J. P., Mantyh, P. W. and Maggio, J. E., 2000. Alzheimer's disease amyloid propagation by a template-dependent dock-lock mechanism. Biochemistry. 39, 6288-6295.

Esposito, L., Gan, L., Yu, G. Q., Essrich, C. and Mucke, L., 2004. Intracellularly generated amyloid-beta peptide counteracts the antiapoptotic function of its precursor protein and primes proapoptotic pathways for activation by other insults in neuroblastoma cells. J Neurochem. 91, 1260-1274.

Evans, D. A., Hebert, L. E., Beckett, L. A., Scherr, P. A., Albert, M. S., Chown, M. J., Pilgrim, D. M. and Taylor, J. O., 1997. Education and other measures of socioeconomic status and risk of incident Alzheimer disease in a defined population of older persons. Arch Neurol. 54, 1399-1405.

Farrell, E. F., Antaramian, A., Rueda, A., Gomez, A. M. and Valdivia, H. H., 2003. Sorcin inhibits calcium release and modulates excitation-contraction coupling in the heart. J Biol Chem. 278, 34660-34666.

Firestein, G. S. and Pisetsky, D. S., 2002. DNA microarrays: boundless technology or bound by technology? Guidelines for studies using microarray technology. Arthritis Rheum. 46, 859-861.

Frazer, K. A., Ballinger, D. G., Cox, D. R., Hinds, D. A., Stuve, L. L., Gibbs, R. A., Belmont, J. W., Boudreau, A., Hardenbol, P., Leal, S. M., Pasternak, S., Wheeler, D. A., Willis, T. D., Yu, F., Yang, H., Zeng, C., Gao, Y., Hu, H., Hu, W., Li, C., Lin, W., Liu, S., Pan, H., Tang, X., Wang, J., Wang, W., Yu, J., Zhang, B., Zhang, Q., Zhao, H., Zhou, J., Gabriel, S. B., Barry, R., Blumenstiel, B., Camargo, A., Defelice, M., Faggart, M., Goyette, M., Gupta, S., Moore, J., Nguyen, H., Onofrio, R. C., Parkin, M., Roy, J., Stahl, E., Winchester, E., Ziaugra, L., Altshuler, D., Shen, Y., Yao, Z., Huang, W., Chu, X., He, Y., Jin, L., Liu, Y., Sun, W., Wang, H., Wang, Y., Xiong, X., Xu, L., Waye, M. M., Tsui, S. K., Xue, H., Wong, J. T., Galver, L. M., Fan, J. B., Gunderson, K., Murray, S. S., Oliphant, A. R., Chee, M. S., Montpetit, A., Chagnon, F., Ferretti, V., Leboeuf, M., Olivier, J. F., Phillips, M. S., Roumy, S., Sallee, C., Verner, A., Hudson, T. J., Kwok, P. Y., Cai, D., Koboldt, D. C., Miller, R. D., Pawlikowska, L., Taillon-Miller, P., Xiao, M., Tsui, L. C., Mak, W., Song, Y. Q., Tam, P. K., Nakamura, Y., Kawaguchi, T., Kitamoto, T., Morizono, T., Nagashima, A., Ohnishi, Y., Sekine, A., Tanaka, T., Tsunoda, T., Deloukas, P., Bird, C. P., Delgado, M., Dermitzakis, E. T., Gwilliam, R., Hunt, S., Morrison, J., Powell, D., Stranger, B. E., Whittaker, P., Bentley, D.

R., Daly, M. J., de Bakker, P. I., Barrett, J., Chretien, Y. R., Maller, J., McCarroll, S., Patterson, N., Pe'er, I., Price, A., Purcell, S., Richter, D. J., Sabeti, P., Saxena, R., Schaffner, S. F., Sham, P. C., Varilly, P., Stein, L. D., Krishnan, L., Smith, A. V., Tello-Ruiz, M. K., Thorisson, G. A., Chakravarti, A., Chen, P. E., Cutler, D. J., Kashuk, C. S., Lin, S., Abecasis, G. R., Guan, W., Li, Y., Munro, H. M., Qin, Z. S., Thomas, D. J., McVean, G., Auton, A., Bottolo, L., Cardin, N., Eyheramendy, S., Freeman, C., Marchini, J., Myers, S., Spencer, C., Stephens, M., Donnelly, P., Cardon, L. R., Clarke, G., Evans, D. M., Morris, A. P., Weir, B. S., Mullikin, J. C., Sherry, S. T., Feolo, M., Skol, A., Zhang, H., Matsuda, I., Fukushima, Y., Macer, D. R., Suda, E., Rotimi, C. N., Adebamowo, C. A., Ajayi, I., Aniagwu, T., Marshall, P. A., Nkwodimmah, C., Royal, C. D., Leppert, M. F., Dixon, M., Peiffer, A., Qiu, R., Kent, A., Kato, K., Niikawa, N., Adewole, I. F., Knoppers, B. M., Foster, M. W., Clayton, E. W., Watkin, J., Muzny, D., Nazareth, L., Sodergren, E., Weinstock, G. M., Yakub, I., Birren, B. W., Wilson, R. K., Fulton, L. L., Rogers, J., Burton, J., Carter, N. P., Clee, C. M., Griffiths, M., Jones, M. C., McLay, K., Plumb, R. W., Ross, M. T., Sims, S. K., Willey, D. L., Chen, Z., Han, H., Kang, L., Godbout, M., Wallenburg, J. C., L'Archeveque, P., Bellemare, G., Saeki, K., An, D., Fu, H., Li, Q., Wang, Z., Wang, R., Holden, A. L., Brooks, L. D., McEwen, J. E., Guyer, M. S., Wang, V. O., Peterson, J. L., Shi, M., Spiegel, J., Sung, L. M., Zacharia, L. F., Collins, F. S., Kennedy, K., Jamieson, R. and Stewart, J., 2007. A second generation human haplotype map of over 3.1 million SNPs. Nature. 449, 851-861.

Fritz, J. D., Swartz, D. R. and Greaser, M. L., 1989. Factors affecting polyacrylamide gel electrophoresis and electroblotting of high-molecular-weight myofibrillar proteins. Anal Biochem. 180, 205-210.

Fu, H. Y., Minamino, T., Tsukamoto, O., Sawada, T., Asai, M., Kato, H., Asano, Y., Fujita, M., Takashima, S., Hori, M. and Kitakaze, M., 2008. Overexpression of endoplasmic reticulum-resident chaperone attenuates cardiomyocyte death induced by proteasome inhibition. Cardiovasc Res. 79, 600-610.

Fuentes, J. J., Genesca, L., Kingsbury, T. J., Cunningham, K. W., Perez-Riba, M., Estivill, X. and de la Luna, S., 2000. DSCR1, overexpressed in Down syndrome, is an inhibitor of calcineurin-mediated signaling pathways. Hum Mol Genet. 9, 1681-1690.

Fuentes, J. J., Pritchard, M. A. and Estivill, X., 1997. Genomic organization, alternative splicing, and expression patterns of the DSCR1 (Down syndrome candidate region 1) gene. Genomics. 44, 358-361.

Fuentes, J. J., Pritchard, M. A., Planas, A. M., Bosch, A., Ferrer, I. and Estivill, X., 1995. A new human gene from the Down syndrome critical region encodes a proline-rich protein highly expressed in fetal brain and heart. Hum Mol Genet. 4, 1935-1944.

Fukuhara, S., Tomita, S., Nakatani, T., Yutani, C. and Kitamura, S., 2005. Endogenous bone-marrow-derived stem cells contribute only a small proportion of regenerated myocardium in the acute infarction model. J Heart Lung Transplant. 24, 67-72.

Gething, M. J. and Sambrook, J., 1992. Protein folding in the cell. Nature. 355, 33-45.

Glabe, C. G., 2008. Structural classification of toxic amyloid oligomers. J Biol Chem. 283, 29639-29643.

Glabe, C. G. and Kayed, R., 2006. Common structure and toxic function of amyloid oligomers implies a common mechanism of pathogenesis. Neurology. 66, S74-78.

Glickman, M. H. and Ciechanover, A., 2002. The ubiquitin-proteasome proteolytic pathway: destruction for the sake of construction. Physiol Rev. 82, 373-428.

Go, L. O., Moschella, M. C., Watras, J., Handa, K. K., Fyfe, B. S. and Marks, A. R., 1995. Differential regulation of two types of intracellular calcium release channels during end-stage heart failure. J Clin Invest. 95, 888-894.

Goldberg, A. L., 2003. Protein degradation and protection against misfolded or damaged proteins. Nature. 426, 895-899.

Golub, T. R., Slonim, D. K., Tamayo, P., Huard, C., Gaasenbeek, M., Mesirov, J. P., Coller, H., Loh, M. L., Downing, J. R., Caligiuri, M. A., Bloomfield, C. D. and Lander, E. S., 1999. Molecular classification of cancer: class discovery and class prediction by gene expression monitoring. Science. 286, 531-537.

Gong, Y., Chang, L., Viola, K. L., Lacor, P. N., Lambert, M. P., Finch, C. E., Krafft, G. A. and Klein, W. L., 2003. Alzheimer's disease-affected brain: presence of oligomeric A beta ligands (ADDLs) suggests a molecular basis for reversible memory loss. Proc Natl Acad Sci U S A. 100, 10417-10422.

Gorza, L. and del Monte, F., 2005. Protein unfolding in cardiomyopathies. Heart Fail Clin. 1, 237-250.

Govindarajan, S. and Goldstein, R. A., 1998. On the thermodynamic hypothesis of protein folding. Proc Natl Acad Sci U S A. 95, 5545-5549.

Gozal, Y. M., Cheng, D., Duong, D. M., Lah, J. J., Levey, A. I. and Peng, J., 2006. Merger of laser capture microdissection and mass spectrometry: a window into the amyloid plaque proteome. Methods Enzymol. 412, 77-93.

Green, K. N., Demuro, A., Akbari, Y., Hitt, B. D., Smith, I. F., Parker, I. and LaFerla, F. M., 2008. SERCA pump activity is physiologically regulated by presenilin and regulates amyloid beta production. J Cell Biol. 181, 1107-1116.

Groll, M. and Huber, R., 2003. Substrate access and processing by the 20S proteasome core particle. Int J Biochem Cell Biol. 35, 606-616.

Grzeskowiak, R., Witt, H., Drungowski, M., Thermann, R., Hennig, S., Perrot, A., Osterziel, K. J., Klingbiel, D., Scheid, S., Spang, R., Lehrach, H. and Ruiz, P., 2003. Expression profiling of human idiopathic dilated cardiomyopathy. Cardiovasc Res. 59, 400-411.

Guntern, R., Bouras, C., Hof, P. R. and Vallet, P. G., 1992. An improved thioflavine S method for staining neurofibrillary tangles and senile plaques in Alzheimer's disease. Experientia. 48, 8-10.

Haass, C., Schlossmacher, M. G., Hung, A. Y., Vigo-Pelfrey, C., Mellon, A., Ostaszewski, B. L., Lieberburg, I., Koo, E. H., Schenk, D., Teplow, D. B. and et al., 1992. Amyloid beta-peptide is produced by cultured cells during normal metabolism. Nature. 359, 322-325.

Hacihanefioglu, A., Tarkun, P. and Gonullu, E., 2008. Acute severe cardiac failure in a myeloma patient due to proteasome inhibitor bortezomib. Int J Hematol. 88, 219-222.

Haddad, G. E., Saunders, L. J., Crosby, S. D., Carles, M., del Monte, F., King, K., Bristow, M. R., Spinale, F. G., Macgillivray, T. E., Semigran, M. J., Dec, G. W., Williams, S. A., Hajjar, R. J. and Gwathmey, J. K., 2008. Human cardiac-specific cDNA array for idiopathic dilated cardiomyopathy: sex-related differences. Physiol Genomics. 33, 267-277.

Haghighi, K., Kolokathis, F., Pater, L., Lynch, R. A., Asahi, M., Gramolini, A. O., Fan, G. C., Tsiapras, D., Hahn, H. S., Adamopoulos, S., Liggett, S. B., Dorn, G. W., 2nd, MacLennan, D. H., Kremastinos, D. T. and Kranias, E. G., 2003. Human phospholamban null results in lethal dilated cardiomyopathy revealing a critical difference between mouse and human. J Clin Invest. 111, 869-876.

Hajjar, R. J., Kang, J. X., Gwathmey, J. K. and Rosenzweig, A., 1997. Physiological effects of adenoviral gene transfer of sarcoplasmic reticulum calcium ATPase in isolated rat myocytes. Circulation. 95, 423-429.

Hamada, H., Suzuki, M., Yuasa, S., Mimura, N., Shinozuka, N., Takada, Y., Nishino, T., Nakaya, H., Koseki, H. and Aoe, T., 2004. Dilated cardiomyopathy caused by aberrant endoplasmic reticulum quality control in mutant KDEL receptor transgenic mice. Mol Cell Biol. 24, 8007-8017.

Hannenhalli, S., Putt, M. E., Gilmore, J. M., Wang, J., Parmacek, M. S., Epstein, J. A., Morrisey, E. E., Margulies, K. B. and Cappola, T. P., 2006. Transcriptional genomics associates FOX transcription factors with human heart failure. Circulation. 114, 1269-1276.

Hannon, G. J., Casso, D. and Beach, D., 1994. KAP: a dual specificity phosphatase that interacts with cyclin-dependent kinases. Proc Natl Acad Sci U S A. 91, 1731-1735.

Harding, H. P., Novoa, I., Zhang, Y., Zeng, H., Wek, R., Schapira, M. and Ron, D., 2000a. Regulated translation initiation controls stress-induced gene expression in mammalian cells. Mol Cell. 6, 1099-1108.

Harding, H. P., Zhang, Y., Bertolotti, A., Zeng, H. and Ron, D., 2000b. Perk is essential for translational regulation and cell survival during the unfolded protein response. Mol Cell. 5, 897-904.

Harding, H. P., Zhang, Y., Zeng, H., Novoa, I., Lu, P. D., Calfon, M., Sadri, N., Yun, C., Popko, B., Paules, R., Stojdl, D. F., Bell, J. C., Hettmann, T., Leiden, J. M. and Ron, D., 2003. An integrated stress response regulates amino acid metabolism and resistance to oxidative stress. Mol Cell. 11, 619-633.

Hare, J. M., 2004. Atlas of Heart Failure. Current Medicine LLC, Philadelphia.

Hayrapetyan, V., Rybalchenko, V., Rybalchenko, N. and Koulen, P., 2008. The N-terminus of presenilin-2 increases single channel activity of brain ryanodine receptors through direct protein-protein interaction. Cell Calcium. 44, 507-518.

Haze, K., Yoshida, H., Yanagi, H., Yura, T. and Mori, K., 1999. Mammalian transcription factor ATF6 is synthesized as a transmembrane protein and activated by proteolysis in response to endoplasmic reticulum stress. Mol Biol Cell. 10, 3787-3799.

He, H., Meyer, M., Martin, J. L., McDonough, P. M., Ho, P., Lou, X., Lew, W. Y., Hilal-Dandan, R. and Dillmann, W. H., 1999. Effects of mutant and antisense RNA of phospholamban on SR Ca(2+)-ATPase activity and cardiac myocyte contractility. Circulation. 100, 974-980.

He, J., Ogden, L. G., Bazzano, L. A., Vupputuri, S., Loria, C. and Whelton, P. K., 2001. Risk factors for congestive heart failure in US men and women: NHANES I epidemiologic follow-up study. Arch Intern Med. 161, 996-1002.

Heber, S., Herms, J., Gajic, V., Hainfellner, J., Aguzzi, A., Rulicke, T., von Kretzschmar, H., von Koch, C., Sisodia, S., Tremml, P., Lipp, H. P., Wolfer, D. P. and Muller, U., 2000. Mice with combined gene knock-outs reveal essential and partially redundant functions of amyloid precursor protein family members. J Neurosci. 20, 7951-7963.

Heckman, G. A., Patterson, C. J., Demers, C., St Onge, J., Turpie, I. D. and McKelvie, R. S., 2007. Heart failure and cognitive impairment: challenges and opportunities. Clin Interv Aging. 2, 209-218.

Hedgepeth, C. M., Conrad, L. J., Zhang, J., Huang, H. C., Lee, V. M. and Klein, P. S., 1997. Activation of the Wnt signaling pathway: a molecular mechanism for lithium action. Dev Biol. 185, 82-91.

Hein, S., Kostin, S., Heling, A., Maeno, Y. and Schaper, J., 2000. The role of the cytoskeleton in heart failure. Cardiovasc Res. 45, 273-278.

Henry, W. L., Gardin, J. M. and Ware, J. H., 1980. Echocardiographic measurements in normal subjects from infancy to old age. Circulation. 62, 1054-1061.

Hesse, A., Altland, K., Linke, R. P., Almeida, M. R., Saraiva, M. J., Steinmetz, A. and Maisch, B., 1993. Cardiac amyloidosis: a review and report of a new transthyretin (prealbumin) variant. Br Heart J. 70, 111-115.

Hindmarch, C., Yao, S., Beighton, G., Paton, J. and Murphy, D., 2006. A comprehensive description of the transcriptome of the hypothalamoneurohypophyseal system in euhydrated and dehydrated rats. Proc Natl Acad Sci U S A. 103, 1609-1614.

Hirayoshi, K., Kudo, H., Takechi, H., Nakai, A., Iwamatsu, A., Yamada, K. M. and Nagata, K., 1991. HSP47: a tissue-specific, transformation-sensitive, collagen-binding heat shock protein of chicken embryo fibroblasts. Mol Cell Biol. 11, 4036-4044.

Hiromura, K., Pippin, J. W., Fero, M. L., Roberts, J. M. and Shankland, S. J., 1999. Modulation of apoptosis by the cyclin-dependent kinase inhibitor p27(Kip1). J Clin Invest. 103, 597-604.

Hirschfield, G. M., 2004. Amyloidosis: a clinico-pathophysiological synopsis. Semin Cell Dev Biol. 15, 39-44.

Hohfeld, J. and Jentsch, S., 1997. GrpE-like regulation of the hsc70 chaperone by the anti-apoptotic protein BAG-1. Embo J. 16, 6209-6216.

Honda, T., Yasutake, K., Nihonmatsu, N., Mercken, M., Takahashi, H., Murayama, O., Murayama, M., Sato, K., Omori, A., Tsubuki, S., Saido, T. C. and Takashima, A., 1999. Dual roles of proteasome in the metabolism of presenilin 1. J Neurochem. 72, 255-261.

Hone, E., Martins, I. J., Jeoung, M., Ji, T. H., Gandy, S. E. and Martins, R. N., 2005. Alzheimer's disease amyloid-beta peptide modulates apolipoprotein E isoform specific receptor binding. J Alzheimers Dis. 7, 303-314.

Honig, L. S. and Rosenberg, R. N., 2000. Apoptosis and neurologic disease. Am J Med. 108, 317-330.

Hoozemans, J. J., Veerhuis, R., Van Haastert, E. S., Rozemuller, J. M., Baas, F., Eikelenboom, P. and Scheper, W., 2005. The unfolded protein response is activated in Alzheimer's disease. Acta Neuropathol. 110, 165-172.

Hope, J., 1832. Treatise on the Diseases of the Heart and Great Vessels.

Horwich, A. L., Fenton, W. A., Chapman, E. and Farr, G. W., 2007. Two families of chaperonin: physiology and mechanism. Annu Rev Cell Dev Biol. 23, 115-145.

Hosoi, T. and Ozawa, K., Endoplasmic reticulum stress in disease: mechanisms and therapeutic opportunities. Clin Sci (Lond). 118, 19-29.

Huang da, W., Sherman, B. T. and Lempicki, R. A., 2009a. Bioinformatics enrichment tools: paths toward the comprehensive functional analysis of large gene lists. Nucleic Acids Res. 37, 1-13.

Huang da, W., Sherman, B. T. and Lempicki, R. A., 2009b. Systematic and integrative analysis of large gene lists using DAVID bioinformatics resources. Nat Protoc. 4, 44-57.

Hwang, J. J., Allen, P. D., Tseng, G. C., Lam, C. W., Fananapazir, L., Dzau, V. J. and Liew, C. C., 2002. Microarray gene expression profiles in dilated and hypertrophic cardiomyopathic end-stage heart failure. Physiol Genomics. 10, 31-44.

Inestrosa, N. C., Alvarez, A., Dinamarca, M. C., Perez-Acle, T. and Colombres, M., 2005. Acetylcholinesterase-amyloid-beta-peptide interaction: effect of Congo Red and the role of the Wnt pathway. Curr Alzheimer Res. 2, 301-306.

Ito, D., Walker, J. R., Thompson, C. S., Moroz, I., Lin, W., Veselits, M. L., Hakim, A. M., Fienberg, A. A. and Thinakaran, G., 2004. Characterization of stanniocalcin 2, a novel target of the mammalian unfolded protein response with cytoprotective properties. Mol Cell Biol. 24, 9456-9469.

Itoh-Satoh, M., Hayashi, T., Nishi, H., Koga, Y., Arimura, T., Koyanagi, T., Takahashi, M., Hohda, S., Ueda, K., Nouchi, T., Hiroe, M., Marumo, F., Imaizumi, T., Yasunami, M. and Kimura, A., 2002. Titin mutations as the molecular basis for dilated cardiomyopathy. Biochem Biophys Res Commun. 291, 385-393.

Jaqua-Stewart, M. J., Read, W. O. and Steffen, R. P., 1979. Isolation of pure myocardial subcellular organelles. Anal Biochem. 96, 293-297.

Jin, H., Sanjo, N., Uchihara, T., Watabe, K., George-Hyslop, P. S., Fraser, P. E. and Mizusawa, H., Presenilin-1 Holoprotein is an Interacting Partner of Sarco Endoplasmic Reticulum Calcium-ATPase and Confers Resistance to Endoplasmic Reticulum Stress. J Alzheimers Dis.

Kaab, S., Barth, A. S., Margerie, D., Dugas, M., Gebauer, M., Zwermann, L., Merk, S., Pfeufer, A., Steinmeyer, K., Bleich, M., Kreuzer, E., Steinbeck, G. and Nabauer, M., 2004. Global gene expression in human myocardium-oligonucleotide microarray analysis of regional diversity and transcriptional regulation in heart failure. J Mol Med. 82, 308-316.

Kachinsky, A. M., Dominov, J. A. and Miller, J. B., 1995. Intermediate filaments in cardiac myogenesis: nestin in the developing mouse heart. J Histochem Cytochem. 43, 843-847.

Kamal, A., Almenar-Queralt, A., LeBlanc, J. F., Roberts, E. A. and Goldstein, L. S., 2001. Kinesin-mediated axonal transport of a membrane compartment containing beta-secretase and presenilin-1 requires APP. Nature. 414, 643-648.

Kang, M. J., Kim, J. S., Chae, S. W., Koh, K. N. and Koh, G. Y., 1997. Cyclins and cyclin dependent kinases during cardiac development. Mol Cells. 7, 360-366.

Kaplan, B., Shtrasburg, S. and Pras, M., 2003. Micropurification techniques in the analysis of amyloid proteins. J Clin Pathol. 56, 86-90.

Karkkainen, S. and Peuhkurinen, K., 2007. Genetics of dilated cardiomyopathy. Ann Med. 39, 91-107.

Katz, A. M., 1990. Cardiomyopathy of overload. A major determinant of prognosis in congestive heart failure. N Engl J Med. 322, 100-110.

Kaufman, R. J., 2004. Regulation of mRNA translation by protein folding in the endoplasmic reticulum. Trends Biochem Sci. 29, 152-158.

Kawahara, M. and Kuroda, Y., 2000. Molecular mechanism of neurodegeneration induced by Alzheimer's beta-amyloid protein: channel formation and disruption of calcium homeostasis. Brain Res Bull. 53, 389-397.

Kayed, R., Head, E., Thompson, J. L., McIntire, T. M., Milton, S. C., Cotman, C. W. and Glabe, C. G., 2003. Common structure of soluble amyloid oligomers implies common mechanism of pathogenesis. Science. 300, 486-489.

Kelly, D. P. and Strauss, A. W., 1994. Inherited cardiomyopathies. N Engl J Med. 330, 913-919.

Kelly, J. W., Colon, W., Lai, Z., Lashuel, H. A., McCulloch, J., McCutchen, S. L., Miroy, G. J. and Peterson, S. A., 1997. Transthyretin quaternary and tertiary structural changes facilitate misassembly into amyloid. Adv Protein Chem. 50, 161-181.

Keogh, A. M., Baron, D. W. and Hickie, J. B., 1990. Prognostic guides in patients with idiopathic or ischemic dilated cardiomyopathy assessed for cardiac transplantation. Am J Cardiol. 65, 903-908.

Khan, M. F. and Falk, R. H., 2001. Amyloidosis. Postgrad Med J. 77, 686-693.

Kim, J. R., Lee, S. R., Chung, H. J., Kim, S., Baek, S. H., Kim, J. H. and Kim, Y. S., 2003. Identification of amyloid beta-peptide responsive genes by cDNA microarray technology: involvement of RTP801 in amyloid beta-peptide toxicity. Exp Mol Med. 35, 403-411.

Kimura, K., Wakamatsu, A., Suzuki, Y., Ota, T., Nishikawa, T., Yamashita, R., Yamamoto, J., Sekine, M., Tsuritani, K., Wakaguri, H., Ishii, S., Sugiyama, T., Saito, K., Isono, Y., Irie, R., Kushida, N., Yoneyama, T., Otsuka, R., Kanda, K., Yokoi, T., Kondo, H., Wagatsuma, M., Murakawa, K., Ishida, S., Ishibashi, T., Takahashi-Fujii, A., Tanase, T., Nagai, K., Kikuchi, H., Nakai, K., Isogai, T. and Sugano, S., 2006. Diversification of transcriptional modulation: large-scale identification and characterization of putative alternative promoters of human genes. Genome Res. 16, 55-65.

Kiss, E., Ball, N. A., Kranias, E. G. and Walsh, R. A., 1995. Differential changes in cardiac phospholamban and sarcoplasmic reticular Ca(2+)-ATPase protein levels. Effects on Ca2+ transport and mechanics in compensated pressure-overload hypertrophy and congestive heart failure. Circ Res. 77, 759-764.

Kittleson, M. M., Minhas, K. M., Irizarry, R. A., Ye, S. Q., Edness, G., Breton, E., Conte, J. V., Tomaselli, G., Garcia, J. G. and Hare, J. M., 2005. Gene

expression analysis of ischemic and nonischemic cardiomyopathy: shared and distinct genes in the development of heart failure. Physiol Genomics. 21, 299-307.

Kleinman, L. H., Wechsler, A. S., Rembert, J. C., Fedor, J. M. and Greenfield, J. C., Jr., 1978. A reproducible model of moderate to severe concentric left ventricular hypertrophy. Am J Physiol. 234, H515-519.

Klyubin, I., Walsh, D. M., Cullen, W. K., Fadeeva, J. V., Anwyl, R., Selkoe, D. J. and Rowan, M. J., 2004. Soluble Arctic amyloid beta protein inhibits hippocampal long-term potentiation in vivo. Eur J Neurosci. 19, 2839-2846.

Koh, J. Y., Yang, L. L. and Cotman, C. W., 1990. Beta-amyloid protein increases the vulnerability of cultured cortical neurons to excitotoxic damage. Brain Res. 533, 315-320.

Koizumi, K., Hoshiai, M., Ishida, H., Ohyama, K., Sugiyama, H., Naito, A., Toda, T., Nakazawa, H. and Nakazawa, S., 2007. Stanniocalcin 1 prevents cytosolic Ca2+ overload and cell hypercontracture in cardiomyocytes. Circ J. 71, 796-801.

Kopito, R. R. and Ron, D., 2000. Conformational disease. Nat Cell Biol. 2, E207-209.

Korenberg, J. R., Pulst, S. M., Neve, R. L. and West, R., 1989. The Alzheimer amyloid precursor protein maps to human chromosome 21 bands q21.105-q21.05. Genomics. 5, 124-127.

Kostin, S., Hein, S., Arnon, E., Scholz, D. and Schaper, J., 2000. The cytoskeleton and related proteins in the human failing heart. Heart Fail Rev. 5, 271-280.

Kowall, N. W., Beal, M. F., Busciglio, J., Duffy, L. K. and Yankner, B. A., 1991. An in vivo model for the neurodegenerative effects of beta amyloid and protection by substance P. Proc Natl Acad Sci U S A. 88, 7247-7251.

Kryndushkin, D. S., Alexandrov, I. M., Ter-Avanesyan, M. D. and Kushnirov, V. V., 2003. Yeast [PSI+] prion aggregates are formed by small Sup35 polymers fragmented by Hsp104. J Biol Chem. 278, 49636-49643.

Kukekov, V. G., Laywell, E. D., Suslov, O., Davies, K., Scheffler, B., Thomas, L. B., O'Brien, T. F., Kusakabe, M. and Steindler, D. A., 1999. Multipotent stem/progenitor cells with similar properties arise from two neurogenic regions of adult human brain. Exp Neurol. 156, 333-344.

LaFerla, F. M., 2002. Calcium dyshomeostasis and intracellular signalling in Alzheimer's disease. Nat Rev Neurosci. 3, 862-872.

Lansbury, P. T. and Lashuel, H. A., 2006. A century-old debate on protein aggregation and neurodegeneration enters the clinic. Nature. 443, 774-779.

Lashuel, H. A., Hartley, D., Petre, B. M., Walz, T. and Lansbury, P. T., Jr., 2002a. Neurodegenerative disease: amyloid pores from pathogenic mutations. Nature. 418, 291.

Lashuel, H. A., Petre, B. M., Wall, J., Simon, M., Nowak, R. J., Walz, T. and Lansbury, P. T., Jr., 2002b. Alpha-synuclein, especially the Parkinson's disease-associated mutants, forms pore-like annular and tubular protofibrils. J Mol Biol. 322, 1089-1102.

Leahy, K. P. and Crawford, D. R., 2000. adapt78 protects cells against stress damage and suppresses cell growth. Arch Biochem Biophys. 379, 221-228.

Leahy, K. P., Davies, K. J., Dull, M., Kort, J. J., Lawrence, K. W. and Crawford, D. R., 1999. adapt78, a stress-inducible mRNA, is related to the glucose-regulated protein family of genes. Arch Biochem Biophys. 368, 67-74.

Lee, A. H., Iwakoshi, N. N. and Glimcher, L. H., 2003. XBP-1 regulates a subset of endoplasmic reticulum resident chaperone genes in the unfolded protein response. Mol Cell Biol. 23, 7448-7459.

Lehninger, A., 1993. Principles of biochemistry. Worth Publishers.

Leissring, M. A., Murphy, M. P., Mead, T. R., Akbari, Y., Sugarman, M. C., Jannatipour, M., Anliker, B., Muller, U., Saftig, P., De Strooper, B., Wolfe, M. S., Golde, T. E. and LaFerla, F. M., 2002. A physiologic signaling role for the gamma -secretase-derived intracellular fragment of APP. Proc Natl Acad Sci U S A. 99, 4697-4702.

Lemere, C. A., Blusztajn, J. K., Yamaguchi, H., Wisniewski, T., Saido, T. C. and Selkoe, D. J., 1996. Sequence of deposition of heterogeneous amyloid beta-peptides and APO E in Down syndrome: implications for initial events in amyloid plaque formation. Neurobiol Dis. 3, 16-32.

Leonard, B. W., Mastroeni, D., Grover, A., Liu, Q., Yang, K., Gao, M., Wu, J., Pootrakul, D., van den Berge, S. A., Hol, E. M. and Rogers, J., 2009. Subventricular zone neural progenitors from rapid brain autopsies of elderly subjects with and without neurodegenerative disease. J Comp Neurol. 515, 269-294.

Li, D., Parks, S. B., Kushner, J. D., Nauman, D., Burgess, D., Ludwigsen, S., Partain, J., Nixon, R. R., Allen, C. N., Irwin, R. P., Jakobs, P. M., Litt, M. and Hershberger, R. E., 2006. Mutations of presenilin genes in dilated cardiomyopathy and heart failure. Am J Hum Genet. 79, 1030-1039.

Li, D., Tapscoft, T., Gonzalez, O., Burch, P. E., Quinones, M. A., Zoghbi, W. A., Hill, R., Bachinski, L. L., Mann, D. L. and Roberts, R., 1999. Desmin mutation responsible for idiopathic dilated cardiomyopathy. Circulation. 100, 461-464.

Liao, H. S., Kang, P. M., Nagashima, H., Yamasaki, N., Usheva, A., Ding, B., Lorell, B. H. and Izumo, S., 2001. Cardiac-specific overexpression of cyclin-dependent kinase 2 increases smaller mononuclear cardiomyocytes. Circ Res. 88, 443-450.

Liao, R. and Jain, M., 2007. Isolation, culture, and functional analysis of adult mouse cardiomyocytes. Methods Mol Med. 139, 251-262.

Lin, M. C., Mirzabekov, T. and Kagan, B. L., 1997. Channel formation by a neurotoxic prion protein fragment. J Biol Chem. 272, 44-47.

Lindholm, D., Wootz, H. and Korhonen, L., 2006. ER stress and neurodegenerative diseases. Cell Death Differ. 13, 385-392.

Lindner, M., Brandt, M. C., Sauer, H., Hescheler, J., Bohle, T. and Beuckelmann, D. J., 2002. Calcium sparks in human ventricular cardiomyocytes from patients with terminal heart failure. Cell Calcium. 31, 175-182.

Liu, J., Chen, Q., Huang, W., Horak, K. M., Zheng, H., Mestril, R. and Wang, X., 2006a. Impairment of the ubiquitin-proteasome system in desminopathy mouse hearts. Faseb J. 20, 362-364.

Liu, J., Farmer, J. D., Jr., Lane, W. S., Friedman, J., Weissman, I. and Schreiber, S. L., 1991. Calcineurin is a common target of cyclophilin-cyclosporin A and FKBP-FK506 complexes. Cell. 66, 807-815.

Liu, K., Solano, I., Mann, D., Lemere, C., Mercken, M., Trojanowski, J. Q. and Lee, V. M., 2006b. Characterization of Abeta11-40/42 peptide deposition in Alzheimer's disease and young Down's syndrome brains: implication of N-terminally truncated Abeta species in the pathogenesis of Alzheimer's disease. Acta Neuropathol (Berl). 112, 163-174.

Lokuta, A. J., Meyers, M. B., Sander, P. R., Fishman, G. I. and Valdivia, H. H., 1997. Modulation of cardiac ryanodine receptors by sorcin. J Biol Chem. 272, 25333-25338.

Longoni, S., Lattonen, S., Bullock, G. and Chiesi, M., 1990. Cardiac alpha-crystallin. II. Intracellular localization. Mol Cell Biochem. 97, 121-128.

Lovell, M. A., Ehmann, W. D., Butler, S. M. and Markesbery, W. R., 1995. Elevated thiobarbituric acid-reactive substances and antioxidant enzyme activity in the brain in Alzheimer's disease. Neurology. 45, 1594-1601.

Lowe, J., Stock, D., Jap, B., Zwickl, P., Baumeister, W. and Huber, R., 1995. Crystal structure of the 20S proteasome from the archaeon T. acidophilum at 3.4 A resolution. Science. 268, 533-539.

Lowry, O. H., Rosebrough, N. J., Farr, A. L. and Randall, R. J., 1951. Protein measurement with the Folin phenol reagent. J Biol Chem. 193, 265-275.

Lye, T. C. and Shores, E. A., 2000. Traumatic brain injury as a risk factor for Alzheimer's disease: a review. Neuropsychol Rev. 10, 115-129.

Lyon, A. R., Sato, M., Hajjar, R. J., Samulski, R. J. and Harding, S. E., 2008. Gene therapy: targeting the myocardium. Heart. 94, 89-99.

Ma, Y., Brewer, J. W., Diehl, J. A. and Hendershot, L. M., 2002. Two distinct stress signaling pathways converge upon the CHOP promoter during the mammalian unfolded protein response. J Mol Biol. 318, 1351-1365.

Maccioni, R. B., Munoz, J. P. and Barbeito, L., 2001. The molecular bases of Alzheimer's disease and other neurodegenerative disorders. Arch Med Res. 32, 367-381.

Madsen, K. L., Tavernini, M. M., Yachimec, C., Mendrick, D. L., Alfonso, P. J., Buergin, M., Olsen, H. S., Antonaccio, M. J., Thomson, A. B. and Fedorak, R. N., 1998. Stanniocalcin: a novel protein regulating calcium and phosphate transport across mammalian intestine. Am J Physiol. 274, G96-102.

Mah, A. L., Perry, G., Smith, M. A. and Monteiro, M. J., 2000. Identification of ubiquilin, a novel presenilin interactor that increases presenilin protein accumulation. J Cell Biol. 151, 847-862.

Mandelkow, E. M., Stamer, K., Vogel, R., Thies, E. and Mandelkow, E., 2003. Clogging of axons by tau, inhibition of axonal traffic and starvation of synapses. Neurobiol Aging. 24, 1079-1085.

Marenduzzo, D., Finan, K. and Cook, P. R., 2006. The depletion attraction: an underappreciated force driving cellular organization. J Cell Biol. 175, 681-686.

Marijianowski, M. M., Teeling, P., Mann, J. and Becker, A. E., 1995. Dilated cardiomyopathy is associated with an increase in the type I/type III collagen ratio: a quantitative assessment. J Am Coll Cardiol. 25, 1263-1272.

Maron, B. J., Ferrans, V. J. and Roberts, W. C., 1975. Ultrastructural features of degenerated cardiac muscle cells in patients with cardiac hypertrophy. Am J Pathol. 79, 387-434.

Mayeux, R. and Sano, M., 1999. Treatment of Alzheimer's disease. N Engl J Med. 341, 1670-1679.

Maytin, E. V., Ubeda, M., Lin, J. C. and Habener, J. F., 2001. Stress-inducible transcription factor CHOP/gadd153 induces apoptosis in mammalian cells via p38 kinase-dependent and -independent mechanisms. Exp Cell Res. 267, 193-204.

McCarthy, R. E., 3rd and Kasper, E. K., 1998. A review of the amyloidoses that infiltrate the heart. Clin Cardiol. 21, 547-552.

McCullough, K. D., Martindale, J. L., Klotz, L. O., Aw, T. Y. and Holbrook, N. J., 2001. Gadd153 sensitizes cells to endoplasmic reticulum stress by down-regulating Bcl2 and perturbing the cellular redox state. Mol Cell Biol. 21, 1249-1259.

Medicherla, B., Kostova, Z., Schaefer, A. and Wolf, D. H., 2004. A genomic screen identifies Dsk2p and Rad23p as essential components of ER-associated degradation. EMBO Rep. 5, 692-697.

Medin, M., Hermida-Prieto, M., Monserrat, L., Laredo, R., Rodriguez-Rey, J. C., Fernandez, X. and Castro-Beiras, A., 2007. Mutational screening of phospholamban gene in hypertrophic and idiopathic dilated cardiomyopathy and functional study of the PLN -42 C>G mutation. Eur J Heart Fail. 9, 37-43.

Meikrantz, W., Gisselbrecht, S., Tam, S. W. and Schlegel, R., 1994. Activation of cyclin A-dependent protein kinases during apoptosis. Proc Natl Acad Sci U S A. 91, 3754-3758.

Mesquita, T., Chorao, M., Soares, I., Mello e Silva, A. and Abecasis, P., 2005. Primary amyloidosis as a cause of microvascular angina and intermittent claudication. Rev Port Cardiol. 24, 1521-1531.

Messina, E., De Angelis, L., Frati, G., Morrone, S., Chimenti, S., Fiordaliso, F., Salio, M., Battaglia, M., Latronico, M. V., Coletta, M., Vivarelli, E., Frati, L., Cossu, G. and Giacomello, A., 2004. Isolation and expansion of adult cardiac stem cells from human and murine heart. Circ Res. 95, 911-921.

Meunier, L., Usherwood, Y. K., Chung, K. T. and Hendershot, L. M., 2002. A subset of chaperones and folding enzymes form multiprotein complexes in endoplasmic reticulum to bind nascent proteins. Mol Biol Cell. 13, 4456-4469.

Meyer, T. S. and Lamberts, B. L., 1965. Use of coomassie brilliant blue R250 for the electrophoresis of microgram quantities of parotid saliva proteins on acrylamide-gel strips. Biochim Biophys Acta. 107, 144-145.

Minamisawa, S., Hoshijima, M., Chu, G., Ward, C. A., Frank, K., Gu, Y., Martone, M. E., Wang, Y., Ross, J., Jr., Kranias, E. G., Giles, W. R. and Chien, K. R., 1999. Chronic phospholamban-sarcoplasmic reticulum calcium ATPase interaction is the critical calcium cycling defect in dilated cardiomyopathy. Cell. 99, 313-322.

Mirzabekov, T. A., Lin, M. C. and Kagan, B. L., 1996. Pore formation by the cytotoxic islet amyloid peptide amylin. J Biol Chem. 271, 1988-1992.

Molinari, M., Calanca, V., Galli, C., Lucca, P. and Paganetti, P., 2003. Role of EDEM in the release of misfolded glycoproteins from the calnexin cycle. Science. 299, 1397-1400.

Molkentin, J. D., Lu, J. R., Antos, C. L., Markham, B., Richardson, J., Robbins, J., Grant, S. R. and Olson, E. N., 1998. A calcineurin-dependent transcriptional pathway for cardiac hypertrophy. Cell. 93, 215-228.

Morishima, N., Nakanishi, K., Takenouchi, H., Shibata, T. and Yasuhiko, Y., 2002. An endoplasmic reticulum stress-specific caspase cascade in apoptosis. Cytochrome c-independent activation of caspase-9 by caspase-12. J Biol Chem. 277, 34287-34294.

Moulik, M., Vatta, M., Witt, S. H., Arola, A. M., Murphy, R. T., McKenna, W. J., Boriek, A. M., Oka, K., Labeit, S., Bowles, N. E., Arimura, T., Kimura, A. and Towbin, J. A., 2009. ANKRD1, the gene encoding cardiac ankyrin repeat protein, is a novel dilated cardiomyopathy gene. J Am Coll Cardiol. 54, 325-333.

Murphy, C. L., Wang, S., Williams, T., Weiss, D. T. and Solomon, A., 2006. Characterization of systemic amyloid deposits by mass spectrometry. Methods Enzymol. 412, 48-62.

Murray, J. C., Buetow, K. H., Weber, J. L., Ludwigsen, S., Scherpbier-Heddema, T., Manion, F., Quillen, J., Sheffield, V. C., Sunden, S., Duyk, G. M. and et al., 1994. A comprehensive human linkage map with centimorgan density. Cooperative Human Linkage Center (CHLC). Science. 265, 2049-2054.

Mustafa, D., Kros, J. M. and Luider, T., 2008. Combining laser capture microdissection and proteomics techniques. Methods Mol Biol. 428, 159-178.

Nakagawa, T., Zhu, H., Morishima, N., Li, E., Xu, J., Yankner, B. A. and Yuan, J., 2000. Caspase-12 mediates endoplasmic-reticulum-specific apoptosis and cytotoxicity by amyloid-beta. Nature. 403, 98-103.

Nakajima, M., Moriizumi, E., Koseki, H. and Shirasawa, T., 2004. Presenilin 1 is essential for cardiac morphogenesis. Dev Dyn. 230, 795-799.

Nakao, K., Minobe, W., Roden, R., Bristow, M. R. and Leinwand, L. A., 1997. Myosin heavy chain gene expression in human heart failure. J Clin Invest. 100, 2362-2370.

Natsume, T., Koide, T., Yokota, S., Hirayoshi, K. and Nagata, K., 1994. Interactions between collagen-binding stress protein HSP47 and collagen. Analysis of kinetic parameters by surface plasmon resonance biosensor. J Biol Chem. 269, 31224-31228.

Neben-Wittich, M. A., Wittich, C. M., Mueller, P. S., Larson, D. R., Gertz, M. A. and Edwards, W. D., 2005. Obstructive intramural coronary amyloidosis and myocardial ischemia are common in primary amyloidosis. Am J Med. 118, 1287.

Ni, M. and Lee, A. S., 2007. ER chaperones in mammalian development and human diseases. FEBS Lett. 581, 3641-3651.

Ni, Y. G., Berenji, K., Wang, N., Oh, M., Sachan, N., Dey, A., Cheng, J., Lu, G., Morris, D. J., Castrillon, D. H., Gerard, R. D., Rothermel, B. A. and Hill, J. A., 2006. Foxo transcription factors blunt cardiac hypertrophy by inhibiting calcineurin signaling. Circulation. 114, 1159-1168.

Nihoyannopoulos, P. and Dawson, D., 2009. Restrictive cardiomyopathies. Eur J Echocardiogr. 10, iii23-33.

Nishimoto, I., Okamoto, T., Matsuura, Y., Takahashi, S., Murayama, Y. and Ogata, E., 1993. Alzheimer amyloid protein precursor complexes with brain GTP-binding protein G(o). Nature. 362, 75-79.

Nishitoh, H., Matsuzawa, A., Tobiume, K., Saegusa, K., Takeda, K., Inoue, K., Hori, S., Kakizuka, A. and Ichijo, H., 2002. ASK1 is essential for endoplasmic reticulum stress-induced neuronal cell death triggered by expanded polyglutamine repeats. Genes Dev. 16, 1345-1355.

Norgett, E. E., Hatsell, S. J., Carvajal-Huerta, L., Cabezas, J. C., Common, J., Purkis, P. E., Whittock, N., Leigh, I. M., Stevens, H. P. and Kelsell, D. P., 2000. Recessive mutation in desmoplakin disrupts desmoplakin-intermediate filament interactions and causes dilated cardiomyopathy, woolly hair and keratoderma. Hum Mol Genet. 9, 2761-2766.

Novitskaya, V., Bocharova, O. V., Bronstein, I. and Baskakov, I. V., 2006. Amyloid fibrils of mammalian prion protein are highly toxic to cultured cells and primary neurons. J Biol Chem. 281, 13828-13836.

Oda, Y., Hosokawa, N., Wada, I. and Nagata, K., 2003. EDEM as an acceptor of terminally misfolded glycoproteins released from calnexin. Science. 299, 1394-1397.

Okada, K., Minamino, T., Tsukamoto, Y., Liao, Y., Tsukamoto, O., Takashima, S., Hirata, A., Fujita, M., Nagamachi, Y., Nakatani, T., Yutani, C., Ozawa, K., Ogawa, S., Tomoike, H., Hori, M. and Kitakaze, M., 2004. Prolonged endoplasmic reticulum stress in hypertrophic and failing heart after aortic constriction: possible contribution of endoplasmic reticulum stress to cardiac myocyte apoptosis. Circulation. 110, 705-712.

Olson, E. N., 2004. A decade of discoveries in cardiac biology. Nat Med. 10, 467-474.

Oyama, M. A. and Chittur, S., 2005. Genomic expression patterns of cardiac tissues from dogs with dilated cardiomyopathy. Am J Vet Res. 66, 1140-1155.

Pack-Chung, E., Meyers, M. B., Pettingell, W. P., Moir, R. D., Brownawell, A. M., Cheng, I., Tanzi, R. E. and Kim, T. W., 2000. Presenilin 2 interacts with sorcin, a modulator of the ryanodine receptor. J Biol Chem. 275, 14440-14445.

Papp, S., Dziak, E., Michalak, M. and Opas, M., 2003. Is all of the endoplasmic reticulum created equal? The effects of the heterogeneous distribution of endoplasmic reticulum Ca2+-handling proteins. J Cell Biol. 160, 475-479.

Pattison, J. S., Sanbe, A., Maloyan, A., Osinska, H., Klevitsky, R. and Robbins, J., 2008. Cardiomyocyte expression of a polyglutamine preamyloid oligomer causes heart failure. Circulation. 117, 2743-2751.

Pearl, L. H. and Prodromou, C., 2006. Structure and mechanism of the Hsp90 molecular chaperone machinery. Annu Rev Biochem. 75, 271-294.

Petrovitch, H., White, L. R., Izmirilian, G., Ross, G. W., Havlik, R. J., Markesbery, W., Nelson, J., Davis, D. G., Hardman, J., Foley, D. J. and Launer, L. J., 2000. Midlife blood pressure and neuritic plaques, neurofibrillary tangles, and brain weight at death: the HAAS. Honolulu-Asia aging Study. Neurobiol Aging. 21, 57-62.

Philipp, U., Broschk, C., Vollmar, A. and Distl, O., 2007. Evaluation of tafazzin as candidate for dilated cardiomyopathy in Irish wolfhounds. J Hered. 98, 506-509.

Porta, S., Serra, S. A., Huch, M., Valverde, M. A., Llorens, F., Estivill, X., Arbones, M. L. and Marti, E., 2007. RCAN1 (DSCR1) increases neuronal susceptibility to oxidative stress: a potential pathogenic process in neurodegeneration. Hum Mol Genet. 16, 1039-1050.

Pounds, S. B., 2006. Estimation and control of multiple testing error rates for microarray studies. Brief Bioinform. 7, 25-36.

Powell, S. R., Wang, P., Katzeff, H., Shringarpure, R., Teoh, C., Khaliulin, I., Das, D. K., Davies, K. J. and Schwalb, H., 2005. Oxidized and ubiquitinated proteins may predict recovery of postischemic cardiac function: essential role of the proteasome. Antioxid Redox Signal. 7, 538-546.

Priller, C., Bauer, T., Mitteregger, G., Krebs, B., Kretzschmar, H. A. and Herms, J., 2006. Synapse formation and function is modulated by the amyloid precursor protein. J Neurosci. 26, 7212-7221.

Prince, M., Cullen, M. and Mann, A., 1994. Risk factors for Alzheimer's disease and dementia: a case-control study based on the MRC elderly hypertension trial. Neurology. 44, 97-104.

Prusiner, S. B., 1998. Prions. Proc Natl Acad Sci U S A. 95, 13363-13383.

Qiu, C., Winblad, B., Viitanen, M. and Fratiglioni, L., 2003. Pulse pressure and risk of Alzheimer disease in persons aged 75 years and older: a community-based, longitudinal study. Stroke. 34, 594-599.

Quackenbush, J., 2002. Microarray data normalization and transformation. Nat Genet. 32 Suppl, 496-501.

Rademaker, M. T. and Richards, A. M., 2005. Cardiac natriuretic peptides for cardiac health. Clin Sci (Lond). 108, 23-36.

Ramsby, M. L. and Makowski, G. S., 1999. Differential detergent fractionation of eukaryotic cells. Analysis by two-dimensional gel electrophoresis. Methods Mol Biol. 112, 53-66.

Reiss, K., Cheng, W., Kajstura, J., Sonnenblick, E. H., Meggs, L. G. and Anversa, P., 1995. Fibroblast proliferation during myocardial development in rats is regulated by IGF-1 receptors. Am J Physiol. 269, H943-951.

Reyes, A. E., Chacon, M. A., Dinamarca, M. C., Cerpa, W., Morgan, C. and Inestrosa, N. C., 2004. Acetylcholinesterase-Abeta complexes are more toxic than Abeta fibrils in rat hippocampus: effect on rat beta-amyloid aggregation, laminin expression, reactive astrocytosis, and neuronal cell loss. Am J Pathol. 164, 2163-2174.

Rogaev, E. I., Sherrington, R., Wu, C., Levesque, G., Liang, Y., Rogaeva, E. A., Ikeda, M., Holman, K., Lin, C., Lukiw, W. J., de Jong, P. J., Fraser, P. E., Rommens, J. M. and St George-Hyslop, P., 1997. Analysis of the 5' sequence, genomic structure, and alternative splicing of the presenilin-1 gene (PSEN1) associated with early onset Alzheimer disease. Genomics. 40, 415-424.

Rogers, J., Webster, S., Lue, L. F., Brachova, L., Civin, W. H., Emmerling, M., Shivers, B., Walker, D. and McGeer, P., 1996. Inflammation and Alzheimer's disease pathogenesis. Neurobiol Aging. 17, 681-686.

Ross, C. A. and Poirier, M. A., 2004. Protein aggregation and neurodegenerative disease. Nat Med. 10 Suppl, S10-17.

Ross, J., Jr., 2002. Dilated cardiomyopathy: concepts derived from gene deficient and transgenic animal models. Circ J. 66, 219-224.

Rostagno, A. and Ghiso, J., 2009. Isolation and biochemical characterization of amyloid plaques and paired helical filaments. Curr Protoc Cell Biol. Chapter 3, Unit 3 33 33 33 31-33.

Rothermel, B. A., McKinsey, T. A., Vega, R. B., Nicol, R. L., Mammen, P., Yang, J., Antos, C. L., Shelton, J. M., Bassel-Duby, R., Olson, E. N. and Williams, R. S., 2001. Myocyte-enriched calcineurin-interacting protein, MCIP1, inhibits cardiac hypertrophy in vivo. Proc Natl Acad Sci U S A. 98, 3328-3333.

Sack, M. N. and Kelly, D. P., 1998. The energy substrate switch during development of heart failure: gene regulatory mechanisms (Review). Int J Mol Med. 1, 17-24.

Saibil, H. R., 2008. Chaperone machines in action. Curr Opin Struct Biol. 18, 35-42.

Saito, S., Hiroi, Y., Zou, Y., Aikawa, R., Toko, H., Shibasaki, F., Yazaki, Y., Nagai, R. and Komuro, I., 2000. beta-Adrenergic pathway induces apoptosis through calcineurin activation in cardiac myocytes. J Biol Chem. 275, 34528-34533.

Sanbe, A., Osinska, H., Saffitz, J. E., Glabe, C. G., Kayed, R., Maloyan, A. and Robbins, J., 2004. Desmin-related cardiomyopathy in transgenic mice: a cardiac amyloidosis. Proc Natl Acad Sci U S A. 101, 10132-10136.

Sanbe, A., Osinska, H., Villa, C., Gulick, J., Klevitsky, R., Glabe, C. G., Kayed, R. and Robbins, J., 2005. Reversal of amyloid-induced heart disease in desmin-related cardiomyopathy. Proc Natl Acad Sci U S A. 102, 13592-13597.

Sandbrink, R., Zhang, D., Schaeffer, S., Masters, C. L., Bauer, J., Forstl, H. and Beyreuther, K., 1996. Missense mutations of the PS-1/S182 gene in German early-onset Alzheimer's disease patients. Ann Neurol. 40, 265-266.

Saraiva, M. J., 2002. Hereditary transthyretin amyloidosis: molecular basis and therapeutical strategies. Expert Rev Mol Med. 4, 1-11.

Sarikas, A., Carrier, L., Schenke, C., Doll, D., Flavigny, J., Lindenberg, K. S., Eschenhagen, T. and Zolk, O., 2005. Impairment of the ubiquitin-proteasome system by truncated cardiac myosin binding protein C mutants. Cardiovasc Res. 66, 33-44.

Sayre, L. M., Zelasko, D. A., Harris, P. L., Perry, G., Salomon, R. G. and Smith, M. A., 1997. 4-Hydroxynonenal-derived advanced lipid peroxidation end products are increased in Alzheimer's disease. J Neurochem. 68, 2092-2097.

Schmitt, J. P., Kamisago, M., Asahi, M., Li, G. H., Ahmad, F., Mende, U., Kranias, E. G., MacLennan, D. H., Seidman, J. G. and Seidman, C. E., 2003. Dilated cardiomyopathy and heart failure caused by a mutation in phospholamban. Science. 299, 1410-1413.

Schmitz, A., Schneider, A., Kummer, M. P. and Herzog, V., 2004. Endoplasmic reticulum-localized amyloid beta-peptide is degraded in the cytosol by two distinct degradation pathways. Traffic. 5, 89-101.

Schonberger, J. and Seidman, C. E., 2001. Many roads lead to a broken heart: the genetics of dilated cardiomyopathy. Am J Hum Genet. 69, 249-260.

Schonberger, J., Wang, L., Shin, J. T., Kim, S. D., Depreux, F. F., Zhu, H., Zon, L., Pizard, A., Kim, J. B., Macrae, C. A., Mungall, A. J., Seidman, J. G. and Seidman, C. E., 2005. Mutation in the transcriptional coactivator EYA4 causes dilated cardiomyopathy and sensorineural hearing loss. Nat Genet. 37, 418-422.

Schrodel, A. and de Marco, A., 2005. Characterization of the aggregates formed during recombinant protein expression in bacteria. BMC Biochem. 6, 10.

Schroder, M. and Kaufman, R. J., 2005. ER stress and the unfolded protein response. Mutat Res. 569, 29-63.

Schuberth, C. and Buchberger, A., 2005. Membrane-bound Ubx2 recruits Cdc48 to ubiquitin ligases and their substrates to ensure efficient ER-associated protein degradation. Nat Cell Biol. 7, 999-1006.

Sedgwick, S. G. and Smerdon, S. J., 1999. The ankyrin repeat: a diversity of interactions on a common structural framework. Trends Biochem Sci. 24, 311-316.

Seidman, J. G. and Seidman, C., 2001. The genetic basis for cardiomyopathy: from mutation identification to mechanistic paradigms. Cell. 104, 557-567.

Selkoe, D. J., 2003. Folding proteins in fatal ways. Nature. 426, 900-904.

Shamu, C. E. and Walter, P., 1996. Oligomerization and phosphorylation of the Ire1p kinase during intracellular signaling from the endoplasmic reticulum to the nucleus. Embo J. 15, 3028-3039.

Sharma, U. C., Pokharel, S., Evelo, C. T. and Maessen, J. G., 2005. A systematic review of large scale and heterogeneous gene array data in heart failure. J Mol Cell Cardiol. 38, 425-432.

Sheikh-Hamad, D., Bick, R., Wu, G. Y., Christensen, B. M., Razeghi, P., Poindexter, B., Taegtmeyer, H., Wamsley, A., Padda, R., Entman, M., Nielsen, S. and Youker, K., 2003. Stanniocalcin-1 is a naturally occurring L-channel inhibitor in cardiomyocytes: relevance to human heart failure. Am J Physiol Heart Circ Physiol. 285, H442-448.

Shibata, M., Yamada, S., Kumar, S. R., Calero, M., Bading, J., Frangione, B., Holtzman, D. M., Miller, C. A., Strickland, D. K., Ghiso, J. and Zlokovic, B. V., 2000. Clearance of Alzheimer's amyloid-ss(1-40) peptide from brain by LDL receptor-related protein-1 at the blood-brain barrier. J Clin Invest. 106, 1489-1499.

Shimizu, M., Ino, H., Yasuda, T., Fujino, N., Uchiyama, K., Mabuchi, T., Konno, T., Kaneda, T., Fujita, T., Masuta, E., Katoh, M., Funada, A. and Mabuchi, H., 2005. Gene mutations in adult Japanese patients with dilated cardiomyopathy. Circ J. 69, 150-153.

Shoji, M., Golde, T. E., Ghiso, J., Cheung, T. T., Estus, S., Shaffer, L. M., Cai, X. D., McKay, D. M., Tintner, R., Frangione, B. and et al., 1992. Production of the Alzheimer amyloid beta protein by normal proteolytic processing. Science. 258, 126-129.

Sipe, J. D. and Cohen, A. S., 2000. Review: history of the amyloid fibril. J Struct Biol. 130, 88-98.

Sitia, R. and Braakman, I., 2003. Quality control in the endoplasmic reticulum protein factory. Nature. 426, 891-894.

Sousa, M. M., Du Yan, S., Fernandes, R., Guimaraes, A., Stern, D. and Saraiva, M. J., 2001. Familial amyloid polyneuropathy: receptor for advanced glycation end products-dependent triggering of neuronal inflammatory and apoptotic pathways. J Neurosci. 21, 7576-7586.

Sparks, D. L., 1996. Intraneuronal beta-amyloid immunoreactivity in the CNS. Neurobiol Aging. 17, 291-299.

Sparks, D. L., Hunsaker, J. C., 3rd, Scheff, S. W., Kryscio, R. J., Henson, J. L. and Markesbery, W. R., 1990. Cortical senile plaques in coronary artery disease, aging and Alzheimer's disease. Neurobiol Aging. 11, 601-607.

Sparks, D. L., Scheff, S. W., Liu, H., Landers, T. M., Coyne, C. M. and Hunsaker, J. C., 3rd, 1995. Increased incidence of neurofibrillary tangles (NFT) in non-demented individuals with hypertension. J Neurol Sci. 131, 162-169.

Stabler, S. M., Ostrowski, L. L., Janicki, S. M. and Monteiro, M. J., 1999. A myristoylated calcium-binding protein that preferentially interacts with the Alzheimer's disease presenilin 2 protein. J Cell Biol. 145, 1277-1292.

Steenman, M., Chen, Y. W., Le Cunff, M., Lamirault, G., Varro, A., Hoffman, E. and Leger, J. J., 2003. Transcriptomal analysis of failing and nonfailing human hearts. Physiol Genomics. 12, 97-112.

Steiner, H., Winkler, E., Edbauer, D., Prokop, S., Basset, G., Yamasaki, A., Kostka, M. and Haass, C., 2002. PEN-2 is an integral component of the gamma-secretase complex required for coordinated expression of presenilin and nicastrin. J Biol Chem. 277, 39062-39065.

Steiner, I. and Hajkova, P., 2006. Patterns of isolated atrial amyloid: a study of 100 hearts on autopsy. Cardiovasc Pathol. 15, 287-290.

Stevens, F. J. and Argon, Y., 1999. Protein folding in the ER. Semin Cell Dev Biol. 10, 443-454.

Storey, J. D. and Tibshirani, R., 2003. Statistical significance for genomewide studies. Proc Natl Acad Sci U S A. 100, 9440-9445.

Strausberg, R. L., Feingold, E. A., Grouse, L. H., Derge, J. G., Klausner, R. D., Collins, F. S., Wagner, L., Shenmen, C. M., Schuler, G. D., Altschul, S. F., Zeeberg, B., Buetow, K. H., Schaefer, C. F., Bhat, N. K., Hopkins, R. F., Jordan, H., Moore, T., Max, S. I., Wang, J., Hsieh, F., Diatchenko, L., Marusina, K., Farmer, A. A., Rubin, G. M., Hong, L., Stapleton, M., Soares, M. B., Bonaldo, M. F., Casavant, T. L., Scheetz, T. E., Brownstein, M. J., Usdin, T. B., Toshiyuki, S., Carninci, P., Prange, C., Raha, S. S., Loquellano, N. A., Peters, G. J., Abramson, R. D., Mullahy, S. J., Bosak, S. A., McEwan, P. J., McKernan, K. J., Malek, J. A., Gunaratne, P. H., Richards, S., Worley, K. C., Hale, S., Garcia, A. M., Gay, L. J., Hulyk, S. W., Villalon, D. K., Muzny, D. M., Sodergren, E. J., Lu, X., Gibbs, R. A., Fahey, J., Helton, E., Ketteman, M., Madan, A., Rodrigues, S., Sanchez, A., Whiting, M., Young, A. C., Shevchenko, Y., Bouffard, G. G., Blakesley, R. W., Touchman, J. W., Green, E. D., Dickson, M. C., Rodriguez, A. C., Grimwood, J., Schmutz, J., Myers, R. M., Butterfield, Y. S., Krzywinski, M. I., Skalska, U., Smailus, D. E., Schnerch, A., Schein, J. E., Jones, S. J. and Marra, M. A., 2002. Generation and initial analysis of more than 15,000 full-length human and mouse cDNA sequences. Proc Natl Acad Sci U S A. 99, 16899-16903.

Stromer, T. and Serpell, L. C., 2005. Structure and morphology of the Alzheimer's amyloid fibril. Microsc Res Tech. 67, 210-217.

Stutzmann, G. E., Smith, I., Caccamo, A., Oddo, S., Laferla, F. M. and Parker, I., 2006. Enhanced ryanodine receptor recruitment contributes to Ca2+ disruptions in young, adult, and aged Alzheimer's disease mice. J Neurosci. 26, 5180-5189.

Subbarao, K. V., Richardson, J. S. and Ang, L. C., 1990. Autopsy samples of Alzheimer's cortex show increased peroxidation in vitro. J Neurochem. 55, 342-345.

Suckau, L., Fechner, H., Chemaly, E., Krohn, S., Hadri, L., Kockskamper, J., Westermann, D., Bisping, E., Ly, H., Wang, X., Kawase, Y., Chen, J., Liang, L., Sipo, I., Vetter, R., Weger, S., Kurreck, J., Erdmann, V., Tschope, C., Pieske, B., Lebeche, D., Schultheiss, H. P., Hajjar, R. J. and Poller, W. C., 2009. Long-term cardiac-targeted RNA interference for the treatment of heart failure restores cardiac function and reduces pathological hypertrophy. Circulation. 119, 1241-1252.

Sylvius, N., Duboscq-Bidot, L., Bouchier, C., Charron, P., Benaiche, A., Sebillon, P., Komajda, M. and Villard, E., 2003. Mutational analysis of the beta- and delta-sarcoglycan genes in a large number of patients with familial and sporadic dilated cardiomyopathy. Am J Med Genet A. 120A, 8-12.

Taha, M. and Lopaschuk, G. D., 2007. Alterations in energy metabolism in cardiomyopathies. Ann Med. 39, 594-607.

Takasugi, N., Tomita, T., Hayashi, I., Tsuruoka, M., Niimura, M., Takahashi, Y., Thinakaran, G. and Iwatsubo, T., 2003. The role of presenilin cofactors in the gamma-secretase complex. Nature. 422, 438-441.

Tamamori, M., Ito, H., Hiroe, M., Terada, Y., Marumo, F. and Ikeda, M. A., 1998. Essential roles for G1 cyclin-dependent kinase activity in development of cardiomyocyte hypertrophy. Am J Physiol. 275, H2036-2040.

Tamayo, P., Slonim, D., Mesirov, J., Zhu, Q., Kitareewan, S., Dmitrovsky, E., Lander, E. S. and Golub, T. R., 1999. Interpreting patterns of gene expression with self-organizing maps: methods and application to hematopoietic differentiation. Proc Natl Acad Sci U S A. 96, 2907-2912.

Tan, F. L., Moravec, C. S., Li, J., Apperson-Hansen, C., McCarthy, P. M., Young, J. B. and Bond, M., 2002. The gene expression fingerprint of human heart failure. Proc Natl Acad Sci U S A. 99, 11387-11392.

Tanaka, S., Nakamura, S., Ueda, K., Kameyama, M., Shiojiri, S., Takahashi, Y., Kitaguchi, N. and Ito, H., 1988. Three types of amyloid protein precursor mRNA in human brain: their differential expression in Alzheimer's disease. Biochem Biophys Res Commun. 157, 472-479.

Tanzi, R. E., 2005. The synaptic Abeta hypothesis of Alzheimer disease. Nat Neurosci. 8, 977-979.

Tanzi, R. E. and Bertram, L., 2001. New frontiers in Alzheimer's disease genetics. Neuron. 32, 181-184.

Tanzi, R. E. and Bertram, L., 2005. Twenty years of the Alzheimer's disease amyloid hypothesis: a genetic perspective. Cell. 120, 545-555.

Tanzi, R. E., Gusella, J. F., Watkins, P. C., Bruns, G. A., St George-Hyslop, P., Van Keuren, M. L., Patterson, D., Pagan, S., Kurnit, D. M. and Neve, R. L., 1987. Amyloid beta protein gene: cDNA, mRNA distribution, and genetic linkage near the Alzheimer locus. Science. 235, 880-884.

Tanzi, R. E., McClatchey, A. I., Lamperti, E. D., Villa-Komaroff, L., Gusella, J. F. and Neve, R. L., 1988. Protease inhibitor domain encoded by an amyloid protein precursor mRNA associated with Alzheimer's disease. Nature. 331, 528-530.

Terentyev, D., Gyorke, I., Belevych, A. E., Terentyeva, R., Sridhar, A., Nishijima, Y., de Blanco, E. C., Khanna, S., Sen, C. K., Cardounel, A. J., Carnes, C. A. and Gyorke, S., 2008. Redox modification of ryanodine receptors contributes to sarcoplasmic reticulum Ca2+ leak in chronic heart failure. Circ Res. 103, 1466-1472.

Tesson, F., Sylvius, N., Pilotto, A., Dubosq-Bidot, L., Peuchmaurd, M., Bouchier, C., Benaiche, A., Mangin, L., Charron, P., Gavazzi, A., Tavazzi, L., Arbustini, E. and Komajda, M., 2000. Epidemiology of desmin and cardiac actin gene mutations in a european population of dilated cardiomyopathy. Eur Heart J. 21, 1872-1876.

Thinakaran, G., Borchelt, D. R., Lee, M. K., Slunt, H. H., Spitzer, L., Kim, G., Ratovitsky, T., Davenport, F., Nordstedt, C., Seeger, M., Hardy, J., Levey, A. I., Gandy, S. E., Jenkins, N. A., Copeland, N. G., Price, D. L. and Sisodia, S. S., 1996. Endoproteolysis of presenilin 1 and accumulation of processed derivatives in vivo. Neuron. 17, 181-190.

Tidholm, A. and Jonsson, L., 2005. Histologic characterization of canine dilated cardiomyopathy. Vet Pathol. 42, 1-8.

To, M. D., Gokgoz, N., Doyle, T. G., Donoviel, D. B., Knight, J. A., Hyslop, P. S., Bernstein, A. and Andrulis, I. L., 2006. Functional characterization of novel presenilin-2 variants identified in human breast cancers. Oncogene. 25, 3557-3564.

Tolia, A. and De Strooper, B., 2008. Structure and function of gamma-secretase. Semin Cell Dev Biol.

Tomita, Y., Matsumura, K., Wakamatsu, Y., Matsuzaki, Y., Shibuya, I., Kawaguchi, H., Ieda, M., Kanakubo, S., Shimazaki, T., Ogawa, S., Osumi, N., Okano, H. and Fukuda, K., 2005. Cardiac neural crest cells contribute to the dormant multipotent stem cell in the mammalian heart. J Cell Biol. 170, 1135-1146.

Tsukamoto, O., Minamino, T., Okada, K., Shintani, Y., Takashima, S., Kato, H., Liao, Y., Okazaki, H., Asai, M., Hirata, A., Fujita, M., Asano, Y., Yamazaki, S., Asanuma, H., Hori, M. and Kitakaze, M., 2006. Depression of proteasome activities during the progression of cardiac dysfunction in pressure-overloaded heart of mice. Biochem Biophys Res Commun. 340, 1125-1133.

Tu, H., Nelson, O., Bezprozvanny, A., Wang, Z., Lee, S. F., Hao, Y. H., Serneels, L., De Strooper, B., Yu, G. and Bezprozvanny, I., 2006. Presenilins form ER Ca2+ leak channels, a function disrupted by familial Alzheimer's disease-linked mutations. Cell. 126, 981-993.

Ungerer, M., Bohm, M., Elce, J. S., Erdmann, E. and Lohse, M. J., 1993. Altered expression of beta-adrenergic receptor kinase and beta 1-adrenergic receptors in the failing human heart. Circulation. 87, 454-463.

Urbanek, K., Cesselli, D., Rota, M., Nascimbene, A., De Angelis, A., Hosoda, T., Bearzi, C., Boni, A., Bolli, R., Kajstura, J., Anversa, P. and Leri, A., 2006. Stem cell niches in the adult mouse heart. Proc Natl Acad Sci U S A. 103, 9226-9231.

Urmoneit, B., Turner, J. and Dyrks, T., 1998. Cationic lipids (lipofectamine) and disturbance of cellular cholesterol and sphingomyelin distribution modulates gamma-secretase activity within amyloid precursor protein in vitro. Prostaglandins Other Lipid Mediat. 55, 331-343.

van Dijk, S. J., Dooijes, D., Dos Remedios, C., Michels, M., Lamers, J. M., Winegrad, S., Schlossarek, S., Carrier, L., Ten Cate, F. J., Stienen, G. J. and van der Velden, J., 2009. Cardiac Myosin-Binding Protein C Mutations and Hypertrophic Cardiomyopathy. Haploinsufficiency, Deranged Phosphorylation, and Cardiomyocyte Dysfunction. Circulation.

Van Geluwe, F., Dymarkowski, S., Crevits, I., De Wever, W. and Bogaert, J., 2006. Amyloidosis of the heart and respiratory system. Eur Radiol. 16, 2358-2365.

van Laar, T., van der Eb, A. J. and Terleth, C., 2002. A role for Rad23 proteins in 26S proteasome-dependent protein degradation? Mutat Res. 499, 53-61.

Vikstrom, K. L., Bohlmeyer, T., Factor, S. M. and Leinwand, L. A., 1998. Hypertrophy, pathology, and molecular markers of cardiac pathogenesis. Circ Res. 82, 773-778.

Voges, D., Zwickl, P. and Baumeister, W., 1999. The 26S proteasome: a molecular machine designed for controlled proteolysis. Annu Rev Biochem. 68, 1015-1068.

von Koch, C. S., Zheng, H., Chen, H., Trumbauer, M., Thinakaran, G., van der Ploeg, L. H., Price, D. L. and Sisodia, S. S., 1997. Generation of APLP2 KO mice and early postnatal lethality in APLP2/APP double KO mice. Neurobiol Aging. 18, 661-669.

Voortman, J. and Giaccone, G., 2006. Severe reversible cardiac failure after bortezomib treatment combined with chemotherapy in a non-small cell lung cancer patient: a case report. BMC Cancer. 6, 129.

Wagner, N., Wagner, K. D., Scholz, H., Kirschner, K. M. and Schedl, A., 2006. Intermediate filament protein nestin is expressed in developing kidney and heart and might be regulated by the Wilms' tumor suppressor Wt1. Am J Physiol Regul Integr Comp Physiol. 291, R779-787.

Walsh, D. M., Klyubin, I., Fadeeva, J. V., Cullen, W. K., Anwyl, R., Wolfe, M. S., Rowan, M. J. and Selkoe, D. J., 2002. Naturally secreted oligomers of amyloid beta protein potently inhibit hippocampal long-term potentiation in vivo. Nature. 416, 535-539.

Walsh, D. M. and Selkoe, D. J., 2004. Oligomers on the brain: the emerging role of soluble protein aggregates in neurodegeneration. Protein Pept Lett. 11, 213-228.

Walter, J., Capell, A., Grunberg, J., Pesold, B., Schindzielorz, A., Prior, R., Podlisny, M. B., Fraser, P., Hyslop, P. S., Selkoe, D. J. and Haass, C., 1996. The Alzheimer's disease-associated presenilins are differentially phosphorylated proteins located predominantly within the endoplasmic reticulum. Mol Med. 2, 673-691.

Wang, T. and Hebert, D. N., 2003. EDEM an ER quality control receptor. Nat Struct Biol. 10, 319-321.

Wang, X., Klevitsky, R., Huang, W., Glasford, J., Li, F. and Robbins, J., 2003. AlphaB-crystallin modulates protein aggregation of abnormal desmin. Circ Res. 93, 998-1005.

Wang, X., Osinska, H., Gerdes, A. M. and Robbins, J., 2002a. Desmin filaments and cardiac disease: establishing causality. J Card Fail. 8, S287-292.

Wang, Y., De Keulenaer, G. W., Weinberg, E. O., Muangman, S., Gualberto, A., Landschulz, K. T., Turi, T. G., Thompson, J. F. and Lee, R. T., 2002b. Direct

biomechanical induction of endogenous calcineurin inhibitor Down Syndrome Critical Region-1 in cardiac myocytes. Am J Physiol Heart Circ Physiol. 283, H533-539.

Weber, K. T., Janicki, J. S., Pick, R., Abrahams, C., Shroff, S. G., Bashey, R. I. and Chen, R. M., 1987. Collagen in the hypertrophied, pressure-overloaded myocardium. Circulation. 75, I40-47.

Weiss, S., Siebzehnrubl, F. A., Kreutzer, J., Blumcke, I. and Buslei, R., 2009. Evidence for a progenitor cell population in the human pituitary. Clin Neuropathol. 28, 309-318.

Weissman, J. S. and Kim, P. S., 1993. Efficient catalysis of disulphide bond rearrangements by protein disulphide isomerase. Nature. 365, 185-188.

Werner, E. D., Brodsky, J. L. and McCracken, A. A., 1996. Proteasome-dependent endoplasmic reticulum-associated protein degradation: an unconventional route to a familiar fate. Proc Natl Acad Sci U S A. 93, 13797-13801.

Westermark, P., Bergstrom, J., Solomon, A., Murphy, C. and Sletten, K., 2003. Transthyretin-derived senile systemic amyloidosis: clinicopathologic and structural considerations. Amyloid. 10 Suppl 1, 48-54.

Wickenden, A. D., Kaprielian, R., Kassiri, Z., Tsoporis, J. N., Tsushima, R., Fishman, G. I. and Backx, P. H., 1998. The role of action potential prolongation and altered intracellular calcium handling in the pathogenesis of heart failure. Cardiovasc Res. 37, 312-323.

Wolfe, M. S., Xia, W., Ostaszewski, B. L., Diehl, T. S., Kimberly, W. T. and Selkoe, D. J., 1999. Two transmembrane aspartates in presenilin-1 required for presenilin endoproteolysis and gamma-secretase activity. Nature. 398, 513-517.

Wolfe, S. L., 1993. Molecular and Cellular Biology. Wadsworth Publishing Company.

Wright, M. J., Wightman, L. M., Latchman, D. S. and Marber, M. S., 2001. In vivo myocardial gene transfer: optimization and evaluation of intracoronary gene delivery in vivo. Gene Ther. 8, 1833-1839.

Wu, Z. and Irizarry, R. A., 2004. Preprocessing of oligonucleotide array data. Nat Biotechnol. 22, 656-658; author reply 658.

Xia, W., 2008. From presenilinase to gamma-secretase, cleave to capacitate. Curr Alzheimer Res. 5, 172-178.

Xu, C., Bailly-Maitre, B. and Reed, J. C., 2005. Endoplasmic reticulum stress: cell life and death decisions. J Clin Invest. 115, 2656-2664.

Yang, J., Moravec, C. S., Sussman, M. A., DiPaola, N. R., Fu, D., Hawthorn, L., Mitchell, C. A., Young, J. B., Francis, G. S., McCarthy, P. M. and Bond, M., 2000. Decreased SLIM1 expression and increased gelsolin expression in failing human hearts measured by high-density oligonucleotide arrays. Circulation. 102, 3046-3052.

Yang, L., Cao, Z., Li, F., Post, D. E., Van Meir, E. G., Zhong, H. and Wood, W. C., 2004. Tumor-specific gene expression using the survivin promoter is further increased by hypoxia. Gene Ther. 11, 1215-1223.

Yankner, B. A., Dawes, L. R., Fisher, S., Villa-Komaroff, L., Oster-Granite, M. L. and Neve, R. L., 1989. Neurotoxicity of a fragment of the amyloid precursor associated with Alzheimer's disease. Science. 245, 417-420.

Ye, Y., Shibata, Y., Yun, C., Ron, D. and Rapoport, T. A., 2004. A membrane protein complex mediates retro-translocation from the ER lumen into the cytosol. Nature. 429, 841-847.

Yoo, A. S., Cheng, I., Chung, S., Grenfell, T. Z., Lee, H., Pack-Chung, E., Handler, M., Shen, J., Xia, W., Tesco, G., Saunders, A. J., Ding, K., Frosch, M. P., Tanzi, R. E. and Kim, T. W., 2000. Presenilin-mediated modulation of capacitative calcium entry. Neuron. 27, 561-572.

Yoshida, H., Haze, K., Yanagi, H., Yura, T. and Mori, K., 1998. Identification of the cis-acting endoplasmic reticulum stress response element responsible for transcriptional induction of mammalian glucose-regulated proteins. Involvement of basic leucine zipper transcription factors. J Biol Chem. 273, 33741-33749.

Yoshida, H., Matsui, T., Yamamoto, A., Okada, T. and Mori, K., 2001. XBP1 mRNA is induced by ATF6 and spliced by IRE1 in response to ER stress to produce a highly active transcription factor. Cell. 107, 881-891.

Yoshida, H., Okada, T., Haze, K., Yanagi, H., Yura, T., Negishi, M. and Mori, K., 2000. ATF6 activated by proteolysis binds in the presence of NF-Y (CBF) directly to the cis-acting element responsible for the mammalian unfolded protein response. Mol Cell Biol. 20, 6755-6767.

Yoshiike, Y., Chui, D. H., Akagi, T., Tanaka, N. and Takashima, A., 2003. Specific compositions of amyloid-beta peptides as the determinant of toxic beta-aggregation. J Biol Chem. 278, 23648-23655.

Young, J. C., Agashe, V. R., Siegers, K. and Hartl, F. U., 2004. Pathways of chaperone-mediated protein folding in the cytosol. Nat Rev Mol Cell Biol. 5, 781-791.

Young, J. C., Moarefi, I. and Hartl, F. U., 2001. Hsp90: a specialized but essential protein-folding tool. J Cell Biol. 154, 267-273.

Yung, C. K., Halperin, V. L., Tomaselli, G. F. and Winslow, R. L., 2004. Gene expression profiles in end-stage human idiopathic dilated cardiomyopathy: altered expression of apoptotic and cytoskeletal genes. Genomics. 83, 281-297.

Zhang, K. and Kaufman, R. J., 2006. Protein folding in the endoplasmic reticulum and the unfolded protein response. Handb Exp Pharmacol, 69-91.

Zhao, G., Liu, Z., Ilagan, M. X. and Kopan, R., Gamma-secretase composed of PS1/Pen2/Aph1a can cleave notch and amyloid precursor protein in the absence of nicastrin. J Neurosci. 30, 1648-1656.

Zhao, L. and Ackerman, S. L., 2006. Endoplasmic reticulum stress in health and disease. Curr Opin Cell Biol. 18, 444-452.

Zhuo, M., Zhang, W., Son, H., Mansuy, I., Sobel, R. A., Seidman, J. and Kandel, E. R., 1999. A selective role of calcineurin aalpha in synaptic depotentiation in hippocampus. Proc Natl Acad Sci U S A. 96, 4650-4655.

Zubenko, G. S., Moossy, J., Martinez, A. J., Rao, G. R., Kopp, U. and Hanin, I., 1989. A brain regional analysis of morphologic and cholinergic abnormalities in Alzheimer's disease. Arch Neurol. 46, 634-638.